HOLLOW FIBER SORBENTS FOR THE DESULFURIZATION OF PIPELINE NATURAL GAS

A Dissertation
Presented to
The Academic Faculty

By

Dhaval Bhandari

In Partial Fulfillment
Of the Requirements for the Degree
Doctor of Philosophy in the
School of Chemical & Biomolecular Engineering

Georgia Institute of Technology

December 2010

HOLLOW FIBER SORBENTS FOR THE DESULFURIZATION OF PIPELINE NATURAL GAS

Approved by:

Dr. William J. Koros, Advisor
School of Chemical & Biomolecular
Engineering
Georgia Institute of Technology

Dr. Pradeep Agrawal
School of Chemical & Biomolecular
Engineering
Georgia Institute of Technology

Dr. Christopher Jones
School of Chemical & Biomolecular
Engineering
Georgia Institute of Technology

Dr. Satish Kumar
School of Materials Science &
Engineering
Georgia Institute of Technology

Dr. Ronald Rousseau
School of Chemical & Biomolecular
Engineering
Georgia Institute of Technology

Dr. James Stevens
Catchlight Energy LLC
(A Weyerhaeuser/Chevron Joint
Venture)

Date approved: October 28, 2010

Dedicated to my dearest parents

ACKNOWLEDGEMENTS

working style. Dr. Junqiang Liu, Ryan Lively were excellent batchmates and bright researchers whom I will always admire. Chien-chiang, Dr. Shan Wickramanayake, Omo, Liren, Diana, Meha and Nitesh were all good colleagues and were always there to discuss research ideas. Thanks to Ms. Michelle Martin for being friendly and processing last minute supply orders. Many thanks to Bunger Henry building manager - Rod Sefton, for fixing all maintenance related issues and help during lab setup.

I wish to thank my dearest parents for their unconditional love and support throughout my life. Despite being half way around the world, their thoughts and prayers were always with me. My sister, brother-in-law and my cute little nephew and niece are also thanked for their love and encouragement.

I have always been fortunate to have good friends who have been present during good and more importantly tough times. I will always cherish and remember my friendship with Prashant, Ashish and Manoj. They were my support system at Tech and I can never return all the favors and sacrifices they have made for me. Ambarish, Pramod, Divya, Anna, Yanto and Kayode were all great friends and I thank them for all the fun times at GaTech. Shreekrishna, Nagesh, Sandeep, Neel, Rutvik and Nilay were wonderful current and past house mates and are thanked for their support, good food and camaraderie.

I will always treasure my time at Georgia Tech and the amazing people who made my stay special!! Thanks to all of you.

TABLE OF CONTENTS

LIST OF TABLES

xiv

LIST OF FIGURES

SUMMARY

The overarching goal of this research was to create innovations in the field of separations by developing 'fiber sorbents' for on-site hydrogen generation applications. Specifically, this work was focused on the removal of sulfur impurities from pipeline natural gas. Knowledge from membrane science and adsorption technology was drawn upon extensively to enable this new technology.

The concentration of sulfur in odorized pipeline natural gas is about 30 ppm with the acceptable level being <1 ppm. The packed bed technology conventionally applied in industry for this application suffers from disadvantages including particle attrition, high pressure drop and slow regeneration rates.

Hollow fiber sorbents are pseudo monolithic material with a polymer 'binder', impregnated with high loadings of sulfur selective zeolite sorbents as 'fillers'. Temperature swing adsorption (TSA) with steam/water as the regeneration media was identified as the optimal approach to regenerate the fiber sorbents. To allow only thermal interactions with the regeneration media, it was planned to create a dense and thin polymer 'barrier' layer on the sheath side of the fiber sorbents.

Simplified calculations were performed to determine mass and heat transfer, pressure drop, surface area-to-volume ratios for fiber sorbents and were compared with conventional pellet packed bed technology to consider the advantages and limitation of the fiber sorbent approach.

Single-layer fiber sorbents were created by using the dry jet-wet quench spinning technique. Cellulose acetate (CA) / zeolite NaY fiber sorbents with 75 wt. % NaY

loading and polyester urethane/NaY fiber sorbents with 60 wt. % NaY loading were spun successfully. Single-layer fiber sorbent dynamic and equilibrium capacities for model sulfur odorants (tertiary butyl mercaptan (TBM) and hydrogen sulfide (H_2S)) were determined using batch and flow systems.

Dual-layer fiber sorbents were created by simultaneous co-extrusion of PVDC as the 'sheath' layer and CA/NaY as the 'core' layer using the hollow fiber spinning technology. Careful tuning of the various spinning parameters allowed for the creation of dual-layer fibers with a dense and low permeance sheath layer. However, the sheath layer was still defective with Knudsen selectivity. Heat treatment and silicone rubber coating techniques were utilized to seal the minor defects in the sheath layer skin. Alternatively, a new post treatment technique using an aqueous dispersion of PVDC barrier polymer was developed to create either a barrier sheath layer on single-layer fiber sorbents or to caulk a severely defective barrier sheath layer.

A small scale facility was designed and constructed to allow continuous sulfur sorption and steam/water regeneration cycles on the fiber sorbent modules. Barrier sheath layer efficacy was tested by conducting water (25 °C) and steam (110 °C) permeance experiments. Based on these results, challenges in testing fiber sorbents under steam were identified and feasible proof-of-concept experiments were conducted to demonstrate the durability and regenerability of fiber sorbents.

CHAPTER 1

INTRODUCTION

1.1. Current energy scenario

High global demand, national security and climate change issues related to conventional fossil fuels have motivated the development of renewable energy resources and have led to improvements in non-renewable resource usage [1]. Despite the increased awareness, non-renewable resources like oil, natural gas and coal continue to remain the dominant fuel source, with renewable energy sources currently accounting for less than 10 % of the total energy consumption [1] (Figure 1.1 (a)). Also, with the rapid industrialization of non-OECD (Organization for Economic Co-operation and Development) countries, especially China and India, the total world energy consumption will increase significantly (Figure 1.1 (b)).
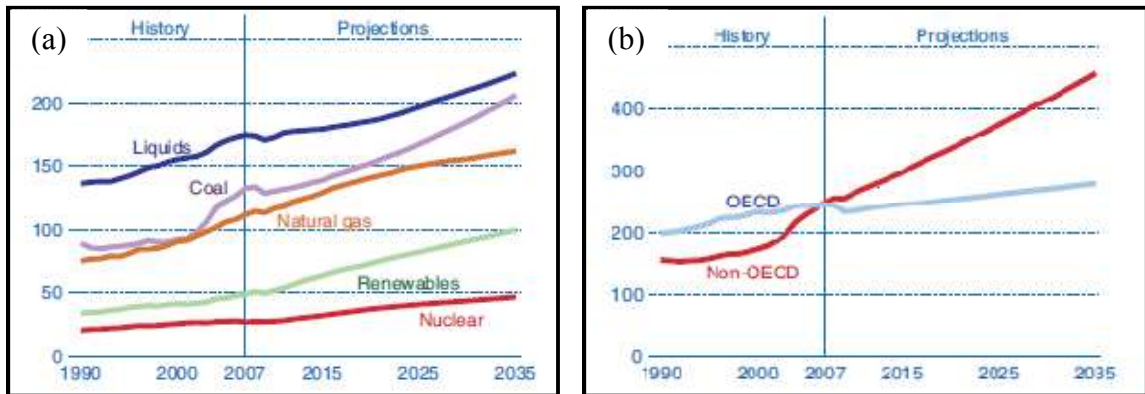
Figure 1.1 (left to right): (a) World marketed energy use by fuel type (quadrillion Btu), 1990-2035 [1] (b) World marketed energy consumption: OECD and Non-OECD (quadrillion Btu), 1990-2035. Reproduced from [1].

For the transition to a renewable energy based economy to occur (Figure 1.1 (a)), there is an urgent need to explore the development of various alternative fuels. This

growth depends on several key factors involving complex inter-relations between the economics, concerns and needs (Figure 1.2).

Economics
- Cost per gallon
- Ease of availability
- Ease of transportation

Concerns
- CO_2 / SOx emissions
- Shrinking natural resources
- Energy security

Needs
- Technology matched to fuel type
- Efficient separations
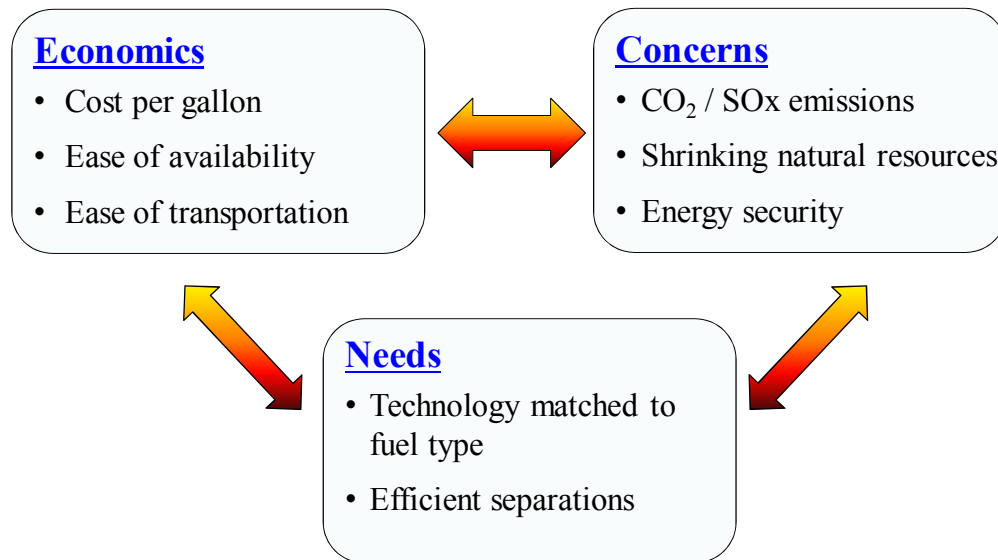
Figure 1.2: Key factors involved in the development of alternative fuels.

1.2. 'Hydrogen' as an alternative fuel

Among the various energy alternatives, hydrogen is particularly attractive as a clean energy carrier and an alternative to fossil fuels in order to reduce emissions of air pollutants and carbon dioxide. Hydrogen can be burned as a fuel, typically in a vehicle, with only water as the combustion product or used in fuel cells, to power an electric motor. This clean burning fuel can mean a significant reduction of pollution in cities [2] and could potentially alter the most polluting sectors in the U.S. i.e. the automobile industry and the electricity generation industry [3].

Hydrogen has been used extensively in the chemical industry as an important feedstock. However, the concept of 'hydrogen economy' (Figure 1.3), with hydrogen as an energy carrier has been visualized recently [4]. For example, a $ 1.2 billion

commitment over five years was announced in the United States in 2003 to research, develop and demonstrate hydrogen and fuel cell technologies [5]. Also, the U.S. department of energy (DOE) started the 'vision 21' program with the goal of developing multi-product energy plants by 2015 that also integrates gasification (hydrogen production) with fuel cell operation [6]. Figure 1.3 shows the essential system elements of hydrogen economy that include supply, production, distribution, dispensing, and end use [7].
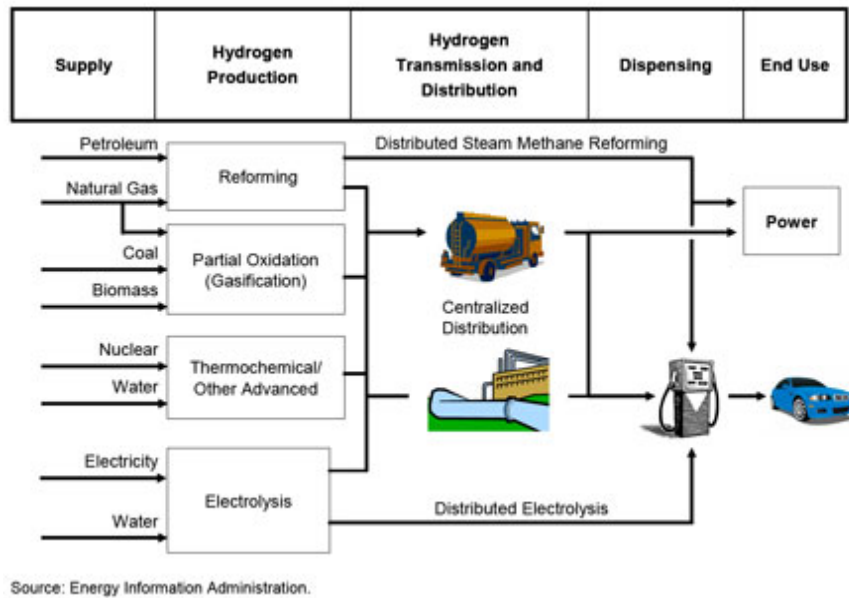
Figure 1.3: Simplified overview of the hydrogen economy. Reproduced from [7].

The transportation sector and stationary power applications are two critical sectors where hydrogen usage can be greatly expanded [8]. Hydrogen can be produced by steam-methane reforming (SMR), partial oxidation (including gasification), and electrolysis. Newer technologies including thermo chemical reactions using renewable resources like fermentation, landfill gas recovery, and municipal waste reformation are also being explored for hydrogen production [7].

SMR is a well-developed technology at the industrial scale and contributes to about 95% of the hydrogen production in the U.S. [9]. It is popular due to high hydrogen content (four hydrogen atoms per carbon atom) of its feedstock - natural gas (NG), extensive NG distribution network and scalability to small end-use applications [10]. For the SMR process, the efficiency at which the feedstock is converted into hydrogen ranges from 67-73 % [7]. For electrolysis, the efficiency of converting water to hydrogen by electric current is 60-63 %, with electricity production itself involving large transformation losses [7].

Currently, small and mid-sized hydrogen consumers use truck, rail, and barge transportation for hydrogen transfer, while larger industrial users rely on pipelines to transport hydrogen [11]. However, pipelines carrying pure hydrogen require special material of construction to avoid steel embrittlement and leakage making hydrogen transportation over longer distances very expensive [11]. Currently, due to the lack of hydrogen distribution infrastructure [4, 12], hydrogen production at the dispensing station by steam-methane reforming [13] and electrolysis [14] processes have been commercialized. The distributed generation approach reduces or eliminates the need for a dedicated hydrogen transmission, storage and distribution infrastructure.

1.3. Hydrogen economy – current scenario

The following discussion is focused on the application in the transportation sector, which is the focus of this research work. For efficient development of the hydrogen economy, both the supply side (the technologies and resources that produce hydrogen) and the demand side (the technologies and devices that convert hydrogen to services desired in the marketplace) must be developed simultaneously [11]. The US-DOE has

partnered with various automobile manufacturers and hydrogen fuel suppliers to simulate

the development of hydrogen as an alternative fuel [2].

Several major automobile manufacturers have begun R&D programs to develop

hydrogen fuel cells. These automobiles with an on-board hydrogen storage tank can be

recharged with hydrogen fuel. As of 2005, two major auto manufacturers, GM and

Daimler Chrysler, acknowledged expenditures of more than $1 billion in fuel cell vehicle

(FCV) development [15]. GM has begun market testing of Chevrolet Equinox fuel cell

sport utility vehicles [16]. Daimler has announced plans to start serial production of its

Mercedes Benz B-Class FCV in 2010 [7]. Honda began commercial leasing of its FCX

Clarity in 2008 [17] (Figure 1.4 (a) and (b)).
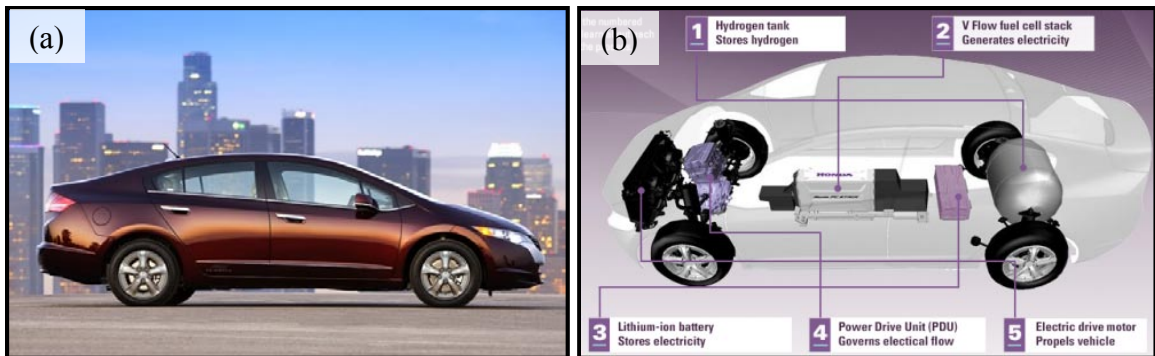
Figure 1.4 (left to right): (a) The exterior of Honda FCX clarity fuel cell electric vehicle (FCEV). Reproduced from [17] (b) Description of the key components of a Honda FCX clarity. Reproduced from [18].

Several major industrial gas and energy companies have partnered with car

makers to open on-site hydrogen generation stations [7] (Figure 1.5 (a) and (b)). There

are currently 72 operational and 24 planned hydrogen fueling stations in the US and in

Canada [19]. Chevron operated five hydrogen refueling stations in the US for five years

under its hydrogen refueling demonstration program [20]. Shell operates three on-site

hydrogen generation stations [14]. The aim of these projects is to understand the consumer behavior, safety and costs associated with hydrogen production [21].
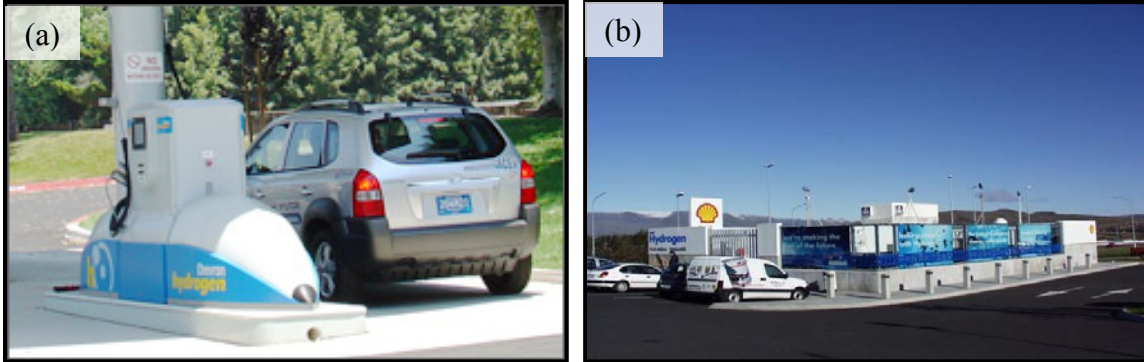
Figure 1.5 (left to right): (a) A hydrogen fuel cell SUV at Chevron hydrogen station in Oakland, CA. Reproduced from [22] (b) Shell hydrogen station in Reykjavik, Iceland. Reproduced from [23].

Even though significant advancements have been made to develop hydrogen fuel for transportation and stationary power applications, the cost of production in medium-to-small scale decentralized plants is still high and in the range of $3 - $10 per kg hydrogen (Figure 1.6), depending on the production method and source [11]. Regardless of the production scale, separation processes are critical to meet the fuel standard requirements and account for around 50 % of the capital investments in hydrogen generation [24]. Hence, improvements in separation processes can significantly reduce the cost of hydrogen production.
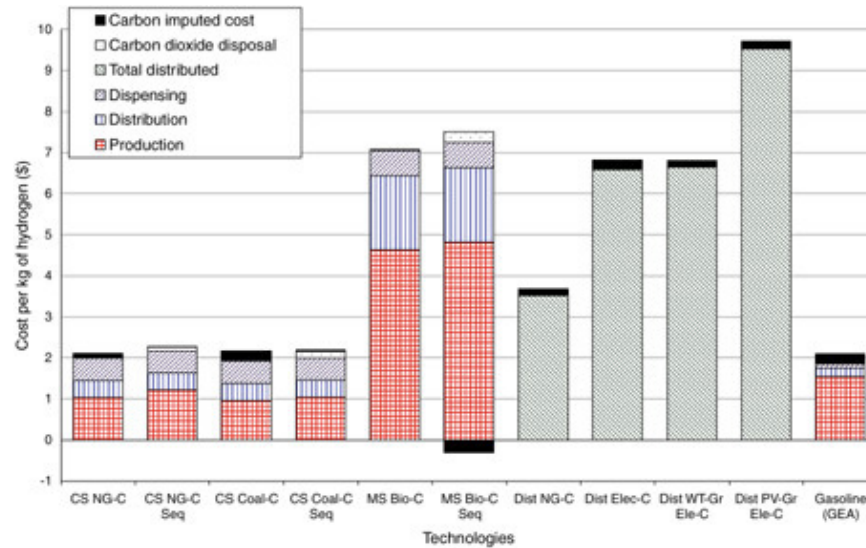
Figure 1.6: Unit cost estimates (cost per kilogram of hydrogen) for the 'current technologies' state of development for 10 hydrogen supply technologies. (GEA = gasoline efficiency adjusted). Reproduced from [11].

1.4. Separations – A key challenge

As described earlier, the SMR process is highly preferred for on-site hydrogen generation and downsizing from an industrial scale to small scales e.g. fueling station involves significant technological challenges. The flow diagram of the SMR process is shown in Figure 1.7. The SMR process consists of the following steps [25]:

Reformation of natural gas

This step involves methane (major component of natural gas (95%)) reacting with steam at ~800°C to produce a synthesis gas (syn-gas), a mixture primarily made up of hydrogen and carbon monoxide.

Shift reaction

In the second step, known as the water gas shift (WGS) reaction, the carbon monoxide from the first step is reacted with steam over a catalyst to form hydrogen and

carbon dioxide. This process occurs in two stages, consisting of a high temperature shift

(HTS) at~350°C and a low temperature shift (LTS) at~200 °C.

The reactions in the process are described below:

$$CH_4 + H_2O \quad \rightarrow \quad CO + 3H_2 \quad - \text{Methane reforming} \qquad (1.1)$$

$$CO + H_2O \quad \rightarrow \quad CO_2 + H_2 \quad - \text{Water gas shift} \qquad (1.2)$$
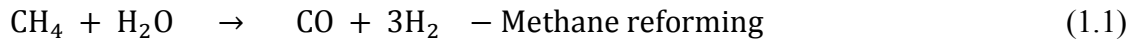
The purity requirements for hydrogen gas in fuel cell operations are very stringent (> 99.99 %) as compared to a hydrogen purity of (70-80 %) required for hydro-cracking operations [26]. The key separation/purification processes in a SMR are summarized below and highlighted in Figure 1.7.
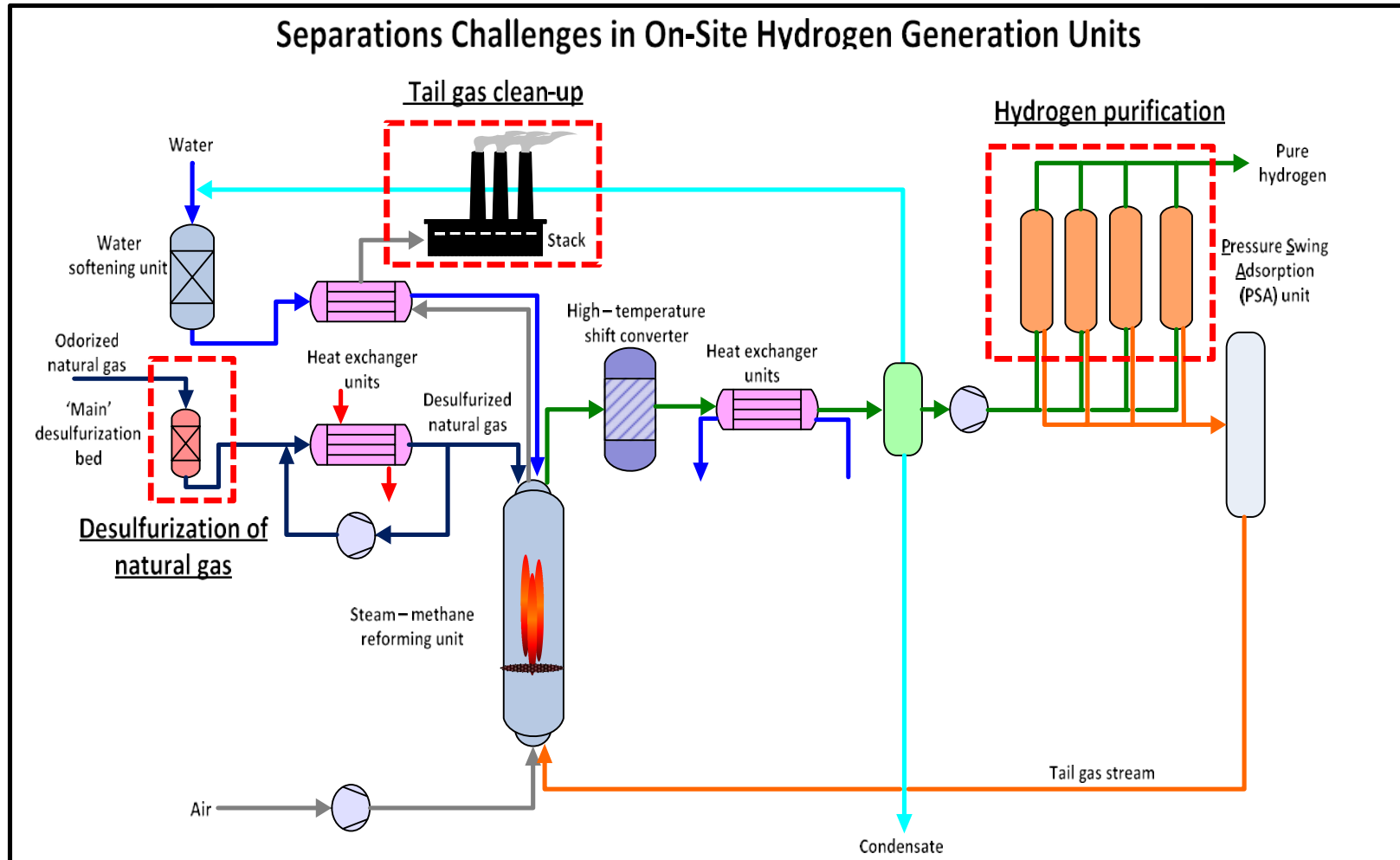
Figure 1.7: Flow diagram of the SMR process. Key separation challenges are highlighted for clarity. Adapted from [27].

- **Removal of sulfur impurities:** Residual hydrogen sulfide (H_2S) contaminant at low concentrations (typically ~ 5–10 ppm) and other organic sulfur species intentionally added as odorants to detect leaks in pipeline natural gas must be removed prior to its use [28-30]. Common odorants include mercaptans, thiols, sulfides and disulfides [31] (Table 1.1) with the concentration in the range of a few ppm to as high as 30 ppm. Metal catalysts used in the fuel processing and in the fuel cell electrodes are irreversibly poisoned by these sulfur compounds above a concentration of 1 ppm [32].

Table 1.1: Common sulfur impurities in pipeline natural gas [33].

Name of the odorant	Mol. Wt.	Boiling point (°C)	Vapor pressure (mm Hg at 25(°C))
Ethyl mercaptan (EM)	62.13	35.1	529
Tertiary butyl mercaptan (TBM)	90.18	64.2	181
Dimethyl sulfide (DMS)	62.13	37.3	502
Hydrogen sulfide (H_2S)	34.08	-60.3	15,600

- **Hydrogen purification:** Carbon dioxide and other residual gases are removed from the product gas to obtain high purity hydrogen. Currently, there are three technologies for hydrogen recovery: cryogenic distillation, pressure swing adsorption (PSA) and membrane processes [34]. PSA is a well-established and mature industrial process operated with multiple packed bed columns giving high purity (99.99%) with high recovery (> 80%) [35].

- **Tail-gas clean up:** Currently, the main sources of hydrogen are hydrocarbon feedstocks like natural gas and coal; however, these feed stocks also produce CO_2.

(Reaction 1.2). Thus, to provide overall emission savings, greenhouse gas (GHG) emissions must be mitigated during hydrogen production through carbon capture and sequestration (CCS). This can be achieved through comparatively greater vehicle efficiency or at other stages in the life cycle of the hydrogen fuel source [7].

1.5. Removal of sulfur impurities from pipeline natural gas

For low concentration and small scale systems, highly energy intensive processes like amine absorption and hydrodesulfurization (HDS) are less attractive. The presence of multiple odorants and low driving force of the feed gas makes the use of membranes less desirable for this application. Traditionally, packed bed adsorbents such as activated carbon and metal oxides have been applied for the desulfurization of pipeline natural gas [30, 36, 37]. Unfortunately, activated carbon can become pyrophoric during regeneration and various metal oxides require high temperature regeneration [38].

In contrast, nano crystalline zeolites are inexpensive, stable and give high sorption capacity at ambient temperatures and pressures. The use of faujasite and MFI type zeolite for removing dimethyl sulfide (DMS) and/or tertiary butyl mercaptan (TBM) present in pipeline natural gas have been reported [28, 39, 40]. Weber et al. have also reported favorable equilibrium sorption of ethyl mercaptan on zeolite NaX [36, 38]. These various studies show that zeolites are attractive adsorbents for the deodorization of natural gas in compact systems.

Zeolite crystals are typically formed into pellets with an inert binding material for the ease of handling. A multi-bed system of pelletized adsorbents can be operated with intermittent adsorption-desorption cycles to achieve continuous treatment of feeds. For bulk separation of the gases containing high levels of contaminant, cycling the operating

pressure known as pressure swing adsorption (PSA) is preferred [41]. For the removal of trace amounts of impurities, such as removal of sulfur impurities from natural gas streams, cycling the temperature of the bed, known as temperature swing adsorption (TSA) is favored [41].

Regeneration media used in TSA are typically a hot stream of purge gas such as nitrogen (N_2) or a fraction of purified feed gas. However, due to low thermal efficiency of gases the regeneration steps take prohibitively long times.

Apart from the regeneration issues, performance of a packed bed can be affected by high pressure drop and large mass transfer resistance. High pressure drop can lead to undesirable high pumping costs and attrition of particles. Large mass transfer resistance can lead to under-utilization of the bed capacity due to slow access of the adsorbate to the adsorption sites. Smaller pellet sizes reduce diffusion path length and allow better utilization of adsorption capacity with sharper breakthrough curves. On the contrary, pressure drop is inversely proportional to the pellet size with smaller crystals leading to a higher pressure drop. These two undesirable factors are oppositely affected by the primary pellet size in packed beds, so optimization is needed.

This research work seeks to develop a novel separation material 'fiber sorbent' to remove sulfur compounds from pipeline natural gas, in which the constraints imposed by the above scaling on primary particle size can be reduced. The feasibility of fiber sorbents will be analyzed, fiber sorbents with desired sorbent loading and morphology will be created and ultimately a process will be designed and developed to efficiently regenerate the fiber sorbents without the loss of its sorption capacity.

1.6. Research objectives

Objective 1: Assess the feasibility of fiber sorbents for the removal of sulfur compounds from natural gas.

This chapter describes the concept of fiber sorbent. This chapter lays down the foundation of a TSA system utilizing hollow fiber geometry with polymer as 'binder', impregnated with high loadings of sulfur selective zeolite sorbents as 'fillers'. These pseudo monolithic materials can be created with high sorbent loading (up to 75 wt%, dry fiber basis) with relative ease by modifying hollow fiber membrane spinning technology. Moreover possible methods to efficiently regenerate fiber sorbent beds without significant loss to zeolite sorption capacity will be considered.

To assess the feasibility of fiber sorbents, simplified calculations are performed to determine mass and heat transfer, pressure drop, surface area to volume ratios as functions of parameters such as outer and inner fiber diameter, fiber length, velocity through the module, fiber porosity and bed packing fraction. Using these calculations as a guiding force, the dimensions and specifications of fiber sorbent operation will be established. Comparisons will be made with the current technology of packed bed adsorbents to illustrate the advantages of fiber sorbent. Knowledge from membrane science and adsorption technology will be drawn upon extensively to enable this new technology.

Objective 2: *Create and characterize single-layer fiber sorbents with high sorbent loading, optimized morphology and desired separation properties.*

Fiber sorbents were made by modifying the dry jet-wet quench spinning technique. Spinning parameters were optimized in a manner to allow fibers to be spun at high take-up rates and at room temperature spinning conditions. CA/NaY fiber sorbents with 75 wt. % NaY loading and polyester urethane/NaY fiber sorbents with 60 wt. % NaY loading were spun successfully. Various spinning parameters like quench bath temperature, air gap, dope flow rates will be discussed in greater detail. Steps taken to eliminate macrovoids in the CA/NaY fiber sorbent morphology will be covered.

SEM images indicated that CA / NaY fiber sorbents had the desired 'sieve-in-a-cage' structure, while polyester urethane fiber sorbents indicated a sieve encapsulated by polymer ('occluded' sieve). *With these advantages CA was pursued as the polymer of choice for the fiber sorbent core layer creation.* EDX image of the CA/NaY fiber sorbents indicated uniform distribution of zeolite crystals. Fiber sorbent capacity under equilibrium conditions with TBM is determined and compared to its individual constituents (Pure CA hollow fiber and zeolite NaY). Fiber sorbent flow testing with TBM/N_2 and H_2S/N_2 test gas mixtures is described. Variation in performance with parameters such as zeolite loading, flow rates, fiber diameter and number of fibers will be considered. Fiber sorbents indicated a sharp, symmetrical S–shaped sorption curve indicating no premature breakthrough under flow conditions. Premature breakthrough was not observed with the variation in flow rate, indicating the expected rapid radial diffusion of gas to the zeolites in the fiber sorbents with relatively small wall thickness.

Objective 3: *Create and characterize dual-layer fiber sorbents with high sorbent loading, optimized morphology and desired separation properties.*

Formation of an impermeable outer layer is crucial for the effective regeneration of the fiber sorbents. This impermeable layer provides a mass transfer barrier for water/steam that would otherwise come into direct contact with the zeolite particles during regeneration. Applicability of various barrier polymers will be analyzed. Based on various iterations polyvinylidene chloride (PVDC) as solvent soluble powder form and in aqueous emulsion form was selected as the polymer of choice. Dual layer spinning with PVDC as the sheath layer and CA/NaY as the core layer will be discussed. The dope compositions and spinning conditions were optimized in a way that the core structure of fiber sorbent is porous while the sheath structure is still dense and impermeable. Challenges in terms of adhesion between the two layers, permeation properties and desired morphology will be addressed. Careful tuning of the various spinning parameters allows for the creation of a close to perfect sheath layer. Various post treatment techniques were explored to caulk the remaining defects in the barrier layer. Spray, dip coating techniques will be compared to a coating method with PVDC emulsion flow on fibers potted in a module with a shell and tube geometry. The optimized post-treatment protocol will be described. SEM, EDX, permeation and DSC techniques will be used to characterize dual/multiple layer fibers.

Objective 4: *Design and build an industrial prototype facility for temperature swing adsorption (TSA) of fiber sorbent modules.*

The design and construction of the TSA setup is also an important part of this work. Safety analysis with regards to sulfur odorant concentration, creation and discharge of high temperature saturated steam will be discussed. The fiber sorbent test rig and the lecture bottles of sulfur gases were located inside the fume hood for safety reasons. The test rig had the ability to perform packed bed and fiber sorbent module operations. A steam generator was installed outside the fume hood to provide saturated steam up to 200 °C in a controlled and safe environment. This chapter will also cover the ability to perform rapid heating and cooling cycles. Proof-of-concept regeneration experiments by heating the modules to 120°C using heat tapes with a nitrogen purge are described. The regeneration of fiber sorbents over a number of cycles is demonstrated to prove the attractiveness of fiber sorbents as a separations material. The barrier layer efficacy will be tested for water vapor permeance with water (25 °C) and steam (110 °C).

1.7. REFERENCES

1. United States. Energy Information Administration. Office of Integrated Analysis and Forecasting. *International Energy Outlook 2010 www.eia.gov/oiaf/ieo/index.html*. Date accessed, October 8th, 2010.

2. Choudhury, B. and Materials Research Society. Meeting Symposium HH., *The hydrogen economy*. 2008, Materials Research Society: Warrendale, PA. p. 1 v. (unpaged papers).

3. *http://www.altenergy.org/renewables/renewables.html*. Date accessed, October 8th, 2010.

4. *A national vision of America's transition to a hydrogen economy: to 2030 and beyond : based on the results of the National Hydrogen Vision Meeting Washington, DC, November 15-16, 2001*. 2001, Washington D.C.: United States Department of Energy.

5. Gronich S. *2010 –2025 Scenario Analysis,http://www1.eere.energy.gov/hydrogenandfuelcells/analysis/pdfs/gronich _scenario_analysis.pdf,*. 2010. Date accessed, October 8th, 2010.

6. U.S. department of energy. *Vision 21 - the Ultimate Power Plant Concept,http://www.fossil.energy.gov/programs/powersystems/vision21/,* 2007. Date accessed, October 8th, 2010.

7. Energy Information Administration - Office of Integrated Analysis and Forecasting, *The Impact of Increased Use of Hydrogen on Petroleum Consumption and Carbon Dioxide Emissions,http://www.eia.doe.gov/oiaf/servicerpt/hydro/pdf/oiafcneaf(08)04.pdf,*. Aug. 2008, U.S. Department of Energy: Washington, DC. Date accessed, October 8th, 2010.

8. Jones, R.H. and G.J. Thomas, *Materials for the hydrogen economy*. 2008, Boca Raton: CRC Press. xxiii, 327 p.

9. U.S. Department of Energy. *Fuel Cell Technologies Program*. http://www1.eere.energy.gov/hydrogenandfuelcells. Date accessed, October 8th, 2010.

10. Xu, J.G. and G.F. Froment, *Methane Steam Reforming, Methanation and Water-Gas Shift .1. Intrinsic Kinetics.* Aiche Journal, 1989. 35(1): p. 88-96.

11. *The Hydrogen Economy: opportunities,costs,barriers and R&D needs*. 2004: National academic press.

12.   Alptekin, G., et al., *Regenerable sorbent for natural gas desulfurization.* Journal of materials engineering and performance, 2006. 15(4): p. 433-438.

13.   *http://technologyventures.chevron.com/commercialize_tech/hydrogen.asp*. Date accessed, October 8th, 2010.

14.   *http://www.shell.com/home/content/environment_society/alternative_energies*. Date accessed, October 8th, 2010.

15.   Fahey J., *Hydrogen Gas*, in *Forbes,May 9, 2005*.

16.   *http://www.chevrolet.com/fuelcell*. Date accessed, October 8th, 2010.

17.   Honda FCX Clarity *http://automobiles.honda.com/fcx-clarity/exterior-photos.aspx*. Date accessed, October 8th, 2010.

18.   Honda Clarity. *http://automobiles.honda.com/fcx-clarity/how-fcx-works.aspx*. Date accessed, October 8th, 2010.

19.   National Hydrogen Assosiation. *http://www.hydrogenassociation.org/general/fuelingSearch.asp#null*. Date accessed, October 8th, 2010.

20.   *http://www.chevron.com/deliveringenergy/hydrogen/*. Date accessed, October 8th, 2010.

21.   *http://www.shell.us/home/content/usa/aboutshell/media_center /news_and_press_releases/2009/jfk_hydrogen_071409.html*. Date accessed, October 8th, 2010.

22.   *http://www.actransit.org/environment/fuelcell_photogallery.html*. Date accessed, October 8th, 2010.

23.   *http://www.icenews.is/index.php/2008/06/23/hydrogen-powered-ships-and-cars-now-available/*. Date accessed, October 8th, 2010.

24.   Nenoff, T.M., R.J. Spontak, and C.M. Aberg, *Membranes for hydrogen purification: An important step toward a hydrogen-based economy.* Mrs Bulletin, 2006. 31(10): p. 735-741.

25.   Kirk, R.E., et al., *Kirk-Othmer encyclopedia of chemical technology*, Wiley: [Hoboken, NJ].

26.   Shao, L., et al., *Polymeric membranes for the hydrogen economy: Contemporary approaches and prospects for the future.* Journal of Membrane Science, 2009. 327(1-2): p. 18-31.

27.   *http://www.global-hydrogen-bus-platform.com/*. Date accessed, October 8th, 2010.

28. Wakita, H., Y. Tachibana, and M. Hosaka, *Removal of dimethyl sulfide and t-butylmercaptan from city gas by adsorption on zeolites.* Microporous and Mesoporous materials, 2001. 46(2-3): p. 237-247.

29. Shimizu, K., et al., *Mechanistic study on adsorptive removal of tert-butanethiol on Ag-Y zeolite under ambient conditions.* Journal of physical chemistry B, 2006. 110(45): p. 22570-22576.

30. Kim, H.T., et al., *Desulfurization of odorant-containing gas: Removal of t-butylmercaptan on Cu/ZnO/Al2O3.* International journal of Hydrogen Energy, 2007. 32(15): p. 3603-3608.

31. de Wild, P.J., et al., *Removal of sulphur-containing odorants from fuel gases for fuel cell-based combined heat and power applications.* Journal of power sources, 2006. 159(2): p. 995-1004.

32. Crespo, D., et al., *Superior sorbent for natural gas desulfurization.* Industrial & Engineering chemistry research, 2008. 47(4): p. 1238-1244.

33. *http://toxnet.nlm.nih.gov/.* Date accessed, October 8th, 2010.

34. Miller, G.Q. and J. Stöcker, *Selection of a Hydrogen Separation Process*, in *National Petrochemical and Refiners Association Annual Meeting, San Francisco.* 1989, UOP Report 3111, January 1999.

35. Sircar, S. and T.C. Golden, *Purification of hydrogen by pressure swing adsorption.* Separation Science and Technology, 2000. 35(5): p. 667-687.

36. Weber, G., et al., *Selective adsorption of ethyl mercaptan on NaX zeolite.* Microporous and Mesoporous materials, 2008. 109(1-3): p. 184-192.

37. Kang, S.H., et al., *Effective removal of odorants in gaseous fuel for the hydrogen station using hydrodesulfurization and adsorption.* Energy & Fuels, 2007. 21(6): p. 3537-3540.

38. Weber, G., et al., *Adsorption equilibrium of light mercaptans on faujasites.* Adsorption-Journal of the International Adsorption Society, 2005. 11: p. 183-188.

39. Garcia, C.L. and J.A. Lercher, *Adsorption and Surface-Chemistry of Light Thiols on Na-Zsm5 and H-Zsm5.* Journal of physical chemistry, 1991. 95(26): p. 10729-10736.

40. Satokawa, S., Y. Kobayashi, and H. Fujiki, *Adsorptive removal of dimethylsulfide and t-butylmercaptan from pipeline natural gas fuel on Ag zeolites under ambient conditions.* Applied Catalysis B-Environmental, 2005. 56(1-2): p. 51-56.

41. Yang, R.T., *Gas separation by adsorption processes*. 1987, Boston: Butterworths.

CHAPTER 2

BACKGROUND AND THEORY

2.1. Concept of fiber sorbent

Structured monoliths with high sorbent loadings are an emerging separations platform with a potential to replace conventional packed bed technology for liquid and gas separations. Hollow fiber sorbents are pseudo monolithic materials with polymer as 'binder', impregnated with high loadings of sulfur selective zeolite sorbents as 'fillers'. Such organic – inorganic hybrid materials are planned to be created with relative ease by modifying the hollow fiber membrane spinning technology [1]. Fiber sorbents have to be created with high sorbent loadings (> 50 wt. %), to achieve sorption capacities comparable to the conventional packed bed technology while removing some of its drawbacks as discussed later. To effectively utilize the fiber sorbents, a process must be developed to efficiently regenerate the fiber sorbent beds without significant loss of zeolite sorption capacity. The goal of this work is to develop a technology by utilizing the key concepts of membrane science and the packed bed technology.

Figure 2.1 shows the schematic view of the proposed fiber sorbent material, a dual-layer mixed matrix membrane (MMM) and a conventional spherical pellet. Key dimensions in each case are shown for clarity.

Fiber sorbents can be identified as modified adsorbent systems where the key disadvantages of a conventional spherical pellet can be removed by manipulating the flow geometry and the morphology (Section 2.2.). However, the key differences between a dual-layer fiber sorbent and a dual-layer MMM need to be identified.

Certain key similarities of obtaining a delamination free structure, high core layer or sub-structure porosity, removal of defects and macrovoids exist in both the forms.
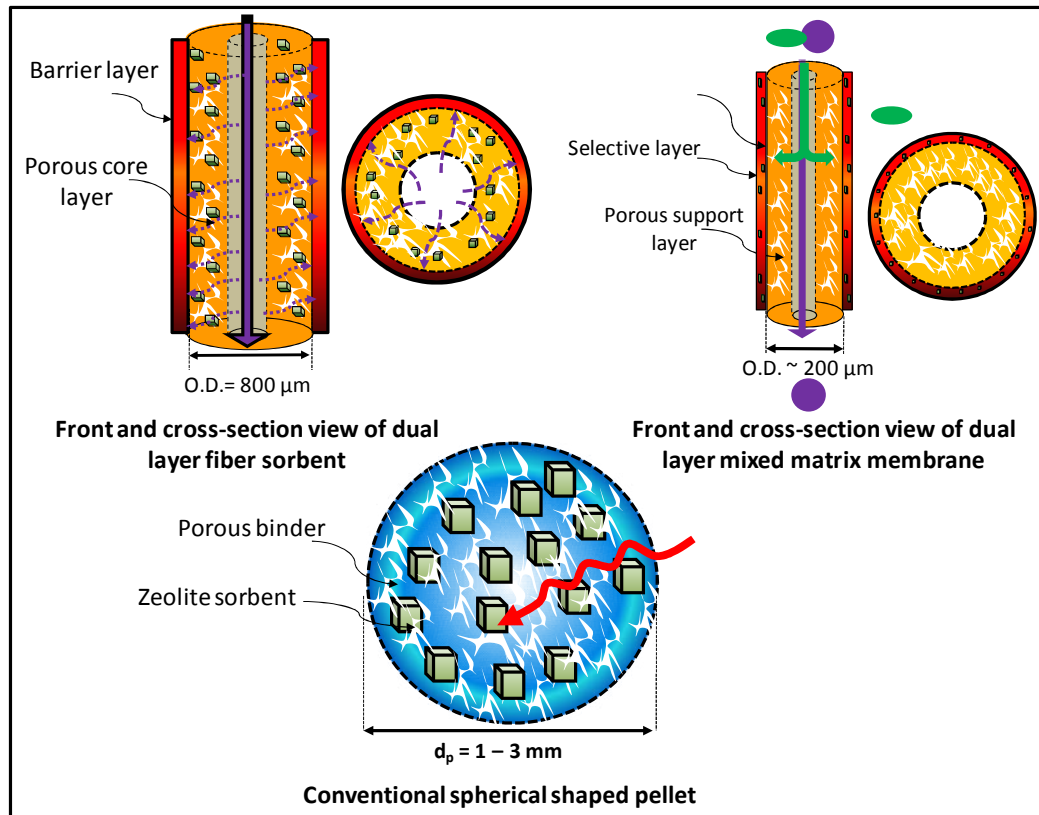
Figure 2.1: Schematic diagram of the proposed dual-layer fiber sorbents vs. a dual-layer mixed matrix membrane and a conventional spherical pellet used in packed bed adsorption.

Table 2.1: Comparison of desired properties in mixed matrix membranes and hollow fiber sorbents.

Dual-layer hollow fiber mixed matrix membranes	Dual-layer hollow fiber sorbents
• 15 - 40 wt. % zeolite loading (sheath layer wt. basis) is desired to obtain performance above Robeson's trade-off line [2]	• 50-75 wt. % zeolite loadings (core layer wt. basis) is desired to obtain loadings comparable to zeolite pellet packed beds
• Pressure or concentration difference across the membrane is the driving force for separation	• Selective adsorption of gas molecules in the zeolite sorbent is the driving force for separation
• The desired sheath is an ultrathin selective layer constituting an expensive, high performance polymer with dispersed zeolite particles that contribute to the separation performance of the membrane	• The desired sheath is a thin, dense layer constituting a gas and water vapor impermeable polymer and does not contribute to the separation performance of the fiber sorbent
• The core is a porous support layer constituting an in-expensive polymer and zeolite fillers (optional) that enables the membrane to withstand high pressures while not providing any contribution to the separation performance of the membrane	• The core is a highly porous layer constituting an inexpensive polymer as binder, and zeolite particles as the sorbent fillers that contribute to the separation performance of the fiber sorbent
• Zeolite and polymer should have good adhesion to get selectivity enchantment. Separation performance is severely impacted by defects at zeolite – polymer interface [3], causing a non-selective flow	• Zeolite and polymer should have intentionally bad adhesion with a sieve-in–a-cage morphology [3] desired. The gas molecules should preferably travel through the voids/pores to reach the zeolite particles improving the kinetics and hence separation performance

2.2. Potential advantages of fiber sorbents

Fiber sorbent morphology and structure is designed to offer numerous advantages over conventional spherical pellets. Some of the advantages are highlighted below and explained in detail with the help of calculations in the appendices.

1. Surface area to volume ratio up to 5-10 times higher than that of a typical spherical pellet of equivalent volume (Appendix A.4.), thereby providing fiber sorbents the capability of rapid cycling with significant downsizing of the main and auxiliary bed sizes (Figure 2.2).

2. Avoidance of particle attrition and poly-dispersity in pellet size, which can cause an undesirable broad breakthrough curve [4], since the fiber sorbents can be created with uniform diameters (up to 2 % variance) and lengths by optimizing the fiber spinning and module making process [5] to obtain sharp breakthrough curves.

3. Simplicity of flow pattern through the hollow fiber bore allows for lower pressure drop and increase in flow pattern reliability for scale-up [6] (Appendix A.6.).

4. Fiber sorbent modules do not require special packing arrangements and can be installed in any orientation.

5. Fiber sorbents provide a better ability to tune the mass transfer resistances compared to a conventional pellet packed bed (Appendix A.5.).
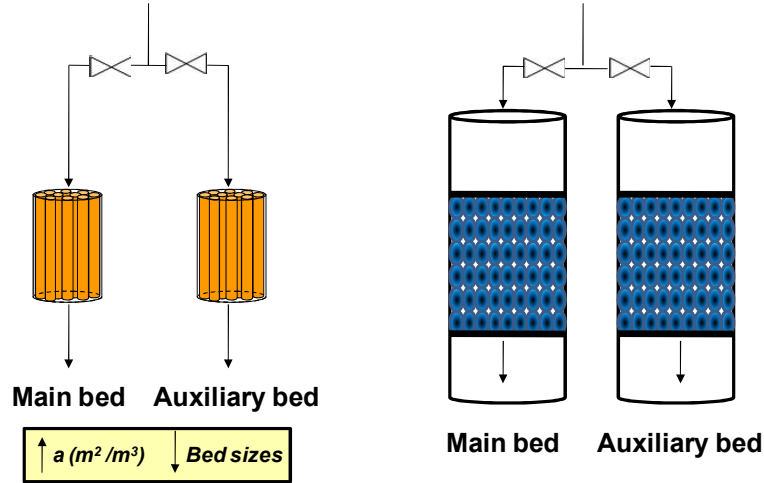
Figure 2.2: Operation of a twin bed fiber sorbent module and pellet packed bed system. With the increase in surface area / volume ratio (a – m^2/m^3), bed sizes can be reduced.

2.3. Fiber sorbent design and key concepts

It is desired to optimize the fiber sorbent geometry and operation to achieve a higher surface area for a given bed volume, minimize pressure drop and maximize the mass and heat transfer. Optimum fiber sorbent design will be a compromise between these various conflicting parameters. Appendices A.1. – A.11. describe the optimization of these factors by the variation of fiber outer diameter (O.D.), fiber inner diameter (I.D.), fiber length (L_f) and velocity through the module (v_s).

Design calculations for on-site hydrogen generation stations for the purification of about 2000 kg of pipeline natural gas per day at 25°C, 5 psig pressure with a sulfur odorant concentration of about 30 ppm (Appendix A.1.), indicated optimum fiber characteristics with a 800 μm (O.D.), 400 μm (I.D.) (Appendix A.2.), and with a desired zeolite loading (w_{ads}) of 75 wt. % (dry fiber wt basis) (Appendix A.3.). Design calculations were conducted taking 30 ppm H_2S as the model odorant. The rationale behind this selection is described in detail in sections 3.1.4 and 4.8. The hypothetical

module dimensions were set with, 0.2 m diameter (d_t) with a length of around 1.2 m (L_t) with roughly 37,500 fibers (N_f) (Appendix A.2.).
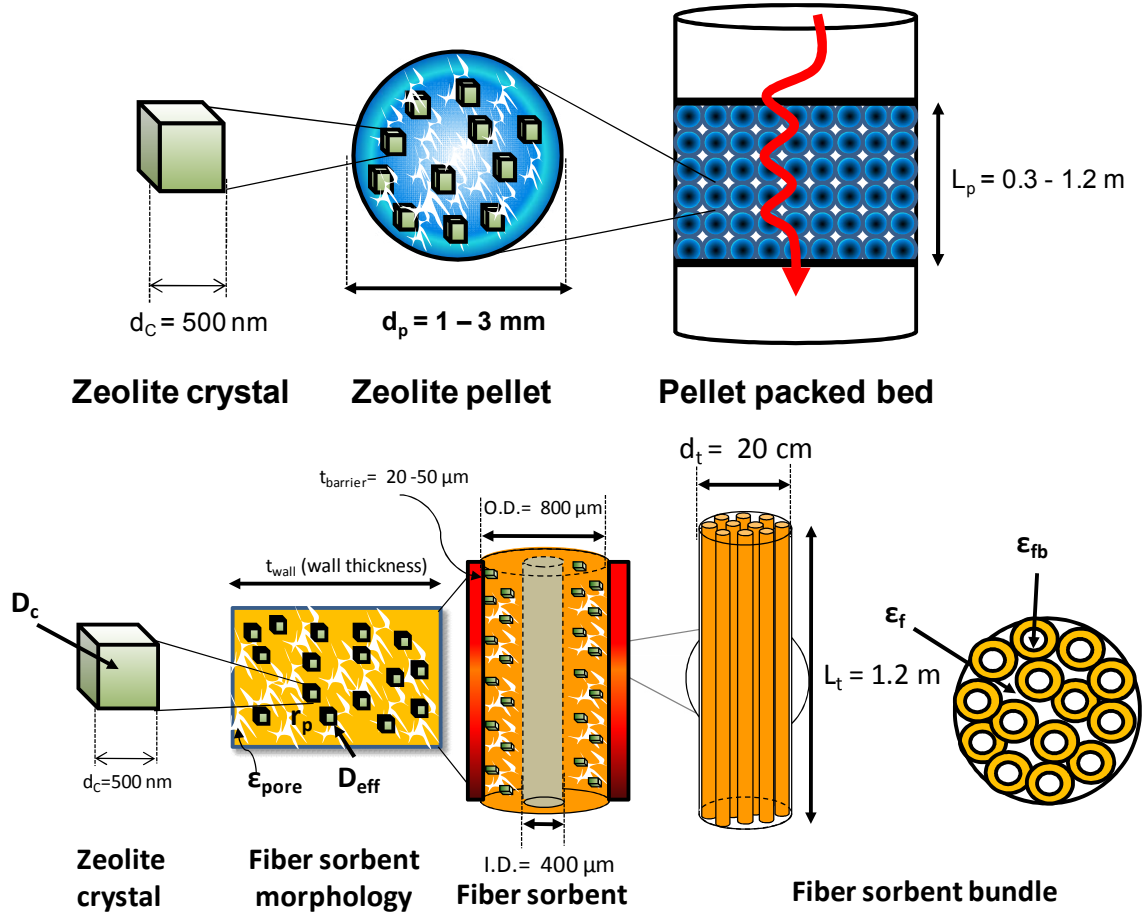
Figure 2.3: Various key dimensions and components of a (a) pellet packed bed and a (b) fiber sorbent module for on-site hydrogen generation.

Key differences in a conventional spherical pellet are compared with the proposed fiber sorbent design, indicated in Figure 2.3. Such pellets comprise small microporous zeolite crystals (d_c), formed into a macro porous pellet with the aid of a binder. Pellet diameters (d_p) ranging from 1–3 mm, with a bed depth (L_p) between 0.3–1.2 m are common in standard packed bed operations [7, 8].

2.3.1. Regeneration of the fiber sorbents

The macroscopic process of removing the adsorbate from the adsorbent pores is known as regeneration of the adsorbent bed and the detailed molecular scale process is called desorption. Economic factors dominate the consideration regarding the regeneration of an adsorbent bed.

Currently, the adsorbents used for sulfur odorant removal are disposed after one-cycle due to the high regeneration cost. Hence, regeneration of the fiber sorbents is crucial for the realization and commercialization of this technology. For the regeneration of fiber sorbents the following options can be considered:

1. Pressure swing adsorption (PSA)

2. Microwave heating

3. Electrical swing adsorption (ESA)

4. Temperature swing adsorption (TSA)

The following factors need to be considered in selecting the appropriate regeneration method:

- From equilibrium sorption experiments (section 4.5.) it was observed that even at 10 mm Hg (~ 0.01 atm) pressure, pure sulfur odorant (TBM) gave almost complete saturation for zeolite NaY. The pipeline natural gas feed stream had a pressure of ~5 psig (1.3 atm) (appendix A.1.).

$$Depressurization\ ratio = \frac{P_{inlet}}{P_{ads}} = \frac{1.3\ atm}{0.01\ atm} = 130 \tag{2.1}$$

From a very high depressurization ratio, it is clear that the PSA process will require significant vacuum during the depressurization step [9].

- Microwave heating requires introduction of large amount of energy and special designs to provide a uniform regeneration [10, 11].

- ESA concept has been successfully utilized for adsorbent monoliths [12], but in case of fiber sorbents lower conductivity of polymers and discontinuity between the zeolite crystals can lead to a very high electric resistance and breaking of the electric circuit.

- In pipeline natural gas, concentration of the sulfur odorants is roughly 30 – 60 ppm indicating the presence of a small amount of adsorbate gas and the applicability of the TSA process.

From the above discussion it follows that using less proven technologies likes ESA and microwave heating are not reliable in terms of scale-up. Also, the depressurization ratio is very high in case of PSA. Clearly, the TSA mode of regeneration is better suited for this application.

For small-scale operations (e.g. on-site hydrogen generation), either a heated purge [13] (Appendix A.8.2.) or a heated feed [14] gas can be effectively used; however, the use of steam and cold water as heat transfer fluids is preferable (Appendix A.8.1.). Steam is an inexpensive TSA regeneration medium easily available in industries as a utility. Also, steam provides higher heat compared to other purge gases due to high latent heat of condensation and high specific heat of water (C_p = 4186 J/kg.K) compared to a purge gas like Nitrogen (C_p = 1044 J/kg.K) [15, 16] (Appendix A.11.). Water can either be used to cool the fibers before the start of the next sorption cycle or to maintain isothermal operating conditions in the case of concentrated gas stream with high heat of sorption on zeolites. This is probably of less importance for the dilute sulfur streams

considered here, but could be very important if this approach is extended for the removal of higher concentrations of sulfur species (Appendix A.9.).

Unfortunately, the capacity of the hydrophilic zeolites drops considerably when in direct contact with water-vapor or steam [17]. Advantageously, an impermeable, thin polymer barrier layer can be created on the outside of the fiber sorbents to allow only thermal interactions with the regeneration media, thereby promoting consistent sorption capacity over repeated cycles. Such a barrier layer can also prevent the escape of natural gas through the porous core layer during the sorption step and can improve the desulfurized natural gas recovery.

In this research, it is planned to create the barrier layer by a one step dual-layer fiber spinning process with simultaneous co-extrusion of a barrier polymer 'sheath' spin dope along with the fiber sorbent 'core' spin dope. Alternatively, a barrier layer can be created on the single layer fiber sorbents by post-treating with the latex solution of the barrier polymer [18].

Also, high silica zeolites or metal ion-exchanged zeolites can be used as a replacement for hydrophilic zeolites. Some studies indicate that the decrease in sorption capacity of these zeolites is comparatively less when in contact with water vapor [19, 20].

2.4. Fiber sorbent transport properties

2.4.1. Permeation

Pure gas permeation tests can be used to determine and compare the flux through the core and the sheath layer in single and dual-layer fiber sorbents with different dope compositions and created under different spinning conditions. A high permeance (i.e. pressure normalized flux) through the core layer indicates high porosity and is desirable,

while in the case of dual-layer fibers; a low permeance is desired indicating the efficacy of the impermeable barrier layer.

Various probing gases such as nitrogen or oxygen can be used to check the permeance (indicating porosity) and selectivity (indicating defect free structure) of the fiber sorbents. Gases were used as the first step to test the barrier layer efficacy as opposed to water vapor due to operational simplicity. Also, water vapor ($\sigma \sim 2.8$ Å, $T_c = 647$ K) is highly permeable (small molecular diameter (σ)) and highly sorptive (proportional to critical temperature (T_c)), compared to gases like N_2 ($\sigma \sim 3.6$ Å, $T_c = 126$ K). Hence, a defective barrier sheath layer indicating Knudsen selectivity and high permeance for N_2 would surely be defective for a highly permeable water vapor.

Gas permeance is defined as the pressure normalized flux and is calculated as follows:

$$Permeance\ (\frac{P_i}{\ell}) = \frac{Flux\ (n_i)}{\Pr essure\ difference\ (\Delta p_i)} \tag{2.2}$$

Permeance values are reported in terms of gas permeation units (GPU) where

$$1\ \text{GPU} = 1 \times 10^{-6}\ \frac{\text{cm}^3 (STP)}{\text{cm}^2.s.\text{cm Hg}} \tag{2.3}$$

The ratio of pure component permeances is defined as the selectivity and represented as $\alpha_{i/j}$.

$$\alpha_{i/j} = \frac{(P/l)_i}{(P/l)_j} \tag{2.4}$$

2.4.2. Equilibrium adsorption: Adsorption isotherms

Adsorption involves the separation of components in a gas/liquid mixture by the selective transfer of one or more components (the adsorbates) to the adsorbent due to specific interactions between the adsorbate and the adsorbent. The nature of the bond

determines whether the interaction is classified as physical or chemical adsorption. Physical adsorption is due to relatively weak intermolecular (van der Waals) forces, while chemical adsorption involves formation of a strong chemical bond between the adsorbate and the adsorbent [21]. Physical adsorption can hence be reversed by the variation in the properties of the operation like temperature, pressure etc, to remove the adsorbate and hence regenerate the adsorbent.

The adsorption isotherm gives the equilibrium relationship between the concentration of the adsorbate in the fluid phase and its concentration in the adsorbent particles at a given temperature [8]. Experimental isotherms are useful to determine the sorption capacity of the fiber sorbents and its constituents (polymer and sorbent), to help select the most appropriate polymer (binder) and sorbent (filler) for the removal of sulfur impurities.

Glassy polymers typically indicate a dual mode mechanism with Langmuir type sorption in the non-equilibrium regions and Henry's law sorption in the equilibrium region [22], while zeolites mainly indicate adsorption by Langmuir type isotherm [23]. Fiber sorbents are thought to give a mixture of the Langmuir model and the dual mode model. However, due to the low sulfur partial pressure in the natural gas streams and high sulfur sorption capacity of the zeolites, the sorption in the fiber sorbents is dominated by the zeolites.

2.4.2.1. Zeolite adsorption - Langmuir model

The sorption of gases on weakly adsorbed surfaces (e.g. zeolites) is typically represented by the Langmuir model. This model, originally developed for adsorption of gases onto solids, is based on the assumptions that the adsorption energy is constant and

independent of surface coverage; that adsorption occurs on localized sites with no interaction between adsorbate molecules, and that the maximum adsorption occurs when the surface is covered by a monolayer of adsorbate [24]. Since the numbers of sorption sites in the zeolite are limited, the sorption in these sites becomes saturated at high pressures. Mathematically the Langmuir model is expressed by the equation:

$$C_z = \frac{C_{HZ}'b_z p}{(1+b_z p)}$$

(2.5)

Where, C_z(cc(STP)/cc zeolite), is the concentration of the adsorbate in the zeolite, b_z (cm Hg)$^{-1}$ is the Langmuir affinity constant for the zeolite, C_H'(cc(STP)/cc zeolite) is the Langmuir capacity constant, and p (cm Hg) is the partial pressure of the adsorbate exposed to the zeolite.

2.4.2.2. Polymer sorption - dual mode model

The simplest physical description of glassy polymers uses a so-called 'dual mode model' that attributes the non-equilibrium aspect to frozen in 'holes' or packets of un-relaxed free volume distributed in a densified regular matrix or the 'dissolved mode' [25]. Sorption in the non-equilibrium holes follows a Langmuir type mechanism while the rest of the polymer matrix can be described by Henry's law uptake. Mathematically the dual mode sorption model is expressed as [26].

$$C = C_D + C_H$$

(2.6)

$$C = k_D \cdot p + \frac{C_H' bp}{(1+bp)}$$

(2.7)

Where, C (cc(STP)/cc polymer), is the concentration of the adsorbate in the polymer k_D (cc(STP)/(cc polymer·cm Hg)) is the Henry's law constant, C_H'(cc(STP)/cc

polymer) is the saturation capacity of the holes, b (cm Hg)$^{-1}$ is the Langmuir affinity constant, and p (cm Hg) is the partial pressure of the adsorbate exposed to the polymer.

2.4.3. Concentration patterns in fixed beds and breakthrough curves

In a typical industrial-scale adsorption process, the adsorbent particles are formed into pellets with a binder material and placed in a fixed bed, and then a contaminated feed stream is passed through it. Initially, all the adsorbate molecules transfer to the adsorbents and get sorbed, with the exiting stream free of any contaminants. As the adsorption step progresses, the inlet of the bed becomes saturated with the adsorbate, and the mass transfer zone (MTZ) moves towards the bed exit as shown in Figure 2.4. The MTZ is responsible for the mass transfer of the molecules from the feed to adsorbent and can be used to study the influence of the flow pattern. Eventually, a breakthrough point (t_b) is reached where the mass transfer zone exits the bed and the contaminant concentration in the effluent stream increases and gradually becomes equal to the inlet feed concentration (C_o) at time t_f. Appendix A.7. describes the calculation of the breakthrough time (t_b) in a fiber sorbent module used in an on-site hydrogen generation station.

The rate of increase in C/C_o is determined by the sorption kinetics and depends on the adsorbate-adsorbent interaction. Favorable kinetics indicates a sharp breakthrough curve, with a short mass transfer zone (Figure 2.4). However, for poor mass transfer kinetics, a short breakthrough time is observed with a long mass transfer zone length. In an ideal case of no mass transfer resistance and no axial dispersion, the breakthrough curve would be a vertical line from 0 to 1.0 when the entire solid is saturated [8].

Apart from the kinetics of sorption, parameters such as adsorbate concentration in the feed, adsorbent pore accessibility, temperature, pressure during the run along with the properties of the adsorbate and the adsorbent influence the rate of adsorption.
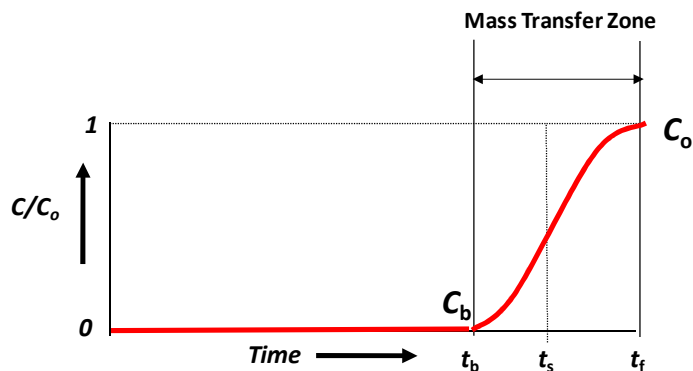
Figure 2.4: Schematic representation of a breakthrough curve and an adsorption profile in a packed bed or a fiber sorbent module.

2.4.3.1. Breakthrough capacity

Initially for the flow testing of the fiber sorbent modules, 30 ppm tertiary butyl mercaptan (TBM)/N_2 was selected as the model odorant stream. However, due to long breakthrough times (~1-3 days), requiring continuous monitoring due to safety reasons and excessive use of bottled gas; 30 ppm H_2S/N_2 gas mixture was then selected as the model odorant for the ease of operation and safety. (Refer sections 3.1.4. and 4.8. for details).

Breakthrough curves are plotted as the ratio of outlet to inlet H_2S concentration as a function of time (Figure 2.4). The breakthrough or dynamic capacity was calculated based on the time taken (t_b) for the outlet H_2S concentration to reach 1 ppm. From an industrial operation viewpoint the inlet gas stream needs to be switched to a fresh bed once breakthrough is reached as the downstream metal catalysts used in fuel processing are irreversibly poisoned by sulfur compounds above a concentration of 1 ppm [20].

33

$$\text{Breakthrough capacity} \ (C_{break}) = \frac{M_{sulfur}.Q_v.p_{bed}.C_o}{10^6.R.T_{bed}}.t_b \tag{2.8}$$

Where, C_{break} is the breakthrough capacity in mg sulfur/g sorbent or fiber, R is the universal gas constant (0.0821 L.atm/mol.K), t_b is the breakthrough time (min), Q_v is the feed flow rate in L/min, M_{sulfur} is the molecular weight of the sulfur species (g/mole), p_{bed} is the pressure of the adsorbent bed, C_o is the sulfur concentration in the feed (ppm), T_{bed} is the temperature of the bed.

2.4.3.2. Saturation capacity

Saturation or equilibrium capacity is defined as the amount of adsorbate, adsorbed by the adsorbent in equilibrium with the feed concentration. Ideally, a higher value of equilibrium capacity is advantageous, resulting in higher contaminant removal. It can be found by numerically calculating the amount of adsorbate, adsorbed till the time taken (t_f) for the outlet sulfur concentration to become equal to the inlet concentration.

$$\textit{Saturation capacity} \ (C_{sat}) = \frac{M_{sulfur}.Q_v.p_{bed}.C_o}{10^6.R.T_{bed}} \int_o^{t_f}(1-\frac{C}{C_o}) \ dt \tag{2.9}$$

2.4.3.3. Length of unused bed

The length of unused bed (LUB) is an important parameter that can be used for scale-up of fiber beds as it depends on the adsorbate-adsorbent combination, the temperature and the fluid velocity and is independent of the column length [8]. The ratio LUB/L_f can give the fraction of un-utilized bed in different modules. A low ratio is desired indicating that the bed has been utilized appropriately. LUB is defines as follows:

$$LUB = (1-\frac{t_b}{t_{0.5}})L_f \tag{2.10}$$

Where, t_b is the breakthrough time (min), $t_{0.5}$ is the time when the ratio of the sulfur outlet concentration to the inlet concentration reaches 0.5, L_f is the overall length of the fiber available for sorption.

2.4.4. Diffusion

In fiber sorbent operation, during the sorption step, a rapid diffusion of gases to reach the zeolite crystals dispersed in the core layer is desired. In the regeneration step, however, a slow gas or water vapor diffusion rate is desired through the barrier polymer, to prevent direct contact between the regeneration media and the core layer. It is thus essential to understand the diffusion through the components of the fiber sorbents (polymers, zeolites and the void/porous space) [27].
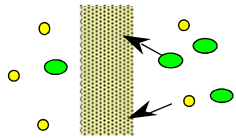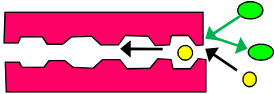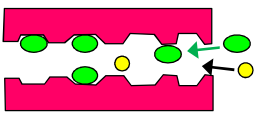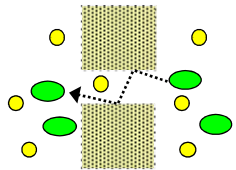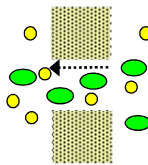
Schematic representation	Separation mechanism	Pore size (nm)	Typical gas diffusion coefficients (cm²/s)
	Polymer (solution-diffusion)	N/A	10^{-6}-10^{-14}
	Small-pore zeolite (Molecular sieving)	$< 10^0$	10^{-6}-10^{-10}
	Large-pore zeolite (Selective adsorption / surface diffusion)	10^1-10^0	$10^{-6} - 10^{-8}$
	Voids (Knudsen diffusion)	$10^2 - 10^0$	10^{-1}-10^{-3}
	Voids (Viscous flow)	$> 10^2$	10^1-10^{-1}

Figure 2.5: Various components of a fiber sorbent and their separation mechanism for a gas mixture. Modified from [28].

2.4.4.1. Diffusion through polymers

The rate of diffusion of gas molecules through a dense polymer depends on the free volume of the polymer and the length and frequency of the random jumps initiated by the thermal fluctuations of the polymeric chains.

A jump is initiated when an opening is created next to the gas molecule. The molecule jumps into this new opening and the hole left behind by this molecule is closed, thereby trapping the gas molecule into a new position. The mechanism is referred to as "solution-diffusion" (Figure 2.5).

Typically, glassy polymers, due to their rigid back bone structures, have lower amplitude thermal fluctuations and hence lower diffusivity or diffusion coefficients compared to the more flexible rubbery polymers.

2.4.4.2. Diffusion through zeolites

Zeolites are ultra-microporous materials consisting of large cavities interconnected by narrow channels through which the gas molecules diffuse and adsorb into the large cavities.

Zeolites are used as molecular sieves where they separate a gas pair(s) based on the shape and size of the molecules relative to the shape and size of the interconnected channels. The smaller molecules can easily diffuse through the zeolite channel, while the larger molecules are either rejected or have to orient in a particular direction to traverse through the channel (Figure 2.5) thereby lowering their diffusivity and leading to separation of the gas pair(s).

In case of zeolites with larger cavities and having specific interaction or affinity towards certain adsorbates with higher condensability, the transport is dominated by surface diffusion [29].

Sulfur odorants of various molecular sizes (σ) and condensability (proportional to critical temperature (T_c)) are added to pipeline natural gas. Small gaseous sulfur molecules from H_2S (σ~3.6 Å, T_c = 373 K) to large organic sulfur species like tertiary-butyl mercaptan (TBM) (σ~ 6 Å, T_c = 554 K) are typically added and are highly condensable compared to methane (σ~3.8 Å, T_c = 191 K), which is the major component of natural gas (> 95%).

Hence, in the case of fiber sorbents to remove highly condensable and differing diameter molecules, it is desired to select a zeolite where the separation is due to the specific interaction with the zeolite (Figure 2.5). For large cavity zeolites the diffusion coefficients are often of the order of 10^{-6} to 10^{-8} cm^2/s at ambient temperatures.

2.4.4.3. Diffusion through the voids

Viscous flow is observed in large pores typically (>100 nm), if there is a difference in total pressure across the fiber or particle. The viscous flow provides no separation capability, with the equivalent diffusion coefficients being very high ($\sim$0.1-10 cm^2/s). This effect is negligible in fiber sorbents or packed bed since the pressure drop over an individual fiber or particle is very small [30].

The diffusion through the voids or pores in the fiber sorbent morphology occurs via bulk or Knudsen diffusion depending on the size of the pores and pressure (Figure 2.5). Molecular or bulk diffusion occurs when the pore size of the fiber sorbent is large compared to the mean free path of the gas molecules [31].

Molecular transport through the pores/voids which are equivalent or smaller in comparison to the mean free path of the gas takes place via Knudsen flow ($\sim10^{-1} - 10^{-3}$ cm^2/s). In this flow regime, the separation efficiency for a gas mixture is determined by the square root of the molecular weight ratio of the gases and provides very little or no separation selectivity.

As noted in appendix A.5.1., the advantages of fiber sorbents can be realized when they have porous walls comprising a polymer matrix containing dispersed zeolite particles and an interconnected pore network where the diffusion coefficient is

approximately equal to the effective diffusivity (molecular + Knudsen diffusion) through the pores.

2.5. Single and dual-layer hollow fiber sorbent spinning

Fiber sorbents were made by modifying the dry jet-wet quench solution spinning technique [32]. Figure 2.6 shows a schematic representation of the fiber spinning apparatus and a triple orifice spinneret. Table 2.2 summarizes the various spinning parameters. Zeolite suspended polymer solution or 'core dope' is fed to the middle compartment of the spinneret. Simultaneously, a mixture of solvent and non-solvent, referred to as the 'bore fluid' (or internal coagulant), is fed into the inner-most compartment of the spinneret. When dual-layer fibers are to be spun, the 'sheath dope' is fed to the outermost compartment of the spinneret.

The extruded fiber is then drawn through the air-gap and into the water quench bath (external coagulant) where it phase separates. The fiber then passes under a Teflon$^{\circledR}$ guide and is collected onto a rotating take-up drum partially submerged in a water-reservoir and continuously replenished with fresh water.
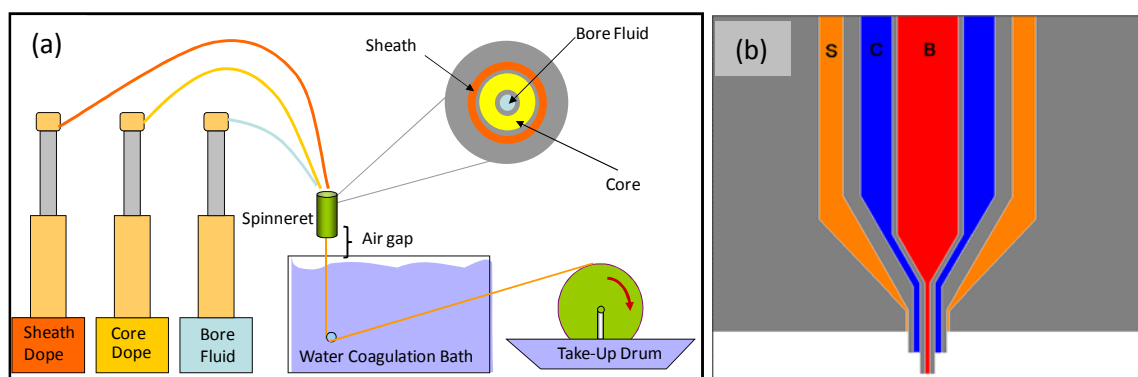
Figure 2.6 (left to right): Schematic diagram of (a) fiber spinning apparatus and (b) triple orifice spinneret (S: Sheath channel (O.D. – 0.195 cm), C: Core channel (O.D. – 0.174 cm), B: Bore channel (O.D. - 0.067 cm)).

Table 2.2: Key parameters affecting fiber-sorbent spinning process

Dope composition	Air gap height	Quench bath temperature
Bore fluid composition	Take-up rate	Quench bath composition
Extrusion rates	Operating temperature	Humidity

Various parameters can be tuned in the spinning process. Extrusion rate, speed of take-up and the size of the annular die determine the diameter of hollow fiber. The air-gap distance helps in the skin layer formation and also contributes to the better interpenetration of the core and sheath layer polymer solutions due to longer mass exchange time. Typically, water is used as an environmentally friendly and easily available quench bath medium. Spinning temperatures (quench bath and spinneret) are also key parameters that can lead to a delamination free fiber structure and improved porosity. These process parameters along with the dope and bore fluid compositions can be changed to obtain a successful hollow fiber sorbent morphology. The effect of each parameter on single and dual-layer fiber spinning are described in greater detail in chapter 4 and 5.

Figure 2.7 shows a qualitative ternary diagram of a polymer, solvent and non-solvent system with qualitative composition paths followed during the skin-layer and the substructure formation. Uniform (one-phase) core and sheath dope compositions are typically chosen close to the binodal curve to facilitate faster phase separation of the nascent fiber using the cloud point technique [33].
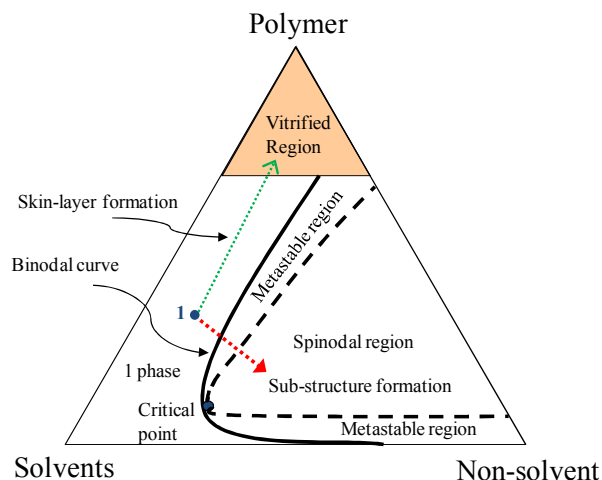
Figure 2.7: Ternary phase diagram of a polymer/solvent/non-solvent system [34].

The binodal curve separates the one and two phase regions. When the one-phase dope is extruded through an adjustable air-gap, volatile solvents and non-solvents evaporate from the fiber driving it closer to the vitrified region as shown in Figure 2.7. Due to the high polymer concentration in the vitrified region, a dense skin layer is formed on the surface of a membrane or a fiber-sorbent. In the case of single-layer fiber sorbent spinning, the skin layer is undesired as this leads to lower porosity in the core layer, while in case of a dual-layer fiber sorbent spinning it is desired that the barrier sheath layer has a thick and dense skin layer.

When the fiber enters the quench bath, the non-solvent from the bath enters the nascent fiber and brings the composition into the two-phase region (Figure 2.7). In the two-phase region, the phase separation of a polymer solution occurs via the 'nucleation and growth' mechanism and/or the 'spinodal decomposition' mechanism [34]. The 'nucleation and growth' mechanism gives either polymer-rich phase dispersed in a

polymer lean matrix or vice versa, while the 'spinodal decomposition' mechanism gives an interpenetrating network of polymer rich and polymer lean phases [34].

2.6. Selection of fiber sorbent module geometry and flow configuration

The key advantage to using hollow fiber sorbents is the high surface area to volume ratio provided by a hollow cylindrical structure, and the ability to pass two fluids simultaneously. This advantage will be negated if mass transfer coefficients are lower than a pellet packed beds [35].

Once the fibers are spun and solvent exchanged, they must be mounted and potted into a module to perform the sorption and regeneration cycles. The fibers must be sealed in a manner to allow high pressure gas / liquid to be applied to the fibers, with minimum possible bypass [36].

Figure 2.8 represents the various flow geometries and module construction designs considered for the fiber sorbent TSA application. Figure 2.8 (a) represents a module with a shell-and-tube module geometry. The flow in these modules is in parallel directions with either co or counter-current flow of steam or natural gas possible. Figure 2.8 (b) and (c) module designs allow a cross flow configuration. The fibers can be arranged in a cylindrical (Figure 2.8 (b)) or rectangular (Figure 2.8 (c)) channel. A detailed optimization of flow geometries is beyond the scope of this work; however, an appropriate geometry must be selected that provides an ease of construction and low bypass with reliability for scale-up.

The flow distribution depends on the inlet manifold type (cylindrical, conical, rectangular), manifold height, tube length (L_M), fiber diameter (O.D./I.D.), shell diameter (d_t), fiber packing density (φ_M) and the Reynolds number (Re) [37]. Channeling or

bypassing of the gas through the fibers due to inefficient packing or flow conditions can lead to instantaneous or premature breakthrough [38].
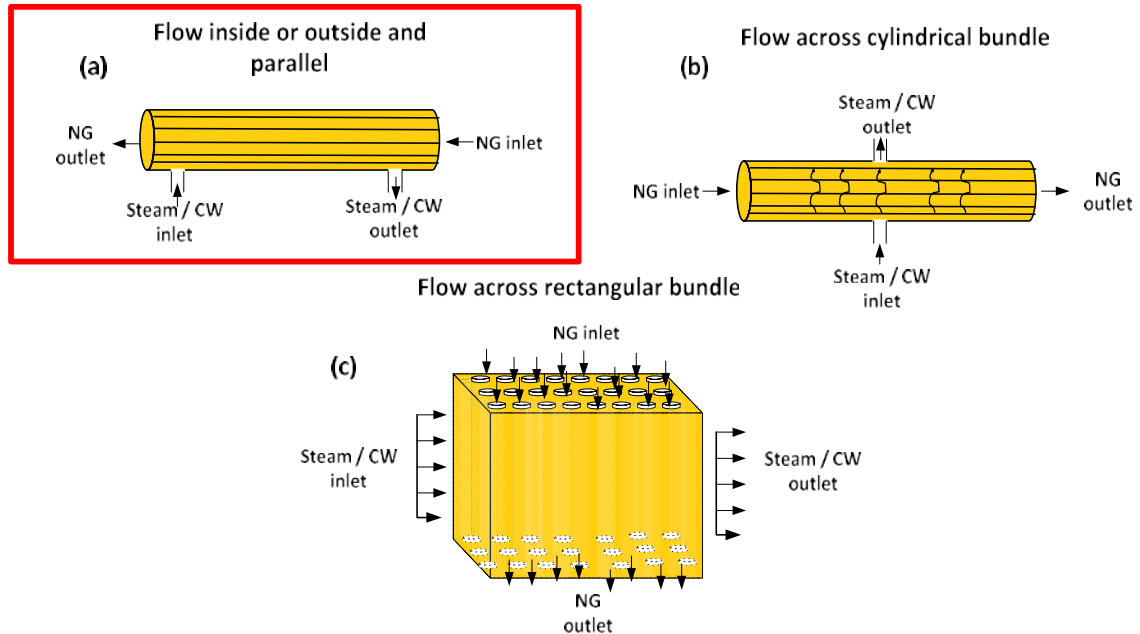
Figure 2.8: Various possible flow geometries and flow conditions in fiber sorbent modules. Adapted from [35].

Mass transfer coefficient in a bore side feed is lower than a shell side feed, due to a lower Reynolds number due to a smaller contact diameter. Also, the pressure drop in a bore side feed is higher than in a shell side feed, due to a smaller flow diameter. However, bore side mass transfer coefficients can be predicted with reasonable accuracy and it provides an advantage of lower bypass and channeling (compared to a shell side feed), which is crucial for the effective operation of this technology [39].

Parallel flow modules are preferred when the bore side mass transfer resistance is controlling, while a cross flow design is preferred when the shell side mass transfer resistance is significant. Flow normal, rather than parallel to the fibers leads to higher

mass transfer coefficients, however; it causes loss of efficiency or capacity due to channeling [40].

Shell and tube geometry offers ease of construction at the lab scale with large number of modules economically manufactured with consistent dimensions without frequent fiber breaks [35].

Baffles can be added to the modules to overcome the shortcomings such as shell side bypassing [40]. However, baffled contractors are tedious to construct at a lab-scale and are not the focus of this proof-of-concept work [41].

Based on the above considerations, a bore side feed of natural gas with a shell side feed of steam / cooling water in a shell and tube geometry was chosen as the starting point.

2.7. REFERENCES

1. Wallace, D.W., C. Staudt-Bickel, and W.J. Koros, *Efficient development of effective hollow fiber membranes for gas separations from novel polymers.* Journal of Membrane Science, 2006. 278(1-2): p. 92-104.

2. Robeson, L.M., *Correlation of Separation Factor Versus Permeability for Polymeric Membranes.* Journal of Membrane Science, 1991. 62(2): p. 165-185.

3. Moore, T.T. and W.J. Koros, *Non-ideal effects in organic-inorganic materials for gas separation membranes.* Journal of Molecular Structure, 2005. 739(1-3): p. 87-98.

4. Gilleskie, G.L., J.L. Parker, and E.L. Cussler, *Gas Separations in Hollow-Fiber Adsorbers.* AIChE Journal, 1995. 41(6): p. 1413-1425.

5. McKelvey, S.A., D.T. Clausi, and W.J. Koros, *A guide to establishing hollow fiber macroscopic properties for membrane applications.* Journal of Membrane Science, 1997. 124(2): p. 223-232.

6. Gabelman, A. and S.T. Hwang, *Hollow fiber membrane contactors.* Journal of Membrane Science, 1999. 159(1-2): p. 61-106.

7. Feng, X.S., et al., *Hollow-fiber-based adsorbers for gas separation by pressure-swing adsorption.* AIChE Journal, 1998. 44(7): p. 1555-1562.

8. McCabe, W.L., J.C. Smith, and P. Harriott, *Unit operations of chemical engineering.* 6th ed. 2001, Boston: McGraw Hill.

9. Yang, R., *Gas separation by adsorption processes.* 1997, London: Imperial college pres.

10. Mezey, E.J., Dinovo, S.T., *Adsorbent regeneration and gas separation utilizing microwave heating,US Patent 4322394.* 1980.

11. K. Sundmacher, A.K., A. Seidel-Morgenstern, *Integrated Chemical Processes: Synthesis, Operation, Analysis, and Control.* 2006: Wiley-VCH.

12. R. Judkins, T.B. *CO2 Removal From Gas Streams Using a Carbon Fiber Composite Molecular Sieve.* http://www.netl.doe.gov/publications/proceedings/01/carbon_seq/3b1.pdf. Date accessed, October 8th, 2010.

13. J. Merel, M.C., F. Meunier, *Carbon dioxide capture by indirect thermal swing adsorption using 13X zeolite.* Environmental Progress, 2006. 25(4): p. 327-333.

14. M. Clausse, J.B., F. Meunier, *Role of presence of CO2 in the feed of an indirect heating TSA process for VOC removal.* Adsorption, 2003. 9: p. 77-85.

15. Schork, J.M. and J.R. Fair, *Steaming of Activated Carbon Beds.* Industrial & Engineering chemistry research, 1988. 27(8): p. 1545-1547.

16. Schweiger, T.A.J. and M.D. Levan, *Steam Regeneration of Solvent Adsorbers.* Industrial & Engineering chemistry research, 1993. 32(10): p. 2418-2429.

17. Bonjour, J., M. Clausse, and F. Meunier, *A TSA process with indirect heating and cooling: parametric analysis and scaling-up to practical sizes.* Chemical Engineering and Processing, 2005. 44(9): p. 969-977.

18. Ekiner, O.M., Kulkarni, S. S., *Process for making hollow fiber mixed matrix membranes,U.S. Patent 6,663,805B1.* 16 December, 2003.

19. Shimizu, K., et al., *Mechanistic study on adsorptive removal of tert-butanethiol on Ag-Y zeolite under ambient conditions.* Journal of physical chemistry B, 2006. 110(45): p. 22570-22576.

20. Crespo, D., et al., *Superior sorbent for natural gas desulfurization.* Industrial & Engineering chemistry research, 2008. 47(4): p. 1238-1244.

21. Yang, R.T., *Gas separation by adsorption processes*. 1987, Boston: Butterworths.

22. Koros, W.J., A.H. Chan, and D.R. Paul, *Sorption and Transport of Various Gases in Polycarbonate.* Journal of Membrane Science, 1977. 2(2): p. 165-190.

23. Langmuir, I., *The adsorption of gases on plane surfaces of glass, mica and platinum.* Journal of the American Chemical Society, 1918. 40(9): p. 1361-1403.

24. Langmuir, I., *A theory of adsorption.* Physical Review, 1915. 6(1): p. 79-80.

25. Stern, S.A., ed. *Gas diffusion in rubbery and glassy polymers,.* Barrier Polymers and Structures, ed. W.J. Koros. 1990, American Chemical Society: Washington DC.

26. Koros, W.J., A.H. Chan, and D.R. Paul, *Sorption and transport of various gases in polycarbonate.* Journal of Membrane Science, 1977. 2(2): p. 165-90.

27. Kiyono, R., et al., *Mixed matrix microporous hollow fibers with ion-exchange functionality.* Journal of Membrane Science, 2004. 231(1-2): p. 109-115.

28. Husain, S., *Mixed matrix dual layer hollow fiber membranes for natural gas separation*. 2006, Georgia Institute of Technology: Atlanta, Ga.

29. Rao, M.B. and S. Sircar, *Nanoporous Carbon Membranes for Separation of Gas-Mixtures by Selective Surface Flow.* Journal of Membrane Science, 1993. 85(3): p. 253-264.

30. Ruthven, D.M., *Principles of adsorption and adsorption processes*. Wiley-Interscience publication. 1984, New York ; Chichester: Wiley. xxiv, 433 p.

31. A. L. Hines, R.N.Maddox, *Mass transfer fundamentals and applications* 1st ed. 1985, Upper Saddle river , NJ: Prentice hall PTR.

32. Pesek, S.C. and W.J. Koros, *Aqueous Quenched Asymmetric Polysulfone Hollow Fibers Prepared by Dry Wet Phase-Separation.* Journal of Membrane Science, 1994. 88(1): p. 1-19.

33. Kosuri, M.R. and W.J. Koros, *Defect-free asymmetric hollow fiber membranes from Torlon (R), a polyamide-imide polymer, for high-pressure CO2 separations.* Journal of Membrane Science, 2008. 320(1-2): p. 65-72.

34. Koros, W.J. and G.K. Fleming, *Membrane-Based Gas Separation.* Journal of Membrane Science, 1993. 83(1): p. 1-80.

35. S.Wickramasinghe, M.S., E. Cussler, *Mass transfer in various hollow fiber geometrics.* Journal of membrane science, 1992. 69: p. 235-250.

36. Park, J.K. and H.N. Chang, *Flow Distribution in the Fiber Lumen Side of a Hollow-Fiber Module.* Aiche Journal, 1986. 32(12): p. 1937-1947.

37. J.Park, H.C., *Flow distribution in the fiber lumen side of a hollow-fiber module.* AIChE Journal, 1985. 32(12): p. 1937-1947.

38. Yang, M.C. and E.L. Cussler, *Designing Hollow-Fiber Contactors.* AIChE Journal, 1986. 32(11): p. 1910-1916.

39. A. Gabelman, S.H., *Hollow- Fiber membrane contactors.* Journal of Membrane Sciences, 1999. 159: p. 61-106.

40. Wang, K.L. and E.L. Cussler, *Baffled Membrane Modules Made with Hollow-Fiber Fabric.* Journal of Membrane Science, 1993. 85(3): p. 265-278.

41. Seibert, A.F. and J.R. Fair, *Scale-up of hollow fiber extractors.* Separation Science and Technology, 1997. 32(1-4): p. 573-583.

CHAPTER 3

MATERIALS AND EXPERIMENTAL METHODS

3.1. Materials

For the creation of fiber sorbents it is important to select appropriate polymers as a 'binder' and 'barrier' material. Also, it is important to identify a zeolite 'sorbent' with high sorption capacity and ease of regeneration for the target separation gases. Different materials were screened to select a good candidate for this proof-of-principal work.

3.1.1. 'Binder' polymer

The material for polymer 'binder' needs to be commercially available at a low cost to realize scale-up of operations. The polymer should have the ability to withstand mechanical wear and tear during continuous cyclic operations while having a desired interface with the zeolite sorbent.

Cellulose acetate (CA) (M_n ~50,000, Sigma-Aldrich, Milwaukee, WI), a glassy polymer with high glass transition temperature (T_g) of ~ 180-210°C was selected as one of the polymers of choice because it is relatively inexpensive, well studied in membrane literature and its properties can be tailored easily by the degree of acetylation and molecular weight.

Polyester urethane (Estane®, grade 58226, Lubrizol, Cleveland, OH), a rubbery polymer with good tensile, chemical resistance properties and a T_g of ~ -25°C was also investigated. Polymers were dried at 110°C for 12 hrs under vacuum before use in spinning dope formulations.

3.1.2. 'Barrier' polymer

Formation of an impermeable outer layer is crucial for the effective regeneration of the fiber sorbents. As described in chapter 2, the barrier layer can either be created by a one step dual-layer fiber spinning process with simultaneous co-extrusion of a barrier 'sheath' and a porous 'core' dope or by post-treating single-layer fiber sorbents with a latex solution to create the barrier sheath.

Relevant properties of different potential barrier layer polymers are summarized in Table 3.1 and compared with the core layer polymers (cellulose acetate and polyester urethane) for reference.

The sheath polymer should be available in powder/resin form soluble in common organic solvents to create a spin dope in case of dual-layer spinning or in latex form in case of post-treatment. A lower glass transition temperature (T_g) could be helpful in annealing or heat treatment of the sheath layer (discussed in section 6.2.). Its maximum working temperature (degradation or melting temperature) should be above the temperature of the regeneration media (>110°C). The barrier layer should also be robust in the presence of continuous thermal cycles, while providing the lowest possible permeability to gases and water vapor.

Polyethylene terephthalate (PET) in spite of having good thermal and barrier properties (Table 3.1) is not soluble in most organic solvents [1] and hence spin dopes could not be made. Polyimides though thermally stable and soluble in common organic solvents, have a high gas and water vapor transmission rate. Neoprene™ had a low melting temperature (Table 3.1) and hence was not shortlisted.

Table 3.1: Comparison of various barrier polymers. Properties of cellulose acetate (CA) and Polyester urethane (Estane®) are provided.

Polymer	Glass transition temperature T_g (°C)	Maximum working temperature (°C)	O_2 Permeability[1] (Barrer[2])	Water vapor transmission rate[3] (WVTR)(Barrer)	Solubility parameter δ (MPa[0.5]) [2]
Polyethylene terephthalate (PET)	67-125 [3]	250-265 [3]	0.017 [3]	207 [3]	22.1
Poly(vinylidene chloride-methyl acrylate) copolymer (IXAN™)	7-18 [4]	150-160 [4]	0.005-0.010 [4, 5]	2-6 [3, 6]	24.9
Polyamide-imide (Torlon®)	275 [7]	400-500 [7]	0.12 [8]	N/A	N/A
Polyacrylonitrile (PAN)	85-95 [3]	250-320 [3]	0.0002 [3]	306 [3]	27.4
Poly(chloroprene) (Neoprene™)	(-45) - (-50) [3]	55-78 [3]	3.9 [3]	908 [3]	18.5
Cellulose acetate (CA)	180-210 [9]	230-290 [9]	0.68-1.22 [9]	5492-7315 [3]	25.1
Polyester urethane (Estane®)	(-13) [10]	140	50 [11]	275-1000 [11]	20.5

---

[1] The reported O_2 permeability are at 25 °C

[2] $1 \text{ Barrer} = 1 \times 10^{-10} \dfrac{\text{cm}^3(STP).\text{cm}}{\text{cm}^2.\text{s.cm Hg}}$

[3] The reported water vapor transmission rate (WVTR) are at 25 °C

Polyvinylidene chloride (PVDC) and polyacrylonitrile (PAN) satisfied the desired criteria (Table 3.1) and were selected for further studies. PVDC (IXAN® PNE-288, VDC/MA copolymer, $M_n \sim 40,600$, PDI = 2.6, Solvay Advanced Polymers, Alpharetta, GA) and polyacrylonitrile (PAN) ($M_n \sim 147,000$, Sigma-Aldrich, Milwaukee, WI) were purchased in solvent soluble powder form.

Polyvinylidene chloride (PVDC) (dispersion grade Diofan® XB-204, Solvay Advanced Polymers, Alpharetta, GA) was used to post treat single and dual-layer fiber sorbents. Diofan® is an anionic aqueous dispersion of PVDC particles in water with a solid content ranging from 45 to 60 wt. % (Table 3.2).

Table 3.2: The key properties of PVDC dispersion (Diofan® XB-204) [6].

Properties	Unit	Value
Aqueous dispersion , solid content	gm / kg	550
Acidic medium	pH	3-5
Emulsion	Type	Anionic
Density at 20 °C	Kg / m^3	1250
Viscosity at 23°C, shear gradient 250 s^{-1}	mPa.s	19
Minimum film forming temperature	°C	5
Particle diameter (average)	μm	0.14
Surface tension	mN/m	33

3.1.3. Zeolite 'sorbent'

Ideally, zeolite for the creation of fiber sorbents should also be commercially available in small, uniform crystal size and with a high sorption capacity for the sulfur odorants. High sorption capacities for various sulfur odorants (especially, TBM and H_2S) with zeolite NaY have been reported [12, 13]. Zeolite NaY, a hydrophilic sieve (CBV-100, Si/Al = 2.6, average crystal size ~ 500 nm, Zeolyst, Valley Forge, PA) satisfied this criteria and was selected as a proof-of-concept adsorbent.

Zeolite Y is a faujasite type zeolite with 7.4Å diameter pores and a three-dimensional pore structure [14]. The basic structural units for Y zeolites are the sodalite cages, which are arranged so as to form supercages that are large enough to accommodate spheres with up to 1.2 nm in diameter [15]. Zeolites were dried at 200°C, under vacuum for 24 h to remove sorbed water vapor and possible organic impurities from synthesis.
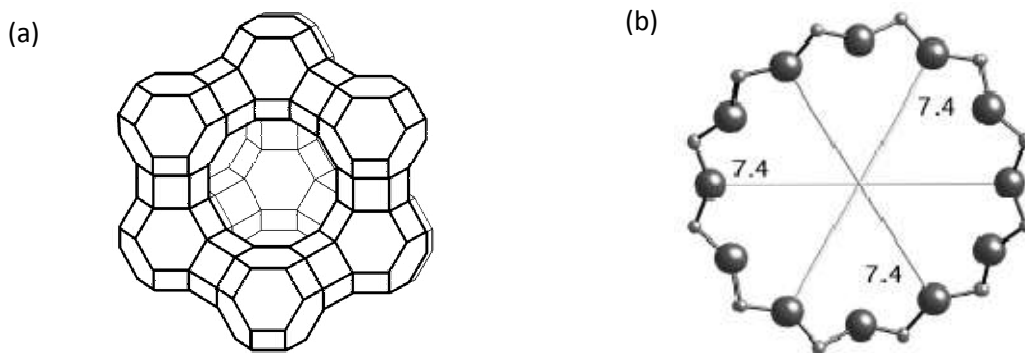
Figure 3.1: (left to right) (a) Framework structure of zeolite Y (b) 12-ring pore window with a 7.4 Å size [16].

3.1.4. Chemicals and gases

N-Methyl-2-Pyrrolidone (NMP) was selected as the spinning solvent due to its strong solvent power, low volatility and good water miscibility. THF was also added in the sheath dope as a high volatility solvent, to facilitate skin layer formation in the sheath layer. Ethanol was also added in the sheath layer as a non-solvent during dope formulation. Methanol and hexane were used for solvent exchange or dehydration of the synthesized fiber sorbents. All liquid chemicals were reagent grade with 99% purity and purchased from Sigma-Aldrich (Milwaukee, WI). De-ionized (DI) water (18 MΩ, Model: D4521, Barnstead International, Dubuque, IA) was added as a non-solvent in the fiber sorbent dope. Lithium nitrate (LiNO$_3$) and polyvinyl pyrrolidone (PVP) ((M$_n$ ~55,000) and (M$_n$ ~1.3 million), Sigma-Aldrich, Milwaukee, WI) was considered as a pore former to the fiber sorbent dope [17, 18]. PVP was dried at 80°C for 12-24 h under vacuum to remove sorbed water vapor.

Tertiary butyl mercaptan (TBM) (99% purity, Sigma-Aldrich, Milwaukee, WI), one of the most common odorants added to pipeline natural gas was selected as the model odorant for characterizing fiber sorbents under equilibrium conditions [12, 13, 19].

Initially for the flow testing of the fiber sorbent modules, 30 ppm TBM/N$_2$ was selected as the model odorant stream. However, during the breakthrough time studies it was found that due to greater condensability (refer section 4.8.) of TBM and hence higher breakthrough capacity (1.8 mmole TBM/g NaY), it took roughly 1-3 days to obtain a breakthrough curve (described in detail in section 4.8.).

Since these experiments were inconveniently long requiring continuous monitoring due to safety reasons and excessive use of bottled gas, for the ease of

operation and safety, 30 ppm *H₂S/N₂ gas mixture was then selected as the model odorant*

for the preliminary flow testing experiments. H$_2$S was found to give lower sorption

capacity, due to lower condensability (refer section 2.4.4.2.) and a breakthrough capacity

of 0.03 mmole H$_2$S/g NaY (section 4.9.). Also in fuel cell applications, the poisoning of

catalyst or voltage drop in fuel cells is measured by exposure to different levels of H$_2$S

[20], thus justifying the selection of H$_2$S as a model odorant in flow testing.

Nitrogen (σ~3.6 Å, T$_c$ = 126 K) was used as a suitable substituent for methane (σ~

3.8 Å, T$_c$ = 191 K), which is the major component of natural gas in the flow testing

experiments because H$_2$S gas cylinders in a nitrogen background were found to have

lower water vapor content (< 5 ppm) [21]. If water content of the test gas is high, certain

sorption capacity of the activated zeolites in fiber sorbents could be lost due to water

vapor sorption. The sorption and diffusion characteristics of methane and nitrogen were

expected to be similar orders of magnitude due to their similar molecular diameters (σ)

and critical temperatures (T$_c$).

Pure gas permeation studies to characterize single and dual-layer fiber sorbents

were performed using oxygen and nitrogen (ultra high purity (UHP) grade, Airgas South,

Atlanta, GA).

Due to the low odor thresholds of pure TBM vapor, iso-butane (C$_4$H$_{10}$, σ~5.2 Å)

was chosen as a surrogate gas for kinetic sorption because of its similar size to that of

TBM (C$_4$H$_{10}$S, σ~6 Å). Their diffusion coefficients were expected to be of similar orders

of magnitude in the large 7.4 Å sieve window (with the Knudsen diffusivity of iso-butane

being~ 1.25 times of that of TBM). Neo–pentane (σ~ 6.4 Å) was found to be a better

stimulant for TBM, but the prohibitively high costs and the non-availability of pure standards made the experiment lower in priority.

3.2. Dense film casting

To analyze the miscibility and interaction between the selected core and sheath layer polymers (section 5.2.), blend solutions with varying compositions of both polymers were made by dissolving in a volatile solvent (THF) at room temperature. The total polymer content in the solutions was about 10 wt. %. The blend was extruded through a syringe onto a metal casting ring placed on top of a level glass plate. The film was covered with a glass funnel and capped with a filter cloth to allow controlled solvent evaporation rate and prevention of contaminants getting onto the film (Figure 3.2). Once vitrified (~ 24 h), the dense, polymer blend film was removed from the glass plate and dried in vacuum oven at 110°C for 12 h.
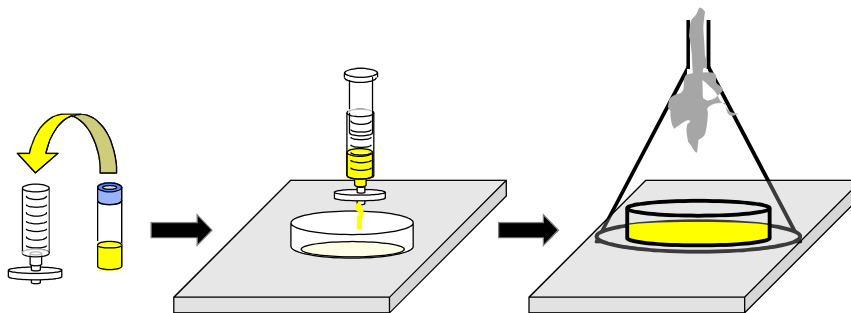
Figure 3.2: Schematic representation of the dense film casting process.

3.3. Fiber-sorbent preparation

3.3.1. Cloud point technique to determine spin dope composition

In fiber-sorbent creation it is desired to choose a one-phase dope composition in close proximity to the binodal curve to ensure a rapid phase separation and high porosity [22].

In the cloud point technique to determine the binodal curve, one-phase dopes in small quantities (15 ml) were initially made with two components (polymer and solvent). Dopes with incremental amounts of non-solvent content were then created, keeping the polymer content constant.

These dope samples were then visually observed to determine a 1-phase solution (transparent and homogenous, Figure 3.3(a)), a 'cloudy' solution (translucent, Figure 3.3(b)) indicating the onset of phase separation and a 2-phase solution (non-homogenous and phase separated, Figure 3.3(c)). The 'cloudy' dope solution composition is defined as the practical binodal point. Figure 3.3 schematically represents the concept of the cloud point technique.

Using similar technique, different binodal points are then found with variable polymer content thus creating the binodal curve. A one-phase dope composition in close proximity to the binodal curve and having appropriate viscosity (determined by viscosity measurements), was selected for scale–up and fiber sorbent dopes in larger quantities were made.

(a)   (b)   (c)

1-phase solution   'Cloudy' solution   2-phase solution
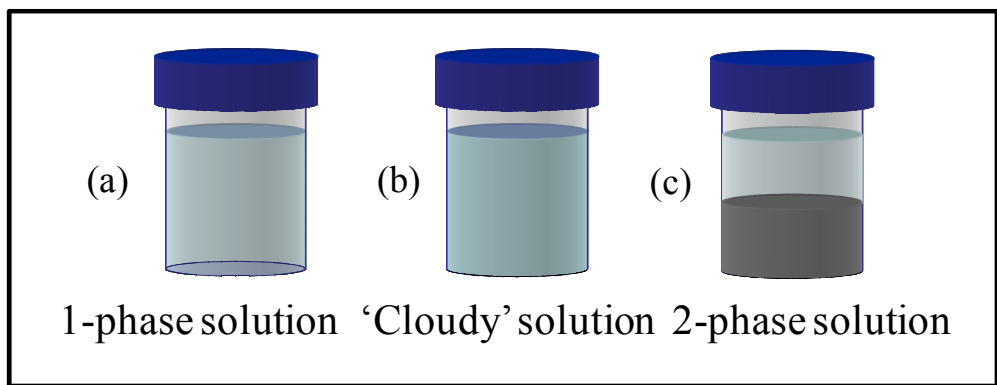
Figure 3.3:   Schematic representation of the cloud point technique to determine the binodal curve.

3.3.2. Asymmetric film casting

Potential core and sheath layer dopes were selected based on binodal experiments (section 3.3.1.) and viscosity measurements (section 3.4.6.). The selected sheath dopes (PAN or PVDC) were cast on top of films casted from the core dope (CA or Estane®/NaY) to check the adhesion of both the layers and simulate spinning conditions.

The dopes (15 ml) were degassed under vacuum for 2 h at room temperature before casting. The core dope was first draw casted onto a pre-cleaned transparent glass plate using a 4-mil thick casting knife, immediately followed by draw casting of barrier polymer dope on top of the casted core dope film with a 6-mil thick knife. The co-casted films were quickly immersed in DI-water coagulation bath to phase separate. The adhesion properties of the dual-layer films were observed in wet and dry states. These asymmetric films were stored in DI-water for 24 h and solvent exchanged with fresh methanol and hexane once followed by drying in vacuum oven at 80°C for 12 h.

3.3.3. 'Core' dope preparation

A general protocol was developed for the creation of fiber sorbent spin dopes. Dried additive (PVP) was dissolved in NMP solvent in a 1000 ml glass jar (Quorpak®, Bridgeville, PA) assisted by sonication (Model 1510R-MTH, Branson Ultrasonics, Danbury, CT). Next, the dried zeolite NaY sorbent was added in three parts with sonication by a powerful 1000 Watt horn (Dukane, Leesburg, VA) twice in one minute bursts for every part added. At very high loadings, clumping of improperly dispersed zeolite crystals can cause clogging of the spinneret during the spinning process in the absence of this procedure. Next, non-solvent (DI-water) was added to the dope and dried polymer binder (CA or polyester urethane) was then slowly added to the mixture.

Polymer was added after the dispersion of zeolites because the polymer increases the solution viscosity as it dissolves and can complicate dispersion of zeolite crystals if added first.

The dope was then heated to 50°C, to reduce its viscosity and stirred with an anchor–gate type impeller using a high torque motor (Model 409, TalBoys laboratory stirrers, Troemner LLC, Thorofare, NJ). The dispersion was stirred for approximately 24 h to ensure complete and uniform dissolution of the polymer. Next, the dope was allowed to mix on a heated roller maintained at 50°C for 24 hours. The fiber sorbent dope was then poured into a syringe pump (Model 500 DM, Teledyne Isco, Lincoln, NE) for spinning. The pump barrel was heated to 50°C and kept undisturbed for 12–24 h to ensure complete degassing of the dope since residual air bubbles trapped in the dope can cause non-uniform fiber sorbents and fiber breaks during spinning.

3.3.4. 'Sheath' dope preparation

For the sheath dope preparation, dried additive (PVP) was dissolved in NMP solvent in a 1000 mL glass jar (Quorpak, Bridgeville, PA) assisted by sonication (Model: 1510R-MTH, Branson Ultrasonics, Danbury, CT), followed by the addition of non-solvent (water). Dried polymer, (PAN or PVDC) was then slowly added to get the desired sheath layer composition. The dope was sealed and put on a roller heated to 40 – 50 °C with the help of an IR lamp, until complete polymer dissolution and dope uniformity was observed. The core and sheath dopes were then poured into syringe pumps (Model: 500 DM, Teledyne Isco, Lincoln, NE) for spinning. The pump barrel was heated to 50°C and kept undisturbed for about 12 h to ensure complete degassing of the dope solution.

3.3.5. Fiber sorbent spinning and solvent exchange protocol

Fiber sorbents were made by modifying the dry jet-wet quench solution spinning technique as described in section 2.5. [23]. By manipulating various spinning parameters, several spinning 'states' were collected and effect of each parameter was analyzed. Single and dual-layer fiber sorbents were found to be brittle compared to pure polymer hollow fiber membranes due to high sorbent loading (up to 75 wt. % - dry fiber wt basis) and were handled carefully. Fibers spun under identical conditions (called a 'spin state') comprising 10-20 fibers approximately 1.2 m long, were removed from the take-up drum, tied and soaked in de-ionized (DI) water for 3-8 days changing with fresh DI-water daily. Conventionally in Koros group, various hollow fiber membrane states are soaked in a water bath (0.5 m (l), 0.3 m (b), 0.15 m (h)) as shown schematically in Figure 3.4(a). This caused considerable entanglement and curling of different fiber states during the solvent exchange process.

The solvent exchange bath was modified such that each spin state was individually soaked in a 1.5 m long, 1 inch diameter solvent exchange tube to prevent curling and entanglement (Figure 3.4(b)). The water present in the fiber sub-structure was then solvent exchanged by immersion of the spin states for 30 minutes each in three batches of fresh methanol followed by three batches of fresh hexane. To remove the residual hexane, fibers were hung in a fume hood at room temperature for 1 hour and dried under vacuum at 80°C for another hour.

(a) Conventional design

(b) New design

Water-bath

Water-bath
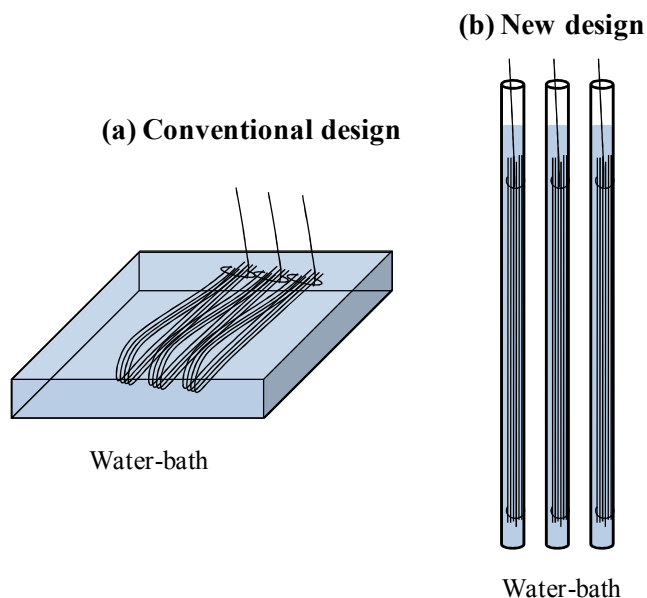
Figure 3.4: (a) Conventional and (b) modified fiber sorbent solvent exchange bath design.

3.3.6. Hollow fiber sorbent module preparation

The fiber sorbent modules were made with stainless steel tubings of various lengths using ¼ inch diameter tube and fittings using a technique similar to potting hollow fiber membranes [24]. Figure 3.5 shows the image of a potted hollow fiber module in a shell and tube configuration. Hollow fiber modules with an active length of 5-60 cm were made with roughly 1-6 fibers.
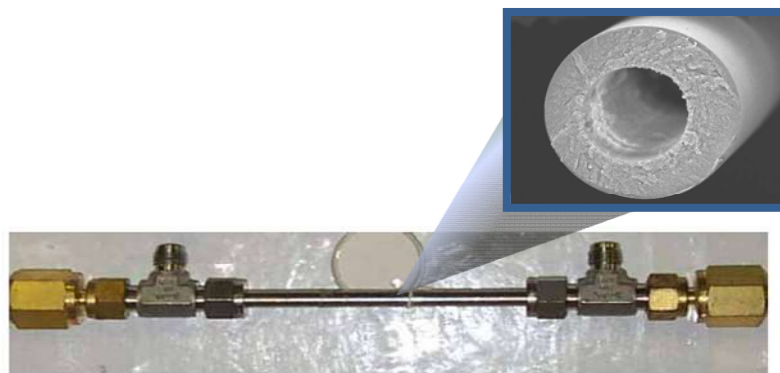
Figure 3.5: Schematic representation of a hollow fiber sorbent module in a shell and tube configuration with parallel flow of fluids.

3.3.7. Post-treatment of the hollow fibers

In case of dual-layer fiber sorbents, a low permeance and a defect-free skin is desired in the sheath layer. A higher permeance and Knudsen selectivity through the dual-layer fiber sorbent indicates higher defects in the sheath layer which could significantly retard its barrier properties. Various post-treatment techniques were explored in this work to remove the defects in the fiber sorbent sheath layer. The post treatment techniques are considered in detail in chapter 6.

3.3.7.1. Heat treatment of dual-layer fibers

Dual-layer fiber sorbents will be exposed to temperatures of around 100-120°C during the temperature swing regeneration cycles using steam or hot purge. The effect of heat exposure on the core and sheath layer morphology was studied in a controlled manner by keeping the fibers under vacuum at various temperatures (100-120 °C), isothermal for various time intervals and allowed to cool down slowly under natural convection of the oven. The glass transition temperature (T_g) of the core layer should be significantly higher than the T_g of the sheath layer polymer. It is desired that during the heat treatment of the fibers, the core layer retains its structure and porosity due to a high T_g, while the sheath layer with a low T_g densifies due to annealing and chain relaxation; thus sealing some of the defects in the sheath layer. The effects of temperature and exposure time during the heat treatment are described in greater detail in section 6.2.

3.3.7.2. Silicone rubber post-treatment

Silicone rubber post treatment method is commonly employed in the membrane literature to plug the skin layer defects of the asymmetric hollow fiber membranes [25]. In this method, a thin layer of silicone rubber was applied on the defective fibers, using a

2 wt. % high molecular weight polydimethylsiloxane (PDMS, Sylgard® 184, Dow chemicals) solution in heptane. The high permeability polydimethylsiloxane (PDMS) layer does not decrease the permeance of the membrane/fiber sorbent significantly; however it plugs the pinhole defects providing a non-selective pathway to the gases. The protocol is described in detail elsewhere [26].

<u>3.3.7.3. Latex post-treatment</u>

A new kind of post treatment technique was employed to either create a low permeability sheath layer on single-layer fiber sorbents or plug the pin-hole defects in a dual-layer fiber sorbent. In this technique, solvent-exchanged and dried fiber sorbents were exposed to PVDC aqueous dispersion solution (Diofan®).

This post-treatment technique was approached in the following manner:

1. **Dip coating of fibers:** In the dip coating of fibers, fiber sorbents were dipped into a tube containing the latex solution, soaked for a certain period of time and then withdrawn at a constant rate. Excess solution was allowed to drain.

2. **Latex flow through fiber sorbent module**: In this method, fiber sorbents were mounted and potted into a module with the finished module having a shell and tube geometry [27, 28]. The fibers were soaked in the latex solution (Diofan®) by passing the solution on the shell side of the module. In case of post treating single-layer fibers, a certain gas pressure could be maintained in the fiber sorbents to prevent latex solution from entering into the porous core layer and blocking the voids. On the contrary, in case of dual-layer fibers, vacuum could be applied on the bore side of the fiber to pull the latex solution into the sheath to effectively

seal the 'barrier' sheath defects. In dual-layer fibers, the dense and thick sheath layer prevents the latex solution from entering the core layer.

This post treatment technique was found to be very flexible where the latex concentration, flow rate and pressure, number of washes, the drying step and the pressure in the fiber were among the various parameters that could be varied to obtain a post-treated layer of desired thickness. The optimization of the post treatment protocol is described in detail in section 6.4.

3.4. Characterization

3.4.1. Scanning electron microscopy (SEM) and Energy-dispersive x-ray spectroscopy (EDX)

Dried fiber sorbents were placed in liquid nitrogen and shear fractured using fine point tweezers. The fibers were mounted on a SEM mount and sputter coated with a 10-20 nm thick gold coating (Model P-S1, ISI, Mountain View, CA). Fiber images were obtained using a high resolution scanning electron microscope (SEM) (Leo 1530, Leo Electron Microscopy, Cambridge, UK). A line spectrum of energy-dispersive x-ray spectroscopy (EDX) (Oxford instruments, Oxfordshire, UK) was applied to the fibers to detect distribution of NaY crystals in core layer and the extent of interpenetration between the core and the sheath layer polymers.

3.4.2. Thermo gravimetric analysis (TGA)

Zeolite loading and drying characteristics of the spun fiber sorbents was verified by thermo gravimetric analysis (TGA) [29] (Model: STA 409 PC, Netzsch Inc., Exton, PA). In a typical TGA experiment, samples are heated to a desired temperature and the sample weight (or weight loss) is monitored simultaneously.

To replicate the drying procedure in a fiber sorbent flow system (section 4.7.), the fiber sorbent or zeolite crystal samples were dried in the TGA under a N_2 purge with a ramp rate of 10 °C /min to 120 °C, and then kept isothermal at 120°C for roughly 48 h at a flow rate of 30 cm^3/min, to estimate the weight loss due to the removal of sorbed water.

The zeolite loading of the spun fiber sorbents was compared with the theoretical loading determined during the creation of the fiber sorbent spin dopes. A good match between the two values indicates that the zeolite loaded core dope was uniform and there was no loss of sorbent particles during the fiber spinning process. A two step heating protocol was followed in which during the first heating step the sorbed water vapor in the polymer and zeolite were removed under a N_2 purge to give dry fiber sorbents with the weight occupied only by the polymer (binder) and the zeolite crystals (sorbent). In the second and the final heating step the polymer template was burned off under an O_2 purge to give only pure zeolite crystals. The temperatures and the soak time in each step were varied depending on the amount of sorbed water vapor (for step 1) and the melting/decomposition temperature of the core and the sheath layer polymers (for step 2).

The residual NMP amount in the solvent exchanged fibers was also estimated by TGA, by heating it to~210 °C (boiling point of NMP) to estimate the weight loss due to the removal of NMP.

3.4.3. Differential Scanning Calorimeter (DSC)

The glass transition temperature (T_g) and melting or degradation temperature (T_m) of pure polymer powders were determined and then compared with polymer blend films using a differential scanning calorimeter (DSC) (Q200, TA instruments, New Castle, DE). Typically, polymers with a large difference in the T_g and showing partial/complete

64

miscibility indicate shifts in T_g upon blending [30]. 7-9 mg sample was placed into aluminum DSC pans and heated from 0°C to 160°C, at a ramp rate of 10°C/min in the first cycle to remove sorbed water vapor and the thermal history of the sample, followed by cooling back to 0°C at a rate of -10°C/min. The protocol was repeated in the second cycle and the T_g was determined at the midpoint of the transition curve.

3.4.4. Ultraviolet-visible spectroscopy (UV-Vis)

Residual NMP in the DI-water exchange solution after subsequent exchanges was analyzed by UV-Vis spectroscopy (Model: DU 720, Backman Coutler, Brea, CA) and was indirectly indicative of residual NMP in the fiber sorbents. Before each measurement a blank run of DI-water was performed and the instrument was calibrated with NMP/DI-water solutions of known composition. The NMP content of a solution was related to the intensity of the experimental peaks. The NMP peaks were observed in the range of 190-220 nm.

3.4.5. Fourier transform infrared spectroscopy (FTIR)

Fourier transform infrared spectroscopy (FTIR) can provide information about the interaction of functional groups in the core and sheath layer and their effect on adhesion. Studies were conducted on polymer blend films (10-20 μm thick) with a FTIR spectrometer (Model: Tensor 27, Bruker Daltonics Inc., Billerica, MA) between 400 – 4000 cm^{-1}.

3.4.6. Rheology experiments

Core and sheath layer dope viscosity was found to be critical to obtain fiber sorbents of desired morphology. Viscosity data was obtained by using a rheometer (Pas

Physica MCR-300, Anton-Paar USA, Ashland,VA) with a shear rate from 0.01 s^{-1}-10 s^{-1},

at temperatures of 25°C and 40°C in collaboration with Dr. Breedveld's research group.

3.4.7. Sorption measurements

3.4.7.1. Equilibrium sorption – quartz spring method

Experimental isotherms are useful to determine the adsorption capacity and for

the selection of the most appropriate sorbent. Equilibrium sorption using a McBain quartz

spring method [31, 32] was performed at 35°C to determine the capacity of fiber sorbents

for the odorant, TBM. This capacity was compared with the capacity of zeolite NaY

crystals and of pure polymer hollow fiber. The gravimetric sorption method involves the

estimation of the change of sample mass due to the adsorption of the penetrant vapor, by

the measurement of the extension of a precise and calibrated quartz spring.
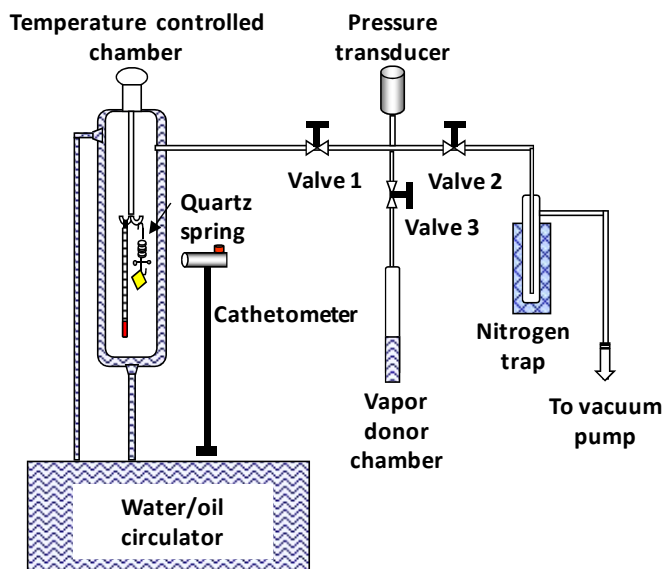
Figure 3.6: Schematic diagram of the quartz spring sorption balance.

The setup involves a jacketed chamber, maintained at a constant temperature by

the circulation of water or colorless silicone oil (Figure 3.6). The chamber lid had a glass

hook, on which a thermometer and/or a quartz spring was hanged. Quartz springs (GE sensing, Houston, TX) were available with maximum loads of 50-100 mg with a maximum extensions of 100-300 mm. A quartz spring with a lower maximum load and a higher extension gives better measurement accuracy.

The springs were calibrated with different masses of stainless steel wires to obtain the spring constant. For the measurement of the zeolite crystals, the samples were placed in a quartz pan, while for the fiber sorbents; the samples were tied to a thin stainless wire and hung from the quartz spring. The sample position was determined by focusing the reference pointer on the spring by a precision cathetometer or an optical reader. The measurement accuracy was 8.3 µg for the cathetometer (least count = 0.05 cm) and 0.83 µg for the optical reader (least count = 0.005 cm), when a spring of 50 mg/300 mm was used.

The remaining manifold was maintained at the same temperature as the jacketed chamber using heat tapes to prevent the condensation of the vapors. The vapors were introduced into the manifold through the vapor donor chamber and the pressure in the system was measured by a 1000 Torr transducer (Model: 127, MKS, Andover, MA). Figure 3.6 shows the schematic of the quartz spring setup, with valve 1 being the chamber isolation valve, valve 2 for vacuum connection and valve 3 was operated to allow the liquid vapor to enter the manifold.

The entire manifold was constructed with glass, with the joints connected by high temperature and solvent resistance Viton™ o-rings. The valves were bakeable Teflon™ plugs (stable up to 140 °C) with Viton™ o-rings.

Before each experiment, the entire system was heated up to 110 °C, under vacuum to remove any condensed residual solvent from the system. The o-rings at the joints and on the valves were changed frequently (usually after two experiments) to minimized leaks in the system. A thin layer of vacuum grease was gently applied to the o-rings to lower the overall system leak rate. The system was leak tested before each experiment and corrections to the adsorption capacity were made accordingly. The system leak rate was about 1.3 Torr/two days. The sample chamber lid was not heated by the chamber jacket and hence a heating tape was used to prevent thermal gradients in the chamber.

The sample was carefully loaded into the chamber and evacuated for 48 h at 110 °C, under vacuum (Valve 1 and 2 open, valve 3 closed) before the sorption test. Care had to be taken to open valve 2 slowly and gradually, to prevent the fragile spring from oscillating and eventually breaking or falling-off the hook. After the drying step, the chamber temperature is lowered to 35 °C and the adsorption tests were conducted. A liquid N_2 trap was used before the vacuum pump to prevent the pump oil from back diffusing into the chamber, thereby preventing the vapors from entering and condensing in the pump.

Due to the low odor threshold of TBM, it was carefully transferred into a vial with activated zeolite 4A to remove trace amounts of water vapor in the as obtained TBM. The purified TBM was then transferred into the vapor donor chamber and connected to the manifold through valve 3. The air in the vapor donor chamber headspace and dissolved in the TBM were removed by conducting 3 freeze-pump-thaw cycles (Valve 1 – closed, valve 2 and 3 open).

Valve 2 connecting the vacuum line was then closed, valve 1 opened, and the valve 3 was opened very slowly to allow the vapor at a certain pressure to enter the manifold. The extension of the spring was measured after regular intervals, and equilibrium was assumed to be attained when the spring position did not change over a course of 24 h. Once equilibrium was reached, pressure was further increased by introducing more vapors into the manifold by opening valve 3. A maximum TBM activity of 0.3 was studied in the experiments. Higher activities were not studied since in actual sulfur impurity removal operation, the sulfur activity in the pipeline natural gas will be around 0.05.

To study, the desorption behavior of the samples; the chamber pressure was gradually decreased by pulling vacuum till a desired lower pressure was reached. The sample was then allowed to equilibrate and desorption behavior of the sample was recorded.

3.4.7.2. Kinetic sorption – pressure decay method

Kinetic measurements using the quartz spring verified extremely rapid equilibration, and could not be accurately quantified because of the short time scale of sorption [33]. Pressure decay sorption was used to determine the sorption kinetics of pure zeolite NaY particles and single-layer fiber sorbents. Due to the low odor thresholds of pure TBM vapor, iso-butane C_4H_{10} ($\sigma \sim 5.2$ Å) was chosen as a surrogate gas for transient sorption because of its similar size to that of TBM $C_4H_{10}S$ ($\sigma \sim 6$ Å).
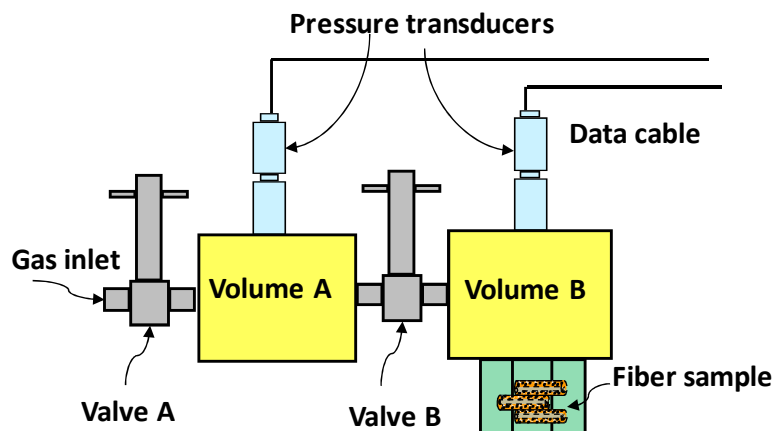
Figure 3.7: Pressure decay sorption system [29, 34].

The schematic diagram of the measurement apparatus is shown in Figure 3.7. The experimental setup consists of two reservoirs of known volume. The volume A is often called as the reservoir cell, while the volume B is called as the sample cell. The two cells were separated by a high precision long handle valves. The pressures in the two volumes were measured by pressure transducers (Ametek, Paoli, PA). The pressure data was recorded real time using Labview®. The sorption cell was immersed in a silicone oil bath maintained at a constant temperature by a heater/circulator (Istotemp 2150, Fisher Scientific, Pittsburgh, PA). The zeolite crystal or the fiber sorbent samples are placed in a sintered stainless steel filter element capped with a aluminum foil tied by a thin stainless steel wire. The weights of the samples were measured before the test.

After loading the cell, the sample was dried for 12-24 h at a temperature of 110°C, by increasing the temperature of the oil bath. After the drying step, the bath was cooled down and maintained constant at 35°C. The sample cell was then isolated by closing the valve B, and gas at a certain pressure was introduced into the reservoir cell. The valve A was then closed to allow the gas to reach equilibrium in the reservoir.

Valve B was then opened for a few seconds to allow a certain amount of gas to expand into the sample cell, before closing it. The final pressure in the reservoir cell was recorded and the pressure decay in the sample cell was monitored over time to indicate the sorption kinetics in a zeolite crystal or fiber sorbents.

3.4.8. Permeation measurements

Pure gas permeation tests can be used to determine and compare the flux through the core layer (in single-layer fiber sorbents) and the sheath layer (in dual-layer fiber sorbents) created with different dope compositions and spun under various spinning conditions. Modules for permeation testing were created with a shell and tube configuration (discussed in section 3.3.6.) and tested in a dead-end module configuration (Figure 3.8 and Figure 3.9) allowing feed gas to be applied either on the bore or the shell side. In permeation testing the active fiber length was taken between the epoxied regions since only this region contributes to permeation (Figure 3.8 and Figure 3.9). Oxygen and nitrogen (ultra high purity (UHP) grade, Airgas South, Atlanta, GA) were used as the probing gases to check the permeance (indicating porosity) and selectivity (indicating defect free structure) of the fiber sorbents.

3.4.8.1. Permeance measurements of single-layer fiber sorbents

In case of single-layer fiber sorbents, the permeance tests were conducted to determine the flux through the core layer which influences the sorption capacity of the fiber sorbents. A bore side feed was selected because in a fiber sorbent module planned to be used in an on-site hydrogen generation station (section 2.6.), the pipeline natural gas will be fed to the bore side. The permeance (i.e. pressure normalized flux) through the core layer was expected to be high due to the high sorbent loading and the porosity of the

core layer wall. Also for high flux gases, if the gas was fed in the shell side then the pressure drop within the bore must be taken into account [28].
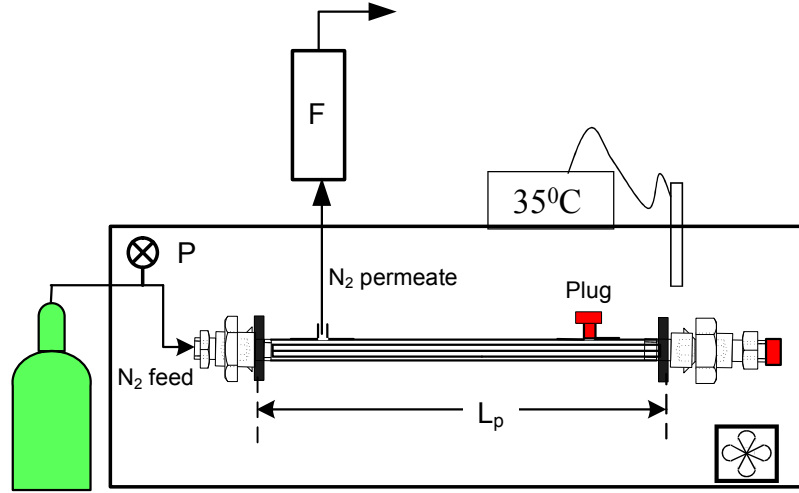
Figure 3.8: Schematic of a constant pressure permeation system for testing hollow fiber sorbents (Fiber module is shown enlarged for better clarity).

In single-layer fibers, the constant pressure (or variable volume) method [23] was preferred (Figure 3.8), in which a constant pressure gas is fed through the bore side of the module and the permeate is collected on the shell side, with the module temperature maintained at 35°C.

The steady state flow rate through the shell side (dV/dt) was measured using a bubble flow meter. The downstream or the sheath side was at atmospheric pressure. Further details of the measurement protocol are described elsewhere [26]. For the constant pressure method:

$$Permeance \left(\frac{P}{\ell}\right) = \frac{(n_{STP})}{(\Delta p)} = \frac{(dV/dt)_{STP}}{(\Delta p)A_f} = \frac{(dV/dt)_{STP}}{(\Delta p)N_f * \pi * O.D. * L_p} \tag{3.1}$$

Where, n_{STP} is the flux through the module at standard conditions of temperature and pressure (STP- T=273.15 K, p=1 atm), Δp is the pressure drop between the upstream

and the downstream of the fiber module, $(dV/dt)_{STP}$ is the permeate flow rate at STP, A_f is the area available for permeation, N_f is the number of fibers in the module, $O.D.$ is the outer diameter of the fiber, and L_p is the length of the module available for gas permeation.

3.4.8.2. Permeance measurements of dual-layer fiber sorbents

In case of testing the barrier layer efficacy in dual-layer fiber sorbents a shell side feed of gas was selected because in the fiber sorbent module planned to be used in an on-site hydrogen generation station (section 2.6.), the regeneration media (steam or water) will be passed on the shell side.

For dual-layer fiber testing, the permeance (i.e. pressure normalized flux) was expected to be low due to the dense and low permeability sheath layer. For fibers indicating a low flux a constant volume method measuring the steady state downstream pressure increase rate (dp/dt) was preferred, due to difficulties in measuring the flow rate $((dV/dt)$ in constant pressure method).

Gases were used as the first step to test the barrier layer efficacy as opposed to water vapor due to operational simplicity. Also, water vapor ($\sigma \sim 2.8$ Å, $T_c = 647$ K) is highly permeable (small molecular diameter (σ)) and highly sorptive (proportional to critical temperature (T_c)), compared to gases like N_2 ($\sigma \sim 3.6$ Å, $T_c = 126$ K). Hence, a defective barrier sheath layer indicating Knudsen selectivity and high permeance for N_2 would surely be defective for a highly permeable water vapor.

In this method, the fiber sorbent module was loaded in a permeation system shown schematically in Figure 3.9. The system (upstream, downstream and the module)

73

are evacuated to remove any sorbed gases. The fibers take less time (~12 h) compared to the dense films to degas (~48 h) due to the small thickness of the dense skin in the sheath layer.
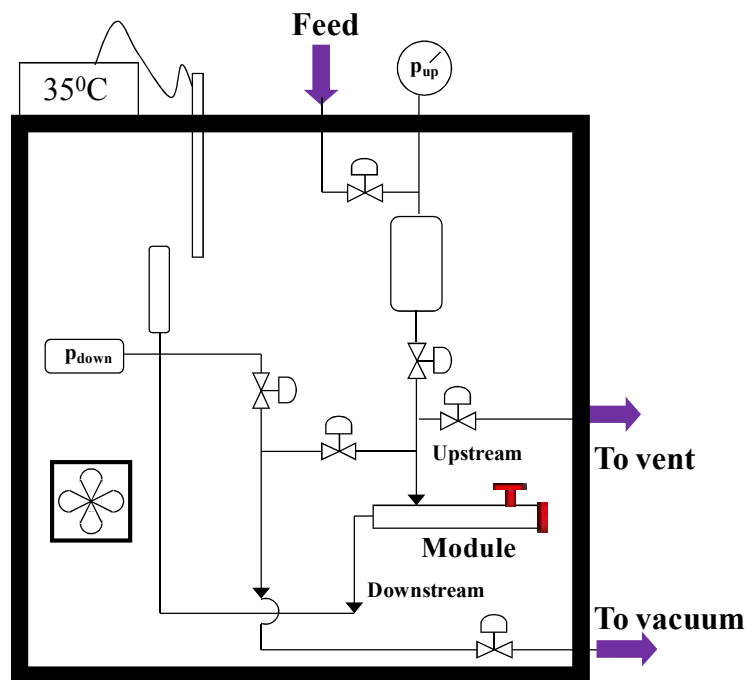
Figure 3.9: Schematic of a constant volume permeation system for testing hollow fiber sorbents.

The system leak rate was measured before each test and should be roughly 1 % of the actual permeance (leak rate~ 10^{-5}-10^{-6} Torr/sec) to avoid erroneous data. A low leak rate indicates no substantial leaks in the system and the removal of any adsorbed gases.

The system was then evacuated again, followed by introduction of gas (N_2 or O_2) at constant pressure in the upstream. The upstream pressure was measured by 1000 psia pressure transducer.

After pressurizing the upstream, the downstream vacuum was closed and the rate of downstream pressure rise due to permeance was monitored with a 1000 Torr transducer. The time lag for gases in fiber sorbent modules was expected to be lower than

dense films since the time lag is directly proportional to the square of the separating layer thickness.

For constant pressure measurement method:

$$Permeance \ (\frac{P}{\ell}) = \frac{(n_{STP})}{(\Delta p)} = \frac{V_d \ (^{dp}/_{dt})_{STP}}{RTp_{up} A_f} = \frac{V_d \ (^{dp}/_{dt})_{STP}}{RTp_{up} N_f \pi.O.D.L_p} \tag{3.2}$$

Where, $(^{dp}/_{dt})_{STP}$ is the rate of downstream pressure change at STP, V_d is the downstream volume, R is the universal gas constant, and T is the module temperature, p_{up} is the upstream pressure.

The ratio of pure component permeances for different gases is defined as selectivity and represented as $\alpha_{i/j}$.

$$\alpha_{i/j} = \frac{(^P/_l)_i}{(^P/_l)_j} \tag{3.3}$$

3.5. REFERENCES

1. Weisskopf, K., *Characterization of Polyethylene Terephthalate by Gel-Permeation Chromatography (Gpc).* Journal of Polymer Science Part a-Polymer Chemistry, 1988. 26(7): p. 1919-1935.

2. Hansen, C.M., *Hansen solubility parameters : a user's handbook.* 2000, Boca Raton, Fla.: CRC Press. 208 p.

3. Brandrup, J., E.H. Immergut, and E.A. Grulke, *Polymer handbook.* 4th ed. 2004, New York ; [Chichester]: Wiley-Interscience.

4. Ixan-Diofan.*http://www.ixan-diofan.com/static//wma/pdf/2/1/7/6/Diofan%20A602%20-%20rév%204%20.pdf.* Date accessed, October 8th, 2010.

5. Koros, W.J., *Barrier Polymers and Structures - Overview.* Acs Symposium Series, 1990. 423: p. 1-21.

6. IXAN-PNE-288. *http://www.ixan-diofan.com/.* Date accessed, October 8th, 2010.

7. *http://www.solvayadvancedpolymers.com/products/bybrand/torlon/0,,329-2-0,00.htm.* Date accessed, October 8th, 2010.

8. Kosuri, M.R. and W.J. Koros, *Defect-free asymmetric hollow fiber membranes from Torlon (R), a polyamide-imide polymer, for high-pressure CO2 separations.* Journal of Membrane Science, 2008. 320(1-2): p. 65-72.

9. Puleo, A.C., D.R. Paul, and S.S. Kelley, *The Effect of Degree of Acetylation on Gas Sorption and Transport Behavior in Cellulose-Acetate.* Journal of Membrane Science, 1989. 47(3): p. 301-332.

10. Lubrizol. *http://www.lubrizol.com/EngineeredPolymers/products/tradename.html.* Date accessed, October 8th, 2010.

11. Massey, L.K., *Permeability Properties of Plastics and Elastomers.* 2nd ed. 2002, Amsterdam: Elsevier.

12. Wakita, H., Y. Tachibana, and M. Hosaka, *Removal of dimethyl sulfide and t-butylmercaptan from city gas by adsorption on zeolites.* Microporous and Mesoporous materials, 2001. 46(2-3): p. 237-247.

13. Satokawa, S., Y. Kobayashi, and H. Fujiki, *Adsorptive removal of dimethylsulfide and t-butylmercaptan from pipeline natural gas fuel on Ag zeolites under ambient conditions.* Applied Catalysis B-Environmental, 2005. 56(1-2): p. 51-56.

14. Gates, B.C., *Catalytic Chemistry.* 1992, New York: Wiley.

15.   Song, W.G., et al., *Development of improved materials for environmental applications: Nanocrystalline NaY zeolites.* Environmental Science & Technology, 2005. 39(5): p. 1214-1220.

16.   Baerlocher, C., W.M. Meier, and D.H. Olson, *Atlas of zeolite framework types.* 5th ed. 2001, Amsterdam: Elsevier.

17.   Duarte, L.T., A.C. Habert, and C.P. Borges, *Preparation and morphological characterization of polyurethane/polyethersulfone composite membranes.* Desalination, 2002. 145(1-3): p. 53-59.

18.   Qin, J.J., et al., *Cellulose acetate hollow fiber ultrafiltration membranes made from CA/PVP 360 K/NMP/water.* Journal of Membrane Science, 2003. 218(1-2): p. 173-183.

19.   Shimizu, K., et al., *Mechanistic study on adsorptive removal of tert-butanethiol on Ag-Y zeolite under ambient conditions.* Journal of physical chemistry B, 2006. 110(45): p. 22570-22576.

20.   Israelson, G., *Results of testing various natural gas desulfurization adsorbents.* Journal of materials engineering and performance, 2004. 13(3): p. 282-286.

21.   Personal communication, *David Haydt, Galvanic applied sciences,.* 2010.

22.   Wallace, D.W., C. Staudt-Bickel, and W.J. Koros, *Efficient development of effective hollow fiber membranes for gas separations from novel polymers.* Journal of Membrane Science, 2006. 278(1-2): p. 92-104.

23.   Pesek, S.C. and W.J. Koros, *Aqueous Quenched Asymmetric Polysulfone Hollow Fibers Prepared by Dry Wet Phase-Separation.* Journal of Membrane Science, 1994. 88(1): p. 1-19.

24.   Carruthers, S.B., G.L. Ramos, and W.J. Koros, *Morphology of integral-skin layers in hollow-fiber gas-separation membranes.* Journal of applied polymer science, 2003. 90(2): p. 399-411.

25.   Henis, J.M.S. and M.K. Tripodi, *Composite Hollow Fiber Membranes for Gas Separation - the Resistance Model Approach.* Journal of Membrane Science, 1981. 8(3): p. 233-246.

26.   Husain, S., *Mixed matrix dual layer hollow fiber membranes for natural gas separation.* 2006, Georgia Institute of Technology: Atlanta, Ga.

27.   Vu, D.Q., W.J. Koros, and S.J. Miller, *High pressure CO2/CH4 separation using carbon molecular sieve hollow fiber membranes.* Industrial & Engineering chemistry research, 2002. 41(3): p. 367-380.

28. Carruthers, S., *Integral-skin formation in hollow fiber membranes for gas separations*, in *Department of Chemical Engineering*. 2001, University of Texas at Austin

29. Lively, R.P., et al., *Hollow Fiber Adsorbents for CO2 Removal from Flue Gas.* Industrial & Engineering chemistry research, 2009. 48(15): p. 7314-7324.

30. Paul, D.R. and S. Newman, *Polymer blends*. 1978, New York: Academic Press.

31. McBain, J.W. and A.M. Bakr, *A new sorption balance.* Journal of the American Chemical Society, 1926. 48(1): p. 690-695.

32. Chandra, P. and W.J. Koros, *Sorption and transport of methanol in poly(ethylene terephthalate).* Polymer, 2009. 50(1): p. 236-244.

33. Karger, J., *Measurement of Diffusion in Zeolites—A Never Ending Challenge?* Adsorption 2003. 9(1): p. 29–35.

34. Koros, W.J. and D.R. Paul, *Design Considerations for Measurement of Gas Sorption in Polymers by Pressure Decay.* Journal of Polymer Science Part B-Polymer Physics, 1976. 14(10): p. 1903-1907.

CHAPTER 4

CREATION AND CHARACTERIZATION OF SINGLE-LAYER

FIBER SORBENTS

Abstract

Single-layer fiber sorbents were made by modifying the dry jet-wet quench spinning technique. Spinning parameters were optimized in a manner to allow fibers to be be spun at high take-up rates and at room temperature spinning conditions. CA/NaY fiber sorbents with 75 wt. % NaY loading and polyester urethane (Estane[®])/NaY fiber sorbents with 60 wt. % NaY loading were spun successfully.

SEM images indicated that CA / NaY fiber sorbents had the desired 'sieve-in-a-cage' structure, while Estane[®] fiber sorbents had a sieve encapsulated by polymer ('occluded' sieve). CA was pursued as the polymer of choice for the fiber sorbent core layer creation. EDX image of the CA/NaY fiber sorbents indicated uniform distribution of zeolite crystals. Fiber sorbents were also characterized for equilibrium and transient sorption in batch and flow systems.

4.1. Literature review

Porous hollow fiber membranes with small adsorbent crystals packed around the fibers have been described previously in the literature as a possible improvement to packed bed operation. Feng et al. [1] and Pan et al. [2] illustrated hydrogen separation by PSA with fine-powder activated carbon and zeolite 5A as adsorbents. Gilleskie et al. [3] illustrated adsorption of ethane from helium using zeolite 13X and 4A. Polypropylene hollow fibers supplied by Hoechst Celanese Corporation were used in these studies. Hollow fiber membranes and adsorbent crystals were used as separate entities *and not as a single hybrid material described here*. The modules prepared in these studies required a rather inconvenient procedure of filling minute zeolite crystals around porous hollow fiber membranes.

Lively et al. [4, 5] describe the concept of fiber sorbent with an internal barrier layer formed by a multi-step process. These fibers were used for the capture of CO_2 from the flue gas streams of coal-fired power plants where bore side feeding was not viable due to low available driving force. They describe temperature swing adsorption (TSA) technique for the regeneration of the fibers. While a shell side feed is useful for reducing the CO_2 concentrations from high levels around 15 mole % to 1 mole % CO_2, for the capture of low concentrations of contaminants considered here, potential bypass or channeling makes the bore feed option preferable.

Kiyono et al. [6] and Avramescu et al. [7] describe the concept of hollow-fiber membrane adsorbers by incorporating cation-exchange particles of loadings up to ($\leq$50 wt %) in hollow fiber membranes for liquid based adsorption processes. Change in the pH by an eluent solution was the preferred regeneration technique. The current work

incorporates zeolite sorbent particles with higher surface area/volume ratio and higher porosities and zeolite loadings (up to 75 wt. %) in the fibers.

Perera et al. [8, 9] describe single and dual layer adsorbent hollow fibers using polyether sulfone (PES) as polymer and zeolite 4A and 13X as active adsorbents for CO_2 and n-butane removal from gas streams. They describe an electrical swing adsorption (ESA) technique for the regeneration of fibers. The outer layers of these fibers are made with a binding polymer and an activated carbon material that carries the current during the regeneration step. The presence of excessive carbon material or carbonization/activation of fibers can cause embrittlement while the presence of excessive low conductivity polymer (e.g., PES) can lead to higher electric resistances and breaking of electric circuit. Moreover, when dealing with flammables like natural gas the ESA process can be potentially dangerous.

4.2. Dope formulation and polymer fiber spinning

Single-layer fiber sorbents are desired to have a highly porous morphology with high loadings of zeolite sorbent uniformly dispersed in a polymer matrix. Contrary to hollow fiber spinning for membrane applications, a dense perm selective skin layer is not desired in fiber sorbents. Hence, during dope formulation for the single-layer fiber sorbents (also called the 'core' layer in dual-layer fiber sorbent spinning), volatile solvents (e.g. acetone or tetrahydrofuran (THF)) or volatile non-solvents (e.g. ethanol) were not added to the dopes.

Different fiber sorbent dope compositions were formulated to get fibers with high zeolite loading, high strength and desired morphology. Spinning parameters were

optimized such that fibers could also be spun at high take-up rates without frequent breaks.

Dope compositions for fiber sorbent spinning were identified by initially creating pure polymer dopes to determine the binodal curve using the cloud point technique described in chapter 3 (section 3.3.1.).

The optimization process started with the selection of cellulose acetate as one of the polymers of choice as discussed in chapter 3 (section 3.1.1.). Initially, cellulose acetate ((CA)-polymer) / N-Methyl-2-pyrrolidone ((NMP)-solvent) / lithium nitrate ((LiNO$_3$)-non-solvent) system was developed.

Addition of inorganic salts (e.g. LiNO$_3$) has been shown to act as a pore former and reduce or eliminate the formation of macrovoids in hollow fiber membrane dopes [10], by increasing the dope viscosity and also lowering the solvent diffusivity by forming Li-ion complexes with NMP molecules [11, 12]. LiNO$_3$ was found to acts as a non-solvent in the polymer dope, with higher concentrations (closer to binodal curve) leading to faster phase separation [13].

The polymer dope appears uniform and translucent when one phase, and cloudy and non-uniform when two-phase as discussed in section 3.3.1. Figure 4.1 shows the binodal diagram of CA/NMP/LiNO$_3$ and CA/NMP/water systems at 25°C. Usually, hydrophilic polymers like CA have a larger miscibility region with 10-15 wt.% non-solvent causing phase separation compared to hydrophobic polymers (e.g. polyimides) where up to 1-5 wt.% non-solvent causes phase separation [13].

Pure polymer fibers with a composition of CA/NMP/LiNO$_3$ - 20/72/8 wt. % were spun successfully and a porous and uniform morphology with an open cell structure was obtained as shown in Figure 4.2.
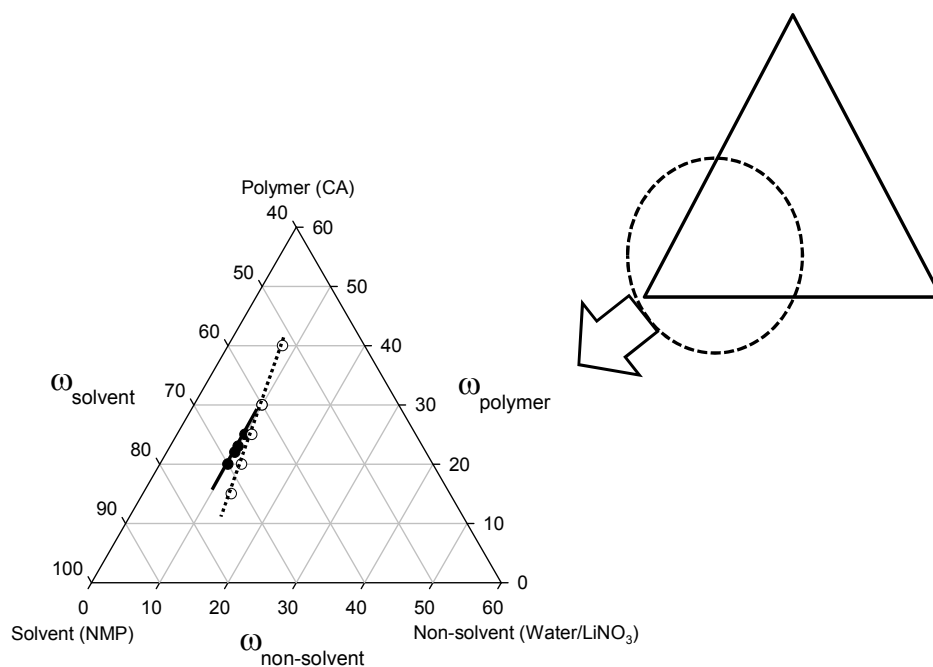
Figure 4.1: Ternary phase diagram of CA with solvent (NMP) and non-solvent (water/LiNO$_3$) system at 25°C in wt. %. The composition to the left of the binodal lines are homogeneous single phase solution, and compositions to the right are two phase. (Solid dots: LiNO$_3$, empty dots: Water).
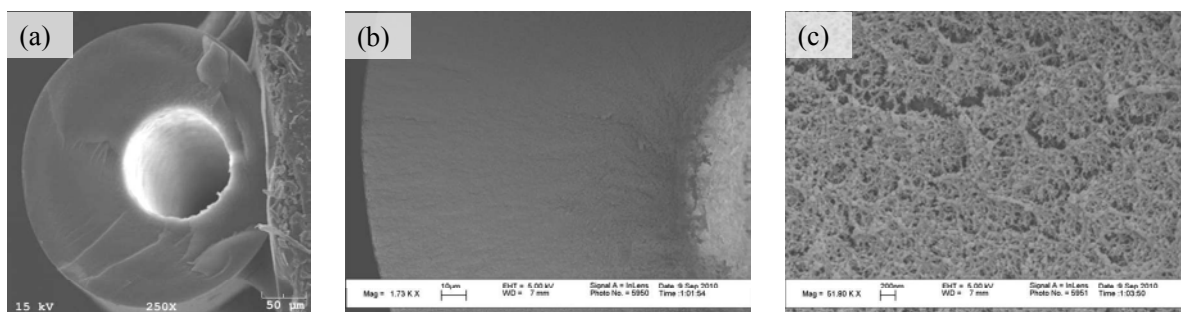
Figure 4.2 (left to right): (a) SEM image of a pure polymer CA fiber sorbent created from a dope with composition: CA/NMP/LiNO$_3$ - 20/72/8 wt. % (b) SEM image close-up of the fiber wall (c) Uniform and porous morphology.

After the successful creation of pure polymer fibers the next goal was to develop fiber sorbent dopes. Various dopes were created by varying the zeolite loading while keeping the ratios of the other components the same as described above. It was found that the already viscous polymer dope (due to 8 wt. % $LiNO_3$ viscosity enhancing non-solvent) became highly viscous due to the addition of zeolite particles leading to difficulties in dope loading and high pressures during the fiber spinning process (refer sections 2.5. and 3.3.3.) Hence, CA fiber sorbent dopes with water as a non-solvent were pursued for further studies. A one phase polymer dope with the composition as CA/NMP/Water – 20/70/10 wt.% was chosen as the starting dope composition to begin the optimization process (based on the binodal curve shown in Figure 4.1).
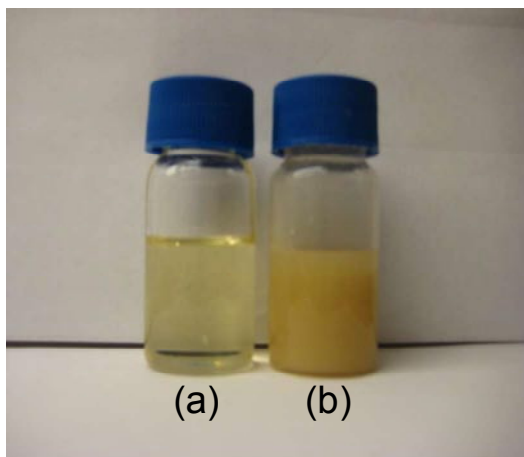
Figure 4.3: Comparison of a homogeneous one-phase (a) cellulose acetate polymer dope and (b) cellulose acetate / NaY fiber sorbent dope.

Fiber sorbent dopes were turbid and highly viscous compared to pure polymer dopes due to the addition of inorganic zeolite fillers. Fiber sorbent dope optimization required considerable trial and error due to the difficulty in determination of one phase mixture purely based on visual observation. The maximum loading was determined based on the viscosity and homogeneity of the fiber sorbent dope. Figure 4.3 shows the

comparison of a cellulose acetate pure polymer dope with composition CA/NMP/Water –
20/70/10 wt. % (Figure 4.3(a)) and a CA/NaY polymer-sorbent dope with 50 wt. %
zeolite loading (Figure 4.3(b)). Selected fiber sorbent dopes were loaded into 10 ml
syringes and extruded into water bath to simulate its spinnability and qualitatively judge
the phase separation kinetics.

4.3. Single-layer fiber sorbent spinning

Table 4.1 describes the fiber sorbents dopes created with different polymer
binders and with different dope compositions. Each dope was defined based on a polymer
solution basis (which does not consider the zeolites dispersed in the dope), fiber sorbent
dope basis (which considers the overall fiber sorbent dope composition) and the dry fiber
sorbent basis (which considers the composition of a dry fiber with only zeolite sorbent
and polymer binder).

The zeolite loading (w_{ads}), defined based on the dry fiber weight basis, was the
ratio of the amount of zeolite sorbent in the dry fiber (W_{ads}) to the overall weight of the
dry fiber (amount of sorbent (W_{ads}) + amount of polymer binder (W_{poly})). The polymer
additives (PVP) in the fiber sorbent dope were not accounted in the overall dry fiber
weight, since the water-soluble PVP leaches out during the solvent exchange of the fibers
with DI water after fiber spinning (section 3.3.5.).

$$Zeolite\ sorbent\ loading, (w_{ads}) = \left(\frac{W_{ads}}{W_{ads} + w_{poly}} \right) \tag{4. 1}$$

$$Polymer\ binder\ loading, (w_{poly}) = 1 - w_{ads} = \left(\frac{W_{poly}}{W_{ads} + w_{poly}} \right) \tag{4. 2}$$

An initial cellulose acetate fiber sorbent dope composition of
CA/NMP/water/NaY – 17/58/8/17 wt.% (Figure 4.3(b) and Table 4.1 (a)) corresponding

to a 50 wt.% zeolite NaY loading (dry fiber wt. % basis) was identified and scaled-up to create 'spin' dopes (section 3.3.3.).

It was found that the CA core dope if kept on the roller for longer periods (up to 3-7 days), could not be spun due to agglomeration and aging of dopes [14] and partial settling of dispersed zeolite particles leading to frequent fiber breaks.

It is hypothesized that the presence of water, acidic conditions (due to acidic zeolites) and high temperatures on the roller could lead to partial hydrolysis of cellulose acetate polymer [15]. Hence fiber sorbents were spun within 48 h of the dope creation, contrary to at least a week in the case of hollow fiber membrane spinning. A fiber sorbent composition with polyester urethane/NMP/water/NaY - 13.5/58.2/8/20.3 wt. % Table 4.1(c)) was also determined using the cloud point technique. This corresponds to a 60 wt % zeolite NaY loading (dry fiber wt basis). The dope composition was scaled-up and Estane$^{®}$ fiber sorbents were spun. Polyester urethane dope had the undesirable tendency to stick to itself and other spinning apparatus including the quench bath and the take-up drum due to the rubbery nature of the polymer.

The fiber sorbent spinning process was briefly explained in section 2.5. A bore fluid (or internal coagulant) composition of 80/20 to 70/30 wt. % NMP/water was found to be a 'neutral' bore fluid based on the binodal curve and experimental observations. A neutral bore fluid prevents the formation of a non-uniform circular bore (in-case of high solvent content) and the formation of an internal skin layer (in-case of high non-solvent content).

Table 4.1: (a) CA/NaY (preliminary), (b) CA/NaY (optimized) and (c) Polyester urethane (Estane$^{®}$) / NaY fiber sorbent dope compositions in wt. %.

	ID	Basis (wt. %)	CA	Estane$^{®}$	NMP	Water	PVP	NaY
(a)	**CA-preliminary**	20% CA/50% loading						
		Polymer solution basis	20.0	-	70.0	10.0	-	-
		Fiber sorbent dope basis	17.0	-	58.0	8.0	-	17.0
		Dry fiber sorbent basis	50.0	-	-	-	-	50.0
(b)	**CA-optimized**	20% CA/60-75% loading						
		Polymer solution basis	20.0	-	68.0	9.0	3.0	-
	1	Fiber sorbent dope basis	12.5	-	42.5	5.6	1.9	37.5
		Dry fiber sorbent basis	25.0	-	-	-	-	75.0
	2	Fiber sorbent dope basis	14.6	-	49.6	6.6	2.2	27.1
		Dry fiber sorbent basis	35.0	-	-	-	-	65.0
	3	Fiber sorbent dope basis	15.4	-	52.3	6.9	2.3	23.1
		Dry fiber sorbent basis	40.0	-	-	-	-	60.0
(c)	**Polyester urethane**	17% Estane$^{®}$/60% loading						
		Polymer solution basis	-	17.0	73.0	10.0	-	-
		Fiber sorbent dope basis	-	13.5	58.2	8.0	-	20.3
		Dry fiber sorbent basis	-	40.0	-	-	-	60.0

Initially, a quench bath (0.4 m deep) with water as the external coagulant was used for the phase separation of the nascent fibers. However, due to the slower phase separation of hydrophilic cellulose acetate, the residence time in the quench bath was not enough to insure complete phase separation of the nascent fiber before contacting the first guide role (section 2.5.). This led to the deformation of the fiber bore which could lead to excessive pressure drop during fiber sorbent testing. Hence, a deeper quench bath (1 m deep) with water as external coagulant was used to achieve efficient phase separation of the extruded fiber and the problem of oval fibers was eliminated.

The effect of quench bath temperatures of 25°C and 50°C were studied with operating temperature (temperature of spinneret, pumps and transfer lines) kept ~25°C (Table 4.2). Air gap was kept low (~ 1-3 cm) to get instantaneous phase separation of the dope and avoid external skin layer formation. Wet spinning (0 cm air-gap) led to the phase separation of the dope at the spinneret annulus leading to the blockage and excessive pressure drop. Internal and external skin layer formation can create an additional layer of mass transfer resistance that are detrimental for fiber sorbent operation (appendix A.5.). The core dope flow rate was varied between 180-600 mL/hr and the bore fluid composition was typically varied between 0.3-0.5 of the core dope flow rate (Table 4.2). As expected, the fiber sorbent dope and bore fluid extrusion rates, take-up speed and the size of the spinneret annular die determine the outer and inner diameter of the hollow fibers [14].

Draw ratio is an important spinning parameter that affects the fiber morphology and productivity. The elongational stresses increase with the take-up velocity (m/min)

and decreases with faster extrusion rate (mL/h) and higher air-gap (cm). The draw ratio is defined as [14]:

$$\text{Draw ratio}, \frac{V_f}{<Vi>} = \frac{V_f \pi (D_c^2 - D_b^2)}{4Q_d} \tag{4.3}$$

Where, $<V_i>$ is average dope extrusion velocity, V_f is the take-up velocity, Q_d the volumetric dope extrusion rate, D_c (spinneret core diameter) and D_b (spinneret bore diameter). D_c and D_b determine the annular cross-section of the dope leaving the spinneret. Take-up rates up to 50 m/min are often achievable in case of pure polymer membrane spinning [16]. Low polymer and high sorbent content reduces the tensile strength of the fibers and a maximum achievable take-up rate of~ 30 m/min was achievable for 50 wt. % zeolite loading CA/NaY fibers (Table 4.1 (a)). Higher take-up rates up to 30 m/min were feasible for fibers with lower loadings i.e. 50 wt. % sorbent loading, but higher take-up rates increased the strain and tensile stress leading to fiber breakage.

It is important to note that some of the spinning parameters and fiber properties are contrary to asymmetric hollow fiber membrane spinning where it is desired to have a high air gap for the vaporization of a high volatility solvent and hence formation of a skin layer for effective separation.

Figure 4.4 shows the SEM images of the preliminary CA/NaY fiber sorbent spun with the above mentioned dope composition. Figure 4.5 shows the SEM images of the polyester urethane/NaY fiber sorbents. Fiber sorbent dope compositions and spinning conditions are summarized in Table 4.1(a), (c) and Table 4.2.
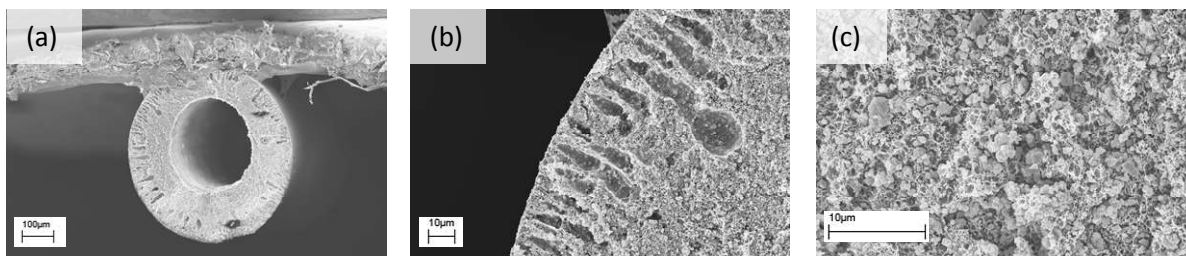
Figure 4.4 (left to right) (a): SEM image of the prelimneary CA/NaY fiber sorbent (50 wt % NaY loading). (b): SEM image close-up of a section of macrovoids in the fiber morphology. (c): NaY crystals exhibiting the desired 'sieve in a cage' morphology.
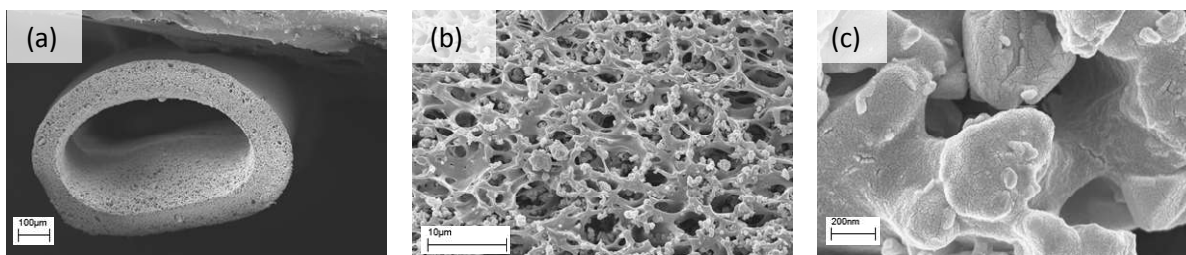
Figure 4.5 (left to right) (a): SEM image of the polyester urethane/NaY fiber sorbent (60 wt % NaY loading). (b): NaY crystal dispersion in the fiber morphology. (c): NaY crystals exhibiting the un-desired 'occluded sieve' morphology.

Table 4.2: Important spinning parameters and conditions for fiber sorbents

Dope (Core)	
Pump temperature	25 °C
In-line temperature	25 °C
Flow rate	180 - 600 mL/h
Bore fluid	
Composition	NMP:Water = 80:20-70:30 wt.%
Temperature	Room temperature
Flow rate	60 - 300 mL/h (0.3-0.5 of core flow rate)
Spinneret temperature	25 °C
Air temperature	Room temperature (~25 °C)
Air-gap	1-3 cm
Quench bath	
Media	Tap water
Depth	1 m
Temperature, T_{quench}	25 and 50 °C
Take-up rate (m/min)	10 - 30

With the creation of fiber sorbents using different polymers it was necessary to check for the desired morphology. SEM images (Figure 4.4 (c) and Figure 4.5(c)) indicated that CA / NaY fiber sorbents had the desired 'sieve-in-a-cage' structure, while polyester urethane fiber sorbents indicated an undesired 'occluded' sieve structure. Both fiber types showed close to Knudsen selectivity, which was expected due to high loading of sorbents, leading to defects in the fiber surface as shown in Figure 4.6(c). Knudsen selectivity shows that the separation does not occur by selective permeation through the fiber sorbent wall. It is rather through the selective sorption in the zeolite NaY dispersed in the fiber morphology as shown later. *With these advantages cellulose acetate was pursued as the polymer of choice for the fiber sorbent creation and the CA/NaY fiber sorbent morphology was further optimized.*

SEM analysis of CA/NaY fiber sorbents (Figure 4.4 (b)) indicated many macrovoids in the outer part of the fiber wall. Macrovoids are polymer lean phase with void sizes~ 10-50 μm, that reduce the mechanical strength of the fiber [17]. It can also lead to non-uniform mass transfer in the fiber sorbent wall, since convection through the macrovoids (~ 10-50 μm), is one-two orders of magnitude faster than the diffusion through the smaller voids (~0.1-1 μm) [18].

Various strategies have been proposed to remove macrovoid formation in the hollow fiber membrane literature [17, 19, 20]. Polyvinyl pyrrolidone (PVP) was added as a water soluble additive to suppress the creation of macrovoids and also act as a pore former [21, 22]. PVP was chosen over $LiNO_3$ (pore former discussed in section 4.2.), since it was commercially available over a large molecular weight window (M_n~20,000 – 1.3 million). Different molecular weight PVP can have varying effects on the fiber

porosity and dope viscosity. Fiber sorbent dopes were then created with varying amounts of PVP of different molecular weights.

The CA fiber sorbent dope composition was further optimized to CA/NMP/PVP (M_n ~ 55,000)/Water – 20/68/3/9 wt. %, and was found to give rapid phase separation in syringe extrusion experiments Table 4.1 (b)).

This composition (polymer solution basis) was fixed, and the zeolite loading was progressively increased to create fiber sorbents with 60, 65 and 75 wt. % zeolite loadings (dry fiber weight basis) Table 4.1 (b-1 to b-3)). A higher sieve loading was desired to obtain higher sorption capacity per unit mass of the fibers. Fiber sorbents with loadings higher than 75 wt. % could not be spun due to poor mechanical strength and inadequate phase separation (due to low polymer binder content).

Typically, for industrial pellets as well, a maximum of 75 wt. % sorbent loading was achievable. CA/NaY fiber sorbent spun with 75 wt. % sorbent loading Table 4.1 (b-1)) had a high sorbent loading with adequate mechanical strength to create fiber sorbent modules (section 3.3.6.). Spinning parameters for the CA/NaY fiber (optimized) were similar to the parameters for the CA/NaY fiber (preliminary) and are summarized in Table 4.2. However, in the case of fiber sorbents with 75 wt. % sorbent loading lower take up-rates (~ 15 m/min) were achievable with a maximum draw ratio of ~ 5, due to lower polymer binder content. Figure 4.6 shows the horizontal cross-section of the fiber sorbent with desired large pores/voids (~ 1-5 μm) due to the engineered dope and spinning conditions.
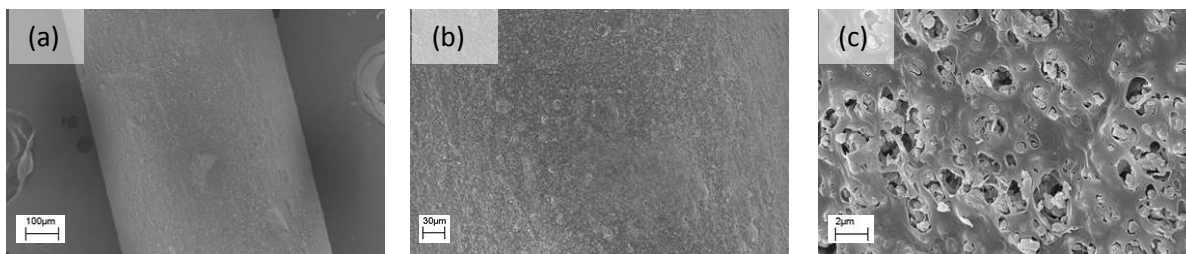
Figure 4.6 (left to right) (a): Horizontal cross-section SEM image of a CA/NaY fiber sorbent (optimized) (75 wt. % sorbent loading). (b): Enlarged view of image (a) showing the horizontal cross-section of a CA/NaY fiber sorbent. (c): Enlarged view of image (b) showing the defects in the fiber sorbent surface due to high sorbent loadings.

Figure 4.7(a) shows the SEM images of the CA/NaY fiber sorbent(optimized) with no visible macrovoids due to the addition of pore former (PVP) and enhanced viscosity (due to higher zeolite loading). Figure 4.7 (b) and (c) indicates zeolite NaY exhibiting the desired sieve-in-a-cage morphology in the cellulose acetate polymer matrix (appendix A.5.).
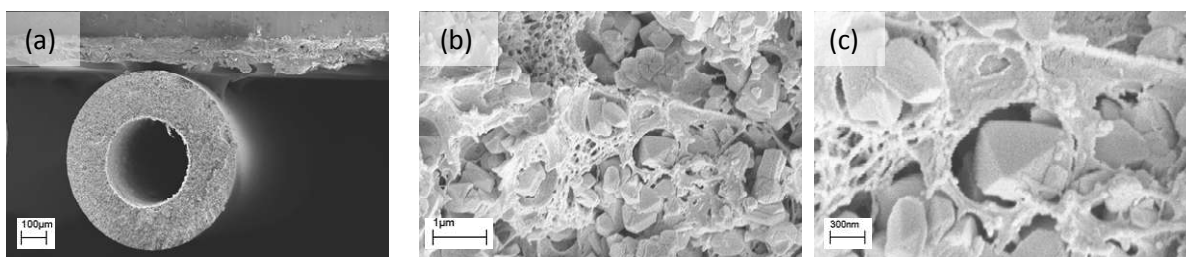
Figure 4.7 (left to right) (a): SEM image of the optimized CA/NaY fiber sorbent (75 wt % NaY loading) with desired dimensions and no macrovoids (b): NaY crystal distribution in cellulose acetate matrix (c): NaY crystal exhibiting the desired 'sieve in a cage' morphology.

EDX analysis can help determine zeolite distribution in the core layer. EDX images of the CA/NaY fiber sorbent (Figure 4.8) indicated a desired uniform distribution of zeolite crystals as evidenced by the uniform detection of sodium or silicon atom present only in zeolite NaY.
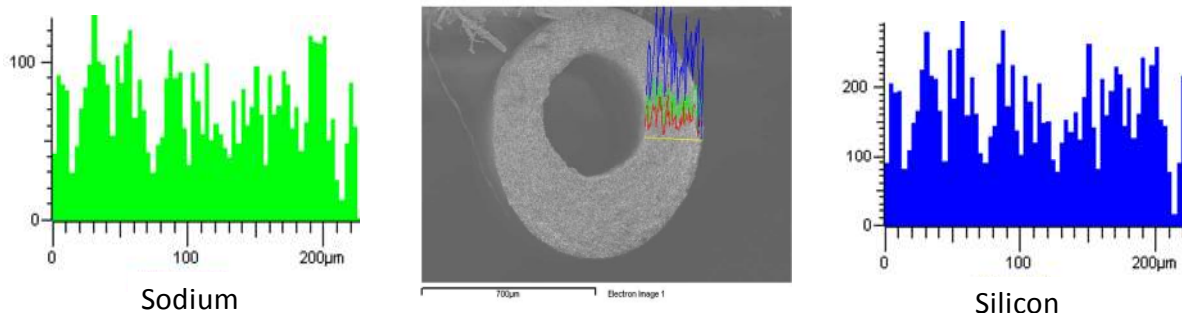
Sodium

Silicon

Figure 4.8: EDX image of CA/NaY fiber sorbent (75 wt% NaY loading) indicating uniform distribution of zeolite NaY crystals in fiber morphology. Line scan spectra of Sodium and Silicon elements are indicated.

4.4. Analysis of fiber sorbent morphologies

Permeance tests using the constant pressure system (described in section 3.4.8.1.) were conducted on single-layer fiber sorbents spun with variable zeolite loading and fiber spinning conditions. Table 4.3 summarizes the permeance (i.e. the pressure normalized flux) obtained in each of the fiber sorbent types. Dope composition (polymer, non-solvent and zeolite content) was found to have a greater effect on the permeance compared to the fiber spinning conditions.

A lower polymer and higher non-solvent concentration in the spin dope caused higher permeance. Fiber sorbents spun at a higher water quench bath temperature (50°C) were found to give higher permeance, possibly due to the faster phase separation of the extruded fiber because of higher diffusivity of water at higher temperatures [23]. Low air-gap (~ 1-3 cm) and the absence of volatile solvents and non-solvents prevented the formation of an external skin layer.

A bore fluid composition of NMP/Water – 70/30 wt. % was found to give a porous bore-core interface (Figure 4.9(a)), while a bore fluid with high non-solvent

content (NMP/Water – 50/50 wt. %) was found to give a dense bore-core interface due to the formation of an internal skin layer (Figure 4.9(c)). Formation of a dense internal skin layer was found to reduce the fiber permeance drastically due to the slower diffusion of gases through the polymer ($D_p \sim 10^{-6}$-10^{-12} cm^2/s) compared to the pores/voids ($D_{voids} \sim 10^{-1}$-10^{-4} cm^2/s) in fiber sorbent operation as discussed in section 2.4.4.

Table 4.3: Comparison of permeance and selectivities of fiber sorbents spun with the dope compositions (a) CA/NaY (preliminary) and (b-1 to b-3) CA/NaY (optimized) with different zeolite loadings. Temperate of measurement = 35 °C.

	Fiber sorbent type	Zeolite loading (wt. %)	Permeance - N_2 (P/ ℓ - GPU) at 30 psig	Selectivity (α_{O_2/N_2})
(a)	CA/NaY fiber (preliminary)	50	15,000 - 20,000	0.92 ± 0.10
(b-1)		75	90,000 - 110,000	0.92 ± 0.10
(b-2)	CA/NaY fiber (optimized)	65	50,000-80,000	0.94± 0.10
(b-3)		60	15,000 - 30,000	0.91± 0.10
$\alpha_{knudsen}$ (O_2/N_2)= 0.93				
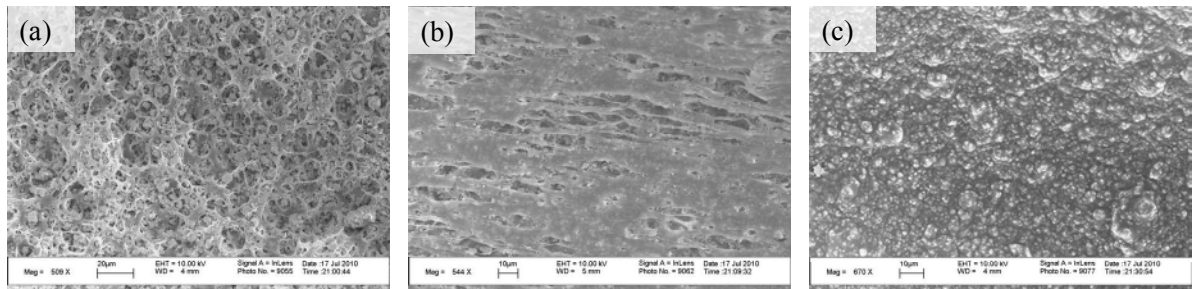
Figure 4.9 (left to right): Variation in the morphology of the bore-core interface with the variation in the bore fluid composition. Horizontal cross-section SEM images of the bore-core interface of a CA/NaY fiber sorbent viewed from the bore with (a) 70/30 wt. % NMP/Water bore fluid (b) 60/40 wt. % NMP/Water bore fluid (c) 50/50 wt. % NMP/Water bore fluid.

Table 4.3 shows the permeance of CA/NaY fiber sorbents was found to increase with higher zeolite loadings. Figure 4.10 shows that with an increase in the zeolite loading, the number and size of voids/pores increases. The bulk flow due to the applied pressure gradient through the fiber increases with higher porosity (ε_{pore}) and larger void

sizes (r_{pore}), thus increasing the permeance with higher sorbent loading as observed in Table 4.3.
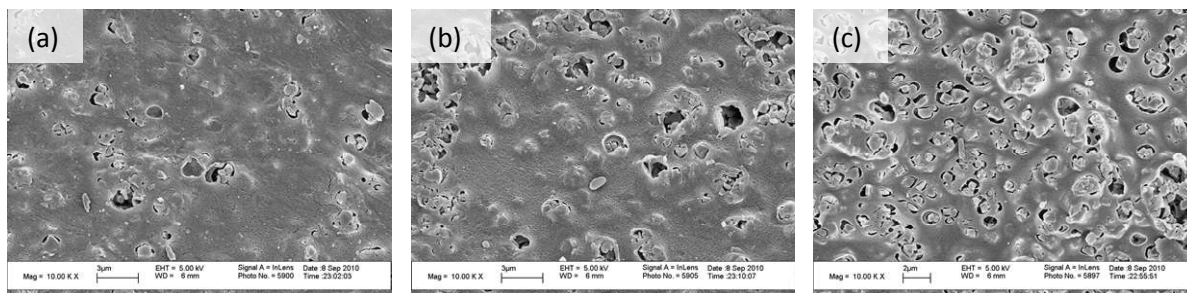
Figure 4.10: Horizontal image showing the outer part of the core layer in a CA/NaY single layer fiber sorbent (optimized) with (a) 60 wt. % sorbent loading (b) 65 wt. % sorbent loading (c) 75 wt. % sorbent loading.

4.5. Equilibrium sorption

Equilibrium sorption was conducted using a quartz spring setup with tertiary butyl mercaptan (TBM) as the odorant as described in section 3.4.7.1. Equilibrium sorption on zeolite NaY indicated high affinity for TBM with saturation capacity of 1.14 mmole TBM/g NaY. The sorption data indicated type – I isotherm, and was fitted to the Langmuir model (section 2.4.2.1.) [24].

The saturation capacity of TBM on zeolite NaY was found to be lower than the capacity of~ 2 mmole TBM / g NaY reported in literature [25, 26]. The reasons for the lower capacity were further explored.

The zeolite samples were loaded into the jacketed chamber and evacuated for 48 h by pulling vacuum to remove the water vapor sorbed in the zeolite crystals (section 3.4.7.1.). It is hypothesized that pulling vacuum was inadequate to remove sorbed water vapor. The jacketed chamber could not be heated above 70°C, due the evaporation of water (circulation fluid).
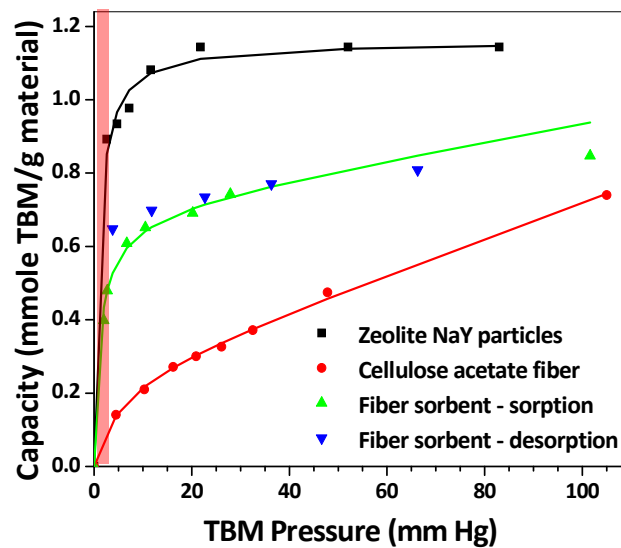
Figure 4.11: Equilibrium isotherms of pure TBM on CA / NaY fiber sorbent (50 wt % NaY loading) and its comparison with zeolite NaY crystals and pure CA hollow fiber measured at 35°C. (The region highlighted in red shows the expected sulfur concentration in actual pipeline natural gas.)

Water was then replaced with silicone oil as the circulating fluid and the chamber could be heated up to 110 °C; however, the silicone oil turned from colorless to dark brown due to continuous circulation at high temperatures. This led to difficulties in accurately observing the reference pointer of the quartz spring and hence the determination of the weight changes due to vapor sorption.

Due to the practical difficulties with silicone oil as the circulation medium, water was preferred and the protocol described above was followed. Since the quartz spring experiments were conducted to demonstrate the nature of the isotherms, the incomplete activation of the zeolite samples can be considered as the worst-case or baseline scenario.

During the flow testing of samples under realistic natural gas (NG) feed conditions the partial pressure of sulfur odorants will be about 0.05 mm Hg as shown by the red highlighted region. In the flow testing of the fibers or zeolite crystals, the samples

could be completely activated or regenerated by drying at 120°C to remove sorbed water vapor as described later in section 4.8.

CA pure polymer hollow fiber sorption data indicated much less sorption capacity for TBM compared to that of zeolite NaY. The data were fitted to the dual mode model (section 2.4.2.2.) [27]. CA / NaY fiber sorbent (50 wt. % zeolite loading, dry fiber wt. basis, Figure 4.11.) demonstrated high sorption capacity for TBM and showed complete regeneration during the desorption step by decrease in pressure, thereby indicating reversible physisorption.

Fiber sorbents gave a capacity identical to the value predicted by adding the capacities of CA polymer hollow fiber and zeolite NaY crystals based on their loadings in the CA/NaY fiber sorbent. This further shows that the CA/NaY fiber sorbents indicated a desired morphology where the zeolite crystals were fully accessible to the sulfur odorant. Very low pressures < 1 mm Hg were difficult to control with the existing equipment and hence this experiment was used to demonstrate the nature of the isotherms, while flow experiments were performed with realistic feeds.

Attempts to perform kinetic sorption measurements using the quartz spring setup verified extremely rapid equilibration (~ seconds), which could not be accurately quantified because of the short time scale of sorption [28].

4.6. Transient sorption

Pressure decay sorption was used to determine the sorption kinetics of pure zeolite NaY particles and single-layer fiber sorbents using iso-butane C_4H_{10} (σ~5.2 Å) as a surrogate gas for TBM $C_4H_{10}S$ (σ~ 6 Å) as explained in sections 3.1.4. and 3.4.7.2. Zeolite adsorption kinetics are difficult to measure accurately due to the exothermic

nature of the adsorption process [29, 30]. These heat effects obscure the nature of the kinetics due to non-isothermal behavior.

Typically, small zeolite crystals (sub-micron scale) reach equilibrium in fraction of seconds [28]. Thus, for the accurate measurement of diffusion coefficients the time scale is lengthened by use of larger zeolite crystals [28].

Transient sorption was used to determine the approximate time scale for diffusion and sorption of gas molecules into the zeolite particles. From the uptake curve (Figure 4.12) it was found that the diffusion of gas molecules in pure NaY crystals and porous CA-NaY fiber sorbents (50 wt. % zeolite loading, dry fiber wt. basis) with the same zeolite crystals were comparable. The small half times (~ 1 s) in both the cases indicated fast diffusion of gas.

Rapid diffusion of gas molecules through the fiber sorbent wall and sorption into the zeolite crystals is crucial to prevent pre-mature breakthrough of sulfur odorants during actual operations (on-site hydrogen generation).
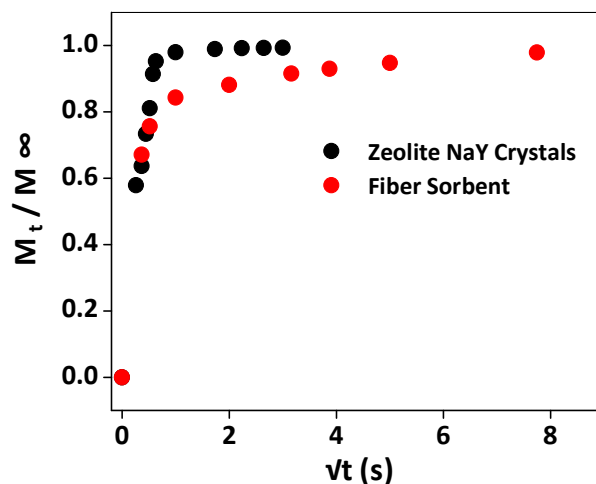
Figure 4.12: Transient sorption isotherm of iso - butane (surrogate gas) on zeolite NaY crystals and CA/NaY fiber sorbent (50 wt % NaY loading, dry fiber wt. basis).

Fiber sorbents reached saturation relatively slowly compared to the zeolite NaY particles after $M_t/M_\infty \approx 0.8$. This can be attributed to the slower diffusion and sorption of gas molecules in the cellulose acetate polymer which acts as the binder material. These experiments justify the selection of small zeolite crystals ($d_c \sim 300\text{-}700$ nm) to minimize micropore diffusional resistance and large pore window zeolite NaY (7.4 Å) which does not cause transport resistance for the sorption of the sulfur gases (3-6 Å). The results can be indicated as the worst case scenario where the kinetics were obscured due to non-isothermal behavior and signal measurement limitations (~ 1 second).

However, in actual experimentation the behavior was expected to be isothermal due to the low concentration of sulfur gases (~ 30 ppm).

4.7. Flow testing procedure and setup

Testing of fiber sorbents under realistic flow conditions is important to determine applicability as a new separations platform. An ideal single and dual-layer fiber sorbent should give dynamic and equilibrium capacity (normalized) equivalent to pure zeolite crystals based on sorbent loading. A small scale facility was designed to replicate conditions similar to an actual plant scale operation. Initially, the setup was constructed with the ability to conduct sorption tests with sulfur gases and regeneration with a purge gas. The system was later modified to enable the regeneration with steam and cooling water (section 7.1.). The gases utilized were 35 ppm TBM / N_2 and 35 ppm H_2S / N_2 as test gases and Nitrogen (UHP grade, Airgas) as the purge gas (section 3.1.4.). The schematic of the flow setup is shown in Figure 4.13. The fiber sorbent test rig and lecture bottles (small compressed gas cylinders, typically 2-3 inches in diameter and 12-18 inches in height) of sulfur gases were located inside a fume hood for safety reasons.

Teflon® tubing (1/8" O.D., 1/16" I.D., McMaster) was used to prevent any sulfur sorption on the working surfaces of the system. The sulfur gases passed through a flow controller (Model: FMA-A2305-SS, Omega engineering Inc., Stamford, CT) to obtain a desired flow rate between 0–500 cm³/min. The sulfur gas concentration could be further diluted by the addition of Nitrogen. The stream would then flow through the module during sorption or bypass it during the sulfur analyzer calibration.
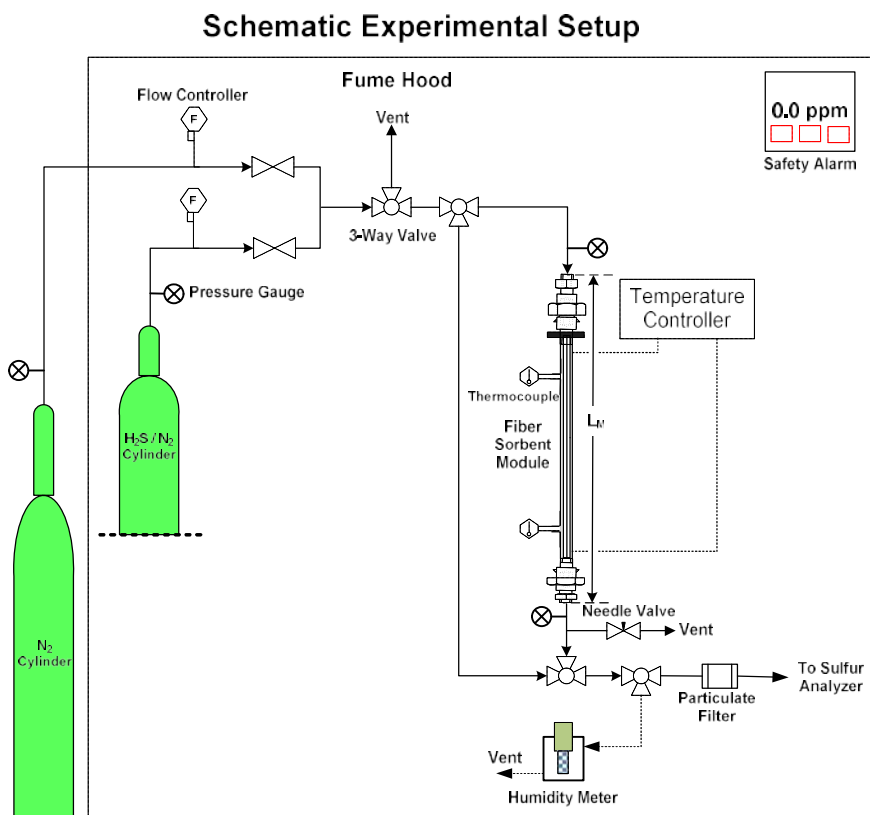
Figure 4.13: Schematic of flow testing setup

The test modules, with a shell and tube configuration, were made using stainless steel ¼ inch tubes and fittings using a technique similar to potting hollow fiber membranes [31]. The modules were made with an active length between 15-55 cm with˷ 1-6 fibers. The active fiber length was taken as the entire module length (L_M) as it

contributes to sorption, (Figure 4.13) as opposed to the module length (L_P) between the epoxied regions taken in the case of permeation testing (section 3.4.8). In flow experiments to determine sulfur sorption capacity of the fibers, a bore side feed of the test gas (30 ppm TBM/N_2 or 30 ppm H_2S/N_2) and a bore side collection was used as it provides advantage of lower bypass and channeling compared to shell side feed as discussed in section 2.6. Sulfur alarms were installed in the fume hood and near the sulfur analyzer to detect any sulfur leakage in the lab.

Studies were also conducted with zeolite NaY crystals packed in a fritted Pyrex® tube (½ inch O.D., wall thickness 1/32 inch, bed depth 1-2 cm). Zeolite NaY crystals (d_c ≈ 500 nm) were dispersed in sand (Fisher scientific, Pittsburgh, PA) to ensure uniform distribution in bed and prevent premature breakthrough. Appropriate correction was applied to account for the finite sorption capacity of the sand particles. The amount of TBM or H_2S adsorbed during the run was calculated by integration from the initial concentration to the final equilibrium concentration using numerical integration (trapezoidal rule) (section 2.4.3.).

Before every adsorption run the modules were heated to 120°C using heating tape (Briskheat^{TM}, Barnstead International, Dubuque, IA) regulated by a temperature controller (Model: EW-02155-52, Cole-Parmer Inc., Vernon Hills, IL) for 24 hours under a nitrogen purge at 200 cm^3/min to remove trace amounts of water sorbed in the beds. The reactor was then cooled down to ambient conditions (~25°C). The nitrogen purge was then shut-off; however a nitrogen pressure of around 10 psig was maintained in the module to prevent sorption of air or water vapor from the atmosphere into the activated fiber sorbents through any leak points. Before each run, averages of 4–5 readings were

taken to calibrate the sulfur analyzer and determine the equilibrium concentration (C_o) of the bottled gas. Once the analyzer readings were stable, the module was depressurized to atmospheric pressure by allowing the N_2 to exit the module, while simultaneously feeding the sulfur gas to the module.

For proof-of-concept regeneration studies on fiber sorbent modules, the same heating protocol was followed. The setup was instrumented with digital pressure gauges (Model: DPG1100B-30G, Omega engineering Inc., Stamford, CT) located at the inlet and outlet of the module. J-type thermocouples were connected on the shell side of the fiber sorbent module to measure the temperature variation during the sorption step. The gas flow from the module was then passed through a t-joint with the gas flow rate to the sulfur analyzer regulated at 80 cm^3/min by a needle valve. The gas was passed though a 0.5 μm filter to remove any entrained fine particles before the sulfur analyzer.

Sample analysis was performed by a H_2S / total sulfur analyzer (Model 902, Galvanic Applied Sciences, Houston, TX) graciously provided by Chevron technology ventures. The analyzer was based on a lead acetate tape detection method. This method relied on the chemical reaction of H_2S with a lead acetate impregnated paper tape to form lead sulfide. The concentration of H_2S was determined by the extent of staining on the tape and displayed on a screen.

The equipment was used for the measurement of sulfur odorants (mercaptan, thiols, and sulfides, section 1.4.) by measuring the total sulfur concentration by mixing of the sample stream with hydrogen and then passing it through a quartz tube heated to 1000°C [32]. This process would quantitatively convert the sulfur bearing compounds to H_2S, which were then measured at the tape. The instrument was calibrated for

concentrations in the range of 0–50 ppm using pre-mixed calibration standard gases. The equipment had a lower detection limit of 0.1 ppm, an accuracy of ± 1 ppm and a sample analysis time of 1-3 minutes. The breakthrough time (t_b) for the flow analysis was taken as the time taken for the outlet sulfur concentration to reach 1 ppm (C_b). Vent gases from the analyzer and the setup were purged-off into the fume hood.

4.8. Sorption studies under flow conditions with TBM/N$_2$

Initially, flows through sorption studies were performed with the stimulant 30 ppm TBM/N$_2$ using the setup as described in section 4.7.

Single-layer CA/NaY fiber sorbent module with 75 wt. % loading (dry fiber wt basis) created by the optimized dope composition mentioned in Table 4.1 (b-1) were tested under 30 ppm TBM/N$_2$. The fibers showed high sorption capacity with the breakthrough capacity 1.4 mmole TBM / g fiber (normalized (based on sorbent loading): 1.86 mmole TBM / g sorbent), and a saturation capacity of 1.5 mmole TBM / g fiber (normalized (based on sorbent loading): 2 mmole TBM / g sorbent) as shown in Table 4.4. The length of unused bed (LUB) and the ratio LUB/L$_M$ (section 2.4.3.3.) were found to be low indicating good utilization of bed capacity.

TGA analysis was used to determine the exact weight loss by CA/NaY fiber sorbents and pure NaY crystals due to the removal of sorbed water when dried at 120°C. CA/NaY fiber sorbents (75 wt % NaY loading) indicated a weight loss of about 16.5 wt%, while pure zeolite NaY crystals indicated a weight loss of 21.5 wt %. Weight loss corrections were applied to accurately determine sulfur sorption capacities. Also, the "void capacity" due to the presence of gas molecules in the module void space (appendix B) was accounted when determining sulfur breakthrough/saturation capacity.

Table 4.4: Breakthrough, saturation capacities and fiber characteristics of a CA / NaY fiber sorbent module (75 wt % NaY loading) tested with 30 ppm TBM/ N_2 (Length of the module - L_M = 53 cm)

CA/NaY fiber weight (g)	0.7
Breakthrough capacity (mmole TBM / g fiber)	1.4
Saturation capacity (mmole TBM / g fiber)	1.5
LUB (cm)	3.6
LUB/L_M	0.07

The saturation capacity was higher than the saturation capacity measured during the quartz spring experiments (section 4.5.). The results matched well with the literature values of TBM sorption on zeolite NaY described in section 4.5. The good match between the literature and experimental values indicates that the zeolite crystals in the fiber sorbents were completely activated and were accessible for gas sorption. This shows that the fiber sorbents can be used effectively for the removal of sulfur impurities from pipeline natural gas.
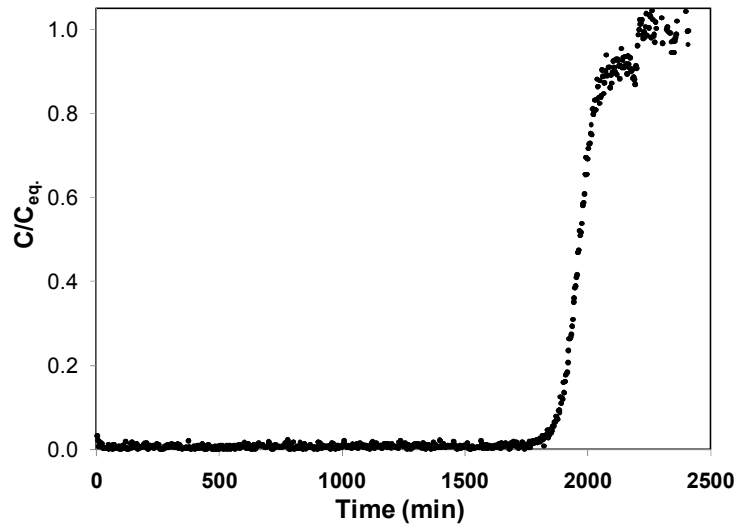
Figure 4.14: Concentration profiles of TBM effluent as a function of time on a CA / NaY fiber sorbent module (75 wt % NaY loading), O.D. ≈ 840 μm, I.D. ≈ 400 μm, L_M = 53 cm, N_f = 5 fibers) (Feed condition: 30 ppm TBM/ N_2, Flow rate = 400 cm^3/min, T = 298 K, p = 1 atm, activation for 48 hours at 393 K under N_2 purge).

However, as noted in section 3.1.4., it took roughly 1-3 days to complete one sorption run (Figure 4.14), which required continuous monitoring of the gases. *For the ease of operation and safety reasons, 30 ppm H_2S/N_2 was selected as the test gas and experiments were performed.*

4.9. Sorption studies under flow conditions with H_2S/N_2

Breakthrough and saturation capacities of three CA/NaY fiber sorbent modules with 75 wt % zeolite loading (dry fiber wt basis) created by the optimized dope composition mentioned earlier Table 4.1 (b)) were tested with 30 ppm H_2S/N_2 gas as indicated in Figure 4.15. Breakthrough, saturation capacities and fiber characteristics of these modules are indicated in Table 4.5.

Table 4.5: Breakthrough, saturation capacities and fiber characteristics of CA / NaY fiber sorbent modules (75 wt % NaY loading)

Sample	Module 1	Module 2	Module 3
CA/NaY fiber weight (g)	0.5	0.6	1.0
Breakthrough capacity (mg H_2S / g fiber)	0.6	0.65	0.53
Saturation capacity (mg H_2S / g fiber)	0.66	0.71	0.63
Outer diameter of fibers (O.D. - μm)	840	840	920
Inner diameter of fibers (I.D. - μm)	400	400	460
Number of fibers (N_f)	4	5	5
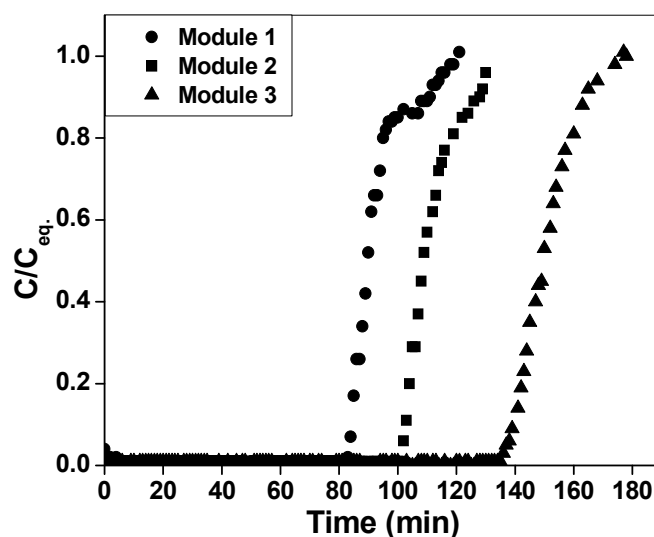
Figure 4.15: Concentration profiles of H_2S effluent as a function of time on three CA / NaY fiber sorbent modules (75 wt % NaY loading, $L_M = 53$ cm) (Feed condition: 30 ppm H_2S / N_2, Flow rate = 80 cm^3/min, T = 298 K, p = 1 atm, activation at 393 K under N_2 purge for 24 hours)

Fiber sorbents showed a sharp, symmetrical S–shaped sorption curve indicating no premature breakthrough. Moreover, channeling of gas through the fiber sorbent bore was not observed, indicating fast diffusion and easy access of gas to zeolites in the fiber sorbent morphology.

Two NaY crystal beds were tested to determine the concentration profiles in case of pure sorbent testing. Zeolite NaY crystals ($d_c \approx 500$ nm) indicated high sorption capacity for H_2S gas under flow conditions as shown by the concentration plot as a function of time in Figure 4.16.

Flow testing on CA polymer particle beds was also performed to determine sorption capacity. It was found that the polymer binder CA, showed negligible sorption capacity at these low concentrations. To maximize sorption capacity, we sought to

minimize the polymer wt % in the fiber sorbent, while balancing negative effects on fiber strength as polymer binder levels are reduced.
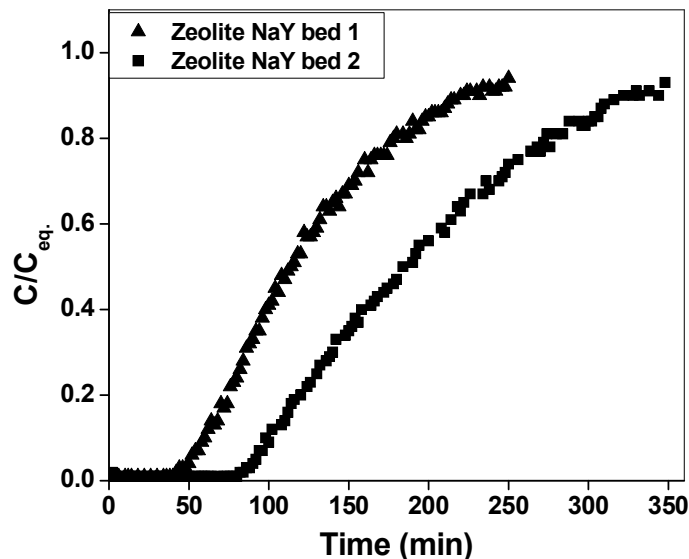
Figure 4.16: Concentration profiles of H_2S effluent as a function of time on two NaY crystal packed bed (Feed condition: 30 ppm H_2S / N_2, Flow rate = 80 cm^3/min, T = 298 K, p = 1 atm, activation at 393 K under N_2 purge for 24 hours)

Table 4.6: Breakthrough and saturation capacities in NaY crystal packed bed

Sample	Bed 1	Bed 2
Zeolite NaY weight (g)	0.25	0.4
Breakthrough capacity (mg H_2S / g sorbent)	0.88	0.82
Saturation capacity (mg H_2S / g sorbent)	1.73	1.6

The average zeolite NaY breakthrough and saturation capacity based on 75 wt % loading in fiber sorbent was calculated to be about 0.7 and 1.24 mg/g respectively. The saturation capacity in fiber sorbents (Table 4.5) was low compared to the zeolite NaY crystal bed and the reasons were further explored. Advantageously, negligible pressure difference was observed in the fiber sorbent, while in the case of NaY crystals bed, the

pressure varied between 2–4 psig depending on the crystal packing. This indicates that due to higher pressure drop, small crystals cannot be used in industrial operations. Variation in temperature of the modules during the sorption step was not observed considering the small amount of sorbent tested and the dilute streams used.

4.10. Regeneration studies on fiber sorbents

Proof-of-concept regeneration experiments indicated that fiber sorbents were regenerable using temperature swing operation. The breakthrough and saturation sorption capacity after five cycles are depicted in Figure 4.17 and is compared to the sorption capacity of zeolite NaY crystal bed. Fiber sorbents gave a capacity identical to the value predicted by adding the capacities of CA polymer binder and zeolite NaY crystal fillers based on their loadings in the CA/NaY fiber sorbent. The predicted capacity in Figure 4.17 indicates the best possible sorption capacity by a 75 wt% CA/NaY fiber sorbent. It should be mentioned that the measured sorption capacity of pure NaY crystals is higher than fiber sorbent mainly due to the absence of a binding material. The binding material gives negligible sorption capacity but is essential to prevent high pressure drop and particle attrition, so for typical pellets with binders, similar capacities per gram of sorbent would be seen.

After each regeneration cycle the fiber sorbent capacity increased slightly, became consistent after the third cycle and approached the maximum possible capacity that can be attained by a 75 wt % loading fiber. It is hypothesized that small amount of water sorbed in the fiber pores was removed after the first few regeneration cycles, thus increasing the capacity and remaining consistent thereafter. The regeneration of fiber sorbents over a number of cycles demonstrates its attractiveness as a separations material.
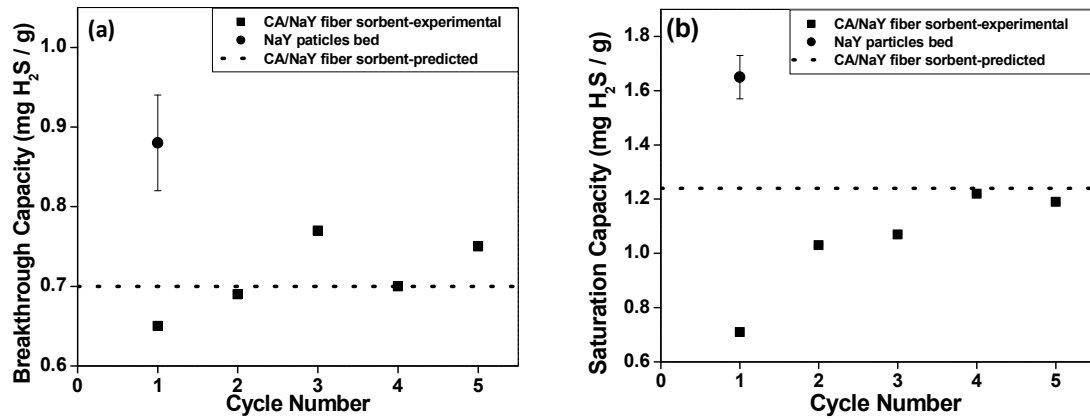
Figure 4.17: (a) Breakthrough capacity (b) saturation capacity of CA / NaY fiber sorbent module (75 wt % NaY loading, O.D. ≈ 840 μm, I.D. ≈ 400 μm, L_M = 53 cm) over 5 cycles and comparison with zeolite NaY crystal bed (Feed condition: 30 ppm H_2S / N_2, dried fiber weight = 0.6 g, flow rate = 80 cm^3/min, T = 298 K, p = 1 atm, activation and regeneration at 393 K under N_2 purge for 24 hours).

4.11. Effect of flow rates on the performance of fiber sorbents

In fiber sorbent operation one of the main concerns is possible channeling of the gas through the bore without sorbing into the zeolites in the fiber sorbent morphology. This was tested by the variation of gas flow rate through the module (Figure 4.18). The gas hourly space velocity (GHSV – flow rate of gas at 25°C and 1 atm pressure (m^3/hr) / volume of fiber bed (m^3)) in typical industrial packed bed operations varies from 5000 hr^{-1} to 20,000 hr^{-1} [33]. A CA/NaY fiber sorbent module with 75 wt % NaY loading used in this study was initially activated for 48 hours and then regenerated for 24 hours after each sorption run. Premature breakthrough was not observed with the variation in flow rate, indicating the expected rapid radial diffusion of gas to the zeolites in the fiber sorbents with relatively small wall thickness (th_{wall} ≈ 200 μm). Also, the breakthrough capacities were not found to vary significantly with the variation of gas flow rates (Table 4.7).
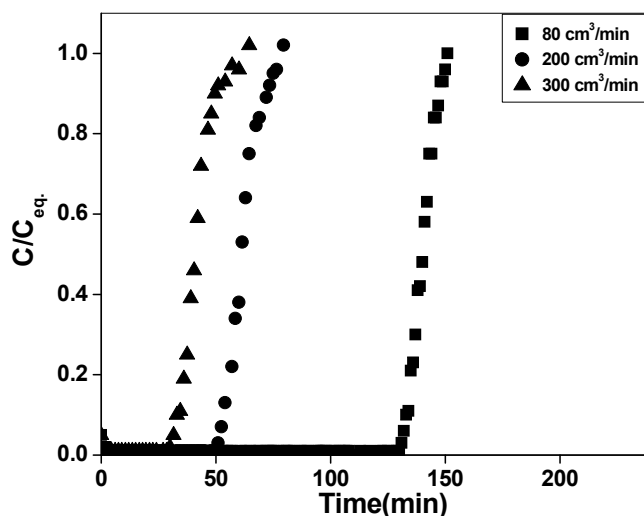
Figure 4.18: Concentration profiles of H_2S effluent as a function of time on a CA / NaY fiber sorbent module (75 wt % NaY loading, O.D $\approx$ 840 μm, I.D. $\approx$ 400 μm, L_M = 53 cm) with varying flow rate (Feed condition: 30 ppm H_2S / N_2, T = 298 K, p = 1 atm, activation for 48 hours and regeneration for 24 hours at 393 K under N_2 purge).

Table 4.7: Effect of variation of flow rate on breakthrough and saturation capacity of a CA / NaY fiber sorbent module (75 wt % NaY loading)

Flow rate (cm³/min)	80	200	300
Gas Hourly Space velocity (GHSV) (h⁻¹)	4600	11,500	17,250
Breakthrough capacity (mg H₂S / g fiber)	0.77	0.75	0.70
Saturation capacity (mg H₂S / g fiber)	1.07	1.19	1.22

4.12. Modifications to the flow setup (water vapor content measurement)

It is important to remove sorbed water vapor and activate the zeolite crystals in the fiber sorbent before each sorption run. In some of the previous experiments the modules were dried for 24-48 h at 120 °C, with a N_2 flow rate of 200 cm³/min. It was observed that up to 48 h were required to completely activate the fiber sorbents.

However, to better quantify this observation, to study the profile of water vapor removal from the fiber sorbents and to detect the water permeance through a dual layer

fiber sorbents (sections 7.4. and 7.5.), a dew point meter (Model: SDT-ZT, Shaw moisture meters, Bradford, UK) was connected downstream of the module as shown in Figure 4.13.

The flow was directed to the dew point meter during the activation or the regeneration step, while the flow was directed towards the sulfur analyzer during the sorption step using a three way valve (Figure 4.13).
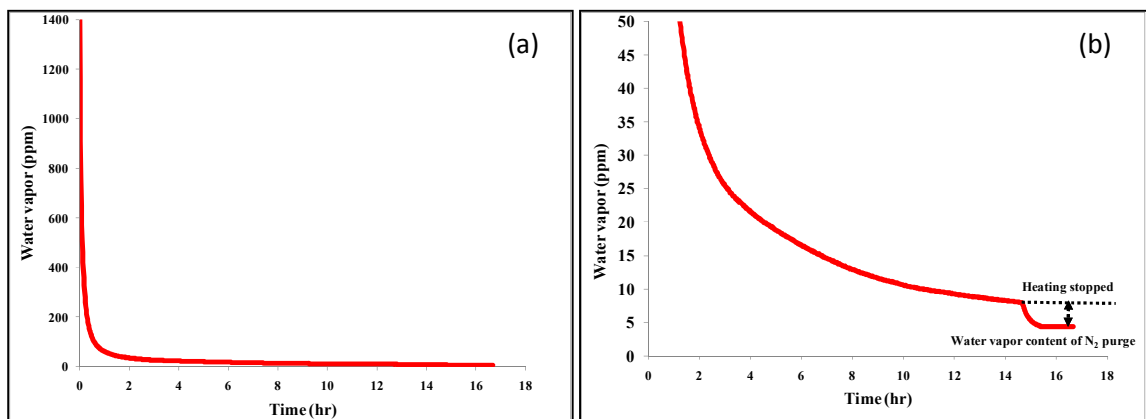
Figure 4.19: Drying profile of a fiber sorbent module heated to 110 °C, with a N_2 purge at 800 cm^3/min flow rate. (a) Indicates the complete drying profile (b) Is the blown-up view of (a) showing the low water vapor concentration region.

The water vapor content of the N_2 purge was indicative of the presence of sorbed water vapor in the zeolite loaded fibers. The water vapor content of bottled N_2 was less than 5 ppm (Figure 4.19 (b)). Most of the sorbed vapor was removed in the first few hours (2-3 h) of drying; however it took 12-48 h to lower the water vapor content to~10 ppm (Figure 4.19 (a) and (b)).

The drying time was found to vary depending on the number of fibers, purge flow rate, humidity, and temperature of activation. The zeolites in the fiber sorbents were considered activated when the water vapor content fell below 10 ppm [34, 35]. The

reactor was then cooled down to ambient conditions (~25°C) and sorption runs were started at atmospheric pressure as described in section 4.7.

The addition of the dew point meter gave a better understanding of the drying characteristics of the fiber sorbent. It was later verified that it took roughly 48 h to dry the fiber sorbent modules tested earlier (sections 4.8. to 4.11.) under a 200 cm^3/min N_2 purge at 120 °C. This can explain the slightly lower breakthrough and saturation capacities in the fiber sorbent modules dried for 24 h (section 4.10.) and would gradually improve after a few regeneration cycles due to further removal of water vapor and eventually become constant (Figure 4.17).

Hence, in future runs the fibers were dried under a variable N_2 purge flow rate which would change the activation time of the module and the drying could be stopped accurately based on the estimation of the water vapor content in the fiber sorbents.

4.13. Effect of zeolite loading on single-layer fiber sorption capacity

Sorption experiments were performed to determine the effect of zeolite loading on the porosity and breakthrough capacity of single-layer fibers. Permeation results indicated a higher permeance in case of fiber sorbents with higher sorbent loading as discussed in section 4.4. and Table 4.3. Sorption experiments were performed on fibers of the same 'spin state' with one and multiple fiber (~4) modules.

It must be realized that high breakthrough or dynamic capacity is crucial for fiber sorbent operation since in the actual industrial operation, the fiber sorbent main bed will be switched (to undergo regeneration) with an auxiliary bed once a breakthrough concentration of 1 ppm is reached.

4.13.1. 'One' fiber module experiments

The breakthrough capacity (Table 4.8) and permeance (Table 4.3) of single-layer fiber sorbents increased with higher loadings. The ratio of length of unused bed to fiber module length (LUB/L_M) decreased with higher loadings, indicating that a smaller fraction of the bed remained un-used. The observations can be explained by examining the mass transfer effects. The external mass transfer coefficients (Appendix A.5.2.) in each case were similar due to the same H_2S/N_2 flow rates (80 cm^3/min) and similar fiber dimensions (inner diameter (I.D.) and fiber length (L_f)) used in the studies [36]. The "void capacity" due to the presence of gas molecules in the module void space (appendix B) was accounted when determining sulfur breakthrough/saturation capacity.

The meso/maco porous mass transfer through the fiber sorbent wall improves with an increase in the diffusion coefficient through the voids/pores. The diffusion coefficient or the permeance through the voids improved with higher sorbent loading as explained in section 4.4. A faster meso/macro mass transfer enables faster access of sulfur molecules to the zeolite crystals in the fiber wall, thus improving the breakthrough capacity.

The breakthrough capacity (normalized) in case of 'one' fiber module experiments (Table 4.8) was found to be lower as compared to the breakthrough capacity of pure zeolite NaY crystals. The reasons for this behavior were further explored.

Table 4.8: Effect of zeolite loading in *one* fiber module experiments of CA/NaY single-layer fiber sorbents created with the optimized dope. Fibers spun under similar spinning conditions. Module length L_M = 53 cm. Feed condition: 30 ppm H_2S / N_2, T = 298 K, p = 1 atm, flow rate = 80 cm^3/min, activated at 393 K under N_2 purge till water vapor concentration < 10 ppm.

Fiber spin ID	Zeolite loading	Breakthrough capacity	Breakthrough capacity (normalized)	LUB/L_M
	(Wt. %)	mg H_2S/g fiber	mg H_2S/g sorbent	
(b-1)	75	0.55	0.73	0.15
(b-2)	65	0.33	0.51	0.22
(b-3)	60	0.24	0.40	0.64

4.13.2. 'Multiple' fiber module experiments

Single-layer CA/NaY fiber sorbents of the 'spin' states used for testing 'one' fiber modules were now potted into a hollow fiber module with 'multiple' fibers (4 fibers) and tested under similar flow conditions (H_2S/N_2 flow rate (80 cm^3/min)).

Table 4.9: Effect of zeolite loading in *multiple* fibers module experiments of CA/NaY single-layer fiber sorbents created with the optimized dope. Fibers spun under similar spinning conditions. Module length L_M = 53 cm, Number of fibers N_f = 4. Feed condition: 30 ppm H_2S / N_2, T = 298 K, p = 1 atm, flow rate = 80 cm^3/min, activated at 393 K under N_2 purge till water vapor concentration < 10 ppm.

Fiber spin ID	Zeolite loading	Breakthrough capacity	Breakthrough capacity (normalized)	LUB/L_M
	(wt. %)	mg H_2S/g fiber	mg H_2S/g sorbent	
(b-1)	75	0.73	0.97	0.03
(b-2)	65	0.6	0.93	0.13
(b-3)	60	0.55	0.91	0.13

Breakthrough capacity of single-layer fibers in 'multiple' fiber modules (Table 4.9) was found to be higher compared to 'one' fiber modules (Table 4.8). The breakthrough capacities (normalized) were found to be slightly higher for higher zeolite

115

loadings, and became equal to or slightly greater than the pure zeolite crystal breakthrough capacity [36].

The improved breakthrough capacities can be explained by considering the improvements in meso/macroporous mass-transfer due to multiple fibers in a module. In single-layer fiber sorbents due to high porosity and voids in the fiber wall, the module is filled with H_2S/N_2 gas during the sorption step.
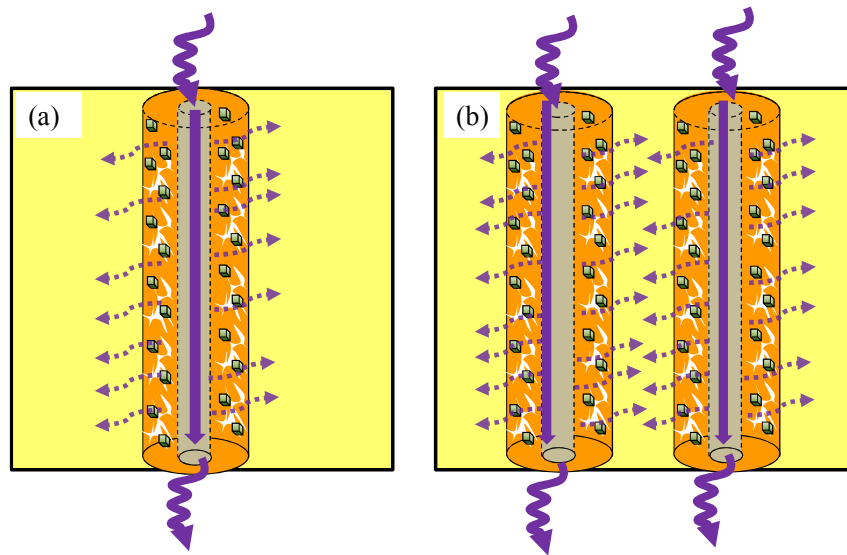
Figure 4.20: Effect of enhanced surface area affecting meso/macro porous resistance in (a) one fiber module compared to (b) multiple fibers module in single-layer fiber sorbents.

In the multiple fiber case, the mass transfer can thus occur through both sides of the fiber wall (Figure 4.20 (b)) compared to mass transfer only through the bore in case of 'one' fiber experiments (Figure 4.20 (a)).

This increase in the contact surface area / volume ratio improves the meso/macro porous mass-transfer rate by a factor of 3 as explained below, thereby improving the breakthrough time and capacity.

$Usually, for \dfrac{M_t}{M_\infty} \leq 0.5$ for various geometries,

$$\frac{M_t}{M_\infty} = 2(a_f)\sqrt{\frac{D_{voids}t}{\pi}} \quad [37] \tag{4.4}$$

Where, M_t is the mass of the transferred into the fiber wall at a time t, M_∞ is the maximum uptake as t becomes infinitely large, D_{eff} is the effective diffusion coefficient through the fiber wall, and (a_f) is the surface area per unit volume of the fiber in contact with the gas.

In 'multiple' fiber modules with gas flow from both sides of the fiber,

$$\frac{Surface\ area}{volume\ of\ the\ fiber\ sorbent} = (a_f)_{multi} = \frac{\pi\,(I.D. + O.D.)L_f}{\dfrac{\pi}{4}(O.D.^2 - I.D.^2)L_f} = \frac{4\,(I.D. + O.D.)}{(O.D.^2 - I.D.^2)} \tag{4.5}$$

While, in the case of 'one' fiber module with the gas flow from the bore side,

$$\frac{Surface\ area}{volume\ of\ the\ fiber\ sorbent} = (a_f)_{one} = \frac{\pi\,(I.D.)L_f}{\dfrac{\pi}{4}(O.D.^2 - I.D.^2)L_f} = \frac{4\,(I.D.)}{(O.D.^2 - I.D.^2)} \tag{4.6}$$

$$\frac{\left[\dfrac{M_t}{M_\infty}\right]_{multi}}{\left[\dfrac{M_t}{M_\infty}\right]_{one}} = \frac{2(a_f)_{multi}\sqrt{\dfrac{D_{eff}t}{\pi}}}{2(a_f)_{one}\sqrt{\dfrac{D_{eff}t}{\pi}}} = \frac{(a_f)_{multi}}{(a_f)_{one}} = \frac{\dfrac{4\,(I.D. + O.D.)}{(O.D.^2 - I.D.^2)}}{\dfrac{4\,(I.D.)}{(O.D.^2 - I.D.^2)}} = \frac{(I.D. + O.D.)}{(I.D.)} \tag{4.7}$$

Where, O.D. is the fiber outer diameter, I.D. is the fiber bore diameter, and L_f is the fiber length.

Hence, for a fiber sorbent with an O.D. of 800 µm and an I.D. of 400 µm, the ratio becomes:

$$\frac{\left[\dfrac{M_t}{M_\infty}\right]_{multi}}{\left[\dfrac{M_t}{M_\infty}\right]_{one}} = \frac{(I.D. + O.D.)}{(I.D.)} = \frac{(400\ \mu m + 800\ \mu m)}{400\ \mu m} = 3 \tag{4.8}$$

Hence, in multiple fiber modules the meso/macroporous mass transfer can be 3 times higher than one fiber module.

It can also be argued that in case of 'one' fiber experiments, bypass or non-uniformity of flow can cause premature breakthrough, while for 'multiple' fiber module experiments, the effect is suppressed [6].

'Multiple' fiber breakthrough capacity (Table 4.9) for high sorbent loadings (75 wt. %, dry fiber wt basis) was found to be slightly higher than in case of pure zeolite crystals testing, possibly due to small amount of clumping in the case of zeolite crystals dispersed in sand, while in the case of fiber sorbents the zeolite particles were uniformly distributed without clumping.

4.14. Summary and conclusions

A polymer-sorbent hybrid single-layer hollow fiber material has been developed. This new material can be used for the removal of sulfur odorants from pipeline natural gas and can be an attractive alternative to the conventional pellet packed bed technology. Such hollow fiber sorbents have been spun using cellulose acetate and zeolite NaY with high sorbent loadings and good strength. Fiber sorbent morphology has been characterized using equilibrium sorption, gas permeation, SEM and EDX.

Performance of fiber sorbent modules has been compared to zeolite crystal packed bed operation under flow conditions. Fiber sorbents have been found to be fully regenerable by application of heat. The concept of fiber sorbent can be extended to other

bulk and specialty separations applications such as ion-exchange, adsorption, catalysis and adsorption chromatography.

4.15. REFERENCES

1. Feng, X.S., et al., *Hollow-fiber-based adsorbers for gas separation by pressure-swing adsorption.* AIChE Journal, 1998. 44(7): p. 1555-1562.

2. Pan, C.Y., McMinis, C.W.. *Hollow Fiber Bundle Element,U.S. Patent 5,139,668* August 18, 1992.

3. Gilleskie, G.L., J.L. Parker, and E.L. Cussler, *Gas Separations in Hollow-Fiber Adsorbers.* AIChE Journal, 1995. 41(6): p. 1413-1425.

4. Lively, R.P., Chance, R. R., Kelley, B. T., Deckman, H.,KorosW. J., *Sorbent Fiber Compositions and Methods of Temperature Swing Adsorption, U.S. Patent 2009/0025555A1.* Jan. 29,2009.

5. Lively, R.P., et al., *Hollow Fiber Adsorbents for CO2 Removal from Flue Gas.* Industrial & Engineering Chemistry Research, 2009. 48(15): p. 7314-7324.

6. Kiyono, R., et al., *Mixed matrix microporous hollow fibers with ion-exchange functionality.* Journal of Membrane Science, 2004. 231(1-2): p. 109-115.

7. Avramescu, M.E., Z. Borneman, and M. Wessling, *Particle-loaded hollow-fiber membrane adsorbers for lysozyme separation.* Journal of Membrane Science, 2008. 322(2): p. 306-313.

8. Perera, S.P., *Hollow Fibres,WO Patent 2007/007051A1.* Jan. 18,2007.

9. Perera, S.P., Tai, C.C., *Regenerable adsorption unit,WO Patent 2008/110820A1.* Sept. 18, 2008.

10. Husain, S. and W.J. Koros, *Macrovoids in Hybrid Organic/Inorganic Hollow Fiber Membranes.* Industrial & Engineering chemistry research, 2009. 48(5): p. 2372-2379.

11. J.Kurdi, A.T., *Improvement in polyetherimide gas separation membranes through the incorporation of nanostructured metal complexes.* Polymer, 2003. 44: p. 4533-4540.

12. J.Kurdi, A.T., *The influence of casting solution structure on the microporosity polyetherimide gas separation membranes by the coagulation post-leaching method.* Journal of membrane science, 2001. 184: p. 175-186.

13. Koros, W.J. and G.K. Fleming, *Membrane-Based Gas Separation.* Journal of Membrane Science, 1993. 83(1): p. 1-80.

14. McKelvey, S.A., D.T. Clausi, and W.J. Koros, *A guide to establishing hollow fiber macroscopic properties for membrane applications.* Journal of Membrane Science, 1997. 124(2): p. 223-232.

15. Vos, K.D., F.O. Burris, and R.L. Riley, *Kinetic Study of Hydrolysis of Cellulose Acetate in Ph Range of 2-10.* Journal of Applied Polymer Science, 1966. 10(5): p. 825-&.

16. Wallace, D.W., C. Staudt-Bickel, and W.J. Koros, *Efficient development of effective hollow fiber membranes for gas separations from novel polymers.* Journal of Membrane Science, 2006. 278(1-2): p. 92-104.

17. McKelvey, S.A. and W.J. Koros, *Phase separation, vitrification, and the manifestation of macrovoids in polymeric asymmetric membranes.* Journal of Membrane Science, 1996. 112(1): p. 29-39.

18. Avramescu, M.E., Z. Borneman, and M. Wessling, *Dynamic behavior of adsorber membranes for protein recovery.* Biotechnology and Bioengineering, 2003. 84(5): p. 564-572.

19. Smolders, C.A., et al., *Microstructures in Phase-Inversion Membranes .1. Formation of Macrovoids.* Journal of Membrane Science, 1992. 73(2-3): p. 259-275.

20. Boom, R.M., et al., *Microstructures in Phase Inversion Membranes .2. The Role of a Polymeric Additive.* Journal of Membrane Science, 1992. 73(2-3): p. 277-292.

21. Qin, J.J., et al., *Cellulose acetate hollow fiber ultrafiltration membranes made from CA/PVP 360 K/NMP/water.* Journal of Membrane Science, 2003. 218(1-2): p. 173-183.

22. Duarte, L.T., A.C. Habert, and C.P. Borges, *Preparation and morphological characterization of polyurethane/polyethersulfone composite membranes.* Desalination, 2002. 145(1-3): p. 53-59.

23. Chou, W.L., D.G. Yu, and M.C. Yang, *Influence of coagulant temperature and on-line drawing on the mechanical properties and permeation performance of cellulose acetate hollow fibers.* Journal of Polymer Research, 2005. 12(3): p. 219-229.

24. Langmuir, I., *The adsorption of gases on plane surfaces of glass, mica and platinum.* Journal of the American Chemical Society, 1918. 40(9): p. 1361-1403.

25. Satokawa, S., Y. Kobayashi, and H. Fujiki, *Adsorptive removal of dimethylsulfide and t-butylmercaptan from pipeline natural gas fuel on Ag zeolites under ambient conditions.* Applied Catalysis B-Environmental, 2005. 56(1-2): p. 51-56.

26.   Lee, D., et al., *Adsorptive removal of tetrahydrothiophene (THT) and tert-butylmercaptan (TBM) using Na-Y and AgNa-Y zeolites for fuel cell applications.* Applied Catalysis a-General, 2008. 334(1-2): p. 129-136.

27.   Koros, W.J., A.H. Chan, and D.R. Paul, *Sorption and Transport of Various Gases in Polycarbonate.* Journal of Membrane Science, 1977. 2(2): p. 165-190.

28.   Karger, J., *Measurement of Diffusion in Zeolites—A Never Ending Challenge?* Adsorption 2003. 9(1): p. 29–35.

29.   Ruthven, D., *Diffusion in zeolite molecular sieves*, in *Introduction to zeolite science and practice*. 2007, Elsevier B. V. .

30.   Yang, R.T., *Adsorbents : fundamentals and applications*. 2003, Hoboken, N.J.: Wiley-Interscience. xii, 410 p.

31.   Carruthers, S.B., G.L. Ramos, and W.J. Koros, *Morphology of integral-skin layers in hollow-fiber gas-separation membranes.* Journal of applied polymer science, 2003. 90(2): p. 399-411.

32.   Haydt, D. *H2S detection and determination*. American School of Gas Measurement Technology (ASGMT) White Papers.

33.   Walas, S.M., *Chemical process equipment : selection and design*. 1988, Boston: Butterworths.

34.   S. Satokawa, Y.K., *Adsorbent for removing sulfur compounds from fuel gases and removal method*. 2005, United States Patent 6875410

35.   Shimizu, K., et al., *Mechanistic study on adsorptive removal of tert-butanethiol on Ag-Y zeolite under ambient conditions.* Journal of physical chemistry B, 2006. 110(45): p. 22570-22576.

36.   Bhandari, D.A., N. Bessho, and W.J. Koros, *Hollow fiber sorbents for desulfurization of natural gas.* Industrial & Engineering chemistry research, In-press.

37.   Crank, J., *The mathematics of diffusion*. 2d ed. 1975, Oxford,: Clarendon Press. viii, 414 p.

CHAPTER 5

CREATION AND CHARACTERIZATION OF DUAL-LAYER

FIBER SORBENTS

Abstract

Hollow fiber sorbents provide a pseudo-monolithic approach with potential applications in natural gas desulfurization [1]. Single-layer hollow fiber sorbents can be created utilizing hollow fiber spinning technology with a polymer 'binder', impregnated with high loadings of sulfur selective zeolite sorbent 'fillers'. Hot purge gases, hot water or steam can be utilized as the thermal media during the regeneration cycles. To minimize natural gas loss during the sorption step and to ensure consistent sorption capacity over repeated cycles, it is desired to create a dense and thin polymer barrier layer on the fiber sorbents to allow only thermal interactions with the heating and cooling media.

This chapter explores materials and methods for the creation and characterization of delamination free dual-layer fiber sorbents, with a porous core and a barrier sheath formed by a simultaneous co-extrusion method. A procedure is described for the selection of low permeability polymer as sheath, with the core layer comprising cellulose acetate polymer as binder and zeolite NaY as sorbent filler. The effects of various spinning conditions, bore fluid and spin dope compositions, and the effect of solvent exchange protocol are examined in detail. Mass transfer effects and morphology of the as-spun fibers are analyzed by TGA, SEM, EDX, permeation and sulfur sorption experiments.

5.1. Introduction

In chapter 4, we described the creation of single-layer hollow fiber sorbents for low concentration sulfur removal and performed proof-of-principle regeneration experiments, exploring the viability of TSA. Steam and water were found to be the most effective heat transfer media (Appendix A.8.). However, the capacity of hydrophilic zeolite goes down considerably when in direct contact with water vapor or steam [2].

This led us to explore the creation of an impermeable, thin polymer barrier layer on the sheath of fiber sorbents to allow only thermal interactions with the regeneration media, thereby promoting consistent sorption capacity over repeated cycles. We envision creating the barrier layer by a one step dual-layer fiber spinning process with simultaneous co-extrusion of a barrier polymer 'sheath' dope along with the fiber sorbent 'core' dope. The creation of dual-layer fiber sorbents is a complicated process requiring simultaneous manipulation of various spinning parameters to obtain mutually contradictory properties in each layer.

Other methods for the creation of the barrier layer, by post-treatment of single-layer fiber sorbent were also explored and are explained in detail in chapter 6.

The creation of dual-layer hollow fiber mixed matrix membranes (MMMs) for gas separations has recently attracted the attention of various researchers due to synergism between organic and in-organic materials [3-6]. Jiang et al. [7] describe the spinning of matrimid/polyethersulfone (PES) dual-layer hollow fibers and studied the effects of spinneret and coagulation temperatures. They found that a spinneret and coagulation bath temperature of 25°C gave improved selectivity. Pereira et al. [8] found polymer spin dopes and air-gap distance to be important factors contributing to the better

interpenetrations of the polymer solutions with longer mass exchange time improving adhesion. Li et al. [9] fabricated fluoropolyimide/PES dual-layer fibers for O_2/N_2 separations and found spin dope compositions and a subsequent heat treatment of fibers helped to obtain delamination free fibers. Higher core polymer viscosity was found to reduce layer shrinkage and improve adhesion. Hosseini et al. [10] have fabricated PBI-matrimid / PES dual-layer membranes for H_2/CO_2 separations. They observed two distinct morphologies in the core and sheath layer due to the dope constituents, dope composition and materials chemistry. Delamination free structure was attributed to the good miscibility of blend polymers, inter-layer diffusion of solvents and close solubility parameters. Li et al. [11] observed high elongation draw ratios and the addition of PEO in the PES inner layer to provide a macrovoid free structure. He et al. [12] discussed the mechanical stability and adhesion of hydrophilic ion-exchange coatings to hydrophobic support material (PES). Knudsen selectivity was obtained due to defects but the charged organic dye retention was high indicating potential as nano filtration membrane.

Widjojo et al. [4] fabricated dual-layer PES hollow fiber membranes with up to 60 wt. % loading of Al_2O_3 nano particles in the core layer and beta zeolite particle in the outer separation layer. Al_2O_3 particles were added to enhance permeation in the substructure and reduce densification during heat treatment of the fibers. Higher particle loading in the core layer, reduction in outer layer dope flow rate and higher elongation draw ratio was found to enhance the permeance and selectivity. Husain et al. [3] successfully spun dual-layer mixed matrix membranes with Ultem$^®$ 1000 polyetherimide polymer and Grignard treated SSZ-13 zeolite particles to obtain improved gas separations. Bonyadi et al. [13] describe a dual-layer hollow fiber for direct contact

membrane distillation (DMCD) process using a hydrophilic outer layer (polyacrylonitrile-PAN) with a hydrophobic inner layer (polyvinylidene fluoride-PVDF). The various studies clearly reveal the applicability of dual-layer fiber spinning technology for various gas and liquid separation applications. The key similarities and differences in a dual-layer fiber sorbents and MMMs were described in section 2.1.

This work uses knowledge from the dual-layer MMM literature and modifies the material selection and spinning process to obtain the desired morphology.

5.2. 'Barrier' sheath polymer selection

It is important to explore the adhesion properties of the core and sheath layer. The sheath polymer should be partially or completely miscible with the core polymer with a thin, seamless interface. Due to the small interaction time scale ($\sim$ 0.1- 3 s) of polymer dopes before phase separation and due to the low diffusion coefficient in viscous dopes, it is difficult for the two layers to interpenetrate to a large extent. Long interaction times ($\sim$ 1-3 days in case of dense film casting – section 3.2.) could lead to the penetration of barrier polymer into the core layer pores/voids causing loss of dynamic sorption capacity.

Polyacrylonitrile (PAN) was selected as one of polymer for barrier sheath layer (section 3.1.2.). NMP was selected as the common spinning solvent in both the core and the sheath layer due to its strong solvent power, low volatility and good water miscibility. A sheath dope composition of PAN/NMP 15/85 wt. % was found to have appropriate viscosity. Unfortunately, PAN and CA/NaY dopes were found to be incompatible with each other and complete delamination was observed upon dual-layer asymmetric film casting (section 3.3.2.). Immiscible core and sheath layer e.g. CA and PAN are undesired, as this could lead to delamination of layers during spinning. PAN is rarely compatible

126

with other polymers due to the strong dipole interaction of its nitrile groups [14, 15]. PVDC was then explored as the sheath layer polymer (section 3.1.2.). PVDC and CA/NaY co-casted asymmetric films showed good adhesion in both wet and dry states. The reason for the good adhesion of both layers was further explored.

Solubility parameters can be used as a first step to predict the miscibility of polymers and their solubility in certain solvents. Similar values of solubility parameters often indicate higher compatibility between the two components. From the solubility parameters of polyvinylidene chloride (PVDC-δ – 24.9 MPa$^{0.5}$) and cellulose acetate (CA-δ – 25.08 MPa$^{0.5}$) (section 3.1.2.), it appears that the polymers might be miscible with each other and soluble in the solvent (NMP-δ– 23.0 MPa$^{0.5}$). Several studies in the patent literature describe the use of PVDC barrier coatings on cellulosic substrates for food storage applications [16, 17]. Also, hydrophilic polymers like cellulose acetate and polysulfone and hydrophobic polymers like polyvinylidene fluoride (PVDF) have been used as composite flat sheet and dual-layer hollow fiber membranes for direct contact membrane distillation(DCMD) [13, 18]. Vazquez-torres et al. [19] report PVDF and CA polymer blends to be partially miscible. Also, the PVDC grade used in this study (IXAN®-PNE-288) was especially suited for coatings on cellulosic films [20].

SEM images of dense polymer blend films of CA and PVDC in Figure 5.1 indicate partial miscibility of the polymers with visible PVDC rich (or CA poor) and PVDC poor (or CA rich) regions depending on the polymer composition. The adhesion between the regions was good and the films appeared uniform. DSC data indicated two compositions dependent T_g's often seen in partially miscible polymers [21].

CA dense film   CA/PVDC 80-20 wt. % film   CA/PVDC 50-50 wt .% film

CA/PVDC 20-80 wt .% film   Pure PVDC film
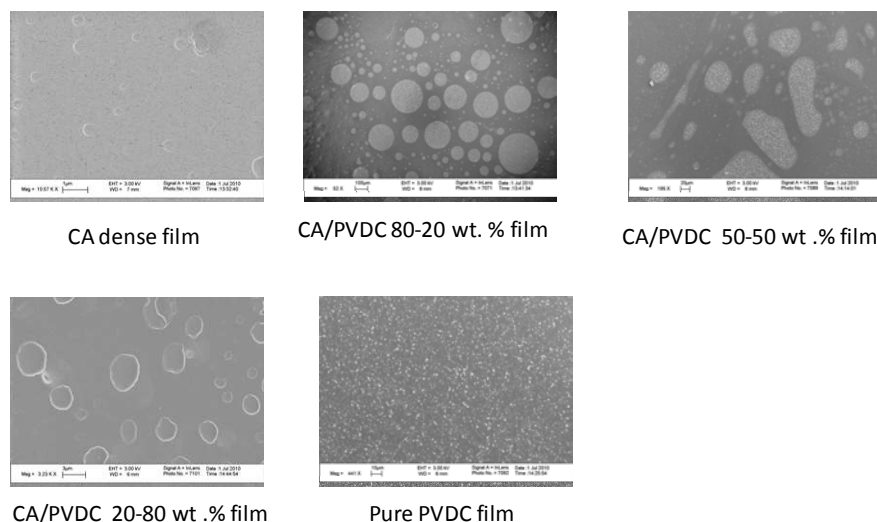
Figure 5.1: SEM images of CA/PVDC dense blend films with varying weight ratios.

IR analysis was used as a tool to examine any specific interactions between PVDC and CA. PVDC is miscible with poly (methyl methacrylate) (PMMA) presumably due to strong specific interactions between vinylidene groups of PVDC and carbonyl groups of PMMA [22]. Similarly, carbonyl groups of CA could interact with vinylidene groups of PVDC. The peak between 3400 and 3700 cm^{-1} indicate a combination of intra and inter-molecular (-OH) hydrogen bonding (Figure 5.2(a)). The high intensity peak for pure CA film indicates the inter-molecular hydrogen bonding of –OH groups in CA, while in pure PVDC films, no corresponding peak is observed due to absence of –OH groups. In blend films the intensity of the intermolecular –OH bonding decreases, while a peak appears around 3250 cm^{-1}.

The peaks near 1748 cm^{-1} indicate –C=O stretching of non-hydrogen bonded carbonyl groups, while the peak near 1700 cm^{-1} is attributed to the –C=O groups involved in hydrogen bonding with –OH groups of CA (Figure 5.2(b)). A decrease in peak intensity at 1748 cm^{-1} and 1700 cm^{-1} indicates less free –C=O to be present and less –C=O groups interacting with –OH groups. This could be possibly be due to the hydrogen

bonding between –C=O groups of CA and C-H groups in PVDC. However, it is difficult to draw exact conclusions because CA shows a strong intermolecular hydrogen bonding tendency and the lower peak intensity could also be due to lower CA concentration in the blend films.
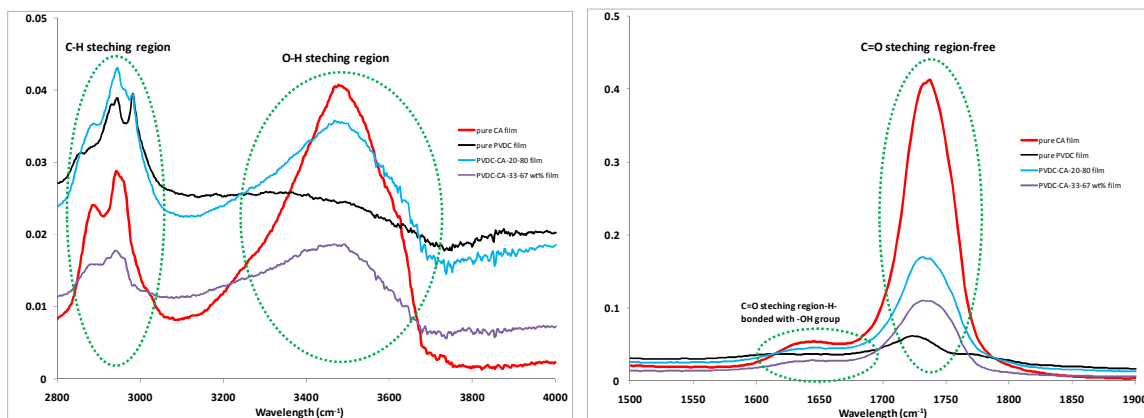
Figure 5.2: Infrared scan showing the differences in the spectra between CA, PVDC and CA/PVDC blend films.

Thus, with the selection of PVDC grade for cellulose material coating, sufficient literature data on CA/PVDC adhesion, and studies on polymer blend films it was concluded that PVDC was a good candidate for the sheath layer.

5.3. Dual-layer fiber sorbent dope preparation

The formulation of appropriate core and sheath spin dopes is a crucial first step in creation of dual-layer fiber sorbents. The core layer should be highly porous with high zeolite sieve loading, while the sheath layer should be dense and defect free. The miscibility region and the binodal curve for the fiber sorbent dopes were investigated using the cloud-point technique described in section 3.3.1. Various dope compositions were prepared in small quantities (15 ml) close to the two phase binodal curve to ensure

rapid phase separation of the dopes. The preparation and optimization of the CA/NaY core dope was described in detail in section 4.2.

A core dope composition of 12.5 wt % CA, 42.5 wt % NMP, 1.9 wt % PVP, 5.6 wt % water, and 37.5 wt % zeolite NaY was found to give rapid phase separation during spinning even with high sorbent loading corresponding to a 75 wt. % zeolite NaY loading (dry fiber wt basis) (section 4.3.). The fibers indicated high porosity and permeance of 90,000-110,000 GPU (section 4.4.), while still indicating the best possible breakthrough capacity of 1.4 mmole TBM/g fiber (normalized: 1.86 mmole TBM/g sorbent) and 0.7 mg H_2S/g fiber (normalized: 0.9 mg H_2S/g sorbent), equivalent to a zeolite crystal packed bed as described in sections 4.8. and 4.9.

Figure 5.3 shows the binodal diagram of PVDC/NMP/water and CA/NMP/water ternary systems at 25°C. PVDC due to its hydrophobic nature presents a small miscibility region with 1-5 wt. % water causing phase separation compared to the more hydrophilic CA, where up to 10-15 wt. % water is needed to cause phase separation (section 4.2.) [23].
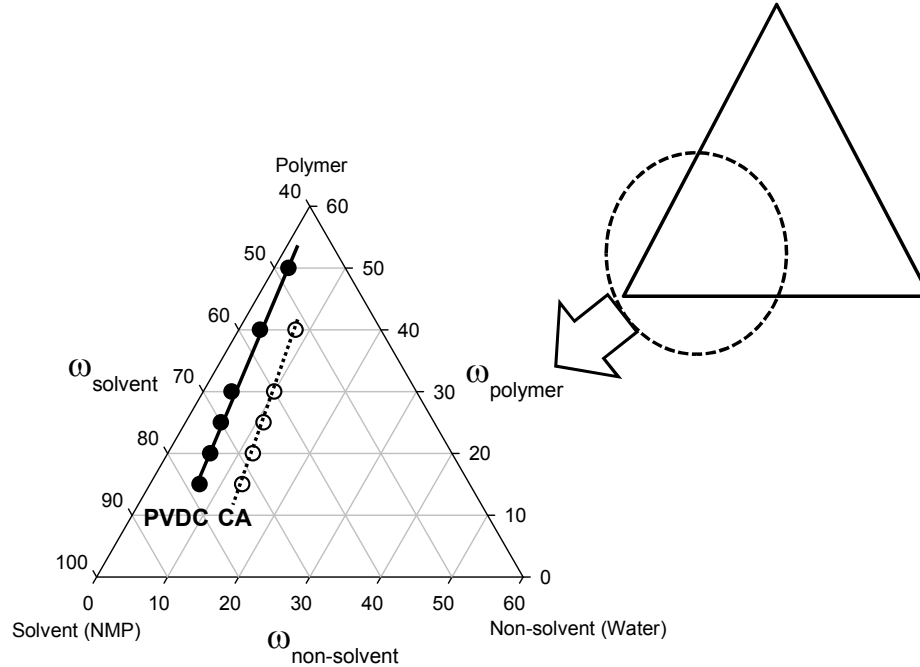
Figure 5.3: Ternary phase diagram of P(VDC-MA) co-polymer and CA with solvent (NMP) and non-solvent (water) system at 25°C. The composition to the left of the binodal lines are homogeneous single phase solution, and compositions to the right are two phase. (Solid dots: PVDC, empty dots: CA).

In dual-layer fiber sorbent spinning, the polymer concentration in the sheath layer and hence the dope viscosity should be carefully adjusted. A higher polymer concentration, though helpful in creating a dense and defect free sheath layer [9], can significantly hinder the phase separation rate of the core layer. A potential way to determine the polymer concentration to minimize defects is the concept of critical polymer concentration (c.p.c.) [9, 10, 24]. Above this critical concentration the dope viscosity is found to drastically increase with the increase in the polymer concentration indicating higher degree of polymer chain entanglement. Figure 5.4 shows the variation in dope viscosity with the changes in polymer concentration at a shear rate of 0.01 s^{-1} and 10 s^{-1} measured at 25°C. The viscosity measured at low shear rates (0.01 s^{-1}) can be used to approximate the dope viscosity in the binodal diagram (Figure 5.3), while the viscosity

at high shear rate (10 s^{-1}), can be approximated as the dope viscosity at the spinneret annulus during the fiber spinning process [24]. The c.p.c. was found to be around 45 wt. % PVDC (polymer) in NMP (solvent). Below the c.p.c. the dope behavior was almost Newtonian with viscosities measured at 0.01 s^{-1} and 10s^{-1} shear rate to be similar, while above it the dope was shear thinning with the behavior increasing with the polymer concentration (Figure 5.4) [25].

Various sheath layers were pursued to determine the best possible spinning conditions. PVP was added to certain sheath dopes. High molecular weight PVP has been found to leach out slowly during solvent exchange and in certain cases block some of the interconnected pores as desired in a dense sheath layer [26, 27]. On the contrary, a low molecular weight PVP leaches out rapidly forming a porous structure as desired in the core layer morphology (section 4.3.). Hydrophilic PVP can enable better compatibility with the core dope and enhance the sheath dope viscosity as well as shown in Figure 5.4 for sheath-2 and sheath-3 dopes. High PVDC polymer content and small amounts of high molecular weight PVP can significantly enhance the dope viscosity (Table 5.4). THF is often added in dopes as a volatile solvent to improve dense skin layer formation. However, THF was found to be a swelling agent for PVDC at room temperature [28]. Sheath dopes with 7 wt. % THF content were not spinnable due to stickiness of the nascent fiber to the guide roles causing inability to be drawn onto the take-up drum.
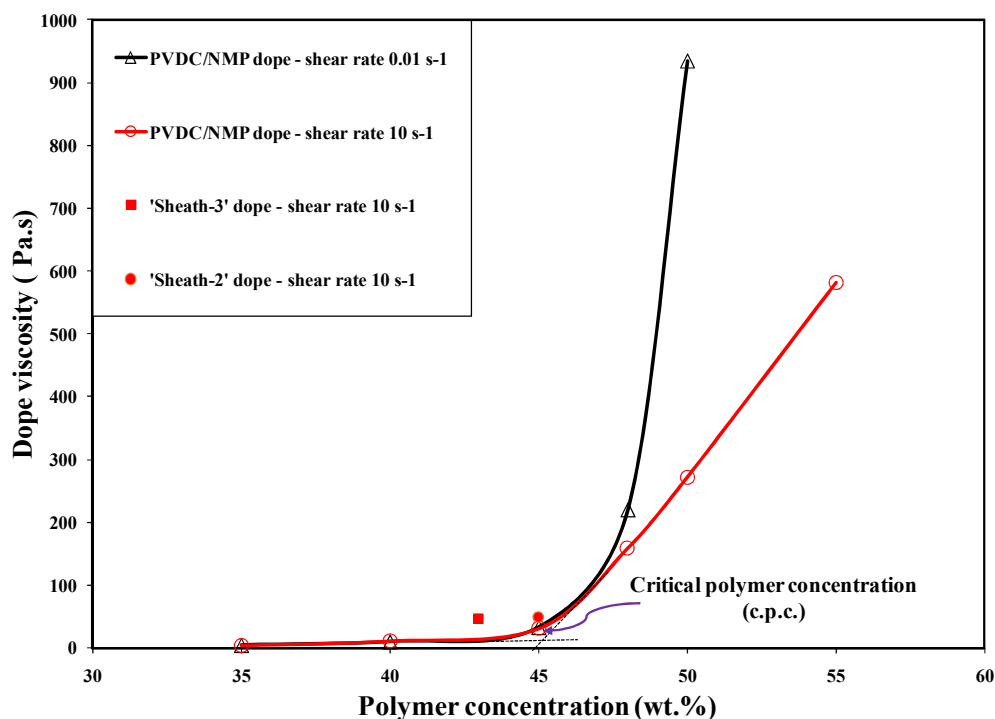
Figure 5.4: variation in dope viscosity as a function of PVDC polymer concentration in solvent NMP under varying shear rate measured at 25°C.

5.4. Dual-layer fiber sorbent spinning

Fiber sorbents were made by modifying the dry jet-wet quench spinning technique as discussed in section 2.5. Table 5.1 summarizes the various spinning parameters in dual-layer fiber spinning. Dual-layer and single-layer fiber spinning had similar tunable parameters; however, the magnitude and importance of the variables were different in each case. Zeolite suspended polymer solution or 'core dope' was fed by a syringe pump to the middle compartment of the spinneret. The core dope flow rate was varied between 180-1000 mL/hr. Simultaneously, a mixture of solvent and non-solvent, referred to as the bore fluid (or internal coagulant), was fed into the innermost compartment of the spinneret. Bore fluid composition was varied between a 50/50 wt. % - 90/10 wt. % NMP/Water mixture (compared to 80/20 to 70/30 wt. % NMP/water in single-layer fiber spinning, section 4.3.). The bore layer flow rate was varied between

0.3-0.5 of the core flow rate. The 'sheath dope' was fed to the outermost compartment of the spinneret (no sheath flow in single-layer fiber spinning). The sheath layer flow rate was varied between 0.2-0.7 of the core layer flow rate.

The bore fluid and the sheath dope were filtered through 15 μm and 40 μm mesh size filters to remove any insoluble particles before entering the spinneret channels. No filter was used for the core dope as the high zeolite content could easily clog the filter creating excessive pressure drop. Spinning temperature (Spinneret, pumps and transfer lines temperature) of 25°C and 40°C maintained by heat tapes (McMaster-Carr, Atlanta, GA) and controlled by PID temperature controllers (Model: CSI-32K, Omega Engineering Inc., Stamford, CT) were studied. The extruded nascent fiber then passed through an adjustable air gap (varied between 0-20 cm, compared to an air-gap of 1-3 cm in single-layer fiber spinning) before entering a quench bath where it phase separates and vitrifies.

Tap water was used as an environmentally friendly and easily available quench bath (1 m deep) medium. Quench bath (or external coagulant) temperatures of 25°C and 50°C were studied. The fiber then passed under a Teflon[®] guide and was collected onto a rotating take-up drum partially submerged in a water-reservoir and continuously replenished with fresh water. The take-up rate was also a variable factor with typical speeds up to 50 m/min. Each collected state was allowed to rotate on the drum at a speed of around (<10 m/min), for about 15 min to allow complete phase separation and vitrification and solvent removal.

By manipulating the various spinning parameters, several spinning 'states' were collected and the effect of each parameter on dual-layer fiber sorbent morphology and separation properties was analyzed.

Table 5.1: Spinning conditions and parameters for dual-layer fiber sorbents.

Dope (Core)	
Pump temperature	25 and 40 °C
In-line temperature	25 and 40 °C
Flow rate	180 - 1000 mL/h
Dope (Sheath)	
Pump temperature	25 and 40 °C
In-line temperature	25 and 40 °C
Flow rate	60- 700 mL/h (0.2-0.7 of core flow rate)
Bore fluid	
Composition	NMP:Water = 90:10-50:50 wt.%
Temperature	Room temperature
Flow rate	60 - 500 mL/h (0.3-0.5 of core flow rate)
Spinneret temperature	25 and 40 °C
Air temperature	Room temperature (~25 °C)
Air-gap	0-20 cm
Quench bath	
Media	Tap water
Depth	1 m
Temperature, T_{quench}	25 and 50 °C
Take-up rate	Up to 50 m/min

To start the optimization process for dual-layer fiber spinning, the CA/NaY (optimized) core dope composition (section 4.3.) was selected. This dope showed the best performance during single-layer fiber sorbent creation and characterization, with high sorbent loading, high permeance and sorption capacity, while still having good mechanical strength. However, fibers spun with the core dope (ID: Core-b1, Table 5.2) and with a sheath dope (ID: Sheath-1, Table 5.3) were found to be brittle and caused frequent fiber breaks. It was observed that the core layer did not phase separate before hitting the first guide role, thereby leading to fiber breakage. It was hypothesized that the

barrier sheath layer significantly retarded the phase separation kinetics of the core layer by hindering the diffusion of external coagulant (water). The low binder loading of the core dope and slow ingress of the external coagulant in the quench bath could lead to inefficient phase separation of the core layer before contacting the first guide role.

With the above observations, the core dope was modified with a lower sorbent loading of 60-65 wt. % (core layer wt. % basis) with the composition on a polymer solution basis being kept constant as discussed in section 4.3. Dual-layer fibers (sheath dope, ID: sheath-1) with core dope (ID: Core-b2 and b3, Table 5.2) were spun with relative ease, possibly due to higher polymer content (or lower sorbent loading) in the core dope validating the hypothesis.

The dual-layer fibers have significant advantages in terms of enabling rapid regeneration cycles with steam; however due to the lower achievable sorbent loading ($\leq$ 65 wt.%, dry fiber wt basis) compared to a maximum of 75 wt. % sorbent loading achievable in single-layer fibers, the fiber sorption capacity per gram fiber in dual-layer fiber sorbents is lower (section 4.9.).

Table 5.2: CA/NaY (optimized) core dope compositions (units in wt. %) (Refer section 4.3. for details on core dope optimization).

ID	Basis (wt. %)	CA	NMP	Water	PVP (M_n~55,000)	NaY
CA-optimized	20% CA/60-75% loading					
	Polymer solution basis	20.0	68.0	9.0	3.0	-
Core-b1	Fiber sorbent dope basis	12.5	42.5	5.6	1.9	37.5
	Dry fiber sorbent basis	25.0	-	-	-	75.0
Core-b2	Fiber sorbent dope basis	14.6	49.5	6.6	2.2	27.1
	Dry fiber sorbent basis	35.0	-	-	-	65.0
Core-b3	Fiber sorbent dope basis	15.4	52.3	6.9	2.3	23.1
	Dry fiber sorbent basis	40.0	-	-	-	60.0

Table 5.3: Various sheath dope compositions studied in this work (units in wt. %).

ID	PVDC	NMP	Water	PVP (M_n~1.3 million)
Sheath-1	25	72	3	-
Sheath-2	45	54	-	1
Sheath-3	43	55	-	2

5.5. Effect of sheath dope viscosity

The core and sheath dope viscosity needs to be adjusted carefully to get delamination free fibers with desired permeation and sorption properties. A higher dope viscosity could be obtained by increasing the solids loadings in the dope. Higher zeolite loading, increasing the polymer content or addition of PVP were all found to increase the viscosity. The viscosity of the core dope (ID: Core-b3, Table 5.2) with 60 wt. % zeolite loading (dry fiber wt. basis) was found to be around 766 Pa.s at 25 °C and a shear rate of $10s^{-1}$ (Table 5.4). Viscosity of core dopes with higher loadings (65 or 75 wt. % zeolite loading) was expected to be even higher. Typically, pure polymer hollow fiber membrane spin dopes have a viscosity of~100 Pa.s [29].

Table 5.4: Summary of viscosity of various spinning dopes at a shear rate of $10s^{-1}$.

Temperature	25°C	40°C
ID	η (Pa.s)	η (Pa.s)
Core-b3	766	287
c.p.c. (PVDC/NMP – 45/55 wt. %)	31	11
Sheath-1	<4	N/A
Sheath-2	50	27
Sheath-3	47	24

Dual-layer fibers were spun with core dope (ID: Core-3) and a low viscosity sheath dope (ID: Sheath-1). The sheath dope did not fill the spinneret compartment uniformly at low flow rates (<400 mL/h) and caused non-uniform coverage of fibers due to low viscosities (Table 5.4). Further increasing the sheath flow rate caused the coverage to be uniform. Good adhesion between the core and the sheath layer was observed (Figure 5.5(b) and Figure 5.6(b)) as expected due to partial miscibility of the core and sheath layer polymers as explained in section 5.3. However, the sheath layer was found to

be porous and defective with large number of 'finger shaped' macrovoids (Figure 5.5 (c)).
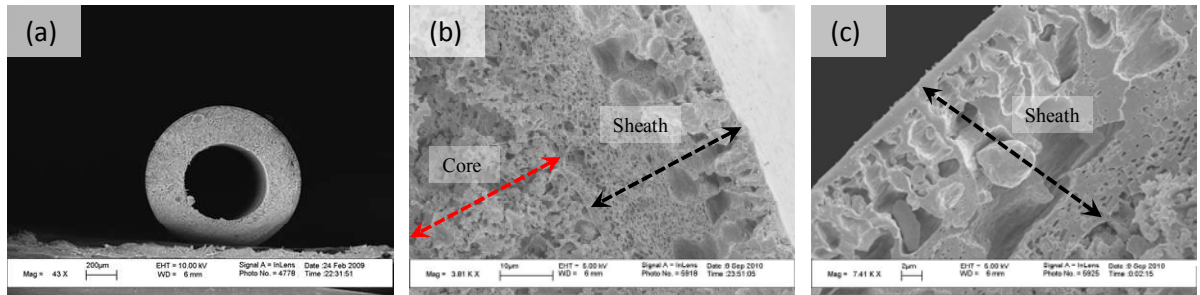
Figure 5.5 (left to right) (a): SEM image of dual-layer fiber sorbents spun with low viscosity sheath dope (ID: Sheath-1) with a 60 wt. % zeolite loading core dope (ID: Core-b1). (b) SEM image showing good adhesion between the core and the sheath layer (c) SEM image close-up of a section of large number of 'finger shaped' macrovoids in the sheath layer morphology.
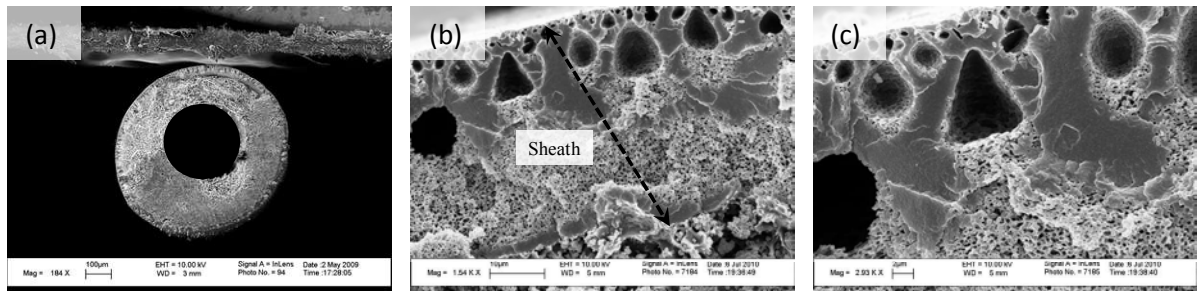
Figure 5.6: (left to right) (a): SEM image of dual-layer fiber sorbents spun with high viscosity sheath dope (ID: Sheath-2) with a 60 wt. % zeolite loading core dope (ID: Core-b1). (b) SEM image showing good adhesion between the core and the sheath layer (c) SEM image close-up of a section of 'tear drop' shaped macrovoids in the sheath layer morphology. The number of macrovoids is also seen to be reduced due to enhanced sheath layer viscosity.

In the case of single-layer fibers (or the core-layer in dual-layer fibers) macrovoids can reduce the mechanical strength and lead to non-uniform mass transfer in the fiber sorbent wall as discussed in section 4.3, while in the case of the sheath layer in dual-layer fiber sorbents, macrovoids can cause non-selective pathways for gas/water vapor flow rendering the barrier layer ineffective.

Macrovoid formation and growth can be reduced by increasing the dope viscosity, which delays the diffusion of solvent into the polymer-lean phase that causes the growth of macrovoids. Hence, the sheath dope viscosity was increased with higher PVDC polymer content and PVP additive and dual-layer fibers were spun with dopes (ID: Core-b3 and Sheath-2,3) as shown in Figure 5.6.

High viscosity sheath dopes (ID: Sheath 2 or 3-Table 5.4) gave uniform coverage of the core layer even at low sheath flow rates ($\sim$ 60 mL/hr). Number of macrovoids reduced dramatically and less developed 'tear-drop' shaped macrovoids were formed (Figure 5.6(c)). The macrovoids through reduced were not completely eliminated possibly due to the hydrophobic nature of the PVDC polymer which causes instantaneous de-mixing of the dope.

Sheath viscosity was not enhanced further as a slower phase separation of the sheath layer could severely affect the phase separation of the core layer making it denser with less pores/voids which could reduce the breakthrough/dynamic capacity during the sorption step. The core-sheath adhesion was found to be good with a dense sheath layer with radially outward porosity gradient (Figure 5.6(b)). The morphology is explained in detail in the mass transfer flux section.

Characterization of fiber sorbent morphologies was quantified with the help of permeation experiments. In case of dual-layer fiber sorbents a low permeance and defect free skin is desired in the sheath layer. Assuming a 1 μm thick defect free skin in a 20-50 μm sheath layer, the ideal permeance for N_2 is around 0.001 GPU, based on a dense film N_2 permeability of 0.001 Barrer and an O_2/N_2 selectivity of$\sim$ 5 [28, 30]. A higher

permeance and Knudsen selectivity through dual-layer fiber sorbent indicates greater defects in the sheath layer, which could undermine its barrier properties.

Table 5.5 compares the permeation rate between dual-layer fiber sorbents, spun with different dope compositions. Single-layer fiber sorbents showed very high permeances ranging between 20,000-110,000 GPU (section 4.4.). The permeance measured in dual-layer fiber sorbents, is indicative of resistance to flow mostly through the dense, barrier sheath layer since the highly porous core layer provides negligible gas transport resistance.

Table 5.5: Comparison of permeances (best case) and selectivity of dual-layer fiber sorbents created with different sheath dope compositions

Fiber type	Permeance - N_2 (P/ ℓ - GPU) at 30 psig	Selectivity (α_{O_2/N_2})
Dual-layer fiber sorbent (ID: core-b3 and sheath-1)	70 - 500	0.94
Dual-layer fiber sorbent (ID: core-b3 and sheath-2)	0.3 - 4	0.91
$\alpha_{knudsen}$ (O_2/N_2)= 0.93		

For fibers spun with low sheath viscosity dope (ID:Sheath-1) the lowest achievable permeance varied between 40-700 GPU, while for fibers spun with high sheath viscosity dope the lowest achievable permeance varied between 0.3-4 GPU (ID:Sheath-2) for N_2. Knudsen selectivity was observed in both the cases. Macrovoids (~ 0.1-50 μm) or other pin-hole defects (as small as 5 Å) in the skin of the sheath layer which could be smaller than the mean free path of gas molecules, cause a non-selective flow leading to Knudsen selectivity. The decrease in permeance for high viscosity sheath dopes could be due to the decrease in the number and size of macrovoids as observed in the horizontal images of fibers Figure 5.7 (b) and (c).

Even though the permeance through the sheath layer is low, a two-three orders of magnitude drop is further required to obtain satisfactory sheath layer barrier properties. Permeance through the core layer in dual-layer fibers could be lower than the core layer in single-layer fibers due to relatively slower phase separation in the presence of a sheath layer. However, it is difficult to predict the core layer porosity or permeance by permeability measurements in dual-layer fibers due to difficulties in completely peeling-off a well adhered sheath layer. Sorption experiments were thus performed to predict the effect of the sheath on the core layer properties as explained later.
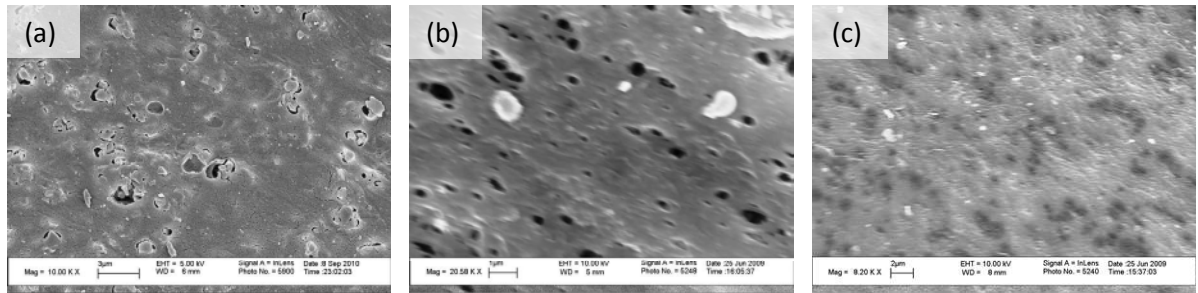
Figure 5.7: Horizontal image of fiber sorbents (left to right) (a) Outer layer of a 60 wt. % zeolite loading CA/NaY single-layer fiber sorbent (ID: Core-b3) indicating large voids due to high sorbent loading (b) Outer layer (sheath layer) of a dual-layer fiber formed with a *low* viscosity sheath (ID: Core-b3, Sheath-1) showing the dense PVDC layer with large macrovoids (c) Outer layer (sheath layer) of a dual-layer fiber formed with a *high* viscosity sheath (ID: Core-b3, Sheath-2) showing the dense PVDC layer with few macrovoids.

5.6. Study of mass transfer effects during dual-layer fiber creation

An understanding of the mass transport phenomenon is required to tailor the fiber sorbent morphology. Due to various coupled factors acting simultaneously, a simplified quantitative model is explained [8]. Directions of mass transfer of the liquids in the various layers are explained pictorially in Figure 5.8(a). The extent of mass transfer between the various layers depends on the concentration of the liquids and viscosity of the core and sheath dopes. The inter-layer mass transfer will occur mostly due to the

142

movement of liquids with the solids either enhancing or reducing the mass transfer rate. The phase separation proceeds from the outer surface of the fiber towards the bore due to the radially inward ingress of the external coagulant (water).
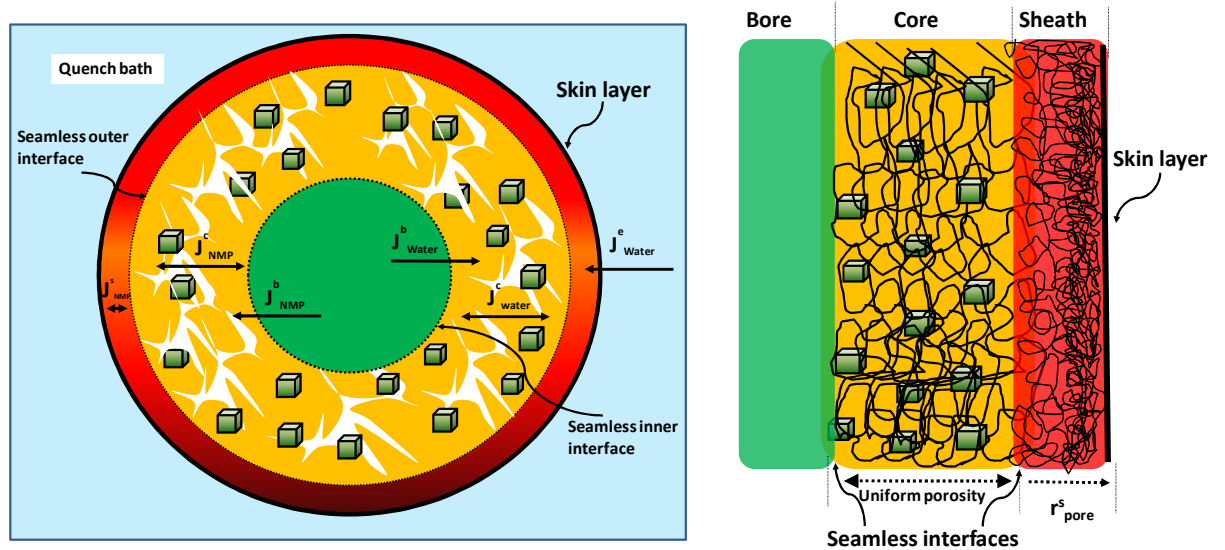
Figure 5.8: (a) Mass exchange between the liquid components of the core and sheath dopes with internal and external coagulants. Bore layer: NMP/Water; Core layer: CA/NaY/PVP (M_n –55,000)/NMP/Water; Sheath layer: PVDC/PVP (M_n – 1.3 Million)/NMP (b) Desired core morphology with uniform interconnected porosity and high zeolite loading. Desired sheath morphology with a porosity gradient and a dense thick skin layer. (J: Flux through the layers, superscripts (b: Bore, c: Core, s: Sheath, e: External coagulant))

The zeolites are assumed to act as "passive fillers" as NMP or water saturate the zeolite pores during the dope making process [1]. Sorption of NMP and water by zeolite crystals could alter the core layer phase separation process. PVP (low and high molecular weight) is a hydrophilic additive that can improve the rate of water influx during phase separation [23]. However, due to its low concentration in the dopes, its effect is not considered to be substantial. Transport of polymer molecules during phase separation is assumed to be negligible with a small amount of interpenetration between the core and sheath layer at the interface.

Solvent in the core and sheath layer should be compatible or miscible to have a seamless interface. Hence, NMP was selected as the solvent of choice in the core, sheath and the bore fluid (section 3.1.4.). The non-solvent (water) is present in the bore fluid, to a small extent in the core and sheath dope, and in the external coagulation bath. Higher temperature of dope or external coagulant enhances the rate of mass transfer, while a higher dope viscosity reduces it [12]. The direction of bore fluid flux (NMP (J_{NMP}^{b}) /Water (J_{water}^{b})) in the air gap is radially outwards towards the core layer. In the core and sheath layer the directions of NMP $(J_{NMP}^{c}\ or\ J_{NMP}^{s})$ and water $(J_{water}^{c}\ or\ J_{water}^{s})$ when in the air gap could be in both directions depending on concentration difference (Figure 5.8(a)). A radially outward direction of NMP flux from the core to sheath layer in the air-gap is preferred, since it prevents instability at the core-sheath interface which can cause poor adhesion [12].

The mass transfer of liquids in the air-gap depends on the dope temperature, presence of volatiles solvents (e.g. THF) in the dopes, and residence time in the air-gap. The solvent (NMP) in all the layers will move radially outwards due to ingress of non-solvent (water) once the nascent fiber enters the external coagulant bath.

With this understanding of mass transfer effects in the various layers, an attempt was made to explain the core and sheath layer morphology. The core layer composition (ID: Core-2 and 3, Table 5.2), sheath layer (ID: Sheath-1, 2 and 3) and bore fluid composition varying between 50/50 - 90/10 wt. % NMP/water were considered. The fiber sorbents were found to have a uniform circular bore due to efficient phase separation of the core layer before hitting the first guide role discussed earlier in section 5.4. Figure 5.9(i) indicates the horizontal image of the fiber cut along the fiber axis showing uniform

144

adhesion between the core and sheath layer. The sheath layer had a dense skin layer (Figure 5.9(b)) with a closed cell sponge sub-structure with increasing porosity towards the core layer (Figure 5.9(d)). A porosity gradient can be helpful if a post treatment step is required to seal the sheath layer defects. It would act as an intrinsic backstop preventing the post treatment solution from getting into the core layer voids and slowing down the mass transfer during the sorption step [31]. The observed sheath layer morphology had a polymer lean dispersed phase with a polymer-rich continuous phase (shown schematically in Figure 5.8(b)) and is often formed due to a "nucleation and growth" process [23]. The desired morphology is usually obtained in case of dopes with a high polymer content, dope composition far from the binodal curve or the slow diffusion of non-solvent leading to phase separation between the binodal and spinodal region (discussed in section 2.5.) [23]. Some macrovoids were observed in the sheath layer (Figure 5.9(b)), possibly due to rapid ingress of water into a hydrophobic PVDC sheath.

During the phase separation of the fiber sorbent in the water quench bath the layer coming in direct contact with the external coagulant (CA/NaY core in case of single-layer fiber sorbents (Figure 5.10(a)) and PVDC sheath in case of dual-layer fiber sorbents (Figure 5.9 (c))) had a dense outer structure due to rapid phase separation of the layer.

Using a similar analogy, the core-sheath interface should be porous in case of good adhesion since it does not come in direct contact with the external coagulant which is diffusing radially inwards from the sheath layer (Figure 5.8 (a)). However, in case of delamination or poor adhesion, the external coagulant ingress between the core-sheath interface leads to the formation of a dense skin layer. To obtain SEM images of a well adhered core and sheath layer, the sheath was carefully peeled-off from the core and fiber

SEM images were taken. Figure 5.9 (a) and Figure 5.10(b) show the horizontal images of the core-sheath interface. Both of the layers were found to be porous, confirming good adhesion.
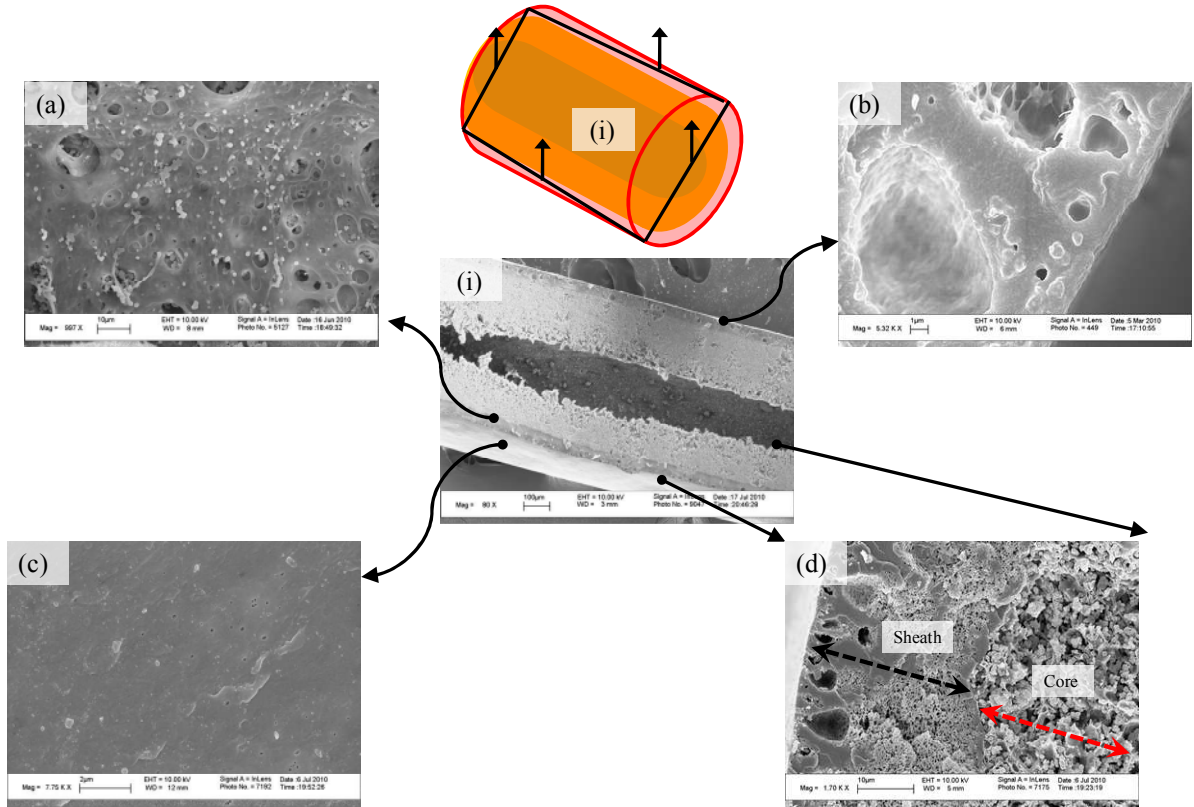
Figure 5.9: (i) horizontal SEM image of fiber sorbent cut axially indicating uniform adhesion between core-sheath layer (a) horizontal image of the inner part of sheath layer (b) Radial image of dense outer skin of the sheath layer (c) Horizontal image of dense outer skin of the sheath layer (d) Radial image indicating porosity gradient in the sheath, good adhesion with core layer and macrovoids on the skin of sheath layer.

Figure 5.11 shows the highly interconnected core morphology observed in pure polymer CA fibers, single and dual-layer CA/NaY fiber sorbents made with the same dope composition (polymer solution basis-Table 5.2) and shown schematically in Figure 5.8(b). A highly porous and uniform structure can reduce meso/macroporous mass transfer limitations and improve fiber sorbent capacity. A non-uniform pore size in the core morphology can cause selective flow through the larger pores through convection,

with a slower diffusive flow through the smaller pores [32]. The observed morphology is thought to be formed by a so called 'spinodal decomposition' (section 2.5.) process with uniform interpenetrated polymer rich and polymer lean phases over the entire region formed due to a rapid phase separation process [23]. The behavior could be due to a low polymer concentration (20 wt. % CA in the dope, polymer solution basis Table 5.2), and close proximity of the core dope to the binodal curve (section 5.3.) [23].
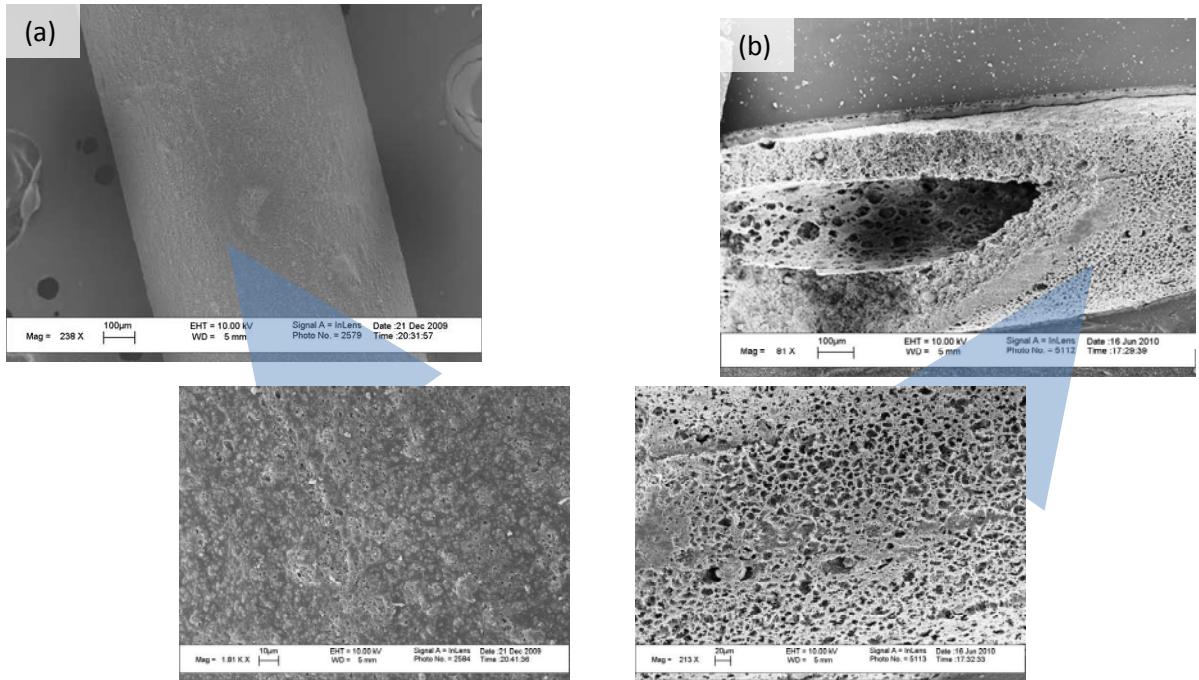
Figure 5.10: Comparison of horizontal images of the core layer in (a) CA/NaY single-layer fiber sorbent and (b) CA/NaY-PVDC dual-layer fiber sorbent (The well-adhered sheath layer is carefully peeled-off to display the porous core layer).
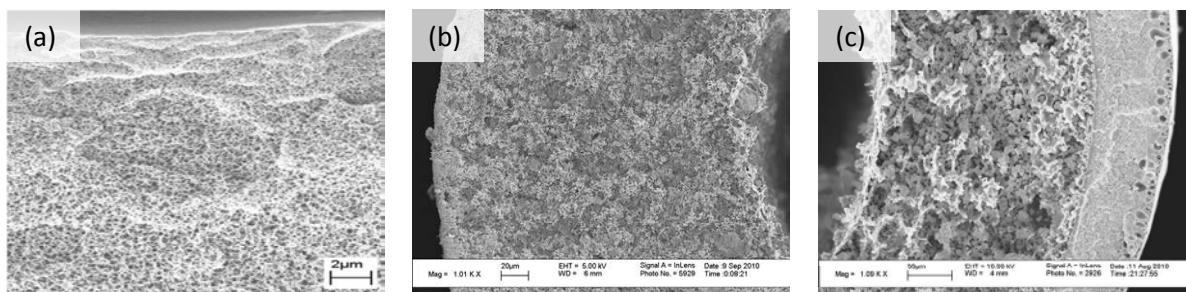
Figure 5.11: Comparison of the core layer morphology in (a) Pure polymer CA single-layer fiber (b) CA/NaY single-layer fiber sorbent (c) CA/NaY dual-layer fiber sorbent.

The bore fluid composition was found to have a significant effect on the bore-core interface with no observed effect on the core-sheath interface possibly due to a short residence time (~0.1-3 s) in the air-gap, described in detail in section 5.13.

5.7. Dope, spinneret and quench bath temperature

Spinning and coagulation bath temperatures are important factors that partially dictate the fiber sorbent morphology by affecting the rate of phase separation.

Single-layer fiber sorbents spun at a higher quench bath temperature (50°C) were found to give higher permeance and porosity possibly due to faster diffusion rate of water at higher temperatures (section 4.4.) [1, 33].
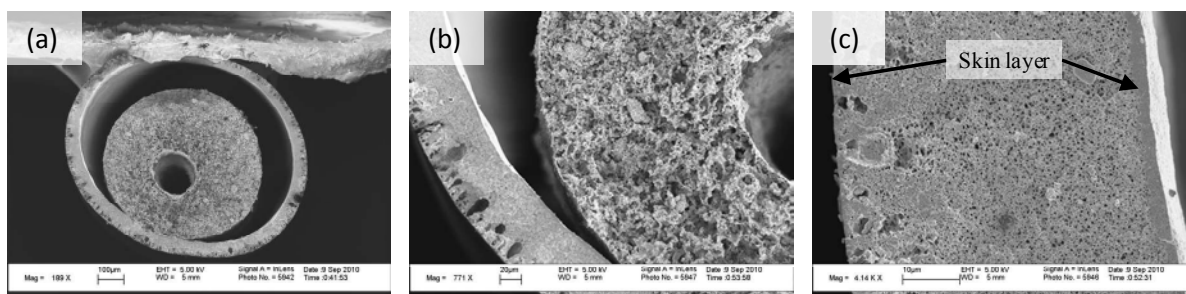
Figure 5.12 (left to right): (a) SEM image of a delaminated dual-layer fiber spun at high coagulant bath temperature (50 °C) (b) Higher number of macrovoids in the sheath layer (c) Skin layer observed on both sides of the delaminated sheath layer.

In the case of dual-layer fibers, the coagulation bath temperature needs to be carefully adjusted. At 50 °C coagulation bath temperature, fiber delamination or

formation of a large number of macrovoids were observed (Figure 5.12 (a) and (b)). SEM images indicated significant shrinkage of the core layer compared to the sheath layer leading to delamination (Figure 5.12). It is hypothesized that the hydrophobic sheath in direct contact with the external coagulant, phase separated rapidly and solidified at higher coagulant temperatures compared to the hydrophilic core, which phase separated relatively slowly and had a dense structure [11].

An apparently well-adhered sheath layer was often found to delaminate during shear fracturing of fibers during SEM sample preparation. It is thus important to determine if the core-sheath interfacial delamination is a sample preparation artifact. A delaminated sheath formed during fiber spinning had a dense skin on both sides due to ingress of external coagulant at the core-sheath interface and formation of a dense skin on in the sheath layer phase separation by external coagulant [8] (Figure 5.12). A sheath layer delaminated during SEM preparation however, indicated an asymmetric structure with a skin only on the outermost part of the fiber.

A delaminated sheath in case of MMMs can lead to poor performance at higher pressures and lower selectivity due to defects [5], while in dual-layer fiber sorbents it can lead to an eventual collapse of the sheath under continuous thermal cycles. Also, delamination can cause bypass of sulfur gases during the sorption step. Sheath layer macrovoids were found to increase at higher coagulant bath temperatures. Fast precipitation due to unbalanced localized stresses and non-solvent diffusion can increase macrovoid formation [7].

Spinning (dope, transfer lines and spinneret) temperatures of 25 °C and 40 °C gave good adhesion, and its effect on fiber sorbent adhesion was found to be secondary.

A higher spinning temperature reduces dope viscosities (Table 5.4), and has been found to give better inter-layer diffusion and adhesion between the polymer layers [7, 12].

5.8. Effect of air-gap height

A minimum critical air-gap is required to ensure interaction between the core and sheath layer before phase separation in the quench bath. Li et al. [9] found an air-gap of 9 cm to be essential for good adhesion between PES dual-layer fibers.

In our work, air-gap lower than~ 3 cm gave delaminated fibers, while a wet-quench spinning with no air-gap caused phase separation of the sheath dope at the spinneret annulus leading to blockage of the spinneret and high pressures in the dope feed line.

Air-gap higher than 15 cm caused the dope line to become unstable leading to fiber curling and frequent breaks. The core and sheath layers were found to be well adhered for air-gaps between 3-15 cm. The typical residence time of the nascent fiber in the air-gap was calculated to vary between 0.1-3 s.

The bore, core and sheath layer thickness were reduced at higher air-gaps; however, the relative ratios remained consistent indicating uniform shrinkage of the layers leading to good adhesion. Less macrovoids were observed in states spun at higher air-gap, possibly due to better orientation of polymer chains in the nascent fiber and partial phase separation in the air gap [10].

5.9. Effect of solvent exchange

Dual-layer fibers showing good adhesion and low permeance were tested to determine their H_2S sorption capacity. The sorption experiments were performed on the flow setup described in section 4.7. and following the protocol described in section 4.12.

TGA analysis was used to determine the weight loss for dual-layer fiber sorbents due to the removal of sorbed water vapor during drying and activation at 120 °C. Zeolite NaY crystals indicated a weight loss of roughly 21.5 wt. %, while CA polymer powder showed roughly 3.8 wt. % and PVDC polymer showed a negligible weight loss of around 0.5 wt. % due to the removal of sorbed water vapor at 120 °C.

The individual weight loss shown by each component (CA,PVDC and zeolite NaY) was then multiplied by its weight fraction in the fiber and then added to find the 'theoretical' weight loss shown by a dual-layer fiber sorbent due to the removal of water vapor.

This was then compared with the 'experimental' weight loss shown by a dual-layer fiber sorbent due to the removal of sorbed water vapor using TGA. A good match between the two values confirmed the weight fraction of each component in the fiber sorbent.

Table 5.6: Spinning conditions of the dual-layer fibers tested in this work.

ID	Core/Sheath composition	Bore fluid composition	Core flow rate	Bore flow rate	Sheath flow rate	Spinning temp.	Quench bath temp.	Air gap	Take-up rate
		NMP/water (wt.%)	(mL/h)	(mL/h)	(mL/h)	(°C)	(°C)	(cm)	m/min
1.	Core-b3/Sheath-2	60 / 40	300	100	150	25	23	10	15
2.	Core-b3/Sheath-2	60 / 40	600	200	200	25	23	10	15
3.	Core-b3/Sheath-2	60 / 40	180	60	60	25	23	10	11
4.	Core-b2/Sheath-3	60 / 40	180	60	60	40	23	3	18

The weight loss during fiber drying was taken into account during fiber capacity determination. Dual-layer fiber sorbents spun at various conditions gave significantly less dynamic capacity (normalized) compared to pure zeolite crystals (Breakthrough capacity: 0.8-0.9 mg H_2S/g sorbent). It was hypothesized that residual NMP may be blocking the sorption sites in the zeolite pores. The activation and regeneration temperature of fiber sorbents was limited to 120 °C, due to the melting of PVDC sheath layer around 150 °C (determined by DSC). However, temperatures of around 180-210°C are often required to remove residual NMP [34]. It was also found difficult to accurately estimate residual NMP amount by TGA due to PVDC degradation (> 160 °C) before the boiling point of NMP (210°C).

The NMP content in the zeolite was indirectly correlated by analyzing the NMP content of the DI water after each solvent exchange using UV-Vis analysis (section 3.4.4.). Three DI water exchanges over three days for single-layer fibers reduced the NMP concentration in the water bath to~1ppm. However, in case of dual-layer fibers six to eight DI water exchanges were found necessary to remove residual NMP ($\leq$ 1 ppm) (section 3.3.5.).

It is hypothesized that the barrier sheath layer significantly slowed down the mass exchange of sorbed NMP with DI water and hence longer durations were required to remove NMP even though the fiber ends were open. Dynamic capacity was found to increase with a longer solvent exchange protocol.

Despite more thorough washing, the dynamic capacity was still found to be less compared to pure zeolite crystals or single-layer fiber sorbents and other factors were explored as described later.

Table 5.7: Comparison of sorption capacities in dual-layer fiber sorbents solvent exchanged with the old and modified protocol. Module length L_M = 53 cm, Number of fibers N_f = 4, fiber spinning conditions summarized in Table 5.6. Feed condition: 30 ppm H_2S / N_2, T = 298 K, p = 1 atm, flow rate = 80 cm^3/min, activated at 393 K under N_2 purge till water vapor concentration < 10 ppm.

Fiber ID	Zeolite loading	Breakthrough capacity	Breakthrough capacity (normalized)	LUB/L_M
	(wt.%)	mg H_2S/g fiber	mg H_2S/g sorbent	-
1. (3 days solvent exchange protocol)	0.60	0.07	0.12	0.82
1. (6-8 days solvent-exchange protocol)	0.60	0.17	0.28	0.50

5.10. Effect of zeolite loading on sorption capacity in dual-layer fibers

Permeation and dynamic sorption experiments in the case of single-layer fiber sorbents indicated an increase in the permeance and the breakthrough sorption capacity of the fibers with higher zeolite loadings (section 4.13.).

Permeation experiments in dual-layer fiber sorbents do not give a clear idea about the core layer porosity since the permeance through the fiber is dominated by the barrier sheath layer (section 5.5.). It was found difficult to create modules of dual-layer fibers with the sheath layer completely peeled-off to test the core layer porosity. Hence, sorption experiments were performed to judge the effect of the sheath layer on the performance of the core-layer.

The breakthrough capacity for dual-layer fibers was found to be lower compared to single-layer fiber sorbents with the same zeolite loading. The lower capacity could be due to the slower phase separation of the core in the presence of the barrier sheath during dual-layer fiber spinning. A denser core layer causes higher meso/macroporous mass transfer resistance leading to lower breakthrough capacity.

Table 5.8: Effect of zeolite loading in CA/NaY-PVDC dual-layer fiber sorbents. Module length L_M = 53 cm. Feed condition: 30 ppm H_2S / N_2, T = 298 K, p = 1 atm, flow rate = 80 cm^3/min, activated at 393 K under N_2 purge till water vapor concentration < 10 ppm.

Fiber ID	Zeolite loading	Breakthrough capacity	Breakthrough capacity (normalized)	LUB/L$_M$
	(wt. %)	mg H$_2$S/g fiber	mg H$_2$S/g sorbent	
3. (4 fibers)	0.6	0.22	0.36	0.57
4. (6 fibers)	0.65	0.44	0.67	0.33

5.11. Effect of elongational draw ratio and tension on take-up drum

Elongation draw ratio is an important spinning parameter that affects the fiber morphology and productivity as described in section 4.3. Due to the low polymer and high sorbent content in the core layer a maximum take-up rate of~ 15 m/min was achievable in single-layer fiber sorbents. The addition of a high polymer content sheath layer in dual-layer fiber sorbent spinning improved the mechanical strength of the core layer by providing good adhesion. The maximum take-up rate was improved to~ 30 m/min with a maximum draw ratio of~ 10 for 65 wt. % (core layer sorbent loading) dual-layer fiber sorbents. Fibers could be collected at higher take-up rates (30-50 m/min) owing to the good 'stretchability' of the sheath layer; however, the fibers had a 'wavy' structure with intermittent broken or variable diameter core layer encapsulated in the sheath. A variable bore diameter or broken core could lead to excessive pressure drop and poor performance of the fiber sorbents. Macrovoids were reduced at higher draw ratios, but could not be completely eliminated as draw ratios above 10 could not be achieved.

In case of dual-layer fibers, keeping the fibers for prolonged periods (> 30 min) on the rotating drum caused higher axial tension on the fibers leading to breakage of the

core layer at certain locations. Also, the take-up drum speed was reduced to <10 m/min to prevent excess axial tension on the spun and collected fiber sorbent states.

5.12. Effect of bore, core and sheath dope flow rates on breakthrough capacity

The flow rates of bore, core and sheath layer need to be adjusted simultaneously during dual-layer fiber spinning. The bore flow rate was typically maintained between 0.3-0.5 of the core layer (section 5.4.). Smaller fiber bore diameter improves the surface area / volume ratio of the fiber (appendix A.4.), while undesirably increasing the pressure drop across the fiber (appendix A.6.).

High core flow rates (>600 ml/hr) and low take-up rates (<10-15 m/min) can lead to formation of a thicker core layer. A thick core layer wall can have a relatively denser structure with a prolonged vitrification process due to the slower ingress of the external coagulant.

The above table indicates a low breakthrough capacity for fiber sorbent with a thicker core layer with the same sheath layer thickness due to higher meso/macroporous diffusion resistance and longer diffusional path length to reach the zeolite particles.

The sheath flow rate was varied between 0.2 – 0.7 of the core layer (section 5.4.). A low sheath flow rate (< 0.3 of the core flow rate) caused a highly defective sheath layer with high permeance. A high sheath flow rate (> 0.5 of the core flow rate) reduced the defects in the sheath layer; however it led to the formation of a less porous core layer with lower breakthrough sorption capacity due to slower core phase separation.

Table 5.9: The effect of core and sheath layer thickness on fiber sorbent performance. Module length L_M = 53 cm, Number of fibers N_f = 4, fiber spinning conditions summarized in Table 5.6. Feed condition: 30 ppm H_2S / N_2, T = 298 K, p = 1 atm, flow rate = 80 cm^3/min, activated at 393 K under N_2 purge till water vapor concentration < 10 ppm.

Fiber ID	Upstream pressure	Breakthrough capacity (normalized)	LUB/L_M	Sheath thickness	Bore diameter	Core thickness
	(psig)	mg H_2S/g fiber		μm	μm	μm
1.	1.5	0.28	0.50	50	295	158
2.	0.2	0.18	0.67	32	460	187
3.	1.0	0.36	0.30	30	330	138

It is clear from the above discussion that considerable optimization is required in the various fiber sorbent layers, and optimization of one layer can adversely affect the performance of the other. This study was found of less relevance for the proof-of-concept work considered here.

5.13. Effect of sulfur gas flow rate through the module

In the case of pellet packed beds the meso/macroporous mass transfer is the slow and rate determining step (Appendix A.5.1.) Hence, an increase in the flow rate through the pellet packed bed which does not affect the meso/macroporous mass transfer rate decreases the breakthrough capacity drastically due to shorter residence time of the gas in the module [35].

Advantageously, the external mass transfer is the rate determining step in a highly porous fiber sorbent with large pores/voids (appendix A.5.) [1]. A higher gas flow rate through the fibers improves the external mass transfer in the fiber sorbents thus improving the performance kinetics. However, the pressure drop across the fiber

increased with higher bore side feed flow rate as calculate by Hagen-Poiseuille's equation (appendix A.6.).

To verify the trend observed from the calculations (appendices A.5. and A.6.), a dual-layer fiber sorbent module was first activated at 120 °C under a N_2 purge and tested at 300 cm^3/min H_2S/N_2 flow rate (Table 5.10). The module was then regenerated using the same protocol (in activation), and the H_2S/N_2 flow rate was varied to study its effect on the breakthrough capacity and the pressure drop across the module.

Table 5.10: Effect of external mass transfer resistance on a dual-layer fiber sorbent (ID: 4, Table 5.6.) by varying the H_2S/N_2 flow rate. Module length L_M = 53 cm, Number of fibers N_f = 6. Feed condition: 30 ppm H_2S / N_2, T = 298 K, p = 1 atm, activated and regenerated at 393 K under N_2 purge till water vapor concentration < 10 ppm.

H_2S/N_2 flow rate	Upstream pressure	Breakthrough capacity	Breakthrough capacity (normalized)	LUB/L_M
(cm^3/min)	(psig)	mg H_2S/g fiber	mg H_2S/g sorbent	
300	5.9	0.4	0.61	0.33
80	1.8	0.44	0.67	0.33
50	1.3	0.4	0.61	0.30
30	0.8	0.36	0.55	0.28

The breakthrough sorption capacity was found to increase with higher flow rate (Table 5.10). Fiber sorbents indicate a laminar flow (appendix A.5.) with a parabolic velocity profile with higher axial velocity and concentration at the center of the bore rather than near the edges. Though, the external mass transfer improves with higher flow rate the breakthrough capacity of fiber sorbent starts decreasing above a certain flow rate due to shorter residence time in module (Table 5.10).

5.14. Effect of bore fluid composition

Appropriate non-solvent content in the bore fluid can improve the phase separation of the core layer in the air-gap, while a high solvent or non-solvent content can be detrimental to fiber sorbent morphology (section 4.3 and 4.4.). High solvent concentration (90/10 wt. % NMP/water) in the bore fluid was found to slow down core layer phase separation forming an undesired radially outward porosity gradient (section 5.6.) observed in Figure 5.13 (a) [23].
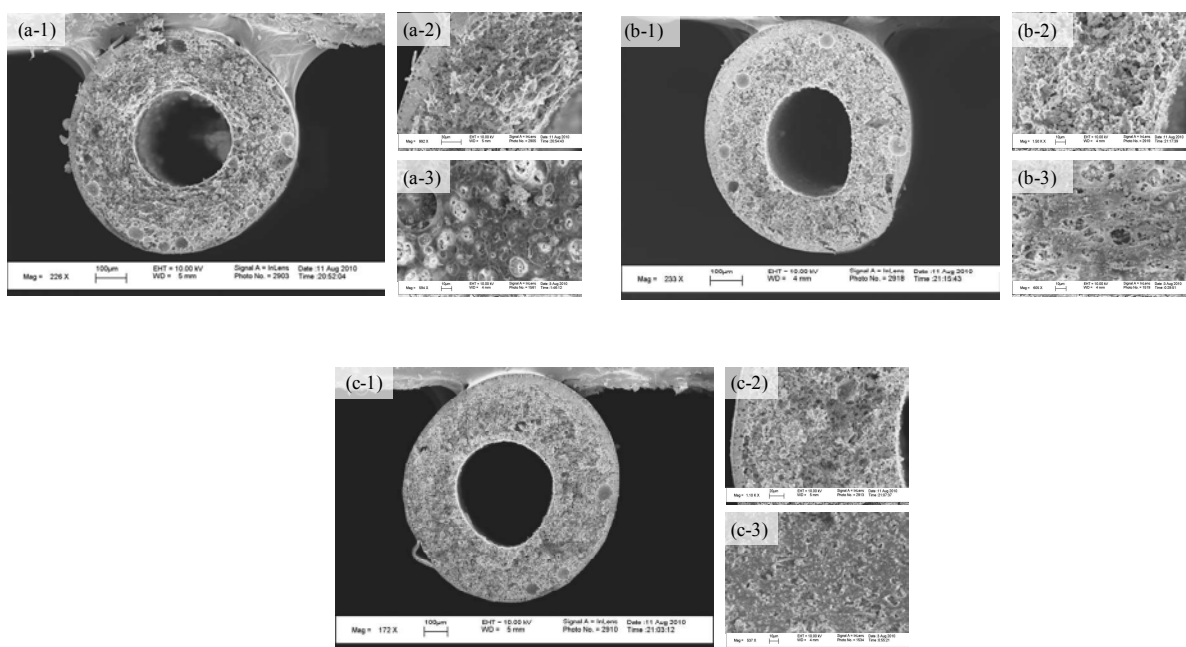
Figure 5.13: Effect of variation in core layer morphology of dual-layer fiber sorbents with variation in the bore fluid composition. (a) NMP/water – 90/10 wt.% (b) NMP/water – 70/30 wt.% (c) NMP/water – 50/50 wt.%. The larger images (a-1,b-1,c-1) show the overall fiber morphology, the smaller top images (a-2,b-2,c-2) show the close-up view of the core-layer morphology and the smaller bottom images (a-3,b-3,c-3) show the horizontal image of the bore-core interface viewed from the bore layer.

On the contrary, very high non-solvent content (50/50 wt. % NMP/water) caused a rapid phase separation at the bore-core interface, leading to a dense inner skin layer that creates an undesirable additional mass transfer resistance (Figure 5.13.(c)). Bore fluid in the range of 80/20 to 60/40 wt. % NMP/Water bore fluid composition gave a uniform

porosity core layer with larger number of small pores in the inner core layer in higher non-solvent content case. The effect of bore fluid composition on the core-sheath interface was found to be negligible.

5.15. EDX analysis

EDX analysis was used to study the adhesion and extent of interpenetration of PVDC and CA/NaY layers. Penetration of PVDC barrier layer into the porous core morphology can lead to reduction in pores/voids causing higher meso/macroporous resistance. In dual-layer fiber sorbents with good adhesion, the chlorine peak present only in PVDC drops sharply at the interface (Figure 5.14), similarly oxygen peak present only in CA drops sharply as well, indicating a small interface. Interface thickness was measured to be approximately 5-10 μm (Figure 5.14). This clearly indicates that with a small contact time (~ 0.1-3 s) between the two layers in the air gap before phase separation in the water quench bath, the interpenetration is limited to the interface.

EDX analysis can also help predict zeolite distribution in the core layer. The Si or Na peak intensity in dual-layer fibers was found to be uniform throughout the core layer (Figure 5.14). A similar trend was observed in single-layer fiber sorbents described in detail in section 4.3. This trend was expected since the CA/NaY core dope compositions in single and dual-layer fibers were the same.
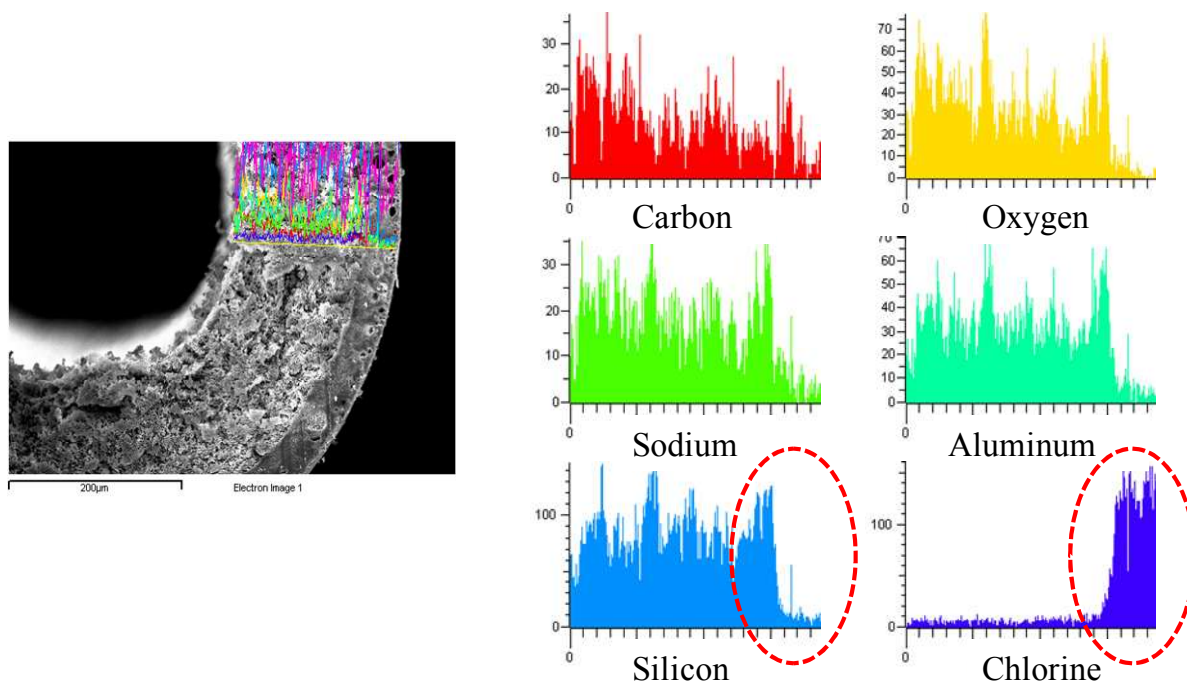
Figure 5.14: SEM-EDX line scan spectra of the cross section of a dual-layer fiber sorbent.

5.16. Obtaining a defect-free sheath layer

Dual-layer fibers with an apparently dense and low permeance sheath layer were successfully created; however, the sheath layer was still defective with Knudsen selectivity. In order to test the barrier layer efficacy under continuous TSA cycles with steam, the sheath layer defects must be removed.

The large difference between the T_g of the CA core ($T_g \sim 180$ °C) and PVDC sheath ($T_g \sim 18$ °C) could be used advantageously by annealing or cross linking the sheath layer at around 120 °C to seal the defects, while still maintaining core layer porosity. Silicon rubber coating [36] or reactive post treatment technique [37] could also be used to seal the sheath layer defects. Alternatively, to avoid the drawbacks of dual-layer spinning, post-treatment of single-layer fiber sorbents with barrier material latex coatings

could also be explored to create a barrier sheath layer [31]. All of the above mentioned post treatment options are considered in detail in chapter 6.

5.17. Summary and conclusions

Dual-layer fiber sorbents with a high sorbent loading, porous core and a barrier sheath layer were successfully created using co-extrusion spinning. Effects of various spinning parameters were studied and the fibers were characterized. The key differences in a single-layer and dual-layer fibers were identified and compared with respect to ease of fabrication and operation. Although the sheath layer was defective indicating Knudsen selectivity, the fibers showed good H_2S sorption capacity under flow conditions.

The dual-layer spinning technology with a hydrophilic core and a hydrophobic sheath layer could also find applications in in-direct contact heat exchangers, membrane contactors and direct contact membrane distillation.

5.18. REFERENCES

1.   Bhandari, D.A., N. Bessho, and W.J. Koros, *Hollow fiber sorbents for desulfurization of natural gas.* Industrial & Engineering chemistry research, In-press.

2.   Bonjour, J., M. Clausse, and F. Meunier, *A TSA process with indirect heating and cooling: parametric analysis and scaling-up to practical sizes.* Chemical Engineering and Processing, 2005. 44(9): p. 969-977.

3.   Husain, S. and W.J. Koros, *Mixed matrix hollow fiber membranes made with modified HSSZ-13 zeolite in polyetherimide polymer matrix for gas separation.* Journal of Membrane Science, 2007. 288(1-2): p. 195-207.

4.   Widjojo, N., T.S. Chung, and S. Kulprathipanja, *The fabrication of hollow fiber membranes with double-layer mixed-matrix materials for gas separation.* Journal of Membrane Science, 2008. 325(1): p. 326-335.

5.   Jiang, L.Y., et al., *Fundamental understanding of nano-sized zeolite distribution in the formation of the mixed matrix single- and dual-layer asymmetric hollow fiber membranes.* Journal of Membrane Science, 2005. 252(1-2): p. 89-100.

6.   Li, Y., et al., *Dual-layer polyethersulfone (PES)/BTDA-TDI/MDI co-polyimide (P84) hollow fiber membranes with a submicron PES-zeolite beta mixed matrix dense-selective layer for gas separation.* Journal of Membrane Science, 2006. 277(1-2): p. 28-37.

7.   Jiang, L.Y., et al., *Fabrication of Matrimid/polyethersulfone dual-layer hollow fiber membranes for gas separation.* Journal of Membrane Science, 2004. 240(1-2): p. 91-103.

8.   Pereira, C.C., et al., *Hollow fiber membranes obtained by simultaneous spinning of two polymer solutions: a morphological study.* Journal of Membrane Science, 2003. 226(1-2): p. 35-50.

9.   Li, D.F., et al., *Fabrication of fluoropolyimide/polyethersulfone (PES) dual-layer asymmetric hollow fiber membranes for gas separation.* Journal of Membrane Science, 2002. 198(2): p. 211-223.

10.   Hosseini, S.S., N. Peng, and T.S. Chung, *Gas separation membranes developed through integration of polymer blending and dual-layer hollow fiber spinning process for hydrogen and natural gas enrichments.* Journal of Membrane Science, 2010. 349(1-2): p. 156-166.

11. Li, D.F., T.S. Chung, and W. Rong, *Morphological aspects and structure control of dual-layer asymmetric hollow fiber membranes formed by a simultaneous co-extrusion approach.* Journal of Membrane Science, 2004. 243(1-2): p. 155-175.

12. He, T., et al., *Preparation of composite hollow fiber membranes: co-extrusion of hydrophilic coatings onto porous hydrophobic support structures.* Journal of Membrane Science, 2002. 207(2): p. 143-156.

13. Bonyadi, S. and T.S. Chung, *Flux enhancement in membrane distillation by fabrication of dual layer hydrophilic-hydrophobic hollow fiber membranes.* Journal of Membrane Science, 2007. 306(1-2): p. 134-146.

14. Kim, B.K., et al., *Modified polyacrylonitrile blends with cellulose acetate: blend properties.* Polymer, 2000. 41(1): p. 385-390.

15. Oh, Y.S., et al., *Modified polyacrylonitrile blends with cellulose acetate: Fibers' properties.* Journal of Applied Polymer Science, 1997. 64(10): p. 1937-1946.

16. Claytor, R.C., Sasthav, M., *Packaging Material having Good Moisture Barrier,U.S. Patent 5,935,664* Aug. 10,1999.

17. Turbak, A.F., Rose, H. J., Ill, D., *Saran Coating of Cellulosic Casing,U.S. Patent 3,794,515.* Feb. 26,1974.

18. Cheng, D.Y., Wiersma, S. J., *Composite Membrane for a Membrane Distillation System,U.S. Patent 4,419,242.* Dec. 6,1983.

19. Vazqueztorres, H. and C.A. Cruzramos, *Poly(Vinylidene Fluoride) Cellulose Acetate-Butyrate Blends - Characterization by Dsc, Waxs, and Ftir.* Polymer Bulletin, 1994. 33(6): p. 673-680.

20. IXAN-PNE-288. *http://www.ixan-diofan.com/.* Date accessed, October 8th, 2010.

21. Paul, D.R. and S. Newman, *Polymer blends.* 1978, New York: Academic Press.

22. Wahrmund, D.C., et al., *Polymer Blends Containing Poly(Vinylidene Fluoride) .1. Poly(Alkyl Acrylates).* Polymer Engineering and Science, 1978. 18(9): p. 677-682.

23. Koros, W.J. and G.K. Fleming, *Membrane-Based Gas Separation.* Journal of Membrane Science, 1993. 83(1): p. 1-80.

24. Chung, T.S., S.K. Teoh, and X.D. Hu, *Formation of ultrathin high-performance polyethersulfone hollow-fiber membranes.* Journal of Membrane Science, 1997. 133(2): p. 161-175.

25. Shilton, S.J., G. Bell, and J. Ferguson, *The Rheology of Fiber Spinning and the Properties of Hollow-Fibre Membranes for Gas Separation.* Polymer, 1994. 35(24): p. 5327-5335.

26. Wang, D.L., K. Li, and W.K. Teo, *Preparation and characterization of polyvinylidene fluoride (PVDF) hollow fiber membranes.* Journal of Membrane Science, 1999. 163(2): p. 211-220.

27. Jung, B., et al., *Effect of molecular weight of polymeric additives on formation, permeation properties and hypochlorite treatment of asymmetric polyacrylonitrile membranes.* Journal of Membrane Science, 2004. 243(1-2): p. 45-57.

28. Brandrup, J., E.H. Immergut, and E.A. Grulke, *Polymer handbook.* 4th ed. 2004, New York ; [Chichester]: Wiley-Interscience.

29. Wallace, D.W., C. Staudt-Bickel, and W.J. Koros, *Efficient development of effective hollow fiber membranes for gas separations from novel polymers.* Journal of Membrane Science, 2006. 278(1-2): p. 92-104.

30. Ixan-Diofan.*http://www.ixan-diofan.com/static//wma/pdf/2/1/7/6/Diofan%20A602%20-%20rév%204%20.pdf*. Date accessed, October 8th, 2010.

31. Lively, R.P., et al., *Hollow Fiber Adsorbents for CO2 Removal from Flue Gas.* Industrial & Engineering chemistry research, 2009. 48(15): p. 7314-7324.

32. Avramescu, M.E., Z. Borneman, and M. Wessling, *Dynamic behavior of adsorber membranes for protein recovery.* Biotechnology and Bioengineering, 2003. 84(5): p. 564-572.

33. Bessho, N., D.A. Bhandari, and W.J. Koros, *Hollow Fiber Sorbents for Hydrogen Recovery.* Chemical Engineeing Science, Submitted.

34. Kosuri, M.R., *Polymeric membranes for super critical carbon dioxide (scCO2) separations*. 2009, Georgia Institute of Technology: Atlanta, Ga. p. 1 v. (various pagings).

35. McCabe, W.L., J.C. Smith, and P. Harriott, *Unit operations of chemical engineering*. 6th ed. 2001, Boston: McGraw Hill.

36. Henis, J.M.S. and M.K. Tripodi, *Composite Hollow Fiber Membranes for Gas Separation - the Resistance Model Approach.* Journal of Membrane Science, 1981. 8(3): p. 233-246.

37. Ekiner, O.M., Kulkarni, S. S., *Process for making hollow fiber mixed matrix membranes,U.S. Patent 6,663,805B1*. 16 December, 2003.

CHAPTER 6

POST-TREATMENT OF SINGLE AND DUAL-LAYER FIBER

SORBENTS

Abstract

Hollow fiber sorbents provide a pseudo monolithic approach with potential applications in gas and liquid separations. In this work, single-layer fiber sorbents were created by hollow fiber spinning technology with a polymer 'binder', impregnated with high loadings of sulfur selective zeolite sorbent 'fillers'. Rapid regeneration using steam/water is a key proposed advantage of fiber sorbents over conventional pellet packed bed operation and valuable for the realization of this technology.

To obtain consistent sorption capacities over repeated cycles, a dense and thin polymer barrier layer is desired to allow only thermal interactions with the heating (steam) and cooling (water) media. Previous chapters (4 and 5) explored the creation and characterization of single and dual-layer fiber sorbents for the removal of sulfur impurities. This chapter explores various post treatment techniques to obtain a defect-free barrier sheath layer on the fiber sorbents.

6.1. Introduction

Creation and characterization of single and dual-layer fiber sorbents was considered in detail in chapter 4 and 5. Proof of concept regeneration experiments with hot purge gas indicated the viability of temperature swing regeneration of fiber sorbents. However, to obtain the full advantage over pellet packed bed technology, rapid regeneration of fiber sorbents with steam and water is required (Appendix A.8.). For the effective regeneration of fiber sorbents, a low permeance defect-free barrier sheath layer is desired.

Dual-layer fibers with a dense and low permeance sheath layer were successfully created (chapter 5); however, the sheath layer was still defective with Knudsen selectivity. Heat treatment or annealing [1, 2], silicone rubber coating [3] and reactive post treatment techniques [4] have been described in conventional membrane literature to seal pin-hole defects in skin layers of hollow fiber membranes. These techniques are also utilized in this work to seal the minor defects in the sheath layer skin. Alternatively, a new post treatment technique using latex solution of a barrier polymer could be developed to create a barrier sheath layer on single-layer fiber sorbents or to caulk a severely defective barrier sheath layer in dual-layer fibers [5].

6.2. Heat treatment of dual-layer fiber sorbents

The large difference between the glass transition temperatures (T_g) of the CA core (T_g ~ 180-210 °C) and the PVDC sheath (T_g ~ 5-25 °C) could be used advantageously by heat treating or densifying the sheath layer at around 110-120 °C to seal the sheath layer defects, while still maintaining the core layer porosity. In gas separation membranes, above T_g annealing is often used to reduce the polymer free volume by chain relaxation.
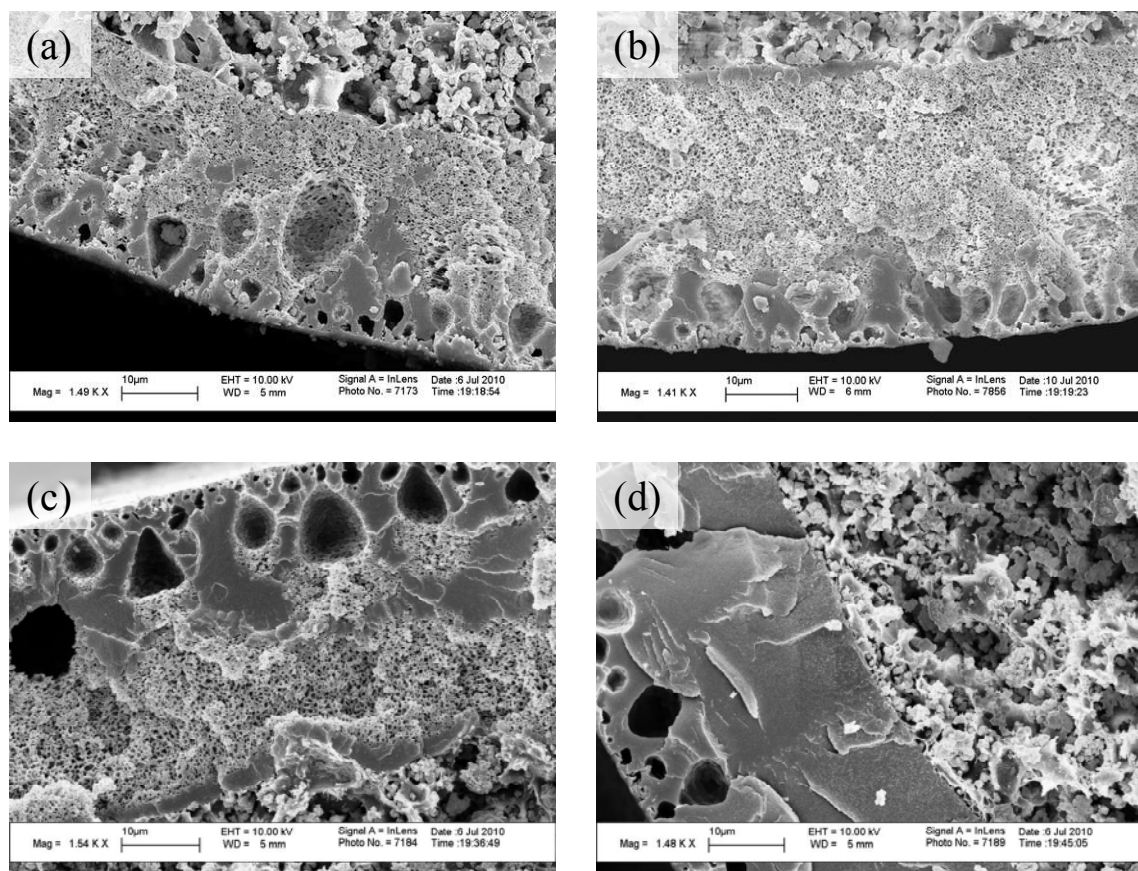
Figure 6.1: SEM images of the sheath layer of a dual-layer fiber sorbent used for heat treatment studies (a) under vacuum at 120 °C for 4 h (b) under vacuum at 120 °C for 24 h (c) under vacuum at 120 °C for 48 h (d) under vacuum at 150 °C for 48 h.

In dual-layer fiber sorbents formed by the dry jet-wet quench spinning technique the PVDC sheath layer has an asymmetric structure with a dense skin and a porous substructure (discussed in section 5.6.). The dense skin layer provides true gas/water vapor barrier properties, while the substructure provides support to the skin layer. It is thus desirable to densify the substructure to enable the entire sheath layer to show dense film barrier properties. The heat treatment was conducted as per the protocol described in section 3.3.7.1. The heat treatment studies were also important since fiber sorbent modules operated under flow conditions will be exposed to high temperatures (110-120

°C) during activation (to remove sorbed water vapor from zeolite crystals in the fiber sorbent) and regeneration (to remove sorbed sulfur species from the sorption step).

In the first study, the fibers were kept at 120 °C under vacuum in an oven for various time intervals, while in the second study the fibers, activated for various time intervals at 110-120 °C under a N_2 purge flow (for sorption experiments discussed in chapter 4 and 5), were investigated.

The sheath layer showed gradual densification on exposure to heat for longer durations as observed from the SEM images in Figure 6.1. The densification was observed to start from the outer part of the sheath layer (Figure 6.1 (a)) and to progress in a radially inward direction (Figure 6.1 (b) and (c)). The fibers exposed to vacuum conditions (first study) and Nitrogen environment (second study) did not show significant variation in the densification process possibly due to inert conditions in both the cases. Hence, in actual operation the barrier efficacy of a dual-layer fiber with a 'defect-free' sheath layer could improve over multiple regeneration cycles due to densification and formation of a thicker barrier skin.

Slight densification of the sheath layer was observed under SEM (Figure 6.1); however, the N_2 permeance did not decrease significantly and Knudsen selectivity (for O_2/N_2) was still observed indicating the presence of defects.

Pure polymer PVDC grades have been shown in literature to undergo degradation by a free-radical chain reaction between 160-200 °C to form an unsaturated crosslinked residue with the elimination of HCl gas [6-8]. The degradation is accelerated at higher temperatures and upon exposure to oxygen or air [8], while high vacuum and inert environment (N_2 or He) retard the degradation process.

Advantageously, the P(VDC-MA) copolymer grade used in this work was found to have a melting point between 150-170 °C with a degradation temperature of around 180 °C (determined by DSC measurements, section 3.4.3).

Also, the polymer powder sample did not indicate any weight loss upon heating to 110 °C under a nitrogen purge for 20 h in TGA (Figure 6.2), confirming its stability. The weight loss, probably due to degradation of the polymer was observed around 160-180 °C in the TGA studies (Figure 6.2).
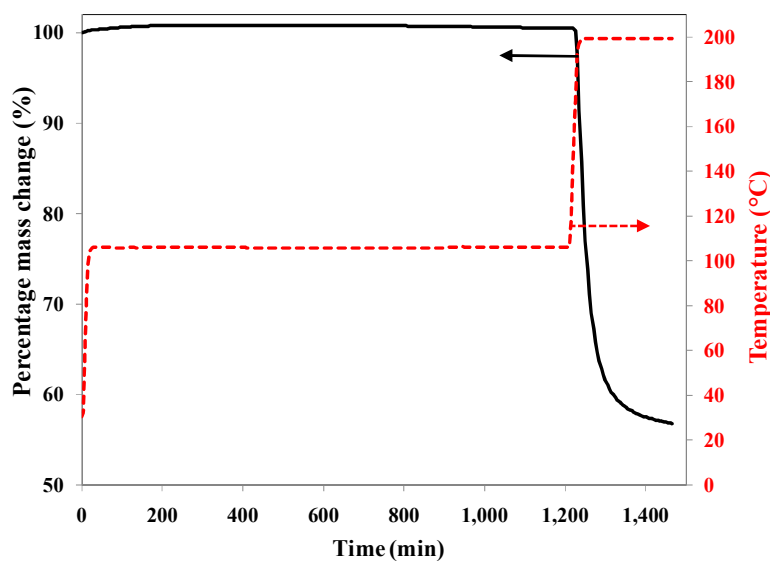
Figure 6.2: TGA results for P(VDC-MA) powder (IXAN®-PNE-288) in N_2 environment at 110 °C for 20 h and 200 °C for 4 h.

To further verify the results from TGA and DSC and to check the effects of high temperature on the PVDC barrier sheath layer, dual-layer fiber sorbent samples were kept at 150 °C under vacuum for 48 h. SEM image (Figure 6.1(d)) and visual observation showed complete densification and substructure collapse of the sheath layer possibly due to degradation and pyrolysis.

Advantageously, in this work the feed gas (natural gas) and the purge gas (natural gas or nitrogen) have negligible oxygen content with a regeneration temperature of 110-120 °C (well below the sheath degradation temperature~150-180 °C).

Though promising, the heat treatment process was not found to be effective to seal the sheath layer defects. However, it showed that the sheath layer was able to sustain high temperatures (110 °C) without degrading and the core layer did not show any undesired matrix densification due to heat treatment.

6.3. Sylgard® (silicone rubber) post treatment

Silicone rubber post treatment method is commonly employed to plug skin layer defects of asymmetric hollow fiber membranes [3]. The high permeability polydimethylsiloxane (PDMS) layer does not decrease the membrane permeance significantly; however minor pin-hole defects providing a non-selective pathway to gases are plugged, thus improving the selectivity. The protocol followed in this work is described in detail in section 3.3.7.2. Pure gas permeance tests with oxygen and nitrogen were conducted using the constant volume system described in section 3.4.8.2.

Gases were used as the first step to test the barrier layer efficacy as opposed to water vapor due to operational simplicity. Also, water vapor (σ~2.8 Å, T_c = 647 K) is highly permeable (small molecular diameter (σ)) and highly sorptive (proportional to critical temperature (T_c)), compared to gases like N_2 (σ~3.6 Å, T_c = 126 K). Hence, a defective barrier sheath layer indicating Knudsen selectivity and high permeance for N_2 would surely be defective for highly permeable water vapor.

Table 6.1: Comparison of permeance in a slightly and highly defective fiber sorbent state before and after silicone rubber post treatment. Module length available for permeation L_p = 15 cm, Number of fibers N_f = 3, Module temperature = 35 °C. The fiber spinning conditions and fiber id are summarized in section 5.9. and Table 5.6.

Fiber ID	Permeance - N_2 (P/ ℓ - GPU) at 30 psig	Selectivity (α_{O_2/N_2})
1. (Before post treatment)	2.2	0.91
1. (After post treatment)	0.0008	1.85
3. (Before post treatment)	387	0.91
3. (After post treatment)	3	0.98
$\alpha_{Knudsen}$ (O_2/N_2)= 0.93		

Table 6.1 compares the permeance properties of two spin states (ID: 1 and 3). Both the fiber spin states had the same core and sheath dope compositions (Table 5.6. and section 5.4.). Fiber ID: 1 showed low permeance of around 2.2 GPU, and ID: 3 indicated a high permeance of around 387 GPU before post treatment with Sylgard®. The reason for lower permeance in ID:1 could be due to a thicker, less defective sheath layer formed by a high sheath layer flow rate. However, as summarized in section 5.12., the fiber ID:1 had a lower breakthrough capacity (normalized : 0.28 mg H_2S/g sorbent) vs. a breakthrough capacity (normalized : 0.36 mg H_2S/g sorbent) for ID: 3 possibly due to a denser and thicker core layer.

Table 6.2: Spinning conditions of the dual-layer fibers tested in this work (refer section 5.9. for details of the table)

ID	Core/Sheath composition	Bore fluid composition	Core flow rate	Bore flow rate	Sheath flow rate	Air gap	Take-up rate
		NMP/water (wt.%)	(mL/h)	(mL/h)	(mL/h)	(cm)	m/min
1.	Core-b3/Sheath-2	60 / 40	300	100	150	10	15
3.	Core-b3/Sheath-2	60 / 40	180	60	60	10	11

Both the fiber modules (ID: 1 and 3) were post treated by Sylgard$^{®}$ using the protocol described above. The permeance of ID: 1 decreased dramatically to 0.0008 GPU with an O_2/N_2 selectivity of 1.85 (higher than O_2/N_2 Knudsen selectivity = 0.93), with a skin layer thickness of ~1-5 μm (measured from SEM). This permeance was found close to the ideal N_2 permeance of~0.001 GPU expected for a 1 μm thick defect-free PVDC skin layer, calculated based on a dense film N_2 permeability of 0.001 Barrer with an O_2/N_2 selectivity of~5. The lower selectivity (compared to the idea selectivity~5) could be due to some remaining defects near the potting region of the hollow fiber module.

It must be emphasized here that the goal of this work is to obtain a barrier sheath layer with low permeance for gas or water vapor flow even if selectivity is less than ideal dense film values. This is contrary to hollow fiber membranes where both permeance (productivity) and selectivity (purity) are equally important for effective operation.

The permeance of ID: 3 decreased from 387 GPU to 3 GPU with an O_2/N_2 selectivity of 0.98 (Knudsen selectivity), indicating that the silicone rubber treatment was not effective in fixing a highly defective sheath layer. Hence, there was found a need to develop a post treatment technique where latex coating of a barrier polymer could be applied to either create a barrier layer on single-layer fiber sorbents or to caulk a highly defective sheath layer in dual-layer fiber sorbents.

6.4. PVDC latex post treatment

A latex solution of PVDC available in an aqueous dispersion form was used in this work. The dry film properties of the PVDC solution (Diofan®-XB-204, section 3.1.2.) were reported to be similar to the film properties of the PVDC powder form (IXAN®-PNE-288, section 3.1.2.) used for the sheath layer formation in dual-layer fiber spinning.

6.4.1. Post treatment of single-layer fiber sorbents

Post treatment of single-layer fiber sorbents was explored as an alternative to dual-layer fiber sorbent spinning as the conflicting properties of a porous core and an impermeable sheath layer could be tailored independently.

Certain advantages in creating the barrier layer by post treatment of single-layer fiber sorbents are described as follows:

1. The maximum achievable zeolite loading in the core layer of dual-layer fibers was 65 wt. % (dry fiber wt. basis, chapter 5) compared to a maximum achievable zeolite loading of 75 wt. % (dry fiber wt. basis, chapter 4) in case of single-layer fiber sorbents.

2. The breakthrough/dynamic capacity of the core layer of a dual-layer fiber sorbent was slightly lower than the capacity observed in single-layer fiber sorbent with similar zeolite loadings, possibly due to the slower phase separation of the core layer in dual-layer fiber spinning (section 5.10.).

3. In case of dual-layer fibers the 20-50 μm sheath layer had an asymmetric structure with a 0.1-1 μm thick skin layer providing the barrier properties. While in the case of post-treatment the entire coating layer is dense and provides barrier properties. Also,

the thickness of the barrier layer could be increased by conducting multiple latex washes (2-3 washes).

On the negative side, however, the post-treatment technique requires an extra step for creation of the barrier layer, while in dual-layer fiber spinning the core and the sheath layer with uniform dimensions can be created simultaneously in one-step. The detailed choice of which barrier layer creation approach would be preferred for actual scale-up will require considerable additional work; however, the work here shows that both approaches are viable.

Single-layer fibers with high sorbent loadings (75 wt.%, dry fiber wt basis) could be spun with a desired morphology as explained in chapter 4. Solvent exchanged and dried fiber sorbents were then exposed to PVDC aqueous dispersion solution.

Spray and dip coating methods (section 3.3.7.3.) did not yield consistent results often leading to cracked coatings due to unstable removal during the withdrawal of fibers. The two techniques required treatment of individual fibers and fine control during immersion and withdrawal and were found difficult to scale-up. These techniques were abandoned for the coating method using a module design.

In this post treatment technique the solvent exchanged fiber sorbents were potted into a module with a shell and tube geometry (section 3.3.6.) [9, 10], to enable further testing of the fibers for permeation (section 3.4.8) and flow through sorption/regeneration experiments (section 4.7.) directly after post treatment. Figure 6.3 shows the schematic of the setup used for the post treatment of single-layer fiber sorbents.
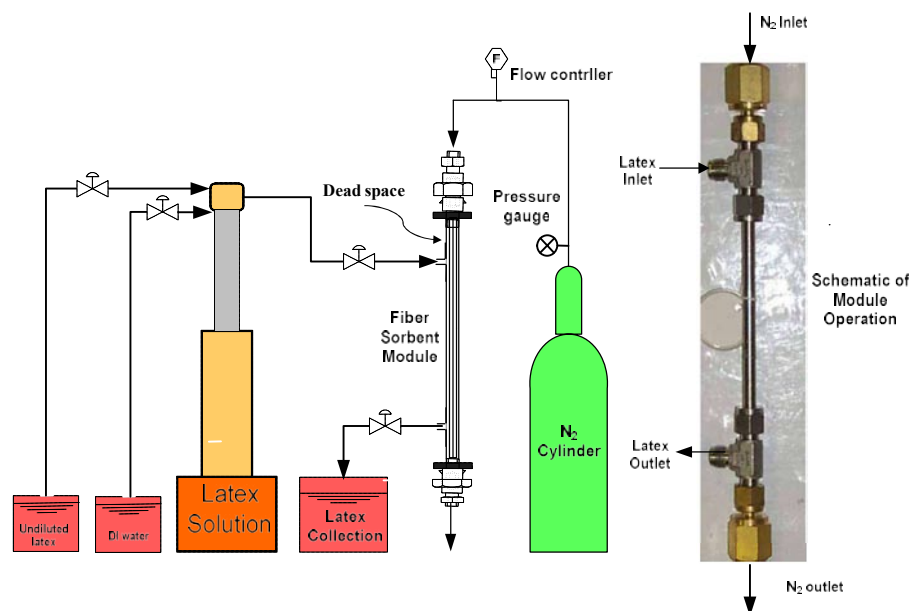
Figure 6.3: Schematic representation of the latex post treatment method for creating a barrier layer on single-layer fiber sorbents (fiber module is shown enlarged for better clarity)

Modules were clamped in a vertical position to provide ease of flow and rapid draining of the post treatment solution. Initially, while developing and modifying the experimental protocol the fibers modules were created with clear Teflon® tubing to carefully observe the flow profile in the modules. The protocol for testing was defined after considerable trial and error to give best results in terms of uniformity and permeance of the coated barrier layer. Once the post treatment protocol was optimized, stainless steel modules were used since it gives low leak rates (important for accurate permeance measurements) and has the ability to sustain high temperatures ($\sim$120 °C, important for the activation and regeneration of fiber sorbents). The optimized protocol and rationale behind each step are described as follows:

A few drops of inert food colorant (blue or green color, ratio: 0.5 g in 500 g latex solution) were added to the milky white latex solution to enhance the observability of the

coating on the CA/NaY fiber sorbents (off-white color). The as-obtained Diofan$^®$ latex solution was diluted from 55 wt. % solids to 10–15 wt. % solid content by the addition of DI Water and supplied at a constant flow rate to the shell side of the module by a syringe pump (Figure 6.3). Dilution helped in reducing viscosity, enabling rapid and adequate spreading of the coating liquid through the fiber module.
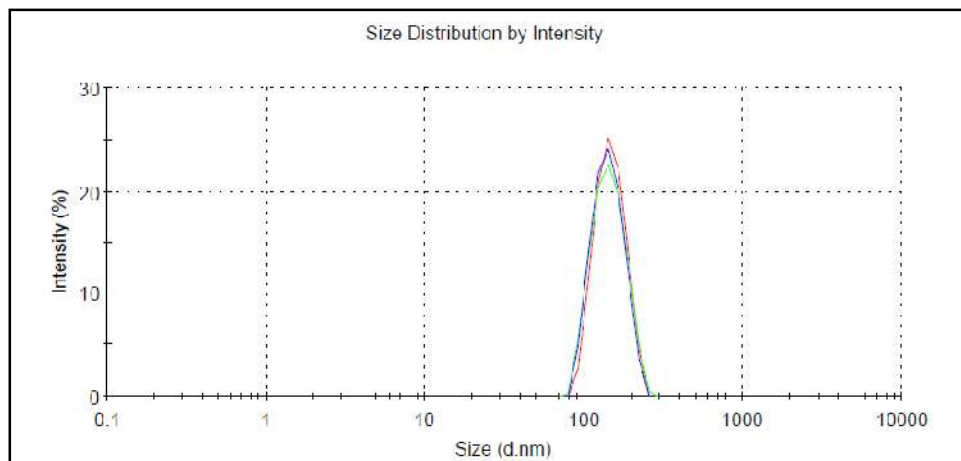
Figure 6.4: Particle size distribution in PVDC latex solution (Diofan$^®$) by light scattering experiments.

Due to the high porosity of the fiber sorbents (void/pores size, 100-300 nm, section 4.4.), PVDC particles ($\sim$50-140 nm, determined by light scattering experiments, Figure 6.4) were found to enter the core layer morphology and block the pores due to capillary suction effect. The blockage of the fiber pores/voids could lead to low breakthrough capacity during the sorption step, due to low diffusivity through the blocked pores (section 4.4.).

Hence, a positive pressure difference was maintained across the fiber sorbent module to prevent the latex solution from entering and blocking the core layer pores. This was accomplished by filling the pores by flowing N_2 through the fiber bore such that neither does it allow the dispersion to get into the pores nor does it blow-off the nascent

coating layer. The concept has been successfully utilized in membrane contactor or extraction processes where the fiber pores are filled with the extraction fluid [11].
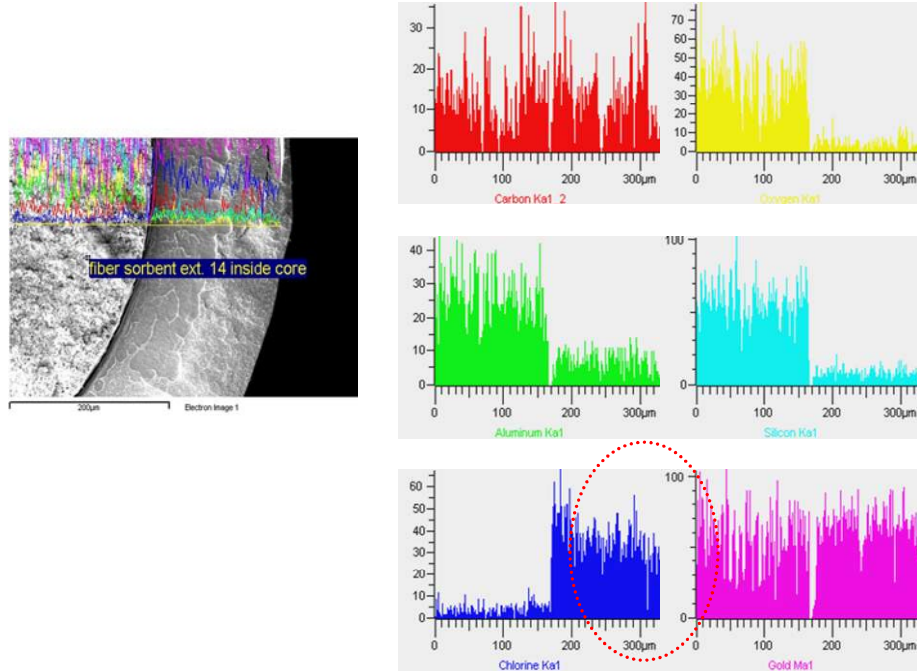
Figure 6.5: SEM-EDX line scan spectra of the cross section of a latex post treated fiber sorbent indicating the absence of PVDC latex particles in the core layer due to the N_2 sweep gas.

The pressure difference required across the fiber module was roughly estimated using the following equation [11].

$$\text{Pr}\,essure\;drop\;(\Delta P) = \frac{2\sigma\cos\Theta}{(r)} \tag{6.1}$$

Where,

Interfacial tension (σ) = 33 mN / m [12]

Contact angle (Θ)= $33^\circ - 40^\circ$ [13]

Pore size (r_{pore}) $\approx$ 300 nm (SEM and permeation measurements)

$$\Delta P = \frac{2 * 33 mN/m * \cos 40^0}{(300 * 10^{-9} m)} \approx 1.7\;atm$$

SEM-EDX was performed on the post treated fiber to confirm the applicability of this methodology (Figure 6.5). Line scan spectra of chlorine atom present only in the PVDC barrier layer clearly indicates that the core layer was not blocked by the PVDC particles.

Three latex washes were conducted with a shell side feed on the module in one flow direction, while simultaneously passing N_2 sweep gas on the bore side (Figure 6.3). In the first wash, the fibers were exposed to diluted Diofan$^®$ ($\sim$10-15 wt.%) at a constant flow rate $\sim$100 ml / min for one minute. This was followed by two slow washes (flow rate$\sim$10-15 ml/min) for 30 minutes each.

During the two slow washes, the latex outlet valve (shell side, Figure 6.3) was closed frequently (every 10 minutes) to allow the module to be filled up with the latex solution to allow access to the dead zones in the module. After filling up the entire module with latex, the inlet valve was also closed and the fibers were soaked for 1 minute. This was followed by opening both the valves (inlet and outlet) and continuing the constant flow rate wash process described above.

The fiber module was then flipped vertically to ensure complete post treatment of the fibers and the above-mentioned washing steps were repeated sequentially. This step ensured that the post treatment solution contacts the dead space near the fiber module potting shown in Figure 6.3.

After, the latex post treatment washes, the N_2 flow through the fiber bore was stopped. The module was then disconnected and excess latex solution was drained. A solvent exchange with hexane could be conducted to remove excess water from the

coating. More number of washes could be conducted if the coating steps did not create a defect-free barrier layer (tested by permeation experiments, section 3.4.8.2.).

Cracked post treatment coating   Non cracked post treatment coating
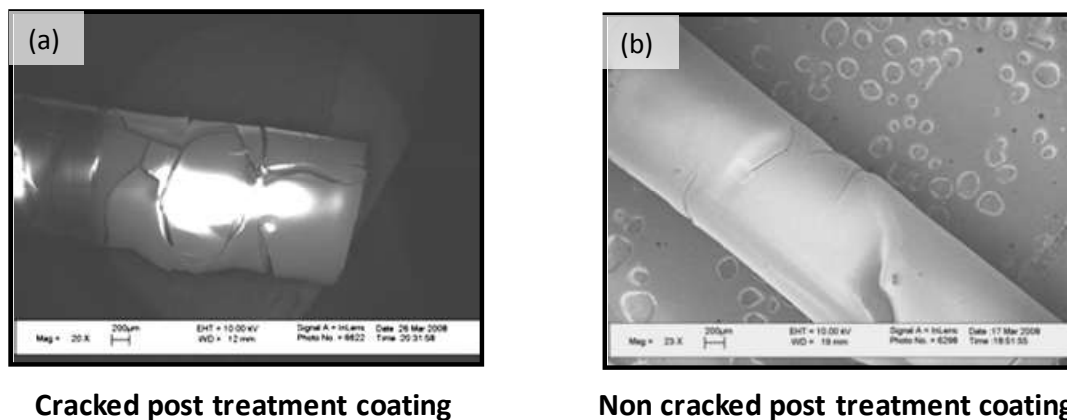
Figure 6.6: SEM images (horizontal) of a post treated single-layer fiber sorbent showing (a) cracked post treatment layer due to rapid drying of the wet coating (b) Uniform post treatment coating layer formed due to a slow and uniform drying.

The post treated module was then vertically mounted and humidified N_2 (70-80 % relative humidity (R.H.)) at 50 cm^3/min flow rate was passed through the shell side of the module for 2-6 h to ensure slow drying of the coating layer. Direct exposure to dry N_2 or heating the module to high temperatures (120 °C) caused rapid and uneven drying of the wet coating leading to cracks as shown in Figure 6.6(a). A cracked coating was found to be defective with high permeance through the barrier layer.

The fibers were then either exposed to dry N_2 (flow rate~50 cm^3/min) for up to 12 h or kept undisturbed in a fume hood for 12 h for slow and uniform drying. The drying protocol (wet N_2 followed by dry N_2) insured the formation of a uniform coating layer with negligible cracks (Figure 6.6 (b)). The post treatment protocol is summarized in Figure 6.7.
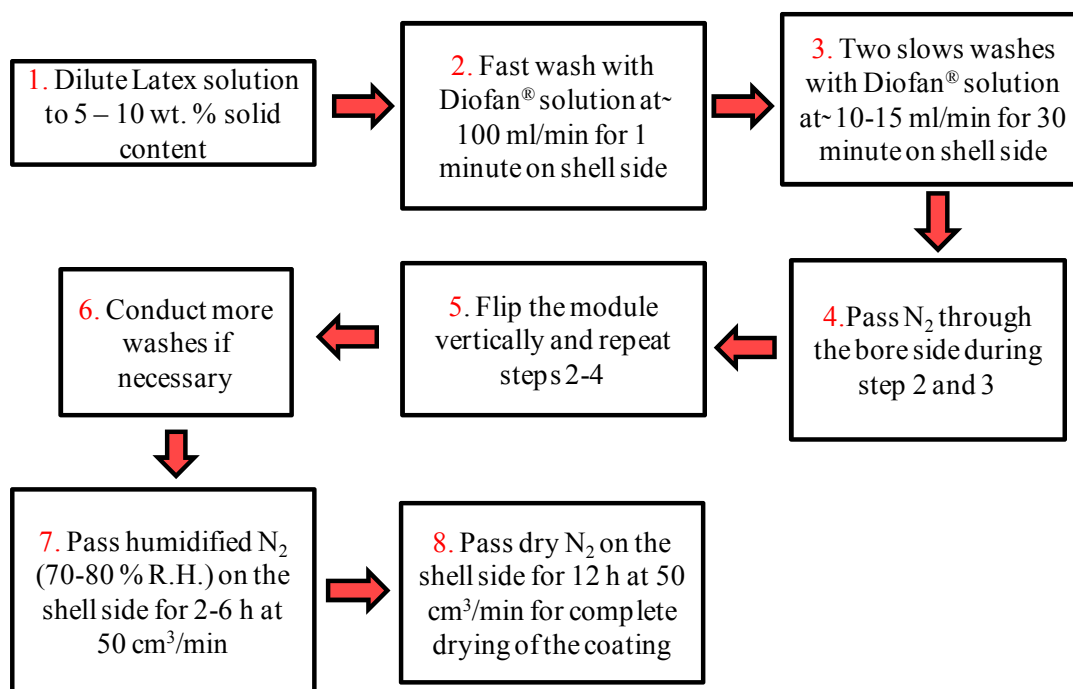
Figure 6.7: Schematic representation of the optimized latex post treatment protocol for single-layer fiber sorbents.

Figure 6.8 shows the SEM images (radial) of a dense and defect free PVDC sheath layer formed on a single-layer fiber sorbent formed by the latex post treatment protocol discussed above.
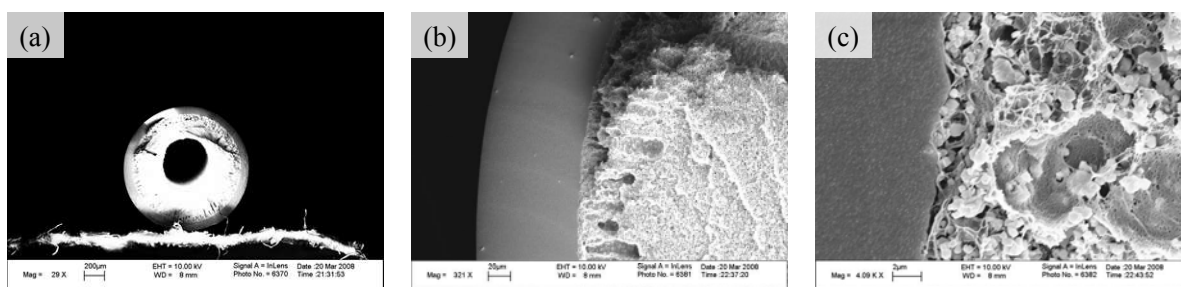
Figure 6.8: SEM images of (a) PVDC latex post treated single-layer fiber sorbent using the protocol shown in Figure 6.7 (b) Dense PVDC barrier coating layer formed on a single-layer fiber sorbent (c) Good adhesion between the post treatment layer and the CA/NaY core layer.

Post treatment methodology, though simple to apply in case of modules with one fiber (Figure 6.9(b)) displayed significant challenges when scaled up for multiple fibers. Post treatment of a multiple fiber module indicated clumping of the fibers as shown in Figure 6.9(a). The clumping of fibers causes uneven and defective coating which leads to poor performance (high permeance) of the barrier sheath layer and could cause slower heat transfer to the fiber sorbent during the regeneration process compared to individual fiber sorbents coated with a sheath layer as shown schematically in Figure 6.10.

Post treatment of fiber bundle   **Post treatment of single fiber**
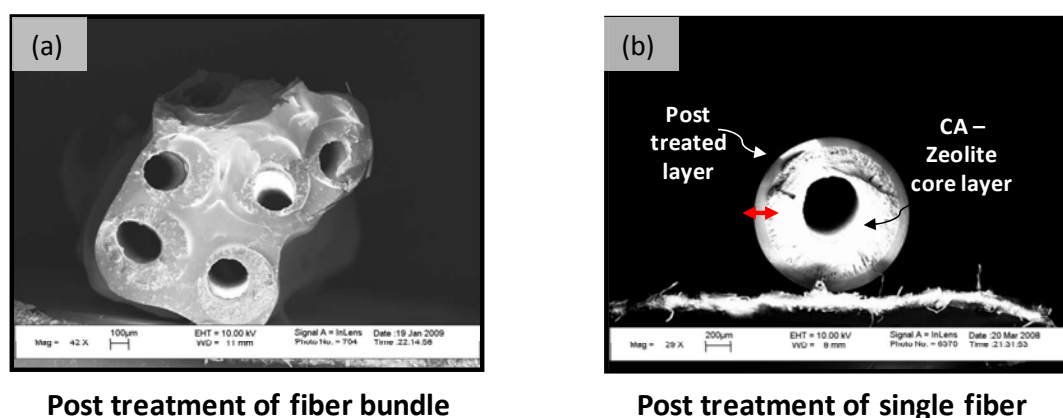
Figure 6.9: (a) SEM image of clumped post treated fibers (b) SEM image of uniformly post treated single fiber.

The clumping was possibly observed due to the hydrophilic nature of the cellulose acetate binder polymer that causes good wettability and spreading of the water based latex solution onto the fiber sorbent surface creating a thick film during post treatment. The tackiness of the latex solution which is useful in creating a uniform barrier layer on individual films or surfaces for industrial applications caused the fibers to stick to each other. As the water was slowly removed in the drying step by a N_2 sweep the high surface tension of water caused the wet coating in the interstitial space of the fibers to coalesce causing clumping.
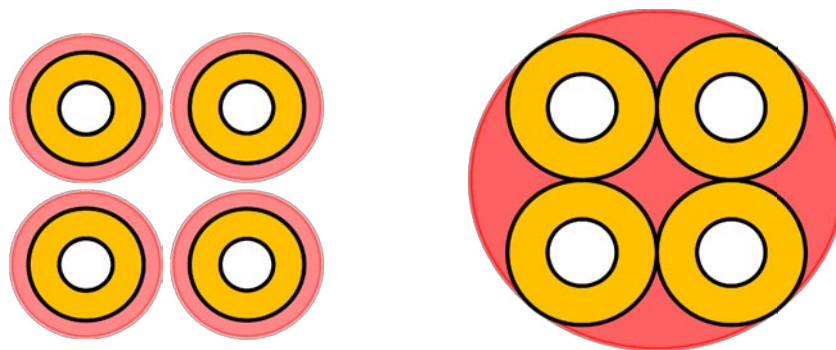
Uniform post treated fiber vs. clumped fiber

Figure 6.10: Schematic representation of a desired barrier layer formation on single-layer fiber sorbents after latex post treatment vs. the undesired fiber clumping actually observed.

Fiber clumping during barrier layer formation on single-layer fiber sorbents could lead to poor barrier layer properties if the post treatment process is scaled-up to treat around 50,000 fiber sorbents for sulfur impurities removal for on-site hydrogen generation stations (appendix A.2.).

Techniques to create repulsion amongst the fibers during post treatment did not yield any positive results. Interestingly, in conventional membrane post treatment techniques [3, 4] , the coating solutes are in a low surface tension, volatile organic solvents (hexane or iso-octane) which are easily removed during the drying step without causing fiber clumping. However, latex solution of barrier polymers (e.g. PVDC, Neoprene™) were found only in water based emulsions.

The post treatment due to drawbacks like fiber clumping, non-uniformity of coating and difficulty in terms of scale-up led us to explore the creation of the barrier sheath layer by dual-layer fiber spinning process explained in detail in Chapter 5.

6.4.2. Post treatment of dual-layer fiber sorbents

Dual-layer fiber sorbents were spun with a porous core and a barrier sheath layer described in detail in chapter 5. The skin layer defects of slightly defective dual-layer fiber sorbents could be sealed with Sylgard® post treatment (Table 6.1).

However, dual-layer fibers with a severely defective sheath layer (Table 6.1) could not be sealed completely by Sylgard® post treatment as explained in section 6.3. A further two-three order of magnitude drop was required to obtain the true barrier properties of PVDC.

The latex post treatment technique was explored to seal the defects in the PVDC sheath layer. The experimental protocol discussed in the previous section for treating single-layer fiber sorbents was modified to enable sealing the defects in dual-layer fiber sorbents (Figure 6.11).

The fiber sorbent module was clamped in a vertical position as shown in Figure 6.11. The module was post treated with a fast latex wash (~100 ml/min, 1 min) followed by a slow latex wash (~10-15 ml/min, 30 min) as described in section 6.4.1.

Advantageously in case of dual-layer fiber sorbents, the 20-50 μm PVDC barrier sheath layer with a dense 0.1-1 μm skin did not allow the PVDC latex particles (~50-140 nm) to enter into the core layer morphology. Hence, a N_2 sweep through the bore was not maintained in case of dual-layer fiber sorbents which was found essential for effective barrier layer creation in single-layer fiber sorbents (section 6.4.1.).

The module was then left idle for 30-60 min to allow the nascent latex coating to dry to a small extent. This was followed by a third latex wash (~10-15 ml/min, 30 min) with vacuum (< 5 Torr) applied on the bore side (Figure 6.11). This step insured that the

PVDC particles were pulled into any remaining defects in the sheath layer. Also, vacuum was applied only in the third wash after the formation of a nascent PVDC barrier coating since pulling vacuum in the previous wash cycles could pull PVDC particles into the core layer through sheath layer defects.

Dual-layer fiber sorbent – latex post treatment
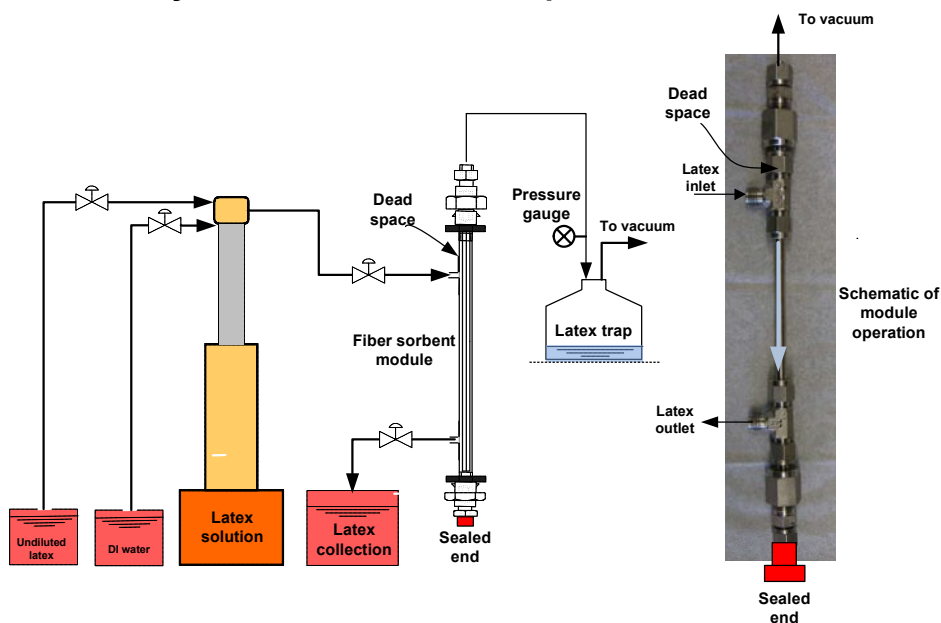
Figure 6.11: Schematic representation of the latex post treatment method for sealing pin-hole defects in the sheath layer of dual-layer fiber sorbents (fiber module is shown enlarged for better clarity).

As an additional safety feature, clear Teflon® tubing was used for the vacuum line to observe if any latex was being pulled in through the module bore. A metallic relief chamber (Figure 6.11) was installed to prevent any latex solution from being pulled into the vacuum pump.

The module was then flipped vertically and the above mentioned washing protocol was repeated sequentially to ensure complete post treatment of the fibers. The slow drying protocol (humid N_2, 2-6 h followed by dry N_2, 12 h) applied for the post

treatment of single-layer fibers (section 6.4.1.), was followed for dual-layer fiber sorbents as well.
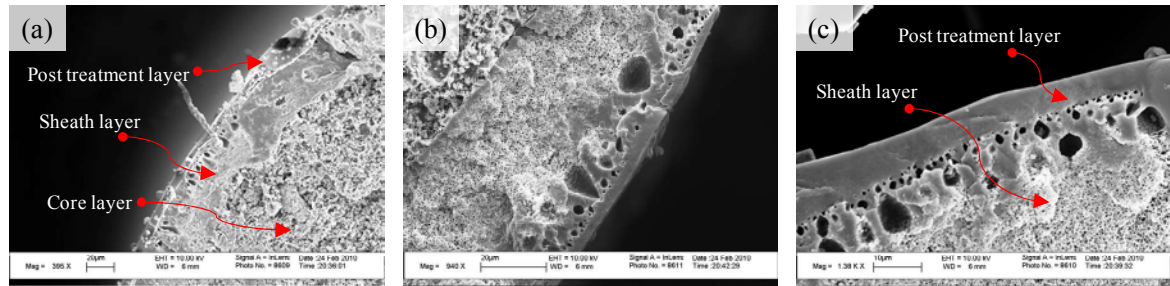
Figure 6.12: Radial SEM image of a latex post treated dual-layer fiber sorbent (Dope compositions: Core-b3, Sheath-2) (left to right) (a) Well adhered core, sheath and post treated layer of a dual-layer fiber sorbent (b) Higher magnification view of image (a), clearly showing good adhesion between the sheath and the PVDC post treatment layer (c) Dense and defect-free post treatment layer.

Advantageously, post treatment of dual-layer fiber sorbent modules even with multiple fibers did not show clumping which was a major drawback in the post treatment of single-layer fibers (section 6.4.1.). Control experiments with modules created with clear Teflon® tubing showed the post treatment solution to trickle down the dual-layer fiber surface without causing the fibers to clump. This was probably due to the highly hydrophobic nature of the existing PVDC sheath layer which did not allow the water to spread preventing the fibers to clump. Figure 6.12 shows the radial SEM image of a PVDC latex post treated dual-layer fiber sorbent with good adhesion between the sheath and the post treatment layer, sealing the defects in the sheath layer.

Figure 6.13 compares the SEM images(horizontal) of a single-layer fiber sorbent surface (Figure 6.13(a)), with a dual-layer fiber sorbent surface (Figure 6.13(b), having the same core as Figure 6.13(a)) and a post treated layer (Figure 6.13(c), post treated layer created on top of a dual-layer fiber sorbent (Figure 6.13(b)).
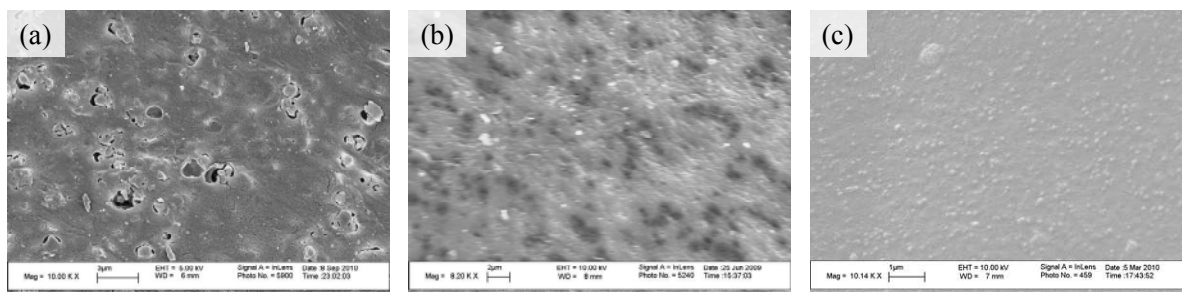
Figure 6.13: Horizontal SEM image of fiber sorbents (left to right) (a) Outer layer of a 60 wt. % zeolite loading CA/NaY single-layer fiber sorbent (ID: Core-b3) indicating large voids due to high sorbent loading (b) Outer layer (sheath layer) of a dual-layer fiber formed with a *high* viscosity sheath (ID: Core-b3, Sheath-2) showing the dense PVDC layer with few macrovoids. (c) Outer layer of a latex post treated dual-layer fiber sorbent (ID: Core-b3, Sheath-2) indicating a dense, uniform barrier coating layer.

PVDC latex post treatment of a dual-layer fiber sorbent module (ID: 1, Table 6.1 and Table 5.6.), showed a significant decrease in N_2 permeance to 0.00007 GPU with an O_2/N_2 selectivity of 2.85 (higher than O_2/N_2 Knudsen selectivity = 0.93) (Table 6.3).

This permeance was found to be lower than the permeance obtained by the Sylgard[®] post treatment of the fiber ID:1 (N_2 permeance ~ 0.0008 GPU, O_2/N_2 selectivity ~1.85, Table 6.1). The lower permeance shown by the latex post treated fiber compared to a Sylgard[®] post treated fiber could be due the formation of a dense PVDC post treated layer (~10-15 μm, Figure 6.12(c)) vs. a highly permeable Sylgard[®] layer on top of the existing PVDC sheath skin layer (~1-5 μm measured from SEM).

The permeance indicated by the PVDC latex post treated fiber was found close to the ideal N_2 permeance of ~0.0001 GPU expected for a 10 μm thick defect-free PVDC skin layer, calculated based on a dense film N_2 permeability of 0.001 Barrer.

Table 6.3: Comparison of permeance in a slightly defective fiber sorbent state before and after latex post treatment. Module length available for permeation L_p =15 cm, Number of fibers N_f = 3, Module temperature = 35 °C. The dual-layer fiber spinning conditions are summarized in Table 5.6.

Fiber ID	Permeance - N_2 (P/ ℓ - GPU) at 30 psig	Selectivity (α_{O_2/N_2})
1. (Before post treatment)	2.2	0.91
1. (After latex post treatment)	0.00007	2.85
$\alpha_{knudsen}$ (O_2/N_2)= 0.93		

6.5. Summary and conclusions

Various post treatment techniques were described in detail to either create a barrier layer on single-layer fiber sorbents or to seal the defects in the sheath layer of dual-layer fiber sorbents.

The PVDC latex post treatment of dual-layer fiber sorbents was found to give defect-free fibers with low gas permeance. The process was also found convenient in terms of scale-up and the protocol was optimized. With the creation of a dense, low gas permeance barrier sheath layer with a high zeolite sorbent loading, porous core layer; it was now necessary to test the barrier efficacy with water and steam as the regeneration media.

6.6. REFERENCES

1.   Widjojo, N., T.S. Chung, and S. Kulprathipanja, *The fabrication of hollow fiber membranes with double-layer mixed-matrix materials for gas separation.* Journal of Membrane Science, 2008. 325(1): p. 326-335.

2.   Widjojo, N., et al., *Enhanced gas separation performance of dual-layer hollow fiber membranes via substructure resistance reduction using mixed matrix materials.* Journal of Membrane Science, 2007. 306(1-2): p. 147-158.

3.   Henis, J.M.S. and M.K. Tripodi, *Composite Hollow Fiber Membranes for Gas Separation - the Resistance Model Approach.* Journal of Membrane Science, 1981. 8(3): p. 233-246.

4.   Ekiner, O.M., Kulkarni, S. S., *Process for making hollow fiber mixed matrix membranes,U.S. Patent 6,663,805B1*. 16 December, 2003.

5.   Lively, R.P., et al., *Hollow Fiber Adsorbents for CO2 Removal from Flue Gas.* Industrial & Engineering chemistry research, 2009. 48(15): p. 7314-7324.

6.   Hsieh, T.H. and K.S. Ho, *Thermal dehydrochlorination of poly(vinylidene chloride).* Journal of Polymer Science Part a-Polymer Chemistry, 1999. 37(13): p. 2035-2044.

7.   Bohme, R.D. and R.A. Wessling, *Thermal-Decomposition of Poly(Vinylidene Chloride) in Solid-State.* Journal of Applied Polymer Science, 1972. 16(7): p. 1761-&.

8.   Hsieh, T.H., *Effects of oxygen on thermal dehydrochlorination of poly(vinylidene chloride).* Polymer Journal, 1999. 31(11): p. 948-954.

9.   Vu, D.Q., W.J. Koros, and S.J. Miller, *High pressure CO2/CH4 separation using carbon molecular sieve hollow fiber membranes.* Industrial & Engineering chemistry research, 2002. 41(3): p. 367-380.

10.   Carruthers, S., *Integral-skin formation in hollow fiber membranes for gas separations*, in *Department of Chemical Engineering.* 2001, University of Texas at Austin

11.   Gabelman, A. and S.T. Hwang, *Hollow fiber membrane contactors.* Journal of Membrane Science, 1999. 159(1-2): p. 61-106.

12.   Diofan-XB-204. *http://www.ixan-diofan.com/*. Date accessed, October 8th, 2010.

13.   K. Grundke, T.B., C. Werner, A. Janke, K. Poschel, H. Jacobasch, *Liquid-fluid contact angle measurements on hydrophilic cellulosic materials.* Colloids and surfaces A: physicochemical and engineering aspects 1996. 116(1-2): p. 79-91.

CHAPTER 7

RAPID TEMPERATURE SWING ADSORPTION (RTSA) STUDIES ON FIBER SORBENTS

Abstract

This chapter considers the design and construction of an industrial prototype rapid temperature swing adsorption (RTSA) setup to enable rapid heating and cooling cycles with steam and water as the regeneration media. An electric steam generator unit was installed near the flow-through sorption setup (chapter 4) to provide saturated steam up to 200°C in a controlled and safe environment.

Rapid heating (steam) and cooling cycles (water) were performed on a fiber sorbent module to demonstrate the system capability. Barrier sheath layer efficacy was tested by conducting water (25 °C) and steam (110 °C) permeance experiments.

7.1. RTSA design and setup

A small scale facility was designed and constructed to allow continuous sulfur sorption and steam/water regeneration cycles on the fiber sorbent modules. The setup design and the constructed lab setup are shown in Figure 7.1 and Figure 7.2.

The facility had three key components as shown in Figure 7.1 and Figure 7.2. The region highlighted in green consisted of the fiber sorbent test rig, lecture bottles of sulfur gases, flow, temperature and pressure measurement devices built inside a fume hood due to safety reasons. The region highlighted in red covered the installation and functioning of the sulfur concentration analysis equipment (H_2S / total sulfur analyzer - Model 902, Galvanic Applied Sciences, Houston, TX). The details of the construction and integration of the two components (green and red region) was considered in detail in sections 4.7. and 4.12. The setup was used to conduct flow-through sorption and regeneration (with purge gas) studies on single and dual-layer fiber sorbent modules (chapter 4 and 5).

The setup was then modified with the design and installation of the third component (highlighted in blue, Figure 7.1 and Figure 7.2) to allow regeneration cycles to be conducted with steam/cooling water as the regeneration media. This component of the lab setup consisted of the steam generator, steam and cooling water supply lines and a blowdown separator for the safe discharge of the steam condensate. This new component was integrated with the main system described above.

Saturated steam was produced by means of an electric steam generator (Model: MBA 3, Sussman electric boilers, Long Island City, NY). The steam temperature could be varied between 100 $^\circ$C – 200 $^\circ$C by changing the pressure settings on the steam generator.
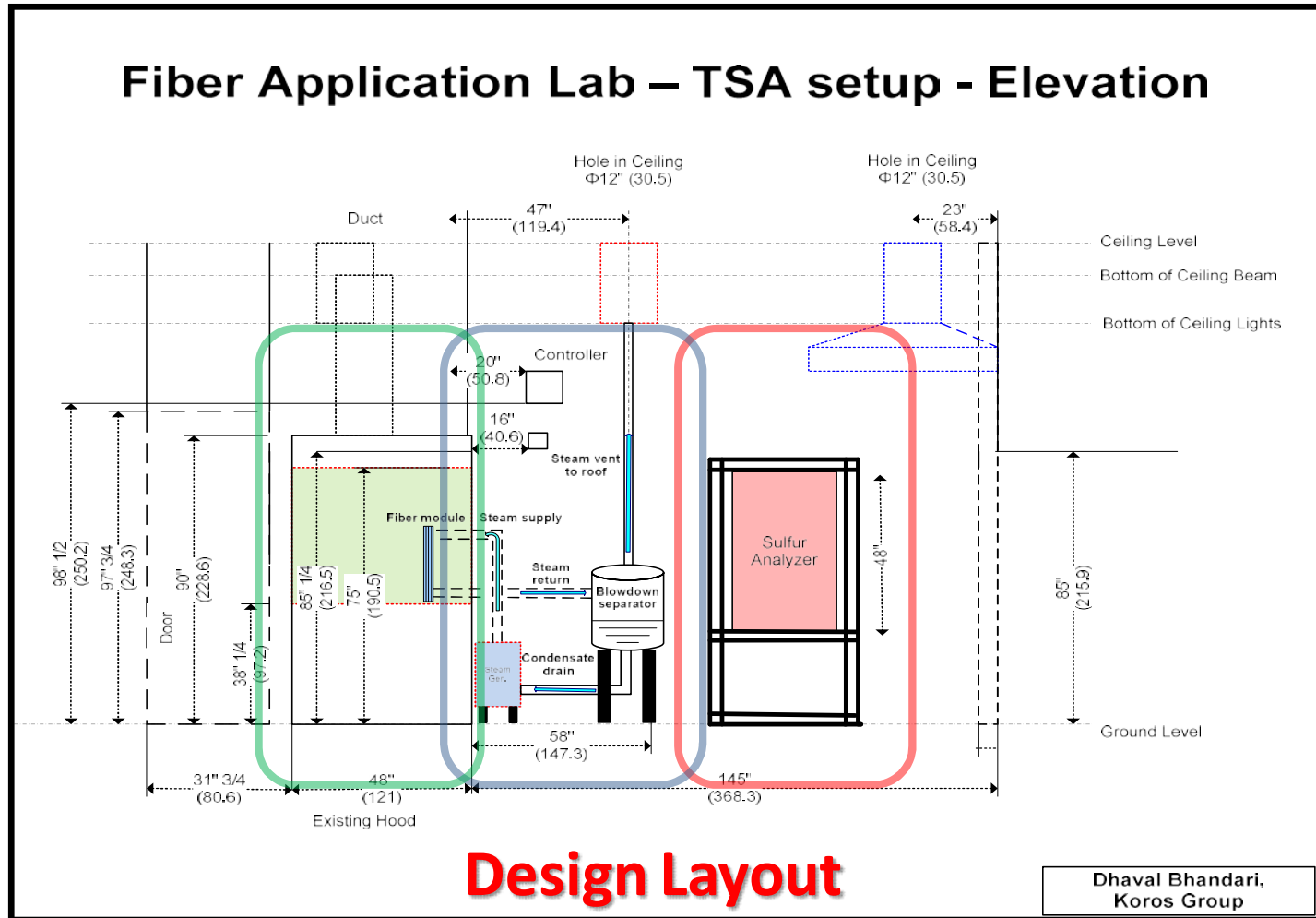
Figure 7.1: Design layout of the proposed TSA setup showing the different key regions of the setup (Green region: fiber sorbent test rig, lecture bottles of sulfur gases, flow, temperature and pressure measurement devices, Blue region: Steam generator, steam/cooling water piping and instrumentation and blowdown separator, Red region: Sulfur analyzer and sulfur gas lines)
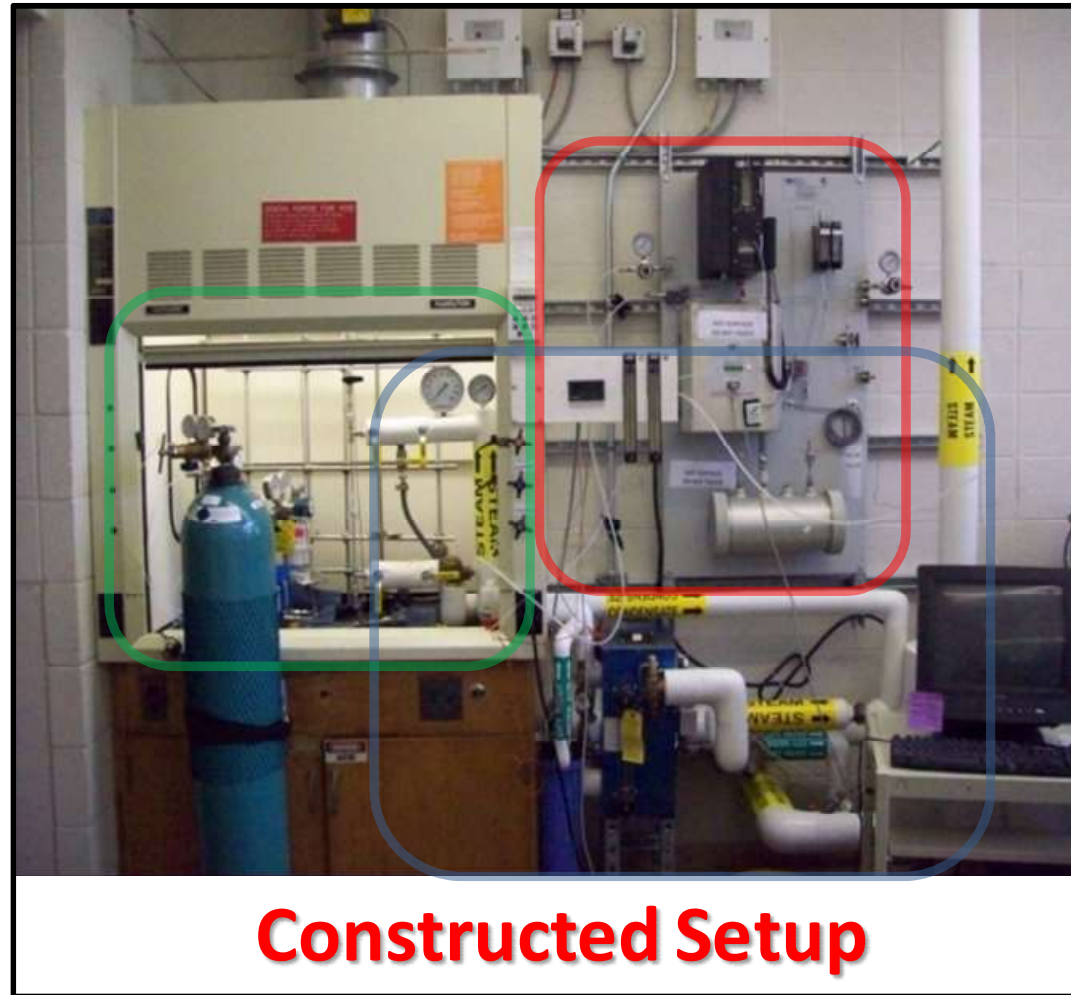
Figure 7.2: Actual lab setup constructed based on the design (Green region: fiber sorbent test rig, lecture bottles of sulfur gases, flow, temperature and pressure measurement devices, Blue region: Steam generator, steam/cooling water piping and instrumentation and blowdown separator, Red region: Sulfur analyzer and sulfur gas lines.)

The steam generator had an explosion proof electric water boiler unit insulated by glass wool to prevent heat loss. The water level in the boiler was maintained during steam generation by an electronic valve connected to the water supply line.

A water purifier was connected before the supply water inlet to remove dissolved impurities which could lead to salt deposition or scale formation in the boiler surface. The steam generator had automatic on-off heating control to maintain the set steam pressure.

The maximum allowable steam pressure in the boiler could be set using an adjustable pressure gauge, which allowed excess steam to be purged through a vent valve. Steam supply and discharge lines (1/2 inch diameter) were wrapped with 1 inch thick fiber glass insulation to lower the heat losses due to the condensation of steam.

Lab supply water was used to cool the fiber sorbent module to ambient conditions (25 °C) after the regeneration cycle with steam. The water flow rate could be regulated between 0-1.5 gallons per minute (gpm) using a flow controller. Steam and water could be supplied sequentially to the shell side of the module during the regeneration step. The direction of heat transfer fluids was oriented from the top to the bottom of the module to assist in draining of the liquids (Figure 7.1 and Figure 7.2). Mechanical ball valves were used to switch between steam and cooling water supply.

Steam condensate from the shell side of the module was collected in a blowdown separator for safe discharge. The condensate drain line from the blowdown separator was maintained at a constant temperature (25 °C) by a pneumatic valve. The valve would open according to the condensate temperature (60-90 °C), to allow the lab supply water to cool down the condensate to ambient conditions (25-40 °C), before discharge to the

building drain lines. The steam/water supply lines were instrumented with thermocouples and pressure gauges to accurately measure the heat transfer characteristics.

7.2. Ideal RTSA cycle definition

The RTSA cycle planned to be used in this work consisted of three steps:

1. In the adsorption step, sulfur containing natural gas would be fed to the tube side of the module. The sulfur odorants sorb into the adsorbents located in the fiber sorbent morphology and a purified stream is continuously detected by the sulfur analyzer. This step ends when the sulfur compound (tertiary butyl mercaptan (TBM) or hydrogen sulfide (H_2S)) breakthrough, with the outlet stream concentration reaching 1 ppm. Due to the low concentration of sulfur compounds used in this work, the increase in the module temperature will be negligible. If a temperature increase is observed in subsequent work due to the heat of adsorption, cooling water can be supplied to limit the temperature overshoot (section 4.7. and appendix A.9.), so the system is quite flexible and adaptable.
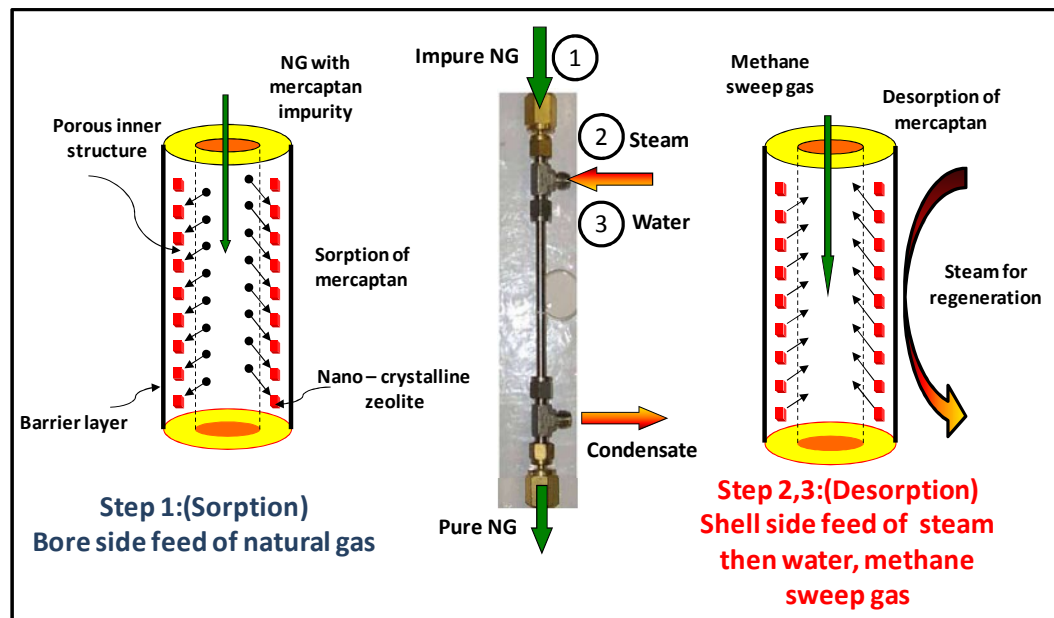
Figure 7.3: Schematic diagram of an RTSA cycle with fiber sorbent modules.

196

2. During the regeneration step, steam at constant temperature will be supplied on the shell side to heat the modules. Simultaneously, a nitrogen sweep is applied through the fiber bore to effectively displace the desorbed sulfur compounds (appendix A.11.) and maintain a low water vapor content in the fiber sorbent (as explained in section 7.4.). The flow rate of the nitrogen sweep is a parameter that can be varied depending on the process requirements. A high flow rate improves desorption, but leads to a dilute desorbed phase. The heating is stopped when the sulfur outlet concentration in the nitrogen sweep reaches below 1 ppm, indicating the completion of the regeneration cycle.

3. The next step will involve the cooling down of the fiber module by water to ambient temperatures (~25 °C) before the start of the next adsorption cycle. The flow rate of water can be varied between 0-1.5 gpm.

7.3. Temperature swing ability of the system
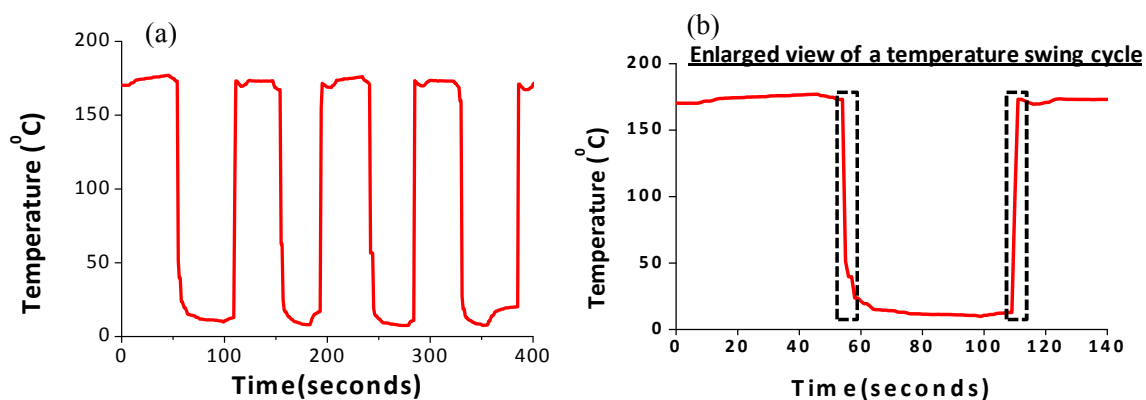
Figure 7.4 (left to right): (a) Graph indicating continuous temperature swing cycles on a fiber sorbent module (b) Expanded view of a heating and cooling cycle indicating the feasibility of rapid cycling.

Continuous temperature swing cycles were performed using the RTSA setup (section 7.1.) to study the time required to heat and cool the fiber sorbent module during

the regeneration step. The steam generator was set to give saturated steam at~180 °C during the heating cycles. Lab supply water at a flow rate of 1.5 gpm was used to cool the modules to~20-25 °C during the cooling cycles. Figure 7.4 (a) depicts the feasibility of rapid continuous temperature swing cycles. Figure 7.4 (b) is a expanded view of one heating/cooling cycle. Continuous and rapid thermal cycles were feasible with typical heating and cooling time of~10-20 s.

In comparison, conventional pellet packed beds can take a few hours to heat using hot purge gases and require proportionally larger beds to handle the same capacity. As noted earlier in section 2.2., a much smaller auxiliary bed will be required due to rapid regeneration with the fiber sorbent approach, thereby saving space and minimizing sorbent use. These experiments verify that fiber sorbent module temperature can be cycled rapidly within a few seconds and rapid thermal cycles were possible using the current setup. Water hammer due to sudden condensation of steam (releasing large amounts of heat, appendix A.8.1.) and pressure fluctuations due to rapid valve switching caused the pipes to vibrate. Adequate support was provided to the steam/water lines to prevent pipelines from breaking due to high pressures.

7.4. Water vapor permeance testing of the fiber sorbents

Sylgard$^®$ post treated dual-layer fiber sorbent (I.D. – 1, section 6.2.) was found to give a low N_2 permeance of 0.0008 GPU with an O_2/N_2 selectivity of 1.85. The module was next tested to determine water vapor permeance through the barrier sheath layer.

The fiber sorbent module was clamped vertically on the test rig (section 4.7.), dried and activated by heating the module to 120 °C under a nitrogen purge till the water vapor level in the module was < 10 ppm (section 4.12.). This drying protocol insured the

removal of sorbed water vapor from zeolite NaY in the fiber sorbent core layer. The heating was then stopped and the module was cooled down to ambient conditions ($\sim$ 25 °C).

The experimental protocol for water vapor permeance measurements was similar to gas permeance measurements using the constant volume system (section 3.4.8.2.), where the upstream (shell side) was pressurized ($\sim$ 30 psig) with gas while the downstream (bore side) had close to vacuum conditions (< 50 Torr). The rate of downstream pressure change was measured with time and the steady state value (dp/dt) was taken for the calculation of permeance.

In water vapor permeance measurements, after the module drying and activation step, lab supply water was fed to the shell side of the module. The shell side was filled with water and the permeance experiment was started with a N_2 sweep gas at a constant flow rate through the fiber bore. The upstream (shell side) had an activity of 1 due to presence of liquid water, while the downstream (bore side) had a water activity close to zero due to the continuous N_2 sweep. The water vapor content of the N_2 sweep gas was recorded with time by a downstream dew point meter (section 4.12.).
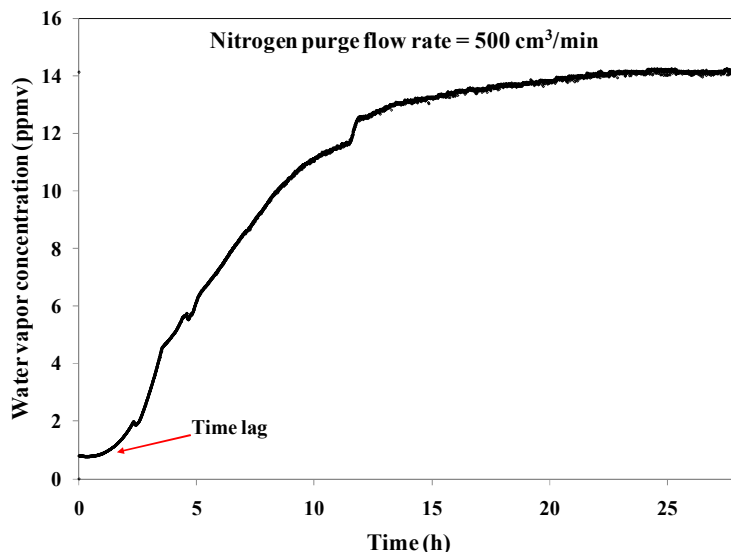
Figure 7.5: Measurement of water vapor permeance through a Sylgard® post treated dual-layer fiber sorbent module. Module length available for permeation L_p = 15 cm, Number of fibers N_f = 3, Module temperature = 25 °C. The fiber spinning conditions of the fibers are summarized in section 6.2. N_2 sweep flow rate = 500 cm³/min, fibers activated at 393 K under N_2 purge till water vapor concentration < 5 ppm.

The water vapor content of the sweep gas at steady state was used to estimate the water vapor flux through the barrier sheath layer. As discussed in section 5.5., the resistance to flow through a dual-layer fiber sorbent was mostly through the dense skin of the PVDC sheath layer, while the resistance to gas/water vapor flow through the porous core was negligible. Figure 7.5 shows the change in the water vapor content of the N_2 sweep gas (flow rate – 500 cm³/min) with time. When the dry and activated fiber sorbents in the module were first exposed to water vapor, a short time lag was observed (Figure 7.5), possibly due to the diffusion of water vapor through the barrier skin layer. The measured water vapor concentration of the N_2 purge was also indicative of the water vapor content in the fiber sorbent. The water vapor content in the fiber sorbent slowly increased till a steady state concentration was obtained with the desired N_2 sweep gas (Figure 7.5).

The calculation of permeance is described below:

Water vapor content of N_2 sweep at steady state from Figure 7.5, $\phi_{wet} = 14.5 \, ppmv$

Water vapor content of dry bottled N_2 sweep gas from Figure 7.5, $\phi_{dry} = 0.8 \, ppmv$

Hence, water vapor content in the sweep gas due to permeation through the fiber sorbent,

$$\phi_{permeance} = \phi_{wet} - \phi_{dry} = 14.5 - 0.8 = 13.7 \, ppmv \quad (7.1)$$

Nitrogen sweep gas flow rate, $Q_{N_2} = 500 \, cm^3 / min$

Hence, steady state water vapor flow rate,

$$Q_{water-vapor} = Q_{N_2} * \phi_{permeance} = 500 \, cm^3 / min * 13.7 * 10^{-6} * \frac{60 \, s}{1 \, min} = 1.14 * 10^{-4} \, cm^3 / s \ (7.2)$$

Temperature of module and humidity measurement device $T_{measure} = 25°C = 298 \, K$

Pressure of N_2 sweep gas at the measurement device, $p_{measure} = 1 \, atm$

Hence, steady state water vapor flow rate at STP,

$$Q_{water-vapor-STP} = Q_{water-vapor} * \frac{T_{measure}}{T_{STP}} * \frac{p_{STP}}{p_{measure}}$$

$$\Rightarrow 1.14 * 10^{-4} \, cm^3 / s * \frac{298K}{273K} * \frac{1atm}{1atm} = 1.25 * 10^{-4} \, cm^3 (STP) / s \quad (7.3)$$

The shell side (or upstream) of the module was filled with liquid water and hence the activity can be assumed to be 1. The partial pressure can be taken to be equal to the vapor pressure of water at the module temperature (25 °C).

Thus, the upstream water vapor pressure, $p_{up} = 2.38 \, cmHg$

Since the bore side (downstream) had a continuous N_2 sweep, the water vapor pressure on the bore side is negligible, $p_{down} \approx 0 \, cmHg$

Hence, the pressure difference across the fiber sorbent,

$$\Delta p = p_{up} - p_{down} = 2.38 - 0 \; cmHg = 2.38 \; cmHg \tag{7.4}$$

Area of fiber sorbent available for permeance,

$$A_f = N_f \pi.O.D.L_p = 3 * \pi * 707 * 10^{-4} \; cm * 14.6 \; cm = 9.73 \; cm^2 \tag{7.5}$$

Where, N_f is the number of fibers in the module, $O.D.$ is the outer diameter of the fiber, and L_p is the length of the module available for gas permeation.

Hence, water vapor permeance (section 3.4.8.2.),

$$Permeance \; (\frac{P}{\ell}) = \frac{(n_{STP})}{(\Delta p)} = \frac{Q_{water-vapor-STP}}{(\Delta p)A_f} = \frac{Q_{water-vapor-STP}}{(\Delta p)N_f * \pi * O.D. * L_p}$$

$$\Rightarrow \frac{1.25 * 10^{-4} \; cm^3 (STP)/s}{2.38 \; cmHg * 9.73 \; cm^2} = 5.4 * 10^{-6} \frac{cm^3 (STP)}{cm^2.s.cm \; Hg} = 5.4 \; GPU \tag{7.6}$$

The dual-layer fiber sorbent module ID: 1, tested here had an approximate PVDC skin layer thickness of ~1-5 µm (section 6.3.) in a 50 µm thick sheath layer.

Assuming a 1 µm thick defect free skin in a 20-50 µm PVDC sheath layer, the ideal permeance for water vapor is around 2-6 GPU, based on a dense film water vapor permeability of 2-6 Barrer at 25 °C (section 3.1.2.) [1, 2]. Hence, the permeance value measured for the fiber sorbent module was close to the expected value from the literature.

The fiber sorbents with a dense barrier layer had a desired low permeance for N_2 gas (section 6.2.) and water vapor as well proving the efficacy of the barrier layer. Thus, the N_2 sweep gas flow rate was varied to observe its effect on the net water vapor content and the water vapor permeance through the PVDC sheath skin layer. The net water vapor content in the sweep gas should change with the flow rate in such a way that the permeance is constant. Permeance of the water vapor through a fiber sorbent module

should vary depending on the pressure difference across the module and the temperature of water vapor while being independent of the sweep gas flow rate.

The sweep gas flow rate through the same module was increased from 500 cm^3/min (Figure 7.5) to 800 cm^3/min (Figure 7.6(a)) followed by reducing the flow rate to 300 cm^3/min (Figure 7.6(b)). Steady state water vapor content was measured in each case and permeance values were calculated and reported in Table 7.1.

Table 7.1: Study of the effect of Nitrogen sweep gas flow rate on the steady state water vapor content and water vapor permeance in a Sylgard$^®$ post treated dual-layer fiber sorbent module. $\Delta p = 2.38$ cm Hg, module temperature $T_{measure} = 25$ °C.

N$_2$ sweep flow rate (cm^3/min)	500	800	300
Net water vapor content in module at steady state ($\phi_{permeance}$ - ppmv)	13.7	6.9	26.3
Water vapor permeance (($\frac{P}{\ell}$)-GPU)	5.4	4.3	6.2
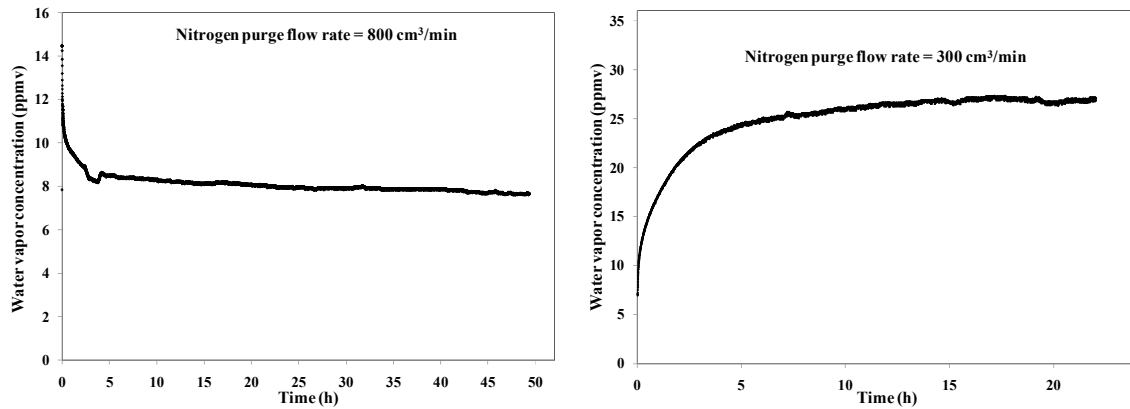
Figure 7.6: Study of the effect of Nitrogen sweep gas flow rate on the water vapor content in a Sylgard$^®$ treated dual-layer fiber sorbent module. Module length available for permeation $L_p = 15$ cm, Number of fibers $N_f = 3$, Module temperature = 25 °C. The fiber spinning conditions of the fibers are summarized in section 6.2. N$_2$ sweep flow rate = 800 and 300 cm^3/min, fibers activated at 393 K under N$_2$ purge till water vapor concentration < 5 ppm.

Time lag was not observed in Figure 7.6 (a) and (b) since the experiments were continuations of the experiment with N$_2$ sweep of 500 cm^3/min. It can be observed from

Table 7.1 that the steady state net water vapor content in the fiber sorbents could be varied by changing the flow rate of the sweep gas.

The control of water vapor content in the fiber sorbent morphology by variation in the sweep gas flow rate is highly advantageous during fiber sorbent regeneration since water vapor content greater than 50-100 ppm can significantly reduce the sulfur sorption capacity of hydrophilic zeolite NaY sorbents [3, 4]. Hence, even if the barrier sheath layer is slightly defective allowing higher water vapor permeance, the fiber sorbents can be kept relatively dry by effectively manipulating the sweep/purge gas temperature and flow rate.

The water vapor permeance (pressure normalized flux) through the fiber sorbent module (Table 7.1) at a certain temperature (25 °C) and water activity ($\sim$1) should remain constant irrespective of the variation in flow rate. However, the permeance was found to fluctuate slightly, possibly due to temperature variation or noise in measurement.

7.5. Steam testing of the fiber sorbent modules

After successfully creating a low permeance barrier layer for dual-layer fiber sorbents (chapter 6), testing its efficacy for gases (sections 6.3. and 6.4.2.) and then water vapor at ambient conditions (section 7.4.) a key challenge was to test its efficacy under steam. The fiber module was dried and activated at 120 °C using heat tapes, as explained in the previous section to remove any sorbed water vapor from the zeolites in the fiber sorbents.

The fiber module was then cooled down to ambient conditions (25 °C), with the nitrogen purge at a constant flow rate through the bore side of the module. The fiber sorbent barrier efficacy was first tested by filling the shell side with water and checking

204

its permeance as described in sections 7.2 and 7.4. After ensuring low permeance of water vapor (Figure 7.7, initial part), water was then drained-off.
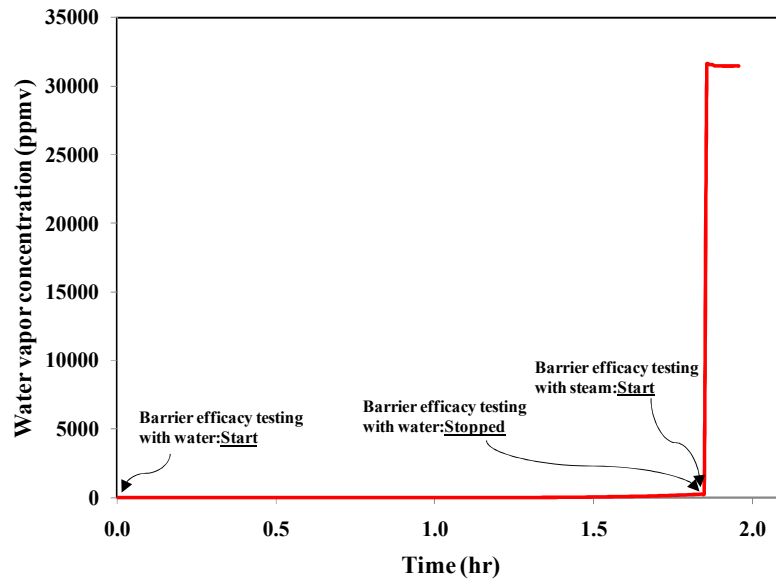
Figure 7.7: Measurement of water vapor permeance through a PVDC latex post treated dual-layer fiber sorbent module on exposure to water followed by steam. Module length available for permeation L_p = 35 cm, Number of fibers N_f = 5, Module temperature = 25 °C and 110 °C. The fiber spinning conditions of the fibers are summarized in section 6.2. N_2 sweep flow rate = 300, fibers activated at 393 K under N_2 purge till water vapor concentration < 10 ppm before testing.

Insulation foam material was wrapped around the module to avoid heat loss and then saturated steam at a constant pressure (~6 psig, equivalent to 110 °C) was supplied to the system. The water vapor permeance at 110 °C was estimated by measuring the net water vapor content of the N_2 sweep gas as described in section 7.4.

Upon introduction of saturate steam, the water vapor content of N_2 suddenly increased from a few ppmv to 32,000 ppmv (maximum measurement limit of the dew point meter) indicating the sudden failure of the barrier layer on exposure to steam (Figure 7.7). Liquid water droplets were observed in the downstream tubing confirming

the failure of the barrier layer. The reasons for the failure of the barrier layer on exposure to steam were further explored.

The steam temperature (~ 110 °C) per se is unlikely to be responsible for the failure or degradation of the barrier layer, since as discussed in section 6.2., the degradation temperature of PVDC grade is around 180 °C. Also, prior to and during activation and drying of the fiber sorbents at elevated temperatures, the fibers were in contact with saturated water (due to sorbed water in zeolites) and eventually steam. Subsequent tests with both pure nitrogen (sections 6.3. and 6.4.2.) and liquid water (Figure 7.5 and Figure 7.7) at ambient temperatures showed the barrier layer and the fibers to be completely intact.

The permeability of gas/water vapor follows an Arrhenius type behavior, with the permeability change with temperature expressed by the following equation [2],

$$P = P_o \exp(-\frac{E_p}{RT}) \tag{7.7}$$

Where, P is the permeability, P_o is the pre exponential factor, E_p is the activation energy of permeation (KJ/mole), R is the gas constant and T is the temperature in K.

The water vapor permeability of PVDC was found to increase from 2-6 Barrer at 25 °C to 82 Barrer at 110 °C (E_p ~ 46.1 KJ/mole). However, if the increase in the permeance at high temperatures was the reason for high water vapor content measurement on exposure to steam, the change in water vapor content would be gradual, while as shown in Figure 7.7, the water vapor increased almost instantaneously to reach the upper limit of the measurement device (~ 32,000 ppmv). Upon carefully opening the

fiber sorbent module, one of the fibers was found to be broken which led to rapid flow of the condensed water vapor into the downstream (Figure 7.8(b)).
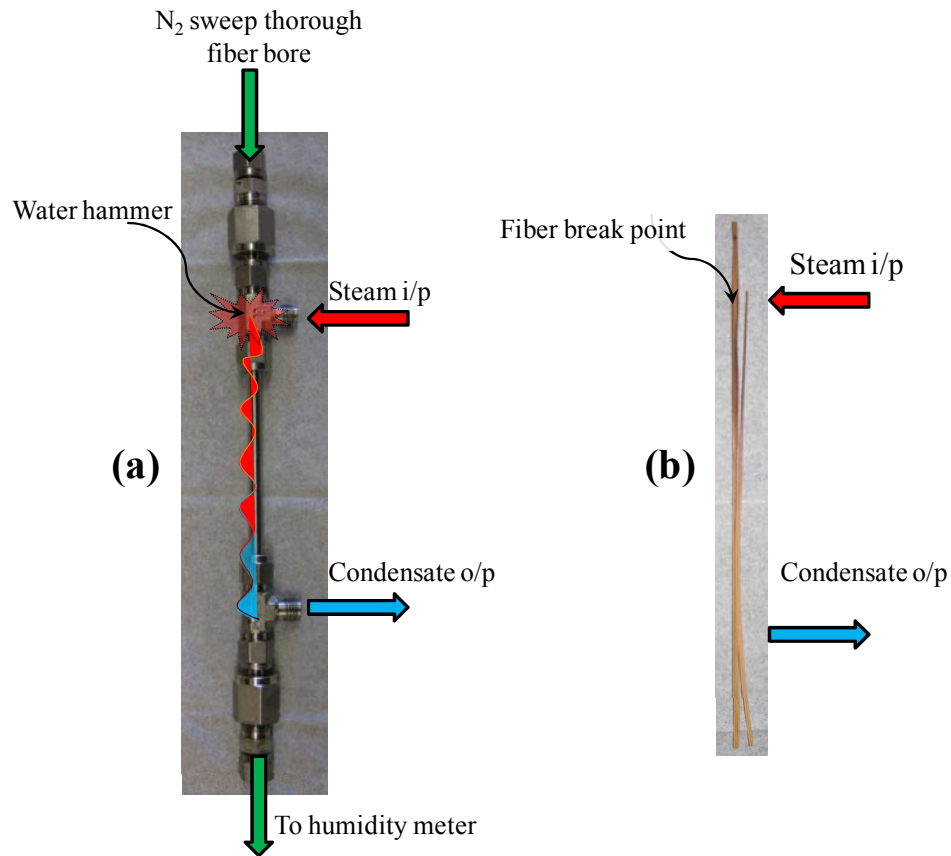
Figure 7.8: (left to right): (a) Sudden condensation of steam on the fiber surface at the shell side inlet causing water hammer or thermal fluctuations (b) Image of the dual-layer fiber sorbent exposed to steam indicating the high temperature of exposure at the inlet possibly causing the fibers to break.

Apparently, the sudden introduction of steam into the ambient temperature module, in direct contact with the constrained fiber bundle can cause excessive stress and failure at the steam entry point, thereby leading to breakage (Figure 7.8 (a)). The fiber sorbents were constrained with less space for expansion due to the potting of the fiber ends in the module. Also, the strong force due to the introduction of steam at high flow rate could cause fiber breakage.

Gradual heating of the fiber modules by hot water, slow introduction and ramping of steam flow rate into the module or the use of a snubber to suppress the pressure transient in the fiber module are potential techniques to reduce the thermal stress on the fiber sorbent during the barrier layer efficacy testing with steam and require further study.

7.6. Proof-of-concept regeneration experiments with N_2 purge

As noted above, the barrier layer efficacy could not be tested adequately with steam due to system and process related difficulties requiring substantial module design and engineering optimization (section 7.5.). This work, while important, requires considerable additional time that would distract us from an efficient proof-of-concept for the fiber sorbent operation.

Therefore, to verify the regenerability of fiber sorbents by the application of heat, proof-of-concept regeneration experiments by heating the module to 110-120 °C under a N_2 purge were conducted. As discussed in sections 4.10. and 5.13., complete regeneration of fiber sorbents and desorption of sulfur impurities was observed. Consistent sorption capacity over 5 regeneration cycles confirmed the durability and regenerability of both single and dual-layer fiber sorbents.

Also, basic design calculations (appendix A.8.) show that N_2 or methane purge gas can also be effectively used for the small scale operation of sulfur impurity removal from pipeline natural gas. However, to obtain the full advantages over pellet packed bed technology, rapid regeneration of fiber sorbents with steam is preferable.

7.7. Summary and conclusions

A rapid temperature swing adsorption (RTSA) system was designed, constructed and tested by conducting rapid heating and cooling cycles with steam and cooling water.

The barrier layer efficacy was successfully tested under water vapor at 25 °C. The barrier layer efficacy could not be effectively tested due to breakage of the fiber sorbents in the module possibly due to a strong thermal shock. Potential techniques to overcome this system related shortcoming were identified. Proof-of-concept regeneration experiments by heating the modules under a N_2 purge gas indicated the complete regenerability of single and dual-layer fiber sorbents.

Continuous heating and cooling cycles need to be performed to test the barrier layer efficacy over multiple cycles. Also, the regeneration cycles need to be complemented with retention of effective sulfur sorption capacity of the hydrophilic zeolite NaY in the sorption cycles to bring this separation technology platform to reality.

7.8. REFERENCES

1. IXAN-PNE-288. *http://www.ixan-diofan.com/*. Date accessed, October 8th, 2010.

2. Brandrup, J., E.H. Immergut, and E.A. Grulke, *Polymer handbook*. 4th ed. 2004, New York ; [Chichester]: Wiley-Interscience.

3. Shimizu, K., et al., *Mechanistic study on adsorptive removal of tert-butanethiol on Ag-Y zeolite under ambient conditions.* Journal of physical chemistry B, 2006. 110(45): p. 22570-22576.

4. S. Satokawa, Y.K., *Adsorbent for removing sulfur compounds from fuel gases and removal method*. 2005, United States Patent 6875410

CHAPTER 8

CONCLUSIONS AND RECOMMENDATIONS

8.1. Summary and conclusions

The overarching goal of this research was to create innovations in the field of separations by developing 'fiber sorbents' for on-site hydrogen generation applications. These sorbents represent a new paradigm that may ultimately have broad applications well beyond the specific proof-of-concept case considered here. Specifically, this work was focused on the removal of sulfur impurities from pipeline natural gas. Knowledge from membrane science and adsorption technology was drawn upon extensively to enable this new technology.

The concentration of sulfur in odorized pipeline natural gas is about 30 ppm with the acceptable level being <1 ppm. The packed bed technology conventionally applied in industry for this application suffers from disadvantages including particle attrition, high pressure drop and slow regeneration rates.

Hollow fiber sorbents are pseudo monolithic material with a polymer 'binder', impregnated with high loadings of sulfur selective zeolite sorbents as 'fillers'. Temperature swing adsorption (TSA) with steam/water as the regeneration media was identified as the optimal approach to regenerate the fiber sorbents. To allow only thermal interactions with the regeneration media, it was planned to create a dense and thin polymer 'barrier' layer on the sheath side of the fiber sorbents.

Simplified calculations were performed to determine mass and heat transfer, pressure drop, surface area-to-volume ratios for fiber sorbents and were compared with

conventional pellet packed bed technology to consider the advantages and limitation of the fiber sorbent approach. Using these calculations as a guiding force, the dimensions and specifications of fiber sorbent were established for this study.

Single-layer fiber sorbents were created by using the dry jet-wet quench spinning technique. Spinning parameters were optimized in a manner to allow fibers to be spun at high take-up rates and at room temperature spinning conditions. Cellulose acetate (CA) / zeolite NaY fiber sorbents with 75 wt. % NaY loading and polyester urethane/NaY fiber sorbents with 60 wt. % NaY loading were spun successfully. Effects of various spinning parameters like quench bath temperature, air gap and dope flow rates was considered in detail.

SEM images indicated that CA / NaY fiber sorbents had the desired 'sieve-in-a-cage' structure, while polyester urethane fiber sorbents indicated a sieve encapsulated by polymer ('occluded' sieve). CA was pursued as the polymer of choice for the fiber sorbent core layer creation.

Single-layer fiber sorbent dynamic and equilibrium capacities for model sulfur odorants (tertiary butyl mercaptan (TBM) and hydrogen sulfide (H_2S)) were determined using batch and flow systems. Variation in performance with parameters such as zeolite loading, flow rates, fiber diameter and number of fibers was considered. Fiber sorbents indicated a sharp, symmetrical S–shaped sorption curve indicating no premature breakthrough under flow conditions.

Formation of an impermeable sheath layer was crucial for the effective regeneration of the fiber sorbents. Applicability of various barrier polymers was

analyzed. Based on various iterations polyvinylidene chloride (PVDC) as solvent soluble powder form and in aqueous emulsion form was selected as the polymer of choice.

Dual-layer fiber sorbents were created by simultaneous co-extrusion of PVDC as the 'sheath' layer and CA/NaY as the 'core' layer using the hollow fiber spinning technology. The dope compositions and spinning conditions were optimized in a way such that the core structure had a porous morphology with high sorbent loadings while the sheath structure was dense and impermeable. Challenges in terms of adhesion between the core and sheath layers, permeation and sorption properties and desired morphology of dual-layer fiber sorbents were addressed.

Careful tuning of the various spinning parameters allowed for the creation of dual-layer fibers with a dense and low permeance sheath layer. However, the sheath layer was still defective with Knudsen selectivity. Heat treatment and silicone rubber coating techniques were utilized to seal the minor defects in the sheath layer skin. Alternatively, a new post treatment technique using an aqueous dispersion of PVDC barrier polymer was developed to create either a barrier sheath layer on single-layer fiber sorbents or to caulk a severely defective barrier sheath layer. The post-treatment protocol was optimized to obtain fiber sorbents with defect-free barrier sheath layer. SEM-EDX, TGA, permeation and DSC techniques were used to characterize the post-treated fiber sorbents.

A small scale facility was designed and constructed to allow continuous sulfur sorption and steam/water regeneration cycles on the fiber sorbent modules. Rapid heating (steam) and cooling cycles (water) were performed on a fiber sorbent module to demonstrate the system capability. Barrier sheath layer efficacy was tested by conducting water (25 °C) and steam (110 °C) permeance experiments. The barrier layer efficacy

could not be tested adequately with steam due to process related difficulties requiring substantial module design and engineering optimization. However, proof-of-concept regeneration experiments by heating the module to 110-120 °C under N_2 purge showed complete regeneration of fiber sorbents and desorption of sulfur impurities. Consistent sorption capacity over 5 cycles confirmed the durability and regenerability of fiber sorbents.

To summarize, the project was successful in meeting most of its key objectives by creating first-generation hollow fiber sorbent material and a cyclic separations platform (TSA system) for the removal of sulfur impurities from natural gas for on-site hydrogen generation application. The concept and basic framework of the technology was established, various key components and materials were iteratively screened and optimized to create single, dual-layer and post treated hollow fiber sorbents with the desired morphology and separation properties. A setup was designed and constructed to conduct sorption experiments with sulfur gases and regeneration with steam/cooling water on the fiber sorbents.

8.2. Recommendations

While this research was successful in demonstrating the key advantages of fiber sorbents, certain challenges must be overcome to improve its industrial viability. Hopefully, this framework acts as a driver for future research on fiber sorbents for various gas and liquid separations applications.

8.2.1. Cyclic sorption and regeneration studies on fiber sorbents

Proof-of-concept regeneration experiments by heating the module under a N_2 purge gas clearly indicated the viability of TSA as a convenient mode of regeneration for

fiber sorbents. For the small scale operation of on-site hydrogen generation, a hot purge could also be effectively used; however, use of steam and cold water as heat transfer fluids is preferable. Barrier layer efficacy was successfully tested with N_2 gas and under water vapor (~25 °C).

However, certain process related difficulties were observed when testing the fiber sorbents with steam due to sudden thermal shock leading to fiber breakage. Gradual heating of the fiber modules by hot water, slow introduction and ramping of steam flow or the use of a snubber to suppress the pressure transients are potential techniques to reduce the mechanical stress on the fiber sorbents.

Once the barrier layer efficacy with steam is successfully tested, continuous heating and cooling cycles need to be performed to test the barrier layer efficacy over multiple cycles. Also, the regeneration cycles need to be complemented with retention of effective sulfur sorption capacity of the hydrophilic zeolite NaY (dispersed in fiber sorbents) in the sorption cycle.

8.2.2. Exploring new materials for fiber sorbent creation

Fiber sorbents had three essential material components. The core layer polymer ('binder'), zeolite ('sorbent') and the sheath layer polymer ('barrier'). Various materials were iteratively screened based on desired separation properties, material costs and ease of availability to create the first generation hollow fiber sorbents.

However, each key component of fiber sorbent can be studied in depth and optimized to enhance its performance.

8.2.2.1. Incorporation of water resistant sorbent material

The 'sorbent' material is the most important component of fiber sorbents. Key attributes of an ideal sorbent for this application are: ease of availability in large quantities, low heat of sorption to insure isothermal operation during the sorption step, high sulfur sorption capacity under wet and dry conditions and ease of regeneration by temperature variation.

Zeolite NaY, a hydrophilic sieve (Si/Al = 2.6) used in this work satisfied most of the criteria described above. However, NaY sorption capacity drops significantly even in the presence of small amount of water vapor ($\sim$ 10 ppm) [1-3]. The presence of large number of surface acidic sites (small Si/Al ratio) usually causes preferential adsorption of water [4, 5].

The key proposed advantage of fiber sorbents is rapid regeneration with steam and cooling water. It was found difficult to maintain very low water vapor content in the fiber sorbent during exposure to water/steam due to finite permeance through the barrier layer.

Hence, new sorbent materials indicating high sorption capacity in dry and wet conditions are desired. Selection of zeolites with small number of acid sites (High Si/Al ratio) and metal ion-exchanged zeolite Y can be used as a replacement for hydrophilic NaY zeolites. Some studies indicate that the decrease in sorption capacity of these zeolites is comparatively less when in contact with water vapor [3, 6, 7].

High silica zeolites are more resistant to water vapor; however, their sulfur sorption capacity is less than dry zeolite NaY. Metal ion-exchanged Y type zeolites (Ag^+, Mg^{2+}) indicate high sorption capacity in dry and wet conditions (up to 1000 ppm);

however, it forms a stronger bond with the sulfur compounds thus requiring higher temperatures for regeneration [2].

A detailed study is hence required to select a sorbent material with the maximum advantages for the sulfur removal process.

<u>8.2.2.2. Selection of a robust thermo-mechanical polymer 'binder' material</u>

The polymer 'binder' is another key component of the fiber sorbent system. The binder material should be an inexpensive polymer, provide good mechanical strength, forming a highly porous matrix with for effective operation. Cellulose acetate (CA) was iteratively selected in this work as the core layer polymer. The T_g of CA used in this work was measured to be∼180 °C in dry form. However, the T_g of CA has been found to drop to∼90-100 °C in presence of excess moisture [8]. A low T_g under wet conditions could lead to the densification of the core layer matrix under steam regeneration cycles at∼110-120 °C. Matrix densification and reduction in porosity could lead to lower dynamic sorption capacity due to slower diffusivity, severely affecting fiber sorbent operation.

Commercially available polyimides (Matrimid[®] or Torlon[®]), have been successfully utilized in Koros group for the creation of hollow fiber gas separation membranes [9-11]. These polymers have good thermal (T_g∼250-300 °C) and chemical stability and could potentially be used as the core layer polymer for fiber sorbents.

8.2.3. Competitive sorption studies with multiple sulfur odorants

In this proof of concept work, the fiber sorbent sulfur sorption capacity was determined under batch and flow conditions using only one model odorant (TBM or H_2S) in the feed gas stream. However, pipeline natural gas can have multiple sulfur impurities including H_2S, mercaptans (e.g., ethyl, isopropyl, and tertiary butyl), thiols (e.g.,

tetrahydrothiophene), and sulfides (e.g., dimethyl, diethyl) [12] with the concentration in the range of a few ppm to as high as 30 - 60 ppm [3, 7, 13].

Competitive sorption on the zeolite active sites and its effect on the dynamic sulfur sorption capacity need to be considered in detail. The industrial scale fiber sorbent module must be designed taking into account the least sorbing species since the main bed will be switched with an auxiliary bed once the sulfur outlet concentration is above 1ppm.

Certain odorants for example tertiary butyl mercaptan (TBM) and tetrahydrothiophene (THT) are highly condensable and have been found to give high sorption capacity compared to less condensable sulfur impurities like hydrogen sulfide (H$_2$S) and dimethyl sulfide (DMS) [7, 12, 14]. Advantageously, fiber sorbents can be spun by dispersing multiple 'odorant specific' sorbents in the core layer spin dope to create a fiber sorbent morphology which then provides high overall dynamic sulfur sorption capacity.

8.2.4. Detailed characterization of fiber sorbents

Though various techniques were used in this work to characterize different fiber sorbents, some further characterizations can be performed to improve the understanding of fiber sorbent operation.

Tensile testing to determine stress-strain behavior and Young's modulus can be used to better quantify the effect of core layer polymer type and zeolite loading on the mechanical strength of the fiber sorbents. BET and mercury porosimetry experiments can be performed to determine the surface area, pore size and porosity of the fiber sorbents.

IR experiments can be conducted to fundamentally understand the zeolite active sites utilized during sorption of various sulfur species.

The effect of different solvent and non-solvent sorption into the zeolites during dope creation needs to be studied in greater detail. Currently, the zeolites crystals in the dopes were assumed to be 'passive' fillers, however certain amount of non-solvent (water) or solvent (NMP) in the dope can sorb into the zeolite, altering the dope composition and effecting the fiber sorbent morphology. Also, the molecular weight and content of additive (PVP) in the dope and its effect on fiber porosity needs to be considered in greater detail.

Shell and tube geometry with parallel flow direction was selected as the preferred module design due to ease of construction and operational simplicity. However, appropriate optimization of the flow geometry, fiber packing and flow profile in a fiber sorbent module can improve external mass transfer and contact surface area, while reducing the pressure drop, thus improving the dynamic sorption capacity [15, 16].

8.2.5. Simulation of physical and transport properties to predict breakthrough times

Reaching the stage of testing fiber sorbent modules is a long and complicated process involving dope making, fiber spinning, checking basis characteristics properties (sorption and permeation), and making modules for flow testing. For peak performance of fiber sorbents experiments have to be augmented with modeling of the process.

In the preliminary calculations basic mass and energy balance equations were established to show the advantages of hollow fiber sorbents in comparison to packed bed pellets. The modeling had considered perfect packing, high porosity, isothermal operation

and complete utilization of zeolites as the gas moves through the fiber. Various non –

idealities need to be included in future models.

8.3. REFERENCES

1. S. Satokawa, Y.K., *Adsorbent for removing sulfur compounds from fuel gases and removal method*. 2005, United States Patent 6875410

2. Satokawa, S., Y. Kobayashi, and H. Fujiki, *Adsorptive removal of dimethylsulfide and t-butylmercaptan from pipeline natural gas fuel on Ag zeolites under ambient conditions.* Applied Catalysis B-Environmental, 2005. 56(1-2): p. 51-56.

3. Shimizu, K., et al., *Mechanistic study on adsorptive removal of tert-butanethiol on Ag-Y zeolite under ambient conditions.* Journal of physical chemistry B, 2006. 110(45): p. 22570-22576.

4. Bekkum, H.v., E.M. Flanigen, and J.C. Jansen, *Introduction to zeolite science and practice*. Studies in surface science and catalysis. 1991, Amsterdam ; Oxford: Elsevier. xvi, 754 p.

5. Rege, S.U. and R.T. Yang, *A novel FTIR method for studying mixed gas adsorption at low concentrations: H2O and CO2 on NaX zeolite and gamma-alumina.* Chemical Engineering Science, 2001. 56(12): p. 3781-3796.

6. Crespo, D., et al., *Superior sorbent for natural gas desulfurization.* Industrial & Engineering chemistry research, 2008. 47(4): p. 1238-1244.

7. Wakita, H., Y. Tachibana, and M. Hosaka, *Removal of dimethyl sulfide and t-butylmercaptan from city gas by adsorption on zeolites.* Microporous and Mesoporous materials, 2001. 46(2-3): p. 237-247.

8. Shogren, R.L., *Preparation, thermal properties, and extrusion of high-amylose starch acetates.* Carbohydrate Polymers, 1996. 29(1): p. 57-62.

9. Kosuri, M.R. and W.J. Koros, *Defect-free asymmetric hollow fiber membranes from Torlon (R), a polyamide-imide polymer, for high-pressure CO2 separations.* Journal of Membrane Science, 2008. 320(1-2): p. 65-72.

10. Kosuri, M.R. and W.J. Koros, *Asymmetric Hollow Fiber Membranes for Separation of CO2 from Hydrocarbons and Fluorocarbons at High-Pressure Conditions Relevant to C2F4 Polymerization.* Industrial & Engineering chemistry research, 2009. 48(23): p. 10577-10583.

11. Carruthers, S.B., G.L. Ramos, and W.J. Koros, *Morphology of integral-skin layers in hollow-fiber gas-separation membranes.* Journal of applied polymer science, 2003. 90(2): p. 399-411.

12.   de Wild, P.J., et al., *Removal of sulphur-containing odorants from fuel gases for fuel cell-based combined heat and power applications.* Journal of power sources, 2006. 159(2): p. 995-1004.

13.   Kim, H.T., et al., *Desulfurization of odorant-containing gas: Removal of t-butylmercaptan on Cu/ZnO/Al2O3.* International journal of Hydrogen Energy, 2007. 32(15): p. 3603-3608.

14.   Alptekin, G., et al., *Regenerable sorbent for natural gas desulfurization.* Journal of materials engineering and performance, 2006. 15(4): p. 433-438.

15.   S.Wickramasinghe, M.S., E. Cussler, *Mass transfer in various hollow fiber geometrics.* Journal of membrane science, 1992. 69: p. 235-250.

16.   Gabelman, A. and S.T. Hwang, *Hollow fiber membrane contactors.* Journal of Membrane Science, 1999. 159(1-2): p. 61-106.

APPENDIX A

The various sections are described to demonstrate the effect of various parameters on the optimization of the fiber sorbent geometry. A spherical pellet is considered as the industrial standard and is compared to fiber sorbent results for better illustration of certain key variables.

If hydrogen (H_2) as a fuel would become a reality as per futuristic estimates, the scale of hydrogen generation can be divided into different categories [1]:

1. **Central generating stations** – Capacity of~1.2 million kg H_2 per day, supporting around 2 million cars. These will be close to a refinery and the scale of operations will be very high. The hydrogen distribution will be through pipelines [1].

2. **Midsize station** – Capacity of~24,000 Kg / H_2 day, supporting around 40,000 cars. The distribution system will be most likely cryogenic trucks [1].

3. **Small size stations** – Capacity of~480 Kg / H_2 day, supporting around 800 cars. These Hydrogen stations would produce hydrogen at the filling station itself and would not require a distribution system [1].

A.1. Process conditions for on-site hydrogen production using pipeline natural gas

In developing fiber sorbents it is desired to develop a natural gas desulfurization technology that can be utilized at all of the above possible stations. At present, due to the lack of distribution infrastructure and other competing alternative fuels, only the on-site filling stations have become a reality [2].

These calculations and equations act as a guiding force to find the parameters for the design and development of fiber sorbents and the TSA system.
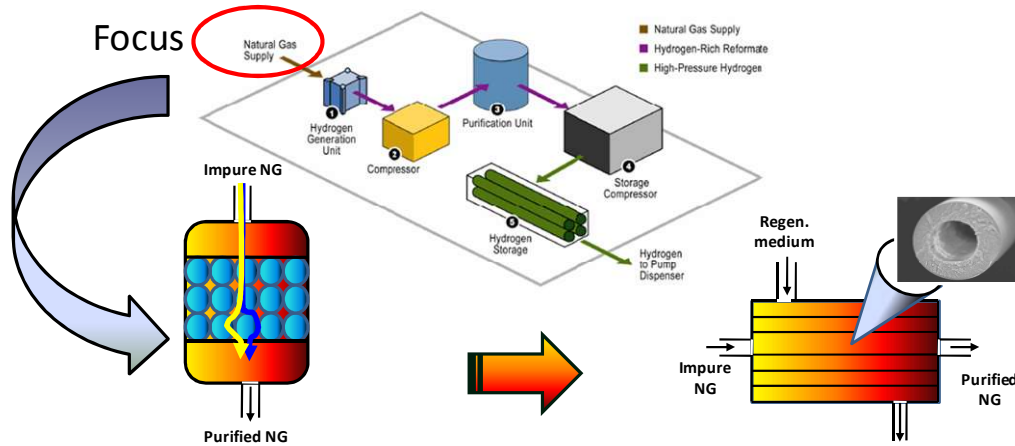
Figure A.1: Prototype of the Chevron hydrogen energy station at Chino, California [3] and the proposed transition from a pellet packed bed to a fiber sorbent based technology.

Design calculations are performed for on-site hydrogen generation station (Figure A.1) considering the feed stream conditions provided by Chevron to analyze the feasibility of using fiber sorbents. The parameters in consideration were fiber diameter (O.D. and I.D.), fiber length, porosity of the fibers and the desired zeolite loading.

Sample calculations are provided for clarity and various parameters are then varied to maximize the mass transfer and the surface area to volume ratio; while, minimizing the pressure drop and the material requirements.

Desired hydrogen output at the pump, $Q_{m-H_2} = 480$ kg/day

An efficiency of 90 % is assumed from the H_2 output from the PSA unit to actual dispensing [1].

Output from the PSA unit, $Q_{M-PSA} = \dfrac{Q_{M-H_2}}{0.9} = \dfrac{480\ kg/day}{0.9} = 533.3\ kg/day$ \qquad (A.1)

From the data provided by Chevron, and stoichometric calculations, the natural gas (NG) inlet to the steam methane reforming (SMR) unit,

$Q_{m-NG} = 1860$ kg/day NG

224

This is the amount of pipeline natural gas (NG) that needs to be desulfurized. The inlet conditions of the gas are as follows:

T_{in} = 25°C or 298 K

p_{in} = 5 psig or 1.34 atm

Typical concentration of odorants in natural gas is around 10 ppm but can be as high as 30 ppm. In our experimental studies 30 ppm H_2S/N_2 (C_o) has been taken as the stimulant gas due to the reasons explained in section 2.4.3.1. and section 3.1.4.) and is taken as the basis here.

Average molecular weight of NG, M_{avg} = 17.14 kg / kmole (weighted average of the components of natural gas stream, methane 95 wt. %, ethane 2 wt. %, CO_2 wt. %, propane 0.4 wt. % etc.)

Temperature and pressure at STP, T_{STP} = 273.15 K, p_{STP} = 1 atm

Determining the flow rate of the gas stream,

Density at feed conditions,

$$\rho_{NG} = \frac{p_{in}M_{avg}}{RT_{in}} = \frac{1.34atm * 17.14\ kg/kmole}{0.082\frac{m^3.atm}{K.kmole} * 298\ K} = 0.94\ kg/m^3 \tag{A.2}$$

Flow rate of the NG stream,

$$Q_v = \frac{Q_{m-NG}}{\rho_{NG}} = \frac{1860\ kg/day}{0.94\ kg/m^3} * \frac{1\ day}{24 * 3600\ sec} = 2.29 * 10^{-2}\ m^3/s \tag{A.3}$$

Flow rate at STP, $Q_{V\text{-STP}} = Q_v * \frac{p}{p_{stp}} * \frac{T_{stp}}{T}$

$$= 2.29 * 10^{-2}\ m^3/s * \frac{1.34\ atm}{1\ atm} * \frac{273\ K}{298\ K} = 0.028\ (STP)\ m^3/s \tag{A.4}$$

A.2. Dimensions of the fiber sorbent module

Fiber sorbent module dimensions can be estimated by two approaches:

1. Module dimensions can be fixed to determine the flow velocity through the module.

2. The flow velocity can be fixed to estimate the module dimensions.

I have decided to base my design as per approach 1.

With the increase in module dimensions (diameter or length) for the same sorbent loading and void fractions, the amount of sorbent in the module increases, thereby increasing the breakthrough time. Based on the desired breakthrough time and the cost of the sorbent we can vary the module dimension. Module dimensions similar to a typical hollow-fiber membrane module were taken as the first step for use in this application.

Diameter of the module, $d_t = 20\,cm \approx 8\,inches$ [4]

Typically, in fiber modules [4], the aspect ratio, $\dfrac{L_t}{d_t} \approx 6$

Hence, the length of the module $L_t = 6 * d_t = 6 * 20\,cm = 120\,cm$ $\hfill$ (A. 5)

The geometry of the module was selected to be cylindrical with shell and tube type arrangement [5, 6]. NG is fed on the bore side of the fiber while steam is fed on the shell side (refer section 2.6.).

The cross-sectional area of the module,

$$S_t = \pi/4 * d_t^2 = \pi/4 * (0.2\,m)^2 = 0.0314\,m^2 \hspace{3em} \text{(A. 6)}$$

Superficial velocity through the module,

$$v_s = \frac{Q_v}{S_t} = \frac{0.0229\,m^3/s}{0.0314\,m^2} = 72.74\,cm/s \hspace{3em} \text{(A.7)}$$

Volume of the module, $V_t = \pi/4 * d_t^2 * L_t = \pi/4 * (0.2\ m)^2 * 1.2\,m = 0.0377\,m^3$ $\quad$ (A.8)

The fiber sorbent bed will be operated at a temperature $T_t = 25$ °C, and a pressure of $p_t = 1$ atm.

For the sake of simplicity, the described optimization is presented taking into account only single-layer fiber sorbents (without the barrier sheath layer). If hot purge gas or product gas is used for the regeneration, then single-layer fiber sorbents can be used effectively.

If it is desired to use steam as the regeneration media, a 20-50 µm thick barrier layer is required on the single-layer fiber to prevent a direct contact between the steam and the zeolite loaded core layer. In that scenario, the outer diameter of the fiber sorbent will increase slightly, taking the sheath layer into account.

Assuming the void fraction in a fiber sorbent module, $\varepsilon_f = 0.4$ (similar to void fraction of pellet packed bed $\varepsilon_b = 0.4$) [7]

Volume occupied by the fibers,

$$V_f = (1 - \varepsilon_f) * V_t = (1 - 0.4) * 0.0377\ m^3 = 0.0226\ m^3 \tag{A.9}$$

The O.D. and I.D. of the fiber sorbent core layer are process parameters. After considerable optimization a fiber sorbent with an O.D. =800 µm and an I.D. =400 µm was found to give the best compromise providing a high breakthrough time and surface area to volume ratio with a low pressure drop as shown in Table A.1. The feed pressure is 1.3 atm, and hence the pressure drop in the module is desired to be less than 0.3 atm.

Detailed calculations for the best case are described in detail in the following sections. Similar calculations can be performed to obtain the variables for different O.D. and I.D. cases shown in Table A.1.

Table A.1: Optimization of the various parameters of the fiber sorbent core layer.

Parameter	Parameter	*Minimize*	*Maximize*	$\Delta p < 0.3$ atm		*Maximize*
Sr. No.	**Outer diameter**	**Inner diameter**	**Amount of zeolite**	**Breakthrough time**	**Pressure drop**	**Number of fibers**	**Surface area to volume ratio**
	O.D. (µm)	**I.D. (µm)**	**W_{ads} (kg)**	**t_b (h)**	**Δp (atm)**	**N_f**	**a_{fb} (cm^2/cm^3)**
1	1200	400	15.9	4.1	0.28	16,667	12.5
2	1200	600	13.4	3.4	0.06	16,667	22.2
3	1000	500	13.4	3.7	0.08	24,000	26.7
4	**800**	**400**	**13.4**	**4.0**	**0.13**	**37,500**	**33.3**
5	500	250	13.4	4.5	0.32	96,000	53.3
6	500	400	6.4	2.2	0.05	96,000	177.7

A.3. Polymer and adsorbent requirements

Illustrative but not restrictive values for key parameters are used in the calculations. *The values were either obtained through experimental measurements or selected through various literature sources.*

Core layer porosity (measured by mercury porosimetry) [8] $\varepsilon_{pore} \approx 0.5$

Usually the amount of binder material in zeolite pellet is roughly 30 wt. % of total zeolite crystal weight that is roughly 75 wt. % loading of zeolite crystals (total pellet wt. basis). In fiber sorbents, the aim will be to achieve zeolite loadings in the range of 50 - 75 wt. % (core layer wt. basis). Very higher sorbent loadings results in brittle fibers due to the smaller content of polymer 'binder' material.

For a 75 wt. % zeolite NaY sorbent loading (core layer wt. basis) and with cellulose acetate polymer as the binder material, the volume and the weight of each component in the fiber sorbent can be calculated as follows:

Taking the volume fraction of the adsorbent as $\phi_{ads} = 0.6$

Thus, the volume fraction of the polymer,

$$\phi_{poly} = (1 - \varepsilon_{pore}) * (1 - \phi_{ads}) = (1 - 0.5) * (1 - 0.6) = 0.2 \tag{A.10}$$

Volume fraction of the pores/voids,

$$\phi_{void} = (\varepsilon_{pore}) * (1 - \phi_{ads}) = (0.5) * (1 - 0.6) = 0.2 \tag{A.11}$$

Density of zeolite NaY, $\rho_{ads} \approx 1320 \ kg/m^3$

Density of polymer cellulose acetate (CA) $\rho_{poly} \approx 1300 \ kg/m^3$ [9]

Hence, density of the fiber, $\rho_{fiber} = \phi_{poly} * \rho_{poly} + \phi_{ads} * \rho_{ads} + \phi_{void} * \rho_{void} \tag{A.12}$

$$\rho_{fiber} = 0.20 * 1300 \ kg/m^3 + 0.6 * 1320 \ kg/m^3 + 0.2 * 0 \ kg/m^3 = 1052 \ kg/m^3$$

Weight fraction of adsorbent, $w_{ads} = \dfrac{\rho_{ads}}{\rho_{fiber}} * \phi_{ads} = \dfrac{1320\ kg/m^3}{1052\ kg/m^3} * 0.6 = 0.75$ (A.13)

Weight fraction of polymer, $w_{poly} = 1 - w_{ads} = 1 - 0.75 = 0.25$

Volume of polymer required, $V_{Poly} = \phi_{poly} * N_f * \pi/4 * (O.D.^2 - I.D.^2) * L_f$ (A.14)

$V_{poly} = 0.2 * 37,5000 * \pi/4 * ((800 * 10^{-4}\ cm)^2 - (400 * 10^{-4}\ cm)^2) * 120\ cm = 3392\ cm^3$

Volume of adsorbent required $V_{ads} = \phi_{ads} * N_f * \pi/4 * (O.D.^2 - I.D.^2) * L_f$ (A.15)

$V_{ads} = 0.60 * 37,500 * \pi/4 * ((800 * 10^{-4}\ cm)^2 - (400 * 10^{-4}\ cm)^2) * 120\ cm = 10180\ cm^3$

Weight of the adsorbent NaY required,

$W_{ads} = \rho_{ads} * V_{ads} = 1.32\ g/cm^3 * 10180\ cm^3 = 13.44\ kg$

Weight of the polymer CA required,

$W_{poly} = \rho_{poly} * V_{poly} = 1.30\ g/cm^3 * 3392\ cm^3 = 4.4\ kg$

A.4. Surface area to volume ratio comparison

Surface area provided by a particular geometry for flow is an important consideration in the determination of the main and auxiliary bed sizes. A higher surface area provides a smaller reactor or bed volume for a similar breakthrough time. This ratio is defined as the surface area available for mass transfer in the material (pellet or fiber) to the volume of the bed. For a given fiber or pellet volume the ratios are defined as:

$$\frac{Surface\ area\ in\ bore\ flow}{volume\ of\ the\ fiber\ sorbent} = a_{fb} = \frac{A_{fb}}{V_f} = \frac{\pi\ I.D.\ L_f}{\dfrac{\pi}{4}(O.D.^2 - I.D.^2)L_f} = \frac{4\ I.D.}{(O.D.^2 - I.D.^2)}$$ (A.16)

$$\frac{Surface\ area\ of\ spherical\ pellet}{volume\ of\ spherical\ pellet} = a_p = \frac{A_p}{V_p} = \frac{\pi\ d_p^2}{\dfrac{\pi}{6}d_p^3} = \frac{6}{d_p}$$ (A.17)

The surface areas in both the cases for equivalent volume are then compared.

volume of a spherical pellet (V_p) = *volume of a fiber* (V_f)

$$\frac{\pi}{6}d_{p,eq}^3 = \frac{\pi}{4}(O.D.^2 - I.D.^2)L_f$$

$$d_{p,eq} = \left[\frac{3}{2}O.D.^2 L_f\left\{1-(\frac{I.D.}{O.D.})^2\right\}\right]^{\frac{1}{3}} \tag{A.18}$$

For equivalent volume of pellet and fiber sorbent,

$$\frac{Surface\ area\ of\ fiber\ sorbent\ in\ bore\ flow}{Surface\ area\ of\ spherical\ pellet} = \frac{A_{f\,b}}{A_{p,eq}} = \frac{\pi\ I.D.\ L_f}{\pi\ d_{p,eq}^2} \tag{A.19}$$

Figure A.2 illustrates the surface area ratio (fiber sorbent/spherical pellet) plotted against diameter ratio (I.D./O.D.), for a range of aspect ratio (L_f/O.D.) values. The results reveal that avoiding impracticable values of (I.D./O.D.) corresponding to solid and very thin fiber sorbents the optimum design range can be between 0.4 < I.D./O.D.< 0.8 [10].
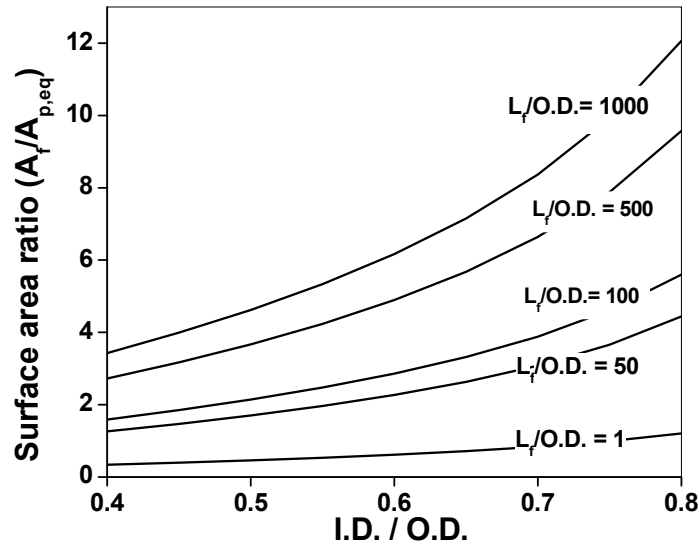

Figure A.2: Effects of aspect ratio and diameter ratio on surface area ratio (fiber sorbent/spherical pellet) for equivalent pellet and fiber volume and packing fraction.

A fiber sorbent with a small bore diameter (Figure A.6) gives a high pressure drop (Table A.1., cases 1 and 5) and a very thin fiber sorbent will have a high voidage giving less sorption capacity for a given bed volume (Table A.1., case 6). Fiber sorbents can have up to 10 times higher surface area compared to a spherical pellet for practically feasible geometries. The results indicate that fiber sorbents are highly advantageous over spherical pellets at high aspect ratio. Unfortunately, increased aspect ratio results in additional pressure drop and lower external mass transfer as explained later.

A.5. Mass transfer considerations

The proposed advantage of faster mass transfer in fiber sorbents arises from the ability to manipulate the morphology of the sorbents. This becomes clear with a comparison of various mass transfer resistances encountered by the gas, during the sorption on a pellet or a fiber sorbent. Similar types of resistances exist in pellets and fiber sorbents; however the relative magnitudes of these resistances are more 'tunable' in the fiber sorbent approach. In general such materials offer multiple resistances to mass transfer [11]:

1. Film transport, of the adsorbate through a hypothetical 'film' or a hydrodynamic boundary layer surrounding the pellet or within the bore of the fiber sorbent

2. The meso/macropore diffusional resistance through a pellet or a fiber sorbent

3. Micropore resistance of the zeolite crystals in a pellet or a fiber sorbent

These resistances are depicted pictorially in Figure A.3. The presence of an internal skin layer in case of fiber sorbents can cause additional mass transfer resistance and must be avoided during its creation. This is explained in detail in the fiber sorbent spinning section in chapter 4.
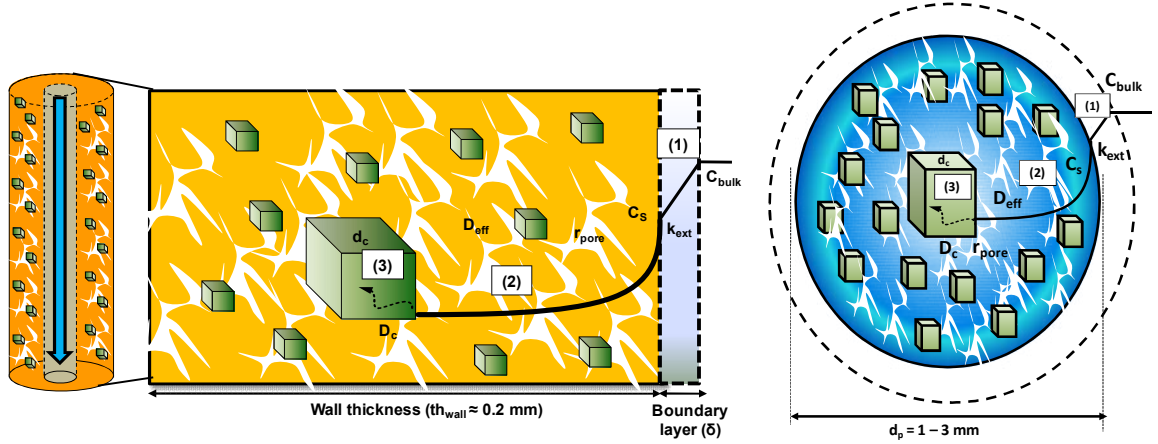
Figure A.3: Mass transfer resistances/coefficients in a single-layer fiber sorbent vs. a spherical pellet.

Due to the small size of zeolite crystals ($d_c \approx 500$ nm) used in both cases, high sulfur sorption affinity [12] and the large pore window of zeolite NaY cage (~7.4 Å) the diffusion ($D_c \sim 10^{-6}$ cm^2/s) of sulfur molecules (3–7 Å) into zeolite cages (step 3) takes place rapidly and is not the rate determining step [11].

A.5.1. Meso/macropore or internal mass transfer coefficient (MTC)

Calculating the binary diffusion coefficient between methane (major component of NG) and H$_2$S

Using the Chapman-Enskog equation [13]:

$$D_M = \frac{1.858*10^{-27} T^{3/2}}{P \sigma_{NG\text{-}H_2S}{}^2 \Omega} * (\frac{1}{M_{NG}} + \frac{1}{M_{H_2S}})^{1/2} \tag{A.20}$$

$$D_M = \frac{1.858*10^{-27} (298.16\, K)^{3/2}}{1.34\, atm * (4.45*10^{-10})^2 * 0.977} * (\frac{1}{17.1} + \frac{1}{34})^{1/2} = 1*10^{-5}\, m^2/s = 0.1\, cm^2/s$$

Also, $r_{pore} \approx 100\text{-}300$ nm (measured from mercury porosimetry) [8], $\varepsilon_{pore} \approx 0.5$ [8] and $\tau \approx 1/\varepsilon_{pore}$ [14]

Knudsen diffusivity [13]

$$D_k = 9.7 * 10^3 * r_{pore} * \sqrt{\frac{T}{M_{H_2S}}}$$

$$\Rightarrow 9.7 * 10^3 * 300 * 10^{-7} cm * \sqrt{\frac{298.15\ K}{34\ gm/gmole}} = 0.86\ cm^2/s$$

(A.21)

The effective diffusion coefficient (D_{eff}) through the pores can be obtained as

$$D_{eff} = \frac{\varepsilon_{pore} D_{combined}}{\tau}$$

(A.22)

Where, $\dfrac{1}{D_{combined}} = \dfrac{1}{D_M} + \dfrac{1}{D_K}$

$$\frac{1}{D_{combined}} = \left(\frac{1}{0.1\ cm^2/s} + \frac{1}{0.86\ cm^2/s}\right) \Rightarrow D_{combined} = 0.09\ cm^2/s$$

$$D_{eff} = \frac{\varepsilon_{pore} D_{combined}}{\tau} = \frac{0.5 * 0.09\ cm^2/s}{2} = 0.022\ cm^2/s$$

(A.23)

It must be noted that the advantages of fiber sorbents can be realized when they have porous walls with an interconnected pore network with the diffusion coefficient approximately equal to the effective diffusivity (molecular + Knudsen diffusion) through the pores. If the polymer interferes or blocks the zeolite surface, this resistance can be significantly higher (i.e. $D_{eff} \approx D_{poly}$), leading to a higher macropore resistance and a smaller breakthrough time. This condition is referred to as 'occluded' sieves [15]. Movement through the porous structure rather than through the polymer is promoted by a so-called 'sieve-in–a–cage' structure [15, 16].

Correlations for meso/macroporous or internal MTC through a hollow cylinder or fiber with a bore side feed and a spherical pellet are given by Patton et. al [17] and Glueckauf [18], using the linear driving force (LDF) approximation (applicable for D_{eff} $t/r^2 > 0.1$)

$$\text{Internal MTC fibers } (k_{int})_f = \cfrac{4D_{eff}}{\{((\frac{r_f}{r_{fb}})-1)(r_f^2 - r_{fb}^2) - (\frac{1}{r_{fb}(r_f - r_{fb})})x[(0.5)(r_f^4 - r_{fb}^4) - (\frac{4r_f}{3})(r_f^3 - r_{fb}^3) + r_f^2(r_f^2 - r_{fb}^2)]\}} / a_f$$

$$\Rightarrow \cfrac{4D_{eff}}{\{((\frac{r_f}{r_{fb}})-1)(r_f^2 - r_{fb}^2) - (\frac{1}{r_{fb}(r_f - r_{fb})})x[(0.5)(r_f^4 - r_{fb}^4) - (\frac{4r_f}{3})(r_f^3 - r_{fb}^3) + r_f^2(r_f^2 - r_{fb}^2)]\}} / \frac{2\,r_{fb}}{(r_f^2 - r_{fb}^2)} \qquad \text{(A.24)}$$

Substituting values,

$$r_f = \frac{O.D.}{2} = \frac{800\ \mu m}{2} = 400\ \mu m$$

$$r_{fb} = \frac{I.D.}{2} = \frac{400\ \mu m}{2} = 200\ \mu m$$

$$D_{eff} = 0.022\ cm^2/s$$

Substituting the values, fiber internal mass transfer coefficient $(k_{int})_f = 3.05\ cm/s$

Calculating meso/macroporous MTC in a spherical pellet of 1 mm diameter and assuming similar diffusion coefficient (D_{eff})

$$\text{Internal MTC pellets } (k_{int})_p = \frac{15 D_{eff}}{r_p^2} / a_p = \frac{15 D_{eff}}{r_p^2} / \frac{3}{r_p} = \frac{5 D_{eff}}{r_p} \qquad \text{(A.25)}$$

$$(k_{int})_p = \frac{5 D_{eff}}{r_p} = \frac{5 * 0.022\ cm^2/s}{0.05\ cm} = 2.2\ cm/s$$

Figure A.4 illustrates the effect of fiber diameter and diameter ratio (I.D./O.D.) on the internal MTC of fiber sorbent $(k_{int})_f$ and compares it with a 1 mm spherical pellet $(k_{int})_p$ for equivalent effective diffusion coefficient (D_{eff}) in fiber sorbents and pellets. The figure reveals that fibers with smaller diameter and higher diameter ratio have a higher internal MTC due to the smaller mass transfer path length. Also, the internal MTC in fiber sorbents is higher compared to a 1 mm spherical pellet. The macropore resistance (step 2) in fiber sorbents is significantly less compared to that of a pellet. This can be

explained by the small fiber wall thickness (th_{wall} = 200 μm or 0.2 mm) vs. the large radius of a commercial spherical pellet (d_p = 1 – 3 mm). Even if an attempt is made to decrease the size of the pellets, the pressure drop summarized in Appendix A.6., increases drastically.
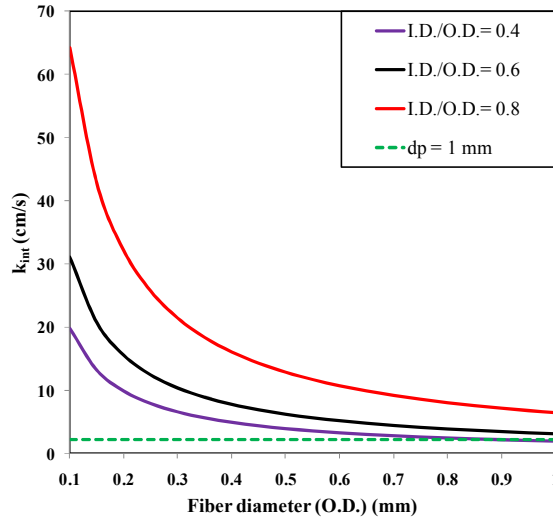

Figure A.4: Variation in the meso/macroporous mass transfer coefficient with fiber diameter and diameter ratio. Coefficients for 1 mm diameter pellet are also shown for comparison. The effective diffusion through the fiber sorbent and pellet wall is assumed to be the same.

A.5.2. External mass transfer coefficient

The Yang – Cussler or Leveque equation [19] for bore side feed in hollow fibers can be used for calculating external MTC

$$\text{Sherwood number, } Sh_f = \frac{(k_{ext})_f \, I.D.}{D_M} = 1.62 \, (\frac{\text{Re}_f \, Sc \, I.D.}{L_f})^{0.33} \tag{A.26}$$

$$\text{Schmidt number, } Sc = \frac{\mu_{NG}}{\rho_{NG*} D_M} = \frac{1.1*10^{-4} \, poise}{0.942*10^{-3} \, g/cm^3 * 0.1 \, cm^2 /s} = 1.167 \tag{A.27}$$

Fraction of the module volume occupied by the fiber bore,

$$\varepsilon_{fb} = \frac{V_{fb}}{V_t} = \frac{N_f * \frac{\pi}{4} * I.D.^2 * L_f}{V_t} = \frac{37,500 * \frac{\pi}{4} * (400 * 10^{-4} \, cm)^2 * 120 \, cm}{37,700 \, cm^3} = 0.15 \quad (A.28)$$

Velocity through the fiber bore,

$$v_{fb} = \frac{Q_v}{S_t * \varepsilon_{fb}} = \frac{2.29 * 10^{-2} \, m^3 / s}{3.142 * 10^{-2} \, m^3 / s * 0.15} = 4.848 \, m/s = 484.8 \, cm/s \quad (A.29)$$

Reynolds number,

$$Re_f = \frac{I.D. * v_{fb} * \rho_{NG}}{\mu_{NG}} = \frac{(400 * 10^{-4} \, cm) * 484.8 \, cm/s * 0.942 * 10^{-3} \, g/cm^3}{1.1 * 10^{-4} \, poise} = 166.1 \, (A.30)$$

$$Sh_f = 1.62 \, (\frac{Re_f \, Sc \, I.D.}{L_f})^{0.33} = 1.62 * (\frac{166.1 * 1.167 * 400 * 10^{-4} \, cm}{120 \, cm})^{0.33} = 0.656 \quad (A.31)$$

$$Sh_f = \frac{(k_{ext})_f \, I.D.}{D_M} \Rightarrow k_{ext} = \frac{Sh * D_M}{I.D.} = \frac{0.656 * 0.1 \, cm^2 / s}{400 * 10^{-4} \, cm} = 1.64 \, cm/s$$

A.5.2.1. Effect of fiber bore diameter on the external mass transfer coefficient

The effect of fiber bore diameter on the external mass transfer coefficient in fiber sorbents is demonstrated and compared it to a standard pellet operation with an equivalent superficial velocity ($v_p = v_f = 1$ m/s) and flow voidage ($\varepsilon_p = \varepsilon_{fb} = 0.4$ [20]) in both the cases.

Figure A.5 illustrates the effect of fiber bore diameter on the external MTC of fiber sorbent and compares it with a 1 mm spherical pellet under similar conditions, The fiber sorbent length (L_f) was taken to be 1.2 m. It can be seen that due to a large aspect ratio (L_f/O.D.) values, the external mass transfer in fiber sorbents is less compared to a 1 mm pellet.

The external mass transfer coefficient for a packed bed (k_{ext})$_p$ with spherical particles (diameter $d_p = 1$ mm) and for Re greater than 10 [21]:

$$Sh = \frac{(k_{ext})_p \, d_p}{D_M} = 1.17 \, Sc^{\frac{1}{3}} \, Re_p^{0.585} \qquad (A.32)$$

In case of pellet packed bed, the Reynolds number,

$$Re_p = \frac{d_p \, v_p \, \rho_{NG}}{\mu_{NG} \, \varepsilon_p} = \frac{(0.1 \, cm) * 100 \, cm/s * 0.942 * 10^{-3} \, g/cm^3}{1.1 * 10^{-4} \, poise * 0.4} = 214 \qquad (A.33)$$

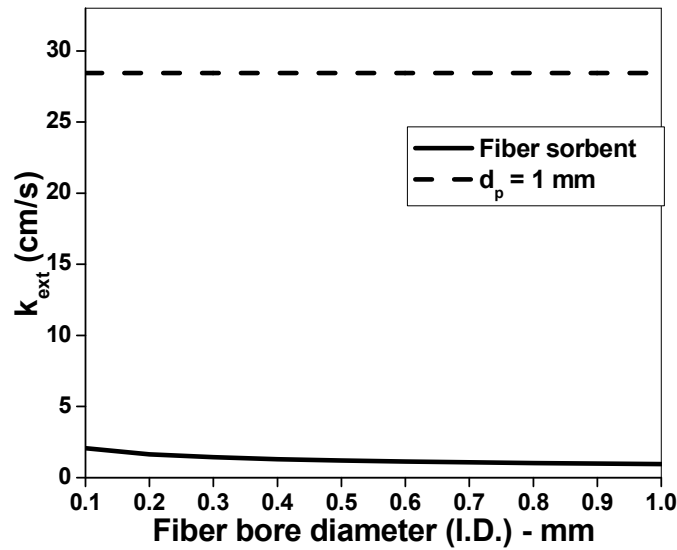Using, calculations similar to above $(K_{ext})_p = 28.4$ cm/s

Figure A.5: Variation in the external mass transfer coefficient with fiber bore diameter. Coefficients for 1 mm diameter pellet are also shown for comparison. The superficial velocity ($v_p = v_f = 1$ m/s) and flow voidage ($\varepsilon_p = \varepsilon_{fb} = 0.4$) in the pellet bed and fiber sorbent module are assumed to be the same.

The above discussion clearly show that in case of fiber sorbents the external mass transfer coefficient is small and the controlling resistance, while in case of spherical pellets macropore or internal mass transfer coefficient is the main controlling factor.

A.6. Pressure drop calculation

Pressure drop considerations are very important for a cyclically operated bed. High pressure drops across the bed can cause significant compression costs and material attrition. For gas flow rates through fiber bore, the pressure drop can be calculated by

Hagen-Poiseuille equation for laminar flow ($Re_f < 2100$) assuming negligible flow through the porous network in the axial direction:

$$\frac{\Delta p}{L_f} = \frac{Q_v * 8 * \mu_{NG}}{N_f * \pi * (I.D./2)^4}$$

(A.34)

Calculating the pressure drop for the demonstration case discussed earlier,

$$\Delta p = \frac{Q_v * 8 * \mu_{NG} * L_f}{N_f * \pi * (I.D./2)^4}$$

$$\Rightarrow \frac{2.29 * 10^{-2} m^3 / s * 8 * 1.1 * 10^{-5} Pa\text{-}sec * 1.2 \, m}{37,500 \, fibers * \pi * (400 * 10^{-6} \, m/2)^4} = 12,801 \, Pa = 0.126 \, atm$$

A.6.1. Effect of superficial velocity and fiber bore diameter on pressure drop

In case of fiber sorbents the pressure drop depends on the gas flow velocity through the fiber bore and the bore diameter and can be estimated by Hagen-Poiseuille equation (shown in terms of superficial velocity instead of flow rate).

$$\frac{\Delta p}{L_f} = \frac{32 \mu_{NG}}{(I.D.)^2} \left[\frac{v_s}{\varepsilon_{fb}} \right]$$

(A.35)

The pressure drop through the packed bed adsorbers over the entire range of flow rates can be evaluated by the Ergun equation [22]:

$$\frac{\Delta p}{L_p} = \frac{150 \mu_{NG}}{d_p^2} \left(\frac{1-\varepsilon_p}{\varepsilon_p} \right)^2 \left(\frac{v_p}{\varepsilon_p} \right) + \frac{1.75 \rho_{NG}}{d_p} \left(\frac{1-\varepsilon_p}{\varepsilon_p} \right) \left(\frac{v_p}{\varepsilon_p} \right)^2$$

(A.36)

The equation predicts that the pressure drop is a quadratic function of the interstitial velocity of the gas flow, pellet size and bed voidage. Figure A.6 shows the variation in pressure drop per unit length plotted against superficial velocity with varying fiber bore diameter and a pellet of 1 mm diameter for a flow voidage of ($\varepsilon_p = \varepsilon_{fb} = 0.4$ [20]). A larger bore diameter and higher voidage though helpful for lower pressure drop (Table A.1., case 2), allows fewer fibers to be packed in a give bed volume.
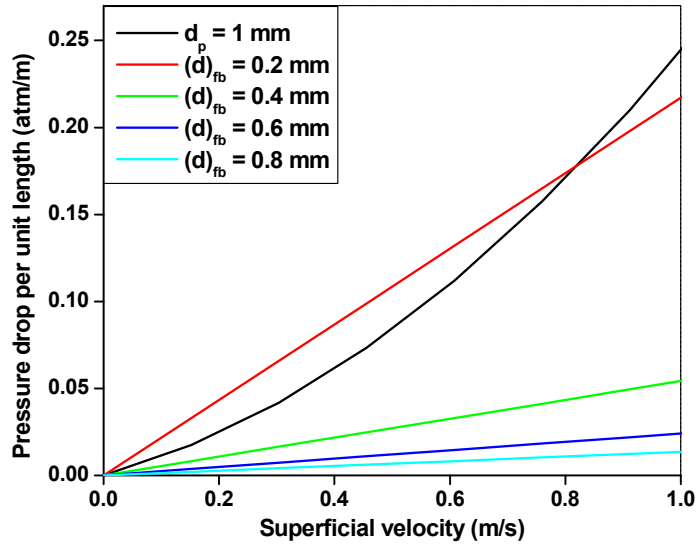
Figure A.6: Variation in pressure drop per unit length with varying superficial velocity for different material diameters. The superficial velocity (v_p = v_f = 1 m/s) and flow voidage (ε_p = ε_{fb} = 0.4) in the pellet bed and fiber sorbent module are assumed to be the same.

A.7. Estimation of the breakthrough time for the fiber sorbent module

Flow rate of H₂S through the module, $Q_{H_2S} = Q_v * C_o$ (A.37)

$$= 2.29*10^{-2}\, m^3/s * 30\, ppm = 2.29*10^{-2}\, m^3/s * 30*10^{-6} = 6.87*10^{-7}\, m^3/s$$

In case of fiber sorbents, at low concentrations of sulfur impurities, only the zeolite sorbent contributes to the sorption capacity, while the polymer binder does not contribute to the sorption capacity (refer chapter 4 for experimental details)

The breakthrough capacity for zeolite NaY in a 30 ppm H₂S/N₂ feed stream at 25°C and 1 atm pressure was found to be,

$$C_b = 1\frac{mg\,H_2S}{g\,zeolite} = 1\frac{mg\,H_2S}{g\,zeolite} * \frac{1}{34\dfrac{mg\,H_2S}{mmole\,H_2S}} = 0.03\frac{mmole\,H_2S}{g\,zeolite}$$

Hence, mass flow rate of H_2S through the module,

$$\dot{m}_{H_2S} = Q_{H_2S} * \rho_{H_2S} = 6.87 * 10^{-7} \, m^3 / s * 1.4 \, kg / m^3 = 9.6 * 10^{-7} \, kg / sec \qquad (A.38)$$

H_2S adsorbed till breakthrough,

$$m_{H_2S} = C_b \frac{mmole \, H_2S}{g \, zeolite} * W_{ads} \, g \, zeolite * M_{H_2S} \frac{g}{mole} \qquad (A.39)$$

$$= 0.03 * 10^{-3} \frac{mole \, H_2S}{gm \, zeolite} * 13.44 * 10^3 \, gm \, zeolite * 34 \frac{gm \, H_2S}{mole} = 13.7 \, gm \, H_2S$$

Hence, breakthrough time $t_b = \dfrac{m_{H_2S}}{\dot{m}_{H_2S}} = \dfrac{13.7 \, g}{9.6 * 10^{-4} \, g / s} * \dfrac{1 hour}{3600 sec} = 4 \, h$

The breakthrough time can thus be varied as per process requirements, either by increasing the zeolite loading in the fiber or by increasing the dimensions of the module.

A.8. Regeneration of fibers

The moles of H_2S adsorbed till breakthrough would be,

$$n_{H_2S} = \frac{\dot{m}_{H_2S} * t_b}{M_{H_2S}} = \frac{9.6 * 10^{-4} \, g / s * 4 \, hours * 3600 \, sec}{34 \, gm / gmole} = 0.41 \, moles \qquad (A.40)$$

The temperature for regeneration is about 100-120°C for desorption of H_2S from the zeolite [23, 24].

Hence, during the regeneration step, steam will heat the fibers to about 115 °C from the temperature at adsorption i.e. 25 °C.

Temperature difference required to heat the components of a single-layer fiber sorbent,

$$\Delta T_{poly} = 90 \, K$$

$$\Delta T_{ads} = 90 \, K$$

Heat capacity of cellulose acetate polymer, $Cp_{poly} = 1600 \, J / kg \, K$

Heat capacity of dry zeolite NaY, $Cp_{ads} = 700\ J/kg\ K$ [25]

Heat of sorption of sulfur impurities on zeolite NaY, $\Delta H_{sorp} \approx -37500\ J/mol$

$\Delta H_{desorp} \approx 37500\ J/mol$ [26]

Heat required,

$$Q_{single-layer} = n_{H_2S} * \Delta H_{desorp} + W_{ads} * Cp_{ads} * \Delta T_{ads} + W_{poly} * Cp_{poly} * \Delta T_{poly} \qquad \text{(A.41)}$$

$$Q_{single-layer} = 0.41\ \text{moles/cycle} * 37500\ \text{J/mole} + 13.44\ kg * 700\ J/kgK * 90\ K + 4.4\ kg * 1600\ J/kgK * 90\ K$$
$$= 1.5 * 10^6\ \text{J/cycle}$$

A.8.1. Regeneration heat provided by steam

To provide this heat saturated steam at 122 °C at 2.1 bar pressure will be used. I will assume that all the heat provided by the steam is <u>only</u> by latent heat of condensation and the steam does not cool down further, not providing any specific heat. This will be the worst case scenario and will give the maximum amount of steam required.

When steam is used as the regeneration media, a barrier layer is required on the fiber sorbents, and hence the amount of heat required to heat the barrier layer must be taken into account as well. The barrier layer is a dense polymer layer with low water vapor / gas permeability.

If, the barrier layer (~50 μm thick) material is selected as PVDC then,

$$\textit{diameter of dual layer fiber}, d_{dual-layer} = O.D. + 2 * t_{barrier}$$
$$= 800\ \mu m + 2 * 50\ \mu m = 900\ \mu m \qquad \text{(A.42)}$$

Volume of the dual layer,

$$V_{sheath} = N_f * \pi/4 * (d_{dual-layer}^2 - O.D.^2) * L_f \qquad \text{(A.43)}$$

$$V_{sheath} = 37,5000 * \pi/4 * ((900*10^{-4}\ cm)^2 - (800*10^{-4}\ cm)^2) * 120\ cm = 6008\ cm^3$$

$$W_{sheath} = V_{sheath} * \rho_{PVDC} = 6008 \, cm^3 * 1.65 \frac{g}{cm^3} = 9.91 \, kg \qquad (A.44)$$

Hence, additional heat required to heat the sheath layer

$$Q_{sheath} = W_{sheath} * Cp_{sheath} * \Delta T_{sheath} = 9.91 \, kg * 1300 \, J / kgK * 90 \, K = 1.15 * 10^6 \, J \qquad (A.45)$$

Latent heat of condensation of steam at 122 °C at 2.1 bar pressure,

$h_{fg} \approx 2196.81 \, KJ / kg$ [25]

Total amount of steam required,

$$m_{steam} * h_{fg} = (Q_{\sin gle-layer} + Q_{sheath})$$

$$\Rightarrow m_{steam} = \frac{(Q_{\sin gle-layer} + Q_{sheath})}{h_{fg}} = \frac{2.65 * 10^6 \, J}{2196.8 * 10^3 \, J / kg} \approx 1.2 \, kg \qquad (A.46)$$

If the barrier layer on the fiber sorbent fails or due to unavailability, steam cannot be used as the source of regeneration for the fiber sorbents. In that case, hot purge gas (N$_2$, air) can be used as the regeneration media on single-layer fibers.

A.8.2. Regeneration heat provided by hot N$_2$ purge

Desired temperature of N$_2$ purge = 120 °C

Heat provided by the purge gas,

$$Q_{\sin gle-layer} = m_{N_2 *} * Cp_{N_2} * \Delta T_{N_2} \qquad (A.47)$$

We assume that the hot N$_2$ cools down from 120 °C to about 40 °C, in turn heating the fibers.

$$\Delta T_{N_2} = 80°C$$
$$Cp_{N_2} = 1044 \, J / kgK \ @ \ 120°C \ [25]$$

$$m_{N_2} = \frac{1.5 * 10^6 \, J}{1044 \, J / kgK * 80°C} = 18 \, kg$$

From the calculations the breakthrough time is roughly 4 hr. Hence, six regeneration cycles need to be performed for the regeneration of the fiber sorbents in a day.

$$m_{N_2\text{-day}-} = m_{N_2} * \frac{regneration\ cycles}{day} = 18\ kg * 6\ \frac{regneration\ cycles}{day} = 108\ kg$$

Density of Nitrogen, $\rho_{N_2} = 1.1\ kg/m^3$

Volume of Nitrogen required, $V_{N_2} = \dfrac{m_{N_2\text{-day}}}{\rho_{N_2}} = \dfrac{108\ kg}{1.1\ kg/m^3} = 98\ m^3$

Cost of 1000 ft^3 or 28.3 m^3 of Nitrogen $\approx$ $ 7.00 [27]

Daily cost of 98 m^3 of Nitrogen $= \dfrac{\$7.00 * 98\ m^3}{28.3 m^3} = \$ 24$

As per our design calculations 480 kg/day of Hydrogen is produced from the small size Hydrogen generation station

Value of 1 kg Hydrogen $\approx$ $ 3 per kg [28]

Total revenue generated by producing 480 Kg H_2 per day = 480 kg/day * 1 day *$ 3 per kg = $ 1440

Cost of Nitrogen as a percentage of cost of Hydrogen produced is,

$$= \frac{\$24\ per\ day}{\$1440\ per\ day} * 100 = 1.7\ \%$$

Hence, cost of using Nitrogen as a source of heat is roughly 1.7 % of the revenue generated from the sale of H_2.

Hot N_2 can be a useful alternative for steam in case of small scale operations (on–site generation). For larger scales of operation steam/cooling water is the preferred regeneration media.

A.9. Mode of operation of fiber bed

Due to the release of heat of sorption of sulfur odorants during adsorption step, there is a possibility of rise in temperature of the fibers. A substantial increase in the temperature can lead to a decrease in the fiber sorbent capacity.

Temperature rise of the system can be calculated as follows:

Heat released during sorption = heat gained by the fiber

$$n_{H_2S} * \Delta H_{sorp} = (W_{ads} * Cp_{ads} + W_{poly} * Cp_{poly}) * \Delta T_{fiber} \tag{A.48}$$

$$\Delta T_{fiber} = \frac{n_{H_2S} * \Delta H_{sorp}}{(W_{ads} * Cp_{ads} + W_{poly} * Cp_{poly})} \Rightarrow \frac{0.41 \text{ moles/cycle} * 37500 \text{ J/mole}}{13.44 \text{ kgs} * 700 J/kgK + 4.4 \text{ kgs} * 1600 J/kgK} \approx 1 K$$

For the low concentration sulfur odorant streams the rise in temperature is not substantial. Isothermal operation can be assumed. However, for high concentration H_2S streams the rise in temperature could be substantial. In these scenarios cooling water can be passed on the impermeable sheath side of the fibers to maintain an isothermal operation.

A.10. Pressure of the desorbed gas after the regeneration step

$$n_{H_2S} = 0.41 \text{ moles/cycle}$$

Temperature of the fibers = 115°C = 388 K

Volume of sulfur odorants in the sorbed state,

$$V_{H_2S} = Q_{H_2S} * t_b = 6.855 * 10^{-7} m^3/s * 4 \, hr * 3600 \frac{\sec}{hr} = 0.009 \ m^3$$

Assuming ideal gas law,

$$p_{H_2S} V_{H_2S} = n_{H_2S} RT \tag{A.49}$$

$$p_{H_2S} = \frac{n_{H_2S}RT}{V_{H_2S}} = \frac{0.41 \; moles/cycle * 8.3143 \; J/mole \; K * 388 \; K}{0.009 \; m^3} = 147000 N/m^2 \approx 1.45 \; atm$$

The resultant pressure can drive the sulfur odorants from the sorbent module. However, a N_2 sweep gas can be passed continuously during the regeneration step to effectively displace the desorbed sulfur odorants.

A.11. Heat transfer Calculations

As described in the previous sections, for the regeneration of the fibers, saturated steam could be passed on the sheath side, with a simultaneous nitrogen sweep gas through the bore layer to effectively displace the desorbed sulfur odorants.
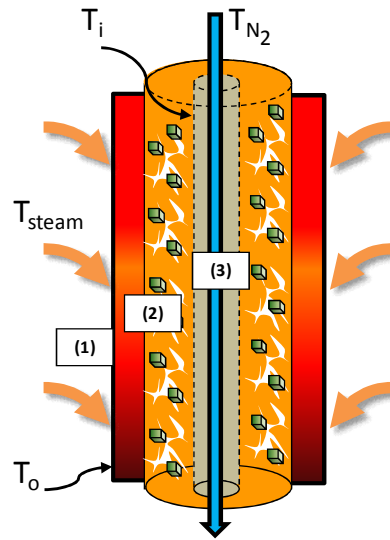

Figure A.7: Scematic diagram indicating the various heat transfer resistances in fiber sorbents.

Different heat transfer resistances encountered during the regeneration step are as follows:

(1) Convective heat transfer by the condensation of steam on the dual-layer fiber surface.

(2) Conduction through the fiber sorbent wall.

(3) Convective heat transfer by the nitrogen sweep gas.

In the calculations, the temperature at the outer surface of the fiber (T_o) and at the inner wall of the fiber (T_i) as indicated in Figure A.7 are the unknown parameters.

A.11.1. Resistance due to convective heat transfer by steam

Saturated steam at 122 °C at 2.1 bar pressure condenses to water at 122 °C.

The properties of the condensate film are evaluated at the film temperature

$$T_{film} = \frac{T_{steam} + T_{fiber}}{2} = \frac{122°C + 25°C}{2} = 73.5°C$$

$$\rho_{film} = 939 \ kg/m^3$$

$$\rho_{steam} \approx 1 \ kg/m^3$$

Thermal conductivity, $k_{film} = 0.68 \ W/m \ K$

Vis cos ity $\mu_{film} = 2.21*10^{-4} \ kg/m.\sec$

Heat of condensation $h_{fg} = 2196.81 \ kJ/kg$

$N_f = 37,500 \ fibers$

diameter of dual layer fiber, $d_{dual-layer} = O.D. + 2 * t_{barrier} = 800 \ \mu m + 2*50 \ \mu m = 900 \ \mu m$

It is assumed that the heat provided by the steam is only due to condensation and it does not cool down further while in contact with fibers. In this worst case scenario the heat transfer will be minimum.

The convection heat transfer coefficient for condensation of steam outside a tube (Assuming a fully developed laminar flow) is given by [29]

$$h_0 = 0.725[\frac{\rho_{film}*(\rho_{film}-\rho_{steam})*g*h_{fg}*k^3_{film}}{N_f*d_{dual-layer}*\mu_{film}*(T_{steam}-T_o)}]^{(1/4)} \tag{A.50}$$

$$h_0 = 0.725 \left[\left(\frac{(939)^2 \ kg/m^3 *9.81 \ m/s^2 *2196.81*10^3 \ J/kg*(0.68)^3 \ W/m.K}{37,500*900*10^{-6} \ m*2.21*10^{-4} \ kg/m.\sec*(122 \ °C - T_o)}\right)\right]^{(1/4)}$$

$$h_0 = 3857*(122 \ °C - T_o)^{-(1/4)} \ W/m^2 \ K$$

$$R_0 = \frac{1}{h_0 A_0} = \frac{1}{h_0 * N_f * \pi * d_{dual-layer} * L_f}$$

$$\Rightarrow \frac{(122\,°C - T_o)^{(1/4)}}{3857\ W/m^2K * 37{,}500\ fibers * \pi * 900 * 10^{-6}\ m * 1.2\ m} = 2.1 * 10^{-6} * (122°C - T_o)^{(1/4)}\ K/W$$

A.11.2. Resistance due to conduction through the fiber sorbent

Average thermal conductivity through the fiber wall including that of zeolite, air in the void, and polymers (CA and PVDC)

$$k_{fiber} = 0.75 * (k_{core}) + 0.25 * (k_{sheath}) \tag{A.51}$$

$$k_{fiber} = 0.75 * (\phi_{poly} * k_{poly} + \phi_{ads} * k_{ads} + \phi_{void} * k_{void/air}) + 0.25 * (k_{PVDC})$$

$$k_{fiber} = 0.75 * (0.2 * 0.5\ W/mK + 0.6 * 0.8\ W/mK + 0.2 * 0.024\ W/mK) + 0.25(0.5\ W/mK)$$
$$k_{fiber} = 0.56\ W/mK$$

$$R_{fiber} = \frac{\ln(r_{dual-layer} / r_{fb})}{2\pi N_f L_f k_{fiber}} \qquad [29] \tag{A.52}$$

$$\Rightarrow \frac{\ln(450\ \mu m. / 200\ \mu m)}{2\pi * 37{,}500\ fibers * 1.2\ m * 0.56\ W/mK} = 5.1 * 10^{-6}\ K/W$$

A.11.3. Convective resistance due to N2 sweep gas

We assume that the N_2 sweep gas is provided at ambient conditions ($T_{N_2\text{-in}}$ = 25 °C) with

a velocity of (v_{N_2}) = superficial velocity of NG through the module (v_s) = 72.7 m/s and

exits the fibers at a temperature ($T_{N_2\text{-out}}$ = 70 °C)

Hence, average N_2 temperature $T_{bulk} = \dfrac{(T_{N_2-in} + T_{N_2-out})}{2} = \dfrac{(25+70)}{2} = 48\ °C$

Properties of N_2 at T_{bulk} are,

Thermal conductivity, $k_{N_2} = 0.02\ W/m\ K$

Vis cos ity, $\mu_{N_2} = 1.78*10^{-5}\ kg/m.\sec$

Density $\rho_{N_2} = 1.14\ kg/m^3$

$\Pr andtl\ number$, $\Pr_{N_2} = 0.69$

Specific heat, $C_{p_{N_2}} = 1040\ J/kg.K$

Hence, the Reynolds number

$$\mathrm{Re}_{N_2} = \frac{I.D.*v_{N_2}*\rho_{N_2}}{\mu_{N_2}} = \frac{(400*10^{-4}\ cm)*72.7\ cm/s*1.14*10^{-3}\ g/cm^3}{1.78*10^{-5}\ poise} = 186 \quad (A.53)$$

For laminar flow of N_2 sweep gas and a fully developed velocity profile [29]

$$k_{N_2} = 0.026\ W/m\ K$$

Using Hausen's equation, [29]

$$Nusselt\ Number\ (Nu) = 3.66 + \frac{0.068(\frac{I..D.}{L_f})\mathrm{Re}_{N_2}\ \Pr_{N_2}}{1+0.04\left[(\frac{I..D.}{L_f})\mathrm{Re}_{N_2}\ \Pr_{N_2}\right]^{2/3}} \quad (A.54)$$

$$Nusselt\ Number\ (Nu) = 3.66 + \frac{0.068(\frac{400*10^{-4}\ cm}{120cm})186*0.69}{1+0.04[(\frac{400*10^{-4}\ cm}{120cm})186*0.69]^{2/3}} \cong 3.66$$

$$h_i = \frac{Nu*k_{N_2}}{I.D.} = \frac{3.66*0.026\ W/m.K}{400*10^{-6}\ m} = 238\ W/m^2.K \quad (A.55)$$

$$R_i = \frac{1}{h_i A_i} = \frac{1}{h_i*N_f*\pi*I.D.*L_f}$$

$$\Rightarrow \frac{1}{238\ W/m^2\ K*37,500\ fibers*\pi*400*10^{-6}\ m*1.2\ m} = 7.4*10^{-5}\ K/W$$

Calculating the temperature at the outer surface of the fiber (T_o) and temperature at the inner wall of the fiber (T_i)

From energy balance, flux at each part [29].

$$\Rightarrow \frac{(T_{steam} - T_o)}{R_O} = \frac{(T_o - T_i)}{R_{fiber}} = \frac{(T_i - T_{N2})}{R_i} \tag{A.56}$$

$$\Rightarrow \frac{(122°C - T_o)}{2.1*10^{-6}*(122°C - T_o)^{(1/4)} \; K/W} = \frac{(T_o - T_i)}{5.1*10^{-6} \; K/W} = \frac{(T_i - 25°C)}{7.4*10^{-5} \; K/W}$$

We have two equations and two unknowns. Hence, solving for T_o and T_i

$$\boxed{\Rightarrow T_0 = 119°C, \; T_i = 112°C}$$

Substituting the values of T_0 we get the value of resistance R_o

Hence, $R_0 = 2.1*10^{-6}*(122°C - 119°C)^{(1/4)} \; K/W = 2.8*10^{-6} \; K/W$ \hfill (A.57)

$$h_0 = 3857*(122 \; °C - T_o)^{-(1/4)} \; W/m^2K = 3756*(122 \; °C - 119°C)^{-(1/4)} \; W/m^2K = 2930 \; W/m^2K$$

A.11.4. Comparison of heat transfer resistances

$$\Rightarrow \frac{\text{Conductive heat transfer resistance through fiber}}{\text{Convective heat transfer resistance by steam condensation}} = \frac{R_{fiber}}{R_0} = \frac{5.1*10^{-6} \; K/W}{2.8*10^{-6} \; K/W} = 1.8$$

$$\Rightarrow \frac{\text{Conductive heat transfer resistance through fiber}}{\text{Convective heat transfer resistance by Nitrogen sweep}} = \frac{R_{fiber}}{R_i} = \frac{5.1*10^{-6} \; K/W}{7.4*10^{-5} \; K/W} = 0.07$$

From the above analysis it can be said that internal heat conduction through the fiber is comparable to heat transfer from convection due to steam. This is due to the high heat transfer coefficient due to steam condensation and the relatively low thermal conductivity of polymers compared to metals.

If the regeneration medium was hot nitrogen instead of steam the convective heat transfer would be lower than the conduction through the fiber.

A.11.5. Calculation of time required for fibers to reach thermal equilibrium

To estimate the time required for the fibers to reach thermal equilibrium an unsteady state process needs to be considered.

In order to simplify the calculations the hollow fiber sorbents can be considered to be an infinite cylinder with a very high aspect ratio.

$$Aspect\ ratio\ of\ the\ fibers = \frac{L_{fiber}}{d_{dual-layer}} = \frac{1.2\ m}{900*10^{-6}\ m} = 1333 \tag{A.58}$$

Density of the fiber,

$$\rho_{fiber} = 0.75*(\phi_{poly}*\rho_{poly} + \phi_{ads}*\rho_{ads} + \phi_{void}*\rho_{void}) + 0.25*(\rho_{PVDC}) \tag{A.59}$$

$$\rho_{fiber} = 0.75(0.2*1300\ kg/m^3 + 0.6*1320\ kg/m^3 + 0.2*0\ kg/m^3) + 0.25*1650\ kg/m^3$$
$$= 1202\ kg/m^3$$

Specific heat of fiber,

$$Cp_{fiber} = 0.75*(\phi_{poly}*Cp_{poly} + \phi_{ads}*Cp_{ads} + \phi_{void}*Cp_{void}) + 0.25*(Cp_{PVDC})$$

$$Cp_{fiber} = 0.75*(0.20*1600\ J/KgK + 0.6*700\ J/KgK + 0.2*1000\ J/KgK) + 0.25*1300\ J/KgK$$
$$= 1030\ J/Kg\text{-}K$$
$$k_{fiber} = 0.56\ W/mK$$

$$h_0 = h_{fiber} = 2930\ W/m^2\ K$$

$$Thermal\ diffusivity\ of\ fiber\ (\alpha) = \frac{k_{fiber}}{\rho_{fiber}*Cp_{fiber}}$$
$$= \frac{0.56\ W/mK}{1202\ kg/m^3 * 1030\ J/KgK} = 4.5*10^{-7}\ m^2/s \tag{A.60}$$

$$\frac{k_{fiber}}{h_{fiber}*r_{dual-layer}} = \frac{0.56\ W/mK}{2930\ W/m^2K * 450*10^{-6}\ m} = 0.43$$

Using Heisler's chart for infinite cylinder and substituting values [29]

We get,

$$\frac{\alpha_{fiber} * \tau_{eq.}}{r_{dual-layer}^2} = 1.4 \qquad (A.61)$$

$$\tau_{eq.} = \frac{1.4 * r_{dual-layer}^2}{\alpha_{fiber}} = \frac{1.4 * (450 * 10^{-6} m)^2}{4.5 * 10^{-7} m^2 / s} = 0.7 \ s$$

This is the time required for the fibers to reach thermal equilibrium once the temperature outside the fiber is isothermal at 122°C. This clearly indicates that the fiber sorbents can be heated rapidly and rapid thermal swing adsorption cycles are feasible.

A.12. REFERENCES

1. *The Hydrogen Economy: opportunities,costs,barriers and R&D needs*. 2004: National academic press.

2. Energy Information Administration - Office of Integrated Analysis and Forecasting, *The Impact of Increased Use of Hydrogen on Petroleum Consumption and Carbon Dioxide Emissions,http://www.eia.doe.gov/oiaf/servicerpt/hydro/pdf/oiafcneaf(08)04.pdf,*. Aug. 2008, U.S. Department of Energy: Washington, DC. Date accessed, October 8th, 2010.

3. *http://technologyventures.chevron.com/commercialize_tech/hydrogen.asp*. Date accessed, October 8th, 2010.

4. Yamamori, H.H., A.; Kobayashi, M.J, *Hollow fiber membrane module*. July 13, 1999.

5. Carruthers, S., *Integral-skin formation in hollow fiber membranes for gas separations*, in *Department of Chemical Engineering*. 2001, University of Texas at Austin

6. Vu, D.Q., W.J. Koros, and S.J. Miller, *High pressure CO2/CH4 separation using carbon molecular sieve hollow fiber membranes.* Industrial & Engineering chemistry research, 2002. 41(3): p. 367-380.

7. Yang, R., *Gas separation by adsorption processes*. 1997, London: Imperial college pres.

8. Bessho, N., D.A. Bhandari, and W.J. Koros, *Hollow Fiber Sorbents for Hydrogen Recovery*. Chemical Engineeing Science, In-Press.

9. Puleo, A.C., D.R. Paul, and S.S. Kelley, *The Effect of Degree of Acetylation on Gas Sorption and Transport Behavior in Cellulose-Acetate.* Journal of Membrane Science, 1989. 47(3): p. 301-332.

10. Afandizadeh, S. and E.A. Foumeny, *Design of packed bed reactors: guides to catalyst shape, size, and loading selection.* Applied Thermal Engineering, 2001. 21(6): p. 669-682.

11. Ruthven, D., *Diffusion in zeolite molecular sieves*, in *Introduction to zeolite science and practice*. 2007, Elsevier B. V. .

12. Wakita, H., Y. Tachibana, and M. Hosaka, *Removal of dimethyl sulfide and t-butylmercaptan from city gas by adsorption on zeolites.* Microporous and Mesoporous materials, 2001. 46(2-3): p. 237-247.

13.	A. L. Hines, R.N.M., *Mass transfer fundamentals and applications* 1st ed. 1985, Upper Saddle river , NJ: Prentice hall PTR.

14.	J. Karger, D.R., *Diffusion in zeolites and other micropore solids*. 1992: John Wiley & sons.

15.	Moore, T.T. and W.J. Koros, *Non-ideal effects in organic-inorganic materials for gas separation membranes*. Journal of Molecular Structure, 2005. 739(1-3): p. 87-98.

16.	Mahajan, R. and W.J. Koros, *Factors controlling successful formation of mixed-matrix gas separation materials*. Industrial & Engineering chemistry research, 2000. 39(8): p. 2692-2696.

17.	Patton, A., B.D. Crittenden, and S.P. Perera, *Use of the linear driving force approximation to guide the design of monolithic adsorbents*. Chemical Engineering Research & Design, 2004. 82(A8): p. 999-1009.

18.	Glueckauf, E., *Theory of Chromatography .10. Formulae for Diffusion into Spheres and Their Application to Chromatography*. Transactions of the Faraday Society, 1955. 51(11): p. 1540-1551.

19.	M. Yang, E.C., *Designing hollow-fiber contactors*. AIChE Journal, 1986. 32(11): p. 1910-1916.

20.	McCabe, W.L., J.C. Smith, and P. Harriott, *Unit operations of chemical engineering*. 6th ed. 2001, Boston: McGraw Hill.

21.	Sherwood, T.K., R.L. Pigford, and C.R. Wilke, *Mass transfer*. 1975, New York: McGraw-Hill.

22.	Ergun, S., *Fluid Flow through Packed Columns*. Chemical Engineering Progress, 1952. 48(2): p. 89-94.

23.	H. Wakita, Y.T., M. Hosaka, *Removal of dimethyl sulfide and t-butylmercaptan from city gas by adsorption on zeolites*. microporous and mesoprorous materials, 2001. 46 (2-3): p. 237.

24.	G. Alptekin, S.D., M. Duboik, J. Monroe, R. Amalfitno. G. Israelson, *Regenerable sorbent for natural gas desulfurization*. Journal of materials engineering and performance, 15(4) (2006): p. 433-438.

25.	R. H. Perry, D.G., ed. *Perry's Chemical Engineers' Handbook*. 7th edition ed. 1997, McGraw-Hill.

26.	G. Weber, F.B., J. Bellat, C. Paulin, P. Mougin, M. Thomas, *Selective adsorption of ethyl mercaptan on NaX Zeolite*. Microporous and Mesoporous materials, 2008. 109: p. 184-192.

27.   themonty.com.
        *http://www.themonty.com/Endothermic%20Gas%20vs%20Methanol%20Producti
        on%20Cost.htm*. Date accessed, October 8th, 2010.

28.   Doty, D. *A Realistic Look at Hydrogen Price
        Projection,http://www.dotynmr.com/PDF/Doty_H2Price.pdf* 2004. Date accessed,
        October 8th, 2010.

29.   Holman, J.P., *Heat Transfer*. 8th ed. 2001: McGraw-Hill Education.

APPENDIX B

It is important to account for the sulfur capacity due to filling up of the void space between the fibers ("void capacity"), while determining the sorption capacity in single and dual-layer fiber sorbents.

Sample calculations for a single-layer fiber sorbent module tested in section 4.13. is described for clarity.

The inlet gas conditions,

Temperature of module and the feed gas,

$$T_{in} = T_t = 25°C \text{ or } 298 \text{ K}$$

Average gas pressure in the module, $p_t = 5 \text{ psig or } 1.35 * 10^5 \text{ N/m}^2$

Diameter of the module, $d_t = 1/4 \text{ inch} = 6.35 * 10^{-3} \text{ m}$

Length of the module $L_t = 53 \text{ cm} = 0.53 \text{ m}$

Here, as the worst case scenario we assume that the entire module volume as the void volume. However, a certain volume will be occupied by the fiber sorbents in the real case.

Volume of the module,

$$V_t = \pi/4 * d_t^2 * L_t = \pi/4 * (6.35 * 10^{-3} \text{ m})^2 * 0.53 \text{ m} = 1.7 * 10^{-5} \text{ m}^3 \quad \text{(B. 1)}$$

Assuming ideal gas law,

$$p_t V_t = n_t R T_t \quad \text{(B. 2)}$$

$$n_t = \frac{p_t V_t}{RT_t} = \frac{1.35 * 10^5 \text{ N/m}^2 * 1.7 * 10^{-5} \text{ m}^3}{8.3143 \text{ J / mole K} * 298 \text{ K}} = 0.0009 \text{ moles}$$

The concentration of sulfur odorant (TBM or H$_2$S) in the H$_2$S/N$_2$ feed gas mixture,

$C_{eq.} = 30$ ppm

Hence, moles of sulfur species in the void space in the module,

$$(n_{sulfur})_t = n_t * C_{eq.} = 0.0009 \ moles * 30 * 10^{-6} = 2.8 * 10^{-8} \ moles \tag{B. 3}$$

The number of moles sorbed in a module depends upon the weight of the fiber (i.e. the weight of active zeolite in the fiber). Here again we take the worst case scenario with a single-layer fiber sorbent module with only one fiber and showing the least capacity (W$_{ads}$=. 0.15 g, zeolite loading 60 wt. %, case b-1, section 4.13.1.).

The moles of H$_2$S sorbed in the module till breakthrough,

$$(n_{sulfur-sorbed})_{measured} = 2 * 10^{-6} \ moles$$

Hence, the actual sulfur sorption capacity taking into account the 'void capacity',

$$(n_{sulfur-sorbed})_{actual} = (n_{sulfur-sorbed})_{measured} - (n_{sulfur})_t$$
$$= (2 * 10^{-6} - 2.8 * 10^{-8}) moles = 1.97 * 10^{-6} \ moles$$

Hence, it can be observed that the sulfur molecules in the module void volume are negligible.